SYNERGISTIC EFFECTS IN CLATHRATE SELECTIVITY

Amina Sayed

A thesis submitted to the Cape Peninsula University of Technology in fulfilment of the requirements for

Master of Technology in Chemistry

In the Faculty of Applied Science
at the

CAPE PENINSULA UNIVERSITY OF TECHNOLOGY

Supervisor: Associate Professor Ayesha Jacobs

Co-supervisor: Professor Luigi R Nassimbeni

Cape Town
September 2012

DECLARATION

I, Amina Sayed, declare that the contents of this dissertation/thesis represent my own work, and that the dissertation/thesis has not previously been submitted for academic examination towards any qualification. Furthermore, it represents my own opinions and not necessarily those of the Cape Peninsula University of Technology.

…… **……**

Signed **Date**

ABSTRACT

The inclusion behaviour of a series of hydroxyl hosts with a variety of liquid guests has been investigated. The host 9-(4-methoxyphenyl)-9*H*-xanthen-9-ol (A1), $C_{20}H_{16}O_3$, forms inclusion compounds with aniline (ANI), 3-picoline (3PIC), morpholine (MORPH), *N*-methylacetamide (NMA) and *N*-methylformamide (NMF). Their structures have been elucidated and correlated with their thermal behaviour. The inclusion compounds A1·ANI and A1·MORPH were successfully solved in space group $P2_1/c$, whereas A1·3PIC was solved in $P\bar{1}$. Non-isothermal kinetics of desolvation were performed for A1·3PIC and A1·MORPH. The packing of A1·3PIC and A1·MORPH is characterized by (Host)···(Guest) hydrogen bonds, whereas A1·ANI is stabilised by (Host)···(Host) hydrogen bonding. Three structures were obtained for the host A1 and the guest *N*-methylacetamide, with structural formulas of $C_{20}H_{16}O_3 \cdot C_3H_7NO$ (A1·NMA), $C_{20}H_{16}O_3 \cdot 2C_3H_7NO$ (A1·2NMA) and $2C_{20}H_{16}O_3 \cdot 2C_3H_7NO$ (2A1·2NMA). The packing of A1·NMA, A1·2NMA and 2A1·2NMA are characterized by (Host)-OH···O-(Guest) and (Guest)-NH···O-(Guest) hydrogen bonds, which gave hydrogen bonding patterns of $C_2^2(7)$, $C_3^3(11)$ and $C_4^2(11)$ respectively. The hydrate A1·NMF·H_2O was successfully solved in the triclinic space group $P\bar{1}$. The A1·NMF·H_2O hydrogen bond pattern may be described according to Etter's notation as $R_4^2(8)$ and $R_6^6(16)$.

The host 9-(3-methoxyphenyl)-9*H*-xanthen-9-ol (A2), $C_{20}H_{16}O_3$, forms inclusion compounds with morpholine (A2·MORPH), *N*-methylacetamide (A2·NMA) and *N*-methylformamide (A2·NMF), with host-guest ratios 1:1. The crystal structure of the apohost was solved in P*bca* with Z=8. The structures of A2·MORPH and A2·NMF were solved in $P\bar{1}$, whereas A2·NMA was solved in $P2_1/n$. The packing of these structures is stabilised by (Host)···(Guest) hydrogen bonds.

The host 5-(4-methoxyphenyl)-5*H*-dibenzo[a,d]cyclohepten-5-ol (A26), $C_{22}H_{18}O_2$, forms inclusion compounds with aniline (A26·ANI) and morpholine (A26·MORPH). A26·MORPH and A26·ANI crystallised in the space groups *Pc* and $P\bar{1}$ respectively. The packing of these structures are characterized by (Host)-OH···O-(Host) hydrogen bonding. A guest exchange reaction was performed.

The host compounds 5-(4-chlorophenyl)-5*H*-dibenzo[a,d]cyclohepten-5-ol ($C_{21}H_{15}OCl$), 5-[3(trifluoromethyl)phenyl]-5*H*-dibenzo[a,d]cyclohepten-5-ol ($C_{22}H_{15}OF_3$) and 5-(naphthalen-1-yl)-5*H*-dibenzo[a,d]cyclohepten-5-ol ($C_{25}H_{18}O$) form inclusion compounds with morpholine. All three structures were solved in $P\bar{1}$ with the host molecules hydrogen bonded to the morpholine guests.

ACKNOWLEDGEMENTS

I wish to thank:

- Associate Professor Ayesha Jacobs
- Professor Luigi R. Nassimbeni

  for their endless support, assistance and encouragement throughout this study. I would be forever indebted to them for giving of their precious time and sharing their knowledge and expertise which they did selflessly and patiently.

- Dr Nikoletta B Báthori for her vital input and assistance throughout this study.
- My family, friends and colleagues for their support.

The financial assistance of the Mauerberger Foundation towards this research is acknowledged. Opinions expressed in this thesis and the conclusions arrived at, are those of the author, and are not necessarily to be attributed to the Mauerberger Foundation.

TABLE OF CONTENTS

LIST OF TABLES

LIST OF FIGURES

ATOM COLOUR SCHEME

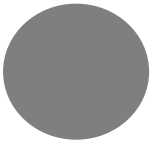

CARBON

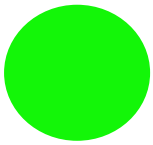

HYDROGEN

NITROGEN

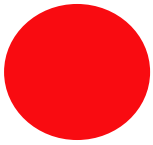

OXYGEN

CHLORINE

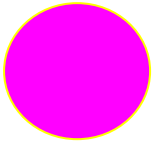

FLUORINE

CHAPTER 1
INTRODUCTION

1.1 Supramolecular Chemistry

Supramolecular chemistry was introduced in the words "Just as there is a field of molecular chemistry based on covalent bonds, there is a field of supramolecular chemistry, the chemistry of molecular assemblies and of the intermolecular bond".[1] Beyond molecular chemistry, supramolecular chemistry aims at constructing highly complex, functional chemical systems from components held together by intermolecular forces.[2] The transformation from molecular to supramolecular chemistry is displayed in Figure 1.1.

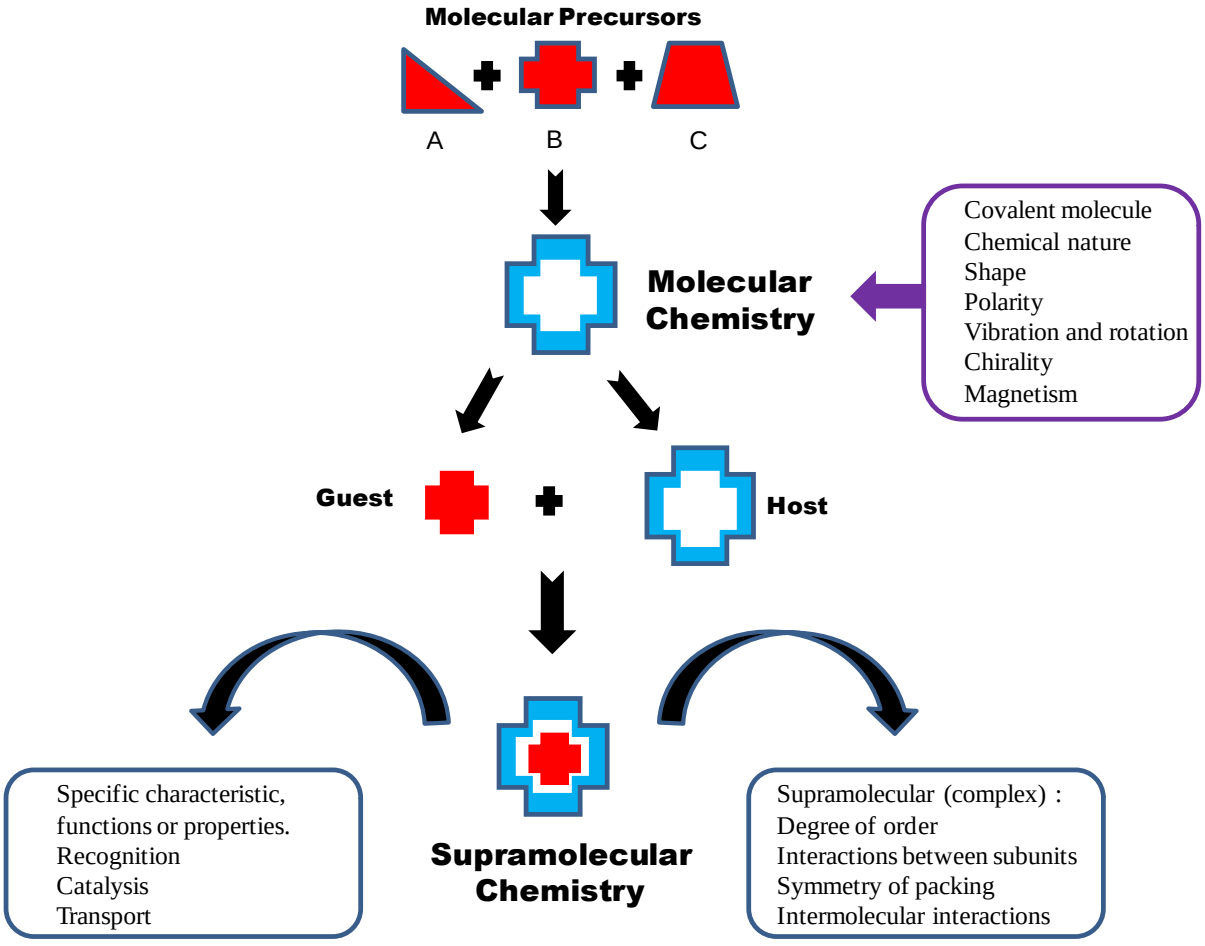

Figure 1.1: Schematic diagram of the transformation from molecular to supramolecular. The diagram also shows the selectivity of the host which preferentially enclathrates guest B.[3, 4]

It appears that the definition of supramolecular chemistry does not have definite boundaries because the field is still in its early stages of development and ever changing as it advances (Table 1.1). Researchers have their own understanding of supramolecular chemistry.

In 1987 the Nobel Prize in chemistry was awarded to Donald Cram, Jean-Marie Lehn and Charles Pedersen for their development and use of molecules with structure-specific interactions of high selectivity. The definition provided by Jean-Marie Lehn states that supramolecular chemistry is the "chemistry of molecular assemblies and of the intermolecular bonds".[1] Owing to the field expanding rapidly, Lehn (2002) added a further functional definition "supramolecular chemistry aims at developing highly complex chemical systems from components interacting by non-covalent intermolecular forces".[5]

Supramolecular chemistry is described by the phrase "chemistry beyond the molecule" owing to the complexity of the outcome when two or more molecules/ions interact with each other and are held together by non-covalent interactions.[6-9] In supramolecular chemistry a supermolecule is the subject of study. The non-covalent interaction defines their tendency to associate or isolate themselves, their selectivity, ability to recognize each other, stability and rigidity.[3]

Supramolecular chemistry includes inclusion complexes, charge-transfer complexes, cyclodextrins, mono- and polylayers, micelles, vesicles, liquid crystals and cocrystals. [7]

Table 1.1 Timeline of significant events in supramolecular chemistry.[10,11]

Year	Author	Event
1811	Davy	Preparation of chlorine hydrate
1823	Faraday	Confirmation of Davy's observation and determines the composition of chlorine hydrate
1849	Wohler	Preparation of β-quinol•H_2S molecular complex
1893	Werner	Co-ordination chemistry
1894	Fischer	Introduction of the lock and key principle
1906	Ehrlich	Introduction of the concept receptor
1940	Bengen	Urea channel inclusion compounds
1947	Palin & Powell	Published the crystal structure of β-quinol•H_2S molecular complex
1948	Powell	Introduces the term "clathrate"
1953	Watson and Crick ; Franklin and Wilkins	Structure of DNA
1953	Perutz	Structure of haemoglobin
1956	Hodgkin	X-ray crystal structure of vitamin B_{12}
1961	Curtis	First Schiff's base macrocycle from acetone and ethylene diamine
1964	Busch & Jager	Schiff's base macrocycle
1967	Pedersen	Preparation of crown ethers
1969	Lehn & co-workers	Synthesis of cryptands
1969	Atwood	Liquid clathrates from alkyl aluminium salts
1978	Lehn	Introduces the concept and term "Supramolecular Chemistry"
1979	Gokel & Okahara	Development of the lariat ethers as a subclass of host
1981	Vögtle and Weber	Podand hosts and development of nomenclature.
1987	Lehn, Cram & Pedersen	Awarded the Nobel prize for their work in the field of supramolecular chemistry
1996	Atwood, Davies, MacNicol & Vögtle	Publication of *Comprehensive Supramolecular Chemistry* containing contributions from many key groups
1996	Kroto, Smalley & Curl	Awarded the Nobel prize for their work on the chemistry of the fullerenes
2003	Agre & Mackinnon	Awarded the Nobel prize for their work on channels in membranes
2011	Shechtman	Awarded the Nobel Prize for the discovery of quasicrystals

1.2 Host-Guest Chemistry

A host-guest complex or supermolecule is formed when a molecule (host) binds to another molecule (guest) to form a larger molecule. The properties of supermolecules are derived from their components. Donald Cram's definition of a host and guest is given by "The host component is an organic molecule/ion whose binding sites converge in the complex…The guest component is any molecule/ion whose binding sites diverge in a complex''.[12]

Host–guest chemistry is based upon three concepts:

1) These aggregates can be of the host-guest type in which one molecule encapsulates the other (Figure 1.2).

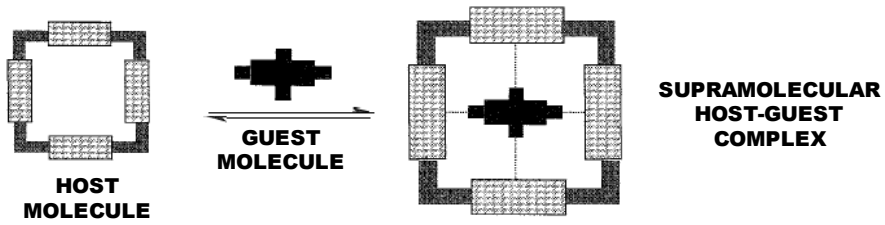

Figure 1.2: Schematic diagram of host-guest complexation.[10]

2) They can involve mutually complementary, self complementary and components of a similar size in which there are no host or guest molecules (Figure 1.3).

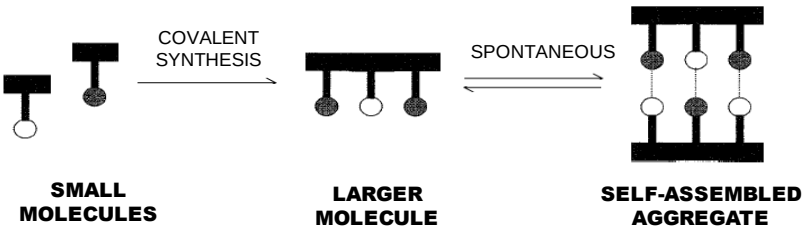

Figure 1.3: Schematic diagram of self-assembly between complementary species (circles represent the binding sites).[10]

3) The guest molecules are packed into the framework between host molecules in the crystal structure (Figure 1.4).

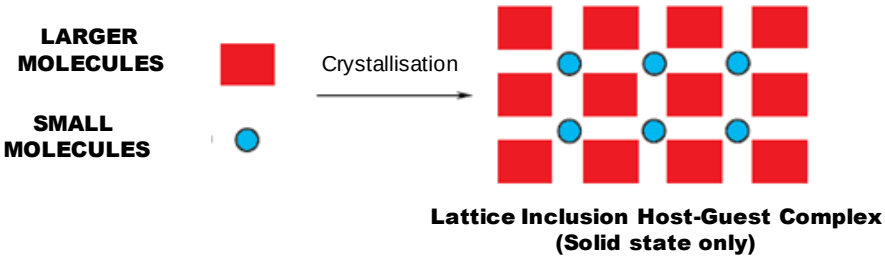

Figure 1.4: Schematic diagram of lattice inclusion host-guest complex. [10]

Inclusion compounds consist of host and guest components in the form of a crystal/polycrystalline material.[13] The study of inclusion compounds is a popular topic in chemical research.[14-22] At the centre of inclusion chemistry lies molecular recognition. The affinity of a host for a given guest depends on the intermolecular interactions between host, guest and solvent molecules under specific conditions of temperature, pressure and concentration.[23] This is dependent on the size, shape, geometry and surface charge distributions of the molecules making up the structure.

The macroscopic properties of crystalline inclusion compounds depend on their structures. A crystal is a supramolecular entity, and the molecules that comprise it interact implicitly among themselves during crystallization.[24] When analyzing a crystal structure it gives us deeper insight into the types of non-covalent interactions that exists in the host-guest complex as well as the lattice energies.[25] By using the lattice energies we are able to predict the relative thermal stabilities of related structures. The topology and stoichiometry of an inclusion compound in the crystalline form (solid state) depends on the degree of molecular recognition which occurs between the host and guest molecules, and the resultant crystal structure relates to reactivity, thermal stability and kinetics of decomposition and formation.[26,27]

A number of techniques that can be used in the study of inclusion compounds are shown in Figure 1.5:

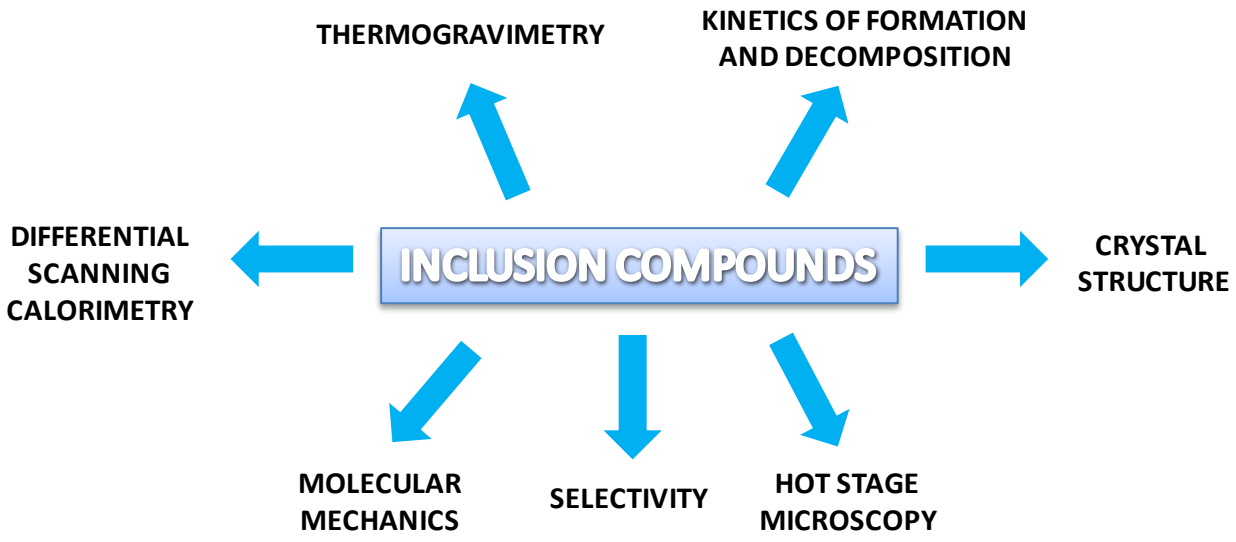

Figure 1.5: Various techniques used in the study of inclusion compounds.[28]

Inclusion compounds can be classified into two broad categories:[11,23]

- **Molecular inclusion**

Molecular complexes are formed by fitting convex guests into the concave cavity of a host. eg. Calixarenes (Figure 1.6).

- **Lattice inclusion**

The guest molecules are packed into the cavities or layers between host molecules in the crystal structure (Figure 1.6).

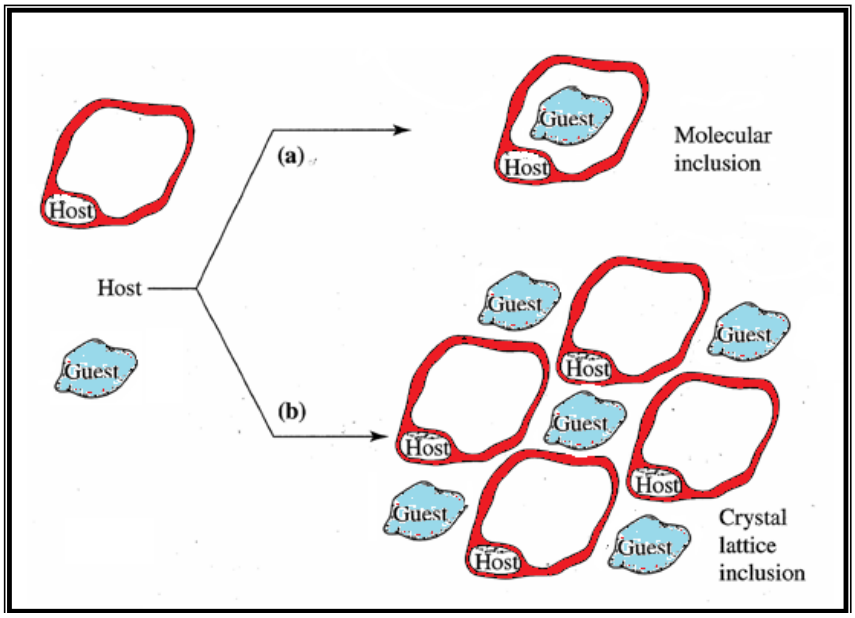

Figure 1.6: Molecular inclusion and crystal lattice inclusion.[6]

The formation of these types of compounds are generally formulated as:

$$H_{(s,\alpha)} + nG_{(l/g)} \rightarrow H \bullet G_{n(s,\beta)}$$

l=liquid phase , s=solid phase , g=gas phase

α = Non porous phase of the pure host H or apohost

β = The phase of the host-guest compound

n = Host : Guest ratio

Figure 1.7 illustrates the formation and decomposition of an inclusion compound.

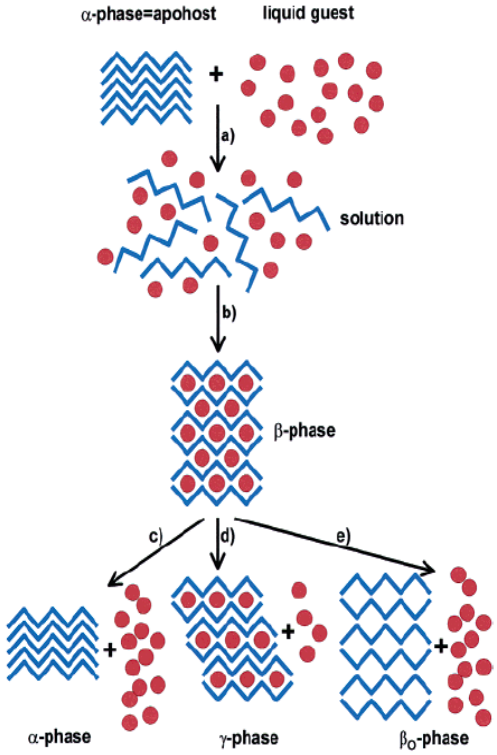

Step a
Gives a solution due to dissolution of the apohost in the liquid guest.

Step b
Crystallization to the β-phase, giving the host-guest complex.

Step c
$H{\bullet}G_{n(s,\beta)} \rightarrow H_{(s,\alpha)} + nG_{(g)} \uparrow$
β-phase reverts to the apohost

Step d
$H{\bullet}G_{n(s,\beta)} \rightarrow H{\bullet}\ G_{(n-m)(s,\gamma)} + mG_{(g)} \uparrow$
β-phase decomposes to form a new γ-phase.

Step e
The host loses the guest but the structure is retained (β_O – phase).

Figure 1.7: The formation and decomposition of an inclusion compound.[23]

Inclusion compounds can be classified according to the type of voids formed, examples are displayed in Figure 1.8.

a	**b**	**c**
Cage-Type Inclusion compound	Channel-Type Inclusion compound	Layered-Type Inclusion compound

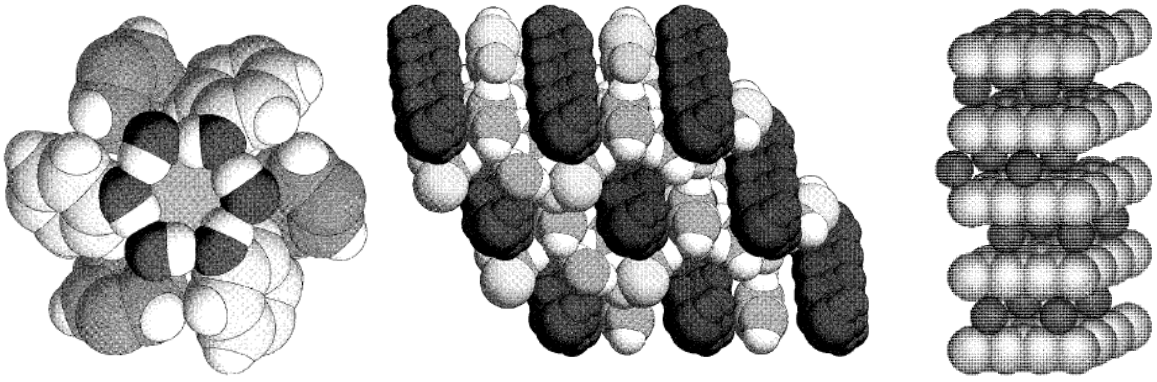

Figure 1.8: a) The cavity in the β-hydroquinone structure with included Xe atom; b) The molecules of n-alkane in the urea channels; c) The stage 1 graphite intercalation compound of potassium, KC_8.[29]

1.2.1 Selectivity

When a host is exposed to a mixture of guests, it may likely combine selectively to form a crystalline inclusion compound with a particular guest(s). When a host molecule shows preference for a specific guest, it is said to show a degree of selectivity towards that guest. There are many factors that influence the selectivity, such as pre-organisation of the host conformation, co-operativity of the binding groups and complementarity of the host and guest binding sites.[30] The selectivity that a host displays towards a guest, has always been the aim of most synthetic supramolecular chemistry studies and is therefore of great interest in the field of crystal engineering.[31,32]

Inclusion compounds with mixed guests are essential as research can show which aspects are important in the selection of different guests, such as steric factors, guest symmetry, solubility and polarity.[33] The possibility of controlling the ratio of mixed guests in a host-guest system gives deeper insight into the chemical and physical properties which have significance in developing chemical sensors, optical and electronic properties of organic crystals.[33]

There are two types of selectivity:

- **Kinetic Selectivity**

  Enzyme-based processes are mostly found when kinetic selectivity studies are carried out. The determining factor for kinetic selectivity is the rate at which competing substrates are transformed, with the enzyme being selective for the fastest-reacting substrate.[1]

- **Thermodynamic Selectivity**

In solution, when a host (H) reacts with a guest (G), the reaction may be formulated as:

$$H + nG \rightarrow H{\cdot}G_n \qquad n = \text{host:guest ratio}$$

The equilibrium constant K is

$$K = \frac{a_{H{\cdot}Gn}}{a_H \times (a_G)^n}$$

where *a* is the activity of the components.

Most chemists simplify the activity to concentration so that

$$K_c = \frac{[\mathrm{H{\cdot}G\ n}]}{[H]\times[G]^n}$$ with the standard state defined as 1mol/L.

The standard Gibbs free energy of this reaction is given by

$$\Delta G° = -RTlnK_c$$

and is a quantitative measure of the molecular recognition which occurs in the formation of the host-guest complex.

When the host is exposed to a mixture of two guests, then the selectivity is defined as[34]

$$\text{Selectivity} = \frac{K_{\text{guest 1}}}{K_{\text{guest 2}}}$$

However, when a solid host-guest crystallises from the mother liquor we can no longer employ the thermodynamic equilibrium constants, because the activity of the pure solids are defined as unity, and we would have to measure the solubilities of the components in the mother liquor. This is not practical, due to the paucity of materials.

We have therefore elected to employ the concept of selectivity coefficient, defined as:[35]

$$K_{A:B} = (K_{B:A})^{-1} = Z_A/ Z_B * X_B/ X_A \qquad (X_A + X_B) = 1$$

X_A and X_B = Mole fraction of the guests A and B in the liquid mixture

Z_A and Z_B = Mole fractions of the guests in the crystal.

The selectivity coefficient of a host towards a specific guest, over a range of compositions of mixtures of guests A and B can be determined. This is done by varying the mole fraction of X_A of the starting mixtures from 0 to 1. The crystals obtained from each mixture are analyzed and the mole fractions (Z_A and Z_B) determined.

A system which contains two components, gives rise to four kinds of selectivity curves (Figure 1.9).

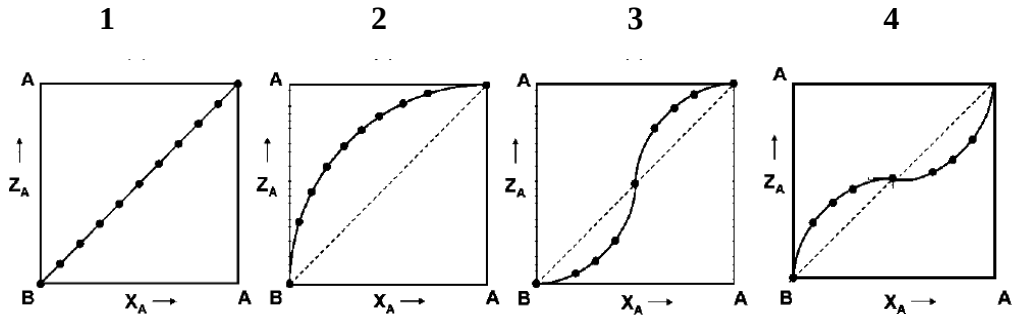

Figure 1.9: Competition experiments selectivity curves for two guests A and B; (1) represents zero selectivity, with $K_{A:B} = 1$; (2) A is preferred to B, $K_{A:B} \approx 6$; (3 and 4) The selectivity is concentration dependent.[35]

Competition experiments may also be successfully achieved by using three guests (Figure 1.10). An equilateral triangle where each apex represents a pure guest is used to illustrate the results. Starting points of the mixtures are chosen sensibly on the inner circle of the triangle.

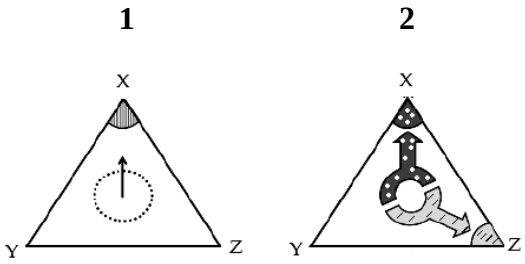

Figure 1.10 : Competition experiments using three guests; (1) displays the results in which guest X is preferentially enclathrated over Y and Z; (2) shows the results of a system in which guest Y is rejected but guests X and Z are favoured, depending on their initial concentrations.[23]

1.2.2 Guest Exchange

The study of guest exchange in crystals is vital due to its various applications, which include the storage of small volatile molecules, component separation of mixtures, catalysis and the formation of materials with optical properties.

The kinetics of host (solid) : guest (vapour) reactions and of guest exchange are important in our understanding of catalytic processes.[23]

The mechanism of guest exchange:[36]

(a) The host-guest system maintains its structure throughout the exchange.

$$H{\cdot}n\,G_{1(s,\beta)} + mG_{2(\text{liquid or vapour})} \rightarrow H{\cdot}mG_{2(s,\beta)} + nG_{1(\text{liquid or vapour})}$$

or

(b) The host-guest system desorbs the original guest G_1 to give the apohost in its α, non porous phase, which in turn forms a new inclusion compound with the incoming guest G_2. This is essentially a recrystallisation process.

$$H{\cdot}n\,G_{1(s,\beta)} \rightarrow H_{(s,\alpha)} + n\,G_{1(\text{liquid or vapour})}$$

$$H_{(s,\alpha)} + mG_2 \rightarrow H{\cdot}mG_{2(s,\beta)}$$

1.2.3 Kinetics of Decomposition

The kinetics of decomposition can be obtained by isothermal or non-isothermal methods.

The kinetics of decomposition is commonly investigated non-isothermally using thermogravimetric analysis. The decomposition at various temperatures yields activation energies.[37] The relationship is described by the Arrhenius equation :

$$k = A^{(-Ea/RT)}$$

k = kinetic rate
A= pre-exponential factor
E_a = activation energy

The E_a (J/mol) represents the energy barrier to the reaction.[38] The *A* value may be regarded as the frequency of the situation which may lead to the conversion of reagents into products. These parameters are often subject to a compensation effect, whereby

$$lnA = aE_a + b, \qquad a \text{ and } b \text{ are constants}$$

The compensation effect "occurs when the decrease in kinetic rate due to increased E_a is offset by an increase in *A*".[38]

A method in which the thermogravimetric rate is analysed with respect to temperature was developed by Flynn,[39] Wall[39] and Ozawa.[40] A series of TG runs are performed at different scan rates (non-isothermal approach) over a selected temperature range.

The thermogravimetric rate is described by the equation

$$dC/dT = A / \beta f(C) e^{-Ea/RT}$$

C = mass loss
β = heating rate

The equation can be reduced to

$$d \log \beta / d (T^{-1}) \approx (0.457/ R)Ea$$

A plot of log β vs. 1/T yields a straight line with slope - (0.457Ea)/R.

1.3. Interactions in Supramolecular Chemistry

1.3.1 Non-covalent Interactions

An understanding of the structure or composition of matter and the nature of non-covalent interactions between molecular species as they exist in close proximity to one another is required to gain insight into structure–property relationships.[41] When a small molecule binds to another molecule(s), a combination of different non-covalent interactions determine the strength and stereochemistry of the interaction.[42] Table 1.2 lists the non-covalent interactions that occur in supramolecular chemistry.

Table 1.2: Supramolecular interactions.[30]

Non-covalent interactions	**Strength (kJ/mol)**
Hydrogen bonding	4 - 120
Van der Waals	< 5 kJ/mol but variable depending on surface area
π- π interaction	0 - 50
Cation – π interaction	5 - 80
Ion – ion	200 - 300
Ion – dipole	50 - 200
Dipole – dipole	5-50
Hydrophobic	Related to solvent-solvent interaction

1.3.1.1 Hydrogen Bond

A definition of hydrogen bonding has been proposed and submitted to the International Union of Pure and Applied Chemistry. The complete definition is quite lengthy and consists of a preamble definition, characteristics of hydrogen bonds, lists of criteria and footnotes. The preamble definition states that "*the hydrogen bond is an attractive interaction between a hydrogen atom from a molecule or a molecular fragment X-H in which X is more electronegative than H, and an atom or a group of atoms in the same or different molecule, in which there is evidence of bond formation*".[43] Desiraju has commented that this definition "is of a very broad scope and should stand the test of time in a general chemical sense''.[44]

The hydrogen bond is without a doubt the most important interaction because it is common, strong and directional.[45] This leads to supramolecular compounds being orientationally specific and structurally robust.[46] The hydrogen bond in its simplest form may be represented by D-H•••A (D=donor; A=acceptor).[47] Various types of hydrogen bonding geometries are shown in Figure 1.11. Hydrogen bonds display an energetic preference for a linear D-H•••A geometry (Figure 1.11a). For many years since the discovery of hydrogen bonds it has been restricted to interactions such as N-H•••O, O-H•••O and F-H•••A. Interactions such as C-H•••O and O-H•••π are weaker interactions which are also classified as hydrogen bonds. The hydrogen bonding interaction is the most frequently observed interaction in the assembly of organic molecules and stabilizes these molecules in the liquid, solid and gas phase.[48]

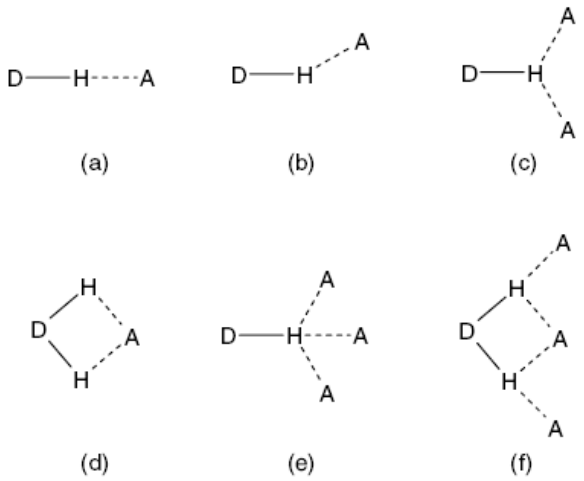

Figure 1.11: Various types of hydrogen bonding geometries: (a) linear (b) bent (c) donating bifurcated (d) accepting bifurcated (e) trifurcated (f) three centre bifurcated.[47,49]

Hydrogen bonds can be classified as: very strong, strong and weak. The properties of the hydrogen bonds are reported in Table 1.3.

Table 1.3: Various properties of very strong, strong and weak hydrogen bonds.[47]

	Very strong	**Strong**	**Weak**
Bond energy (kJ/mol)	62 – 84	16 - 20	< 16
Example	$[F•••H•••F]^-$	O-H•••O	C-H•••O
D•••A range(Å)	2.2 – 2.5	2.5 – 3.2	3.0 – 4.0
H•••A range(Å)	1.2 – 1.5	1.5 – 2.2	2.0 – 3.0
Effect on crystal packing	Dominant	Distinctive	Variable
Utility in crystal engineering	Unknown	Useful	Partly useful

- **Very Strong :** These hydrogen bonds are formed by unusually activated donors and acceptors. They are often assisted by resonance. They are mostly formed by an acid and its conjugate base (D-H•••D^-) or a base and its conjugate acid (D-H•••D^+). It is easy to recognize very strong hydrogen bonds due to comparable distances of D-H and H••A.[47]

- **Strong** : They are usually electrostatic and the most well known examples are ice and DNA. If molecules have the ability to form strong hydrogen bonds they will, unless there are unwanted steric effects. The use of strong directional hydrogen bonding is a good tool in the structural design of specific compounds.[50] It has been used frequently and successfully as structure-directing forces in synthetic and natural supramolecular systems.[51] The most intensively studied interactions of strong hydrogen bonds are O-H•••O, N-H•••O and O-H•••N in organic and biological structures.[52] The formation of α–helices and β–sheets in proteins, base pairing in nucleic acids and many protein-nucleic acid interactions are due to the strong O-H•••O and N-H•••O hydrogen bonds.[51] These bonds are referred to as the "master key" of molecular recognition and crystal engineering. If ever full control of this interaction is gained it will lead to the mastery of supramolecular chemistry.[47] Figure 1.12 shows examples of supramolecular synthons displaying strong hydrogen bonds.

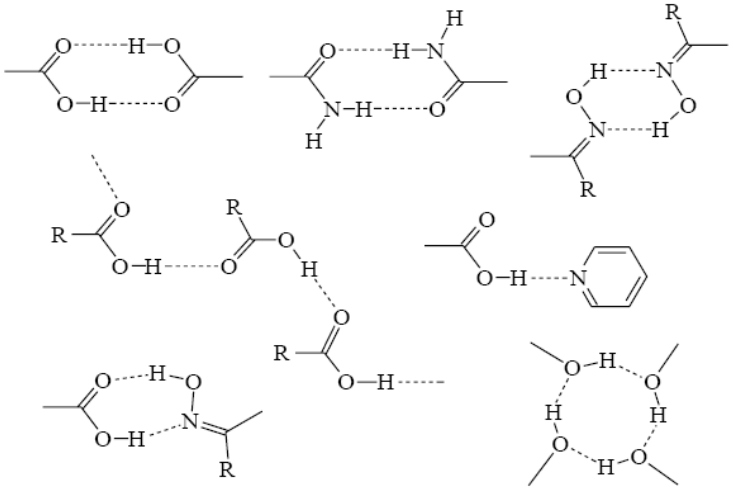

Figure 1.12: Examples of supramolecular synthons displaying strong hydrogen bonds.[53]

- **Weak** : These bonds are electrostatic, they possess components that depend on the nature of the acceptor and donor group. Bonds such as C-H•••O, C-H•••N and N-H••• π are significant in crystal packing.[52] The strongest of these bonds are O-H•••Ph and C≡C-H•••O, which lie in the energy range (8 - 16 kJ/mol). The bond that is formed by unactivated methyl groups are the weakest bonds with energies of approximately 2 kJ/mol.[47] The C-H•••π bonds lie in the energy range 2 - 8 kJ/mol and have displayed a significant role in a number of chemical and biological phenomena.[54] Figure 1.13 shows examples of supramolecular synthons displaying weak hydrogen bonds.

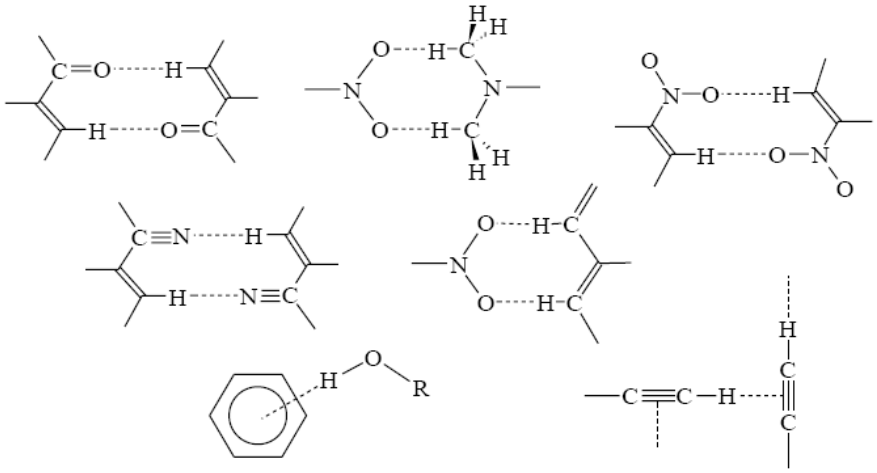

Figure 1.13: Examples of supramolecular synthons displaying weak hydrogen bonds.[53]

1.3.1.2 π- π Interaction

This type of interaction usually occurs between one aromatic ring that is electron-rich (donor) and another aromatic ring that is electron-deficient (acceptor).[55] For this reason they are often called donor-acceptor interactions. It is commonly found in both synthetic and natural systems.[56] The aromatic interaction controls the properties of many crystalline solids, because it dictates the molecular organization.[56] The polar nature of aromatics is known as a significant contributor to molecular recognition. This is mainly due to the large, permanent quadrupole moment of benzene.[57] Hexafluorobenzene has a quadrupole moment that is similar in magnitude but opposite in sign to that of benzene (Figure 1.14).[58,59]

Figure 1.14: Quadrupoles of aromatic π –donors (benzene) and π –acceptors (hexafluorobenzene).[60]

These are the two most common types of π-π interactions:

Off-set face-to-face π-π stacking: This type of π-π interaction is responsible for the slippery feel of graphite. Lubricant properties are achieved and can be very useful. It can be seen in Figure 1.15 that there is not a direct overlap, this is due to repulsive forces.[61]

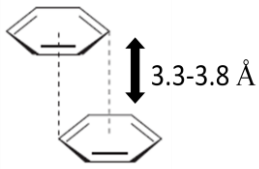

Figure 1.15: Off-set face-to-face π- π stacking.

Edge-to-face π-π interaction: An understanding of the edge-to-face interaction between the edge H atom of an axial aromatic ring and the centre of the facial aromatic ring is of significance (Figure 1.16), due to the conformational changes between T-shape and stacked conformers which could be used as precursors of nanomechanical devices.[62] The substituents on aromatic rings affect their ability to form π-π interactions due to their resonance and inductive effects which change the electronic distribution on these aromatic rings. This interaction is regarded as a weak form of the hydrogen bond.[4] It is frequently found in proteins, and between weakly acidic aromatic C-H bonds and π–moieties.[63] They should be referred to as hydrogen bonds and not π-stacking since there is no stacking of the π-electron surfaces. The edge-to-face geometry is the most stable arrangement for the benzene ring.[64] This type of interaction is responsible for the herringbone packing in the crystal structure (benzene). Due to the interaction between the slightly electron deficient hydrogen atoms of one aromatic ring and the electron rich π-cloud of another, they could be regarded as weak forms of hydrogen bonds.[58]

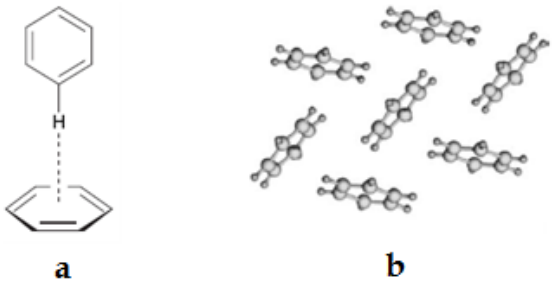

Figure 1.16: (a) Edge-to-face π -π interaction. (b) X-ray crystal structure of benzene showing herringbone pattern.

1.4 Polymorphism

Polymorphism is when a chemical substance in the crystalline state can adopt at least two different crystal packing arrangements.[65] The study of polymorphism is important because two polymorphs of any compound may possess very different properties, e.g. different solubilities or different melting point.[66] Altering crystallisation conditions such as temperature, humidity, solvent and the presence of seeds or additives can lead to different polymorphs.[30] Crystals can change form as a function of pressure, temperature, humidity or time. Changing crystallization methods such as cooling or evaporating a solution to form a new crystal, crystallization from the melt, vapour diffusion, thermal treatment, thermal desolvation of crystalline solvates, grinding, sublimation and precipitation from solution by pH adjustment can lead to the formation of polymorphs.[67] The relationship between "true" polymorphs, solvates, co-crystals, salts and the amorphous phase is shown in Figure 1.17.[68]

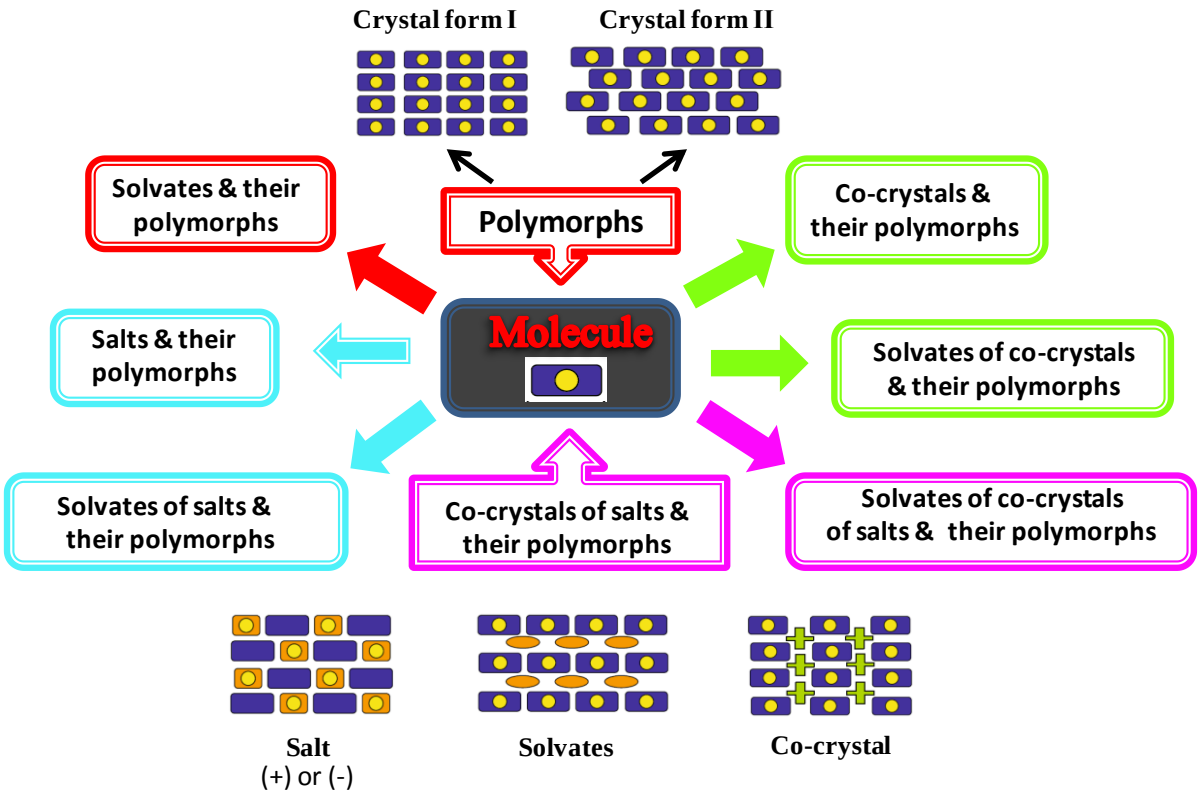

Figure 1.17: The relationship between "true" polymorphs, solvates, co-crystals, salts and the amorphous phase.

Polymorphs may display noticeable differences in their properties, such as thermodynamic, kinetic, surface, mechanical, spectroscopic and chemical properties (Figure 1.18).[68] These differences are of great signifance to the pharmaceutical industry and crystal engineering.[69] Reproducibly obtaining the correct polymorph of a given compound is important, since undesired polymorphs can cause problems during formulation.[70,71] In the paper by Nassimbeni *et al*.[72] They raise the question whether a new polymorph was formed when they proceeded to cool methylparaben to sub ambient temperatures. Threlfall *et al*.,[73] in their paper, responded by claiming that the result obtained by Nassimbeni *et al*. was simply due to anisotropic behaviour and not a new polymorph. They believe that "the changes, although large, fall within those expected for changes of the structure with temperature, without a phase change". Desiraju pointed out the importance of distinguishing whether a compound is a polymorph or a new compound.[74]

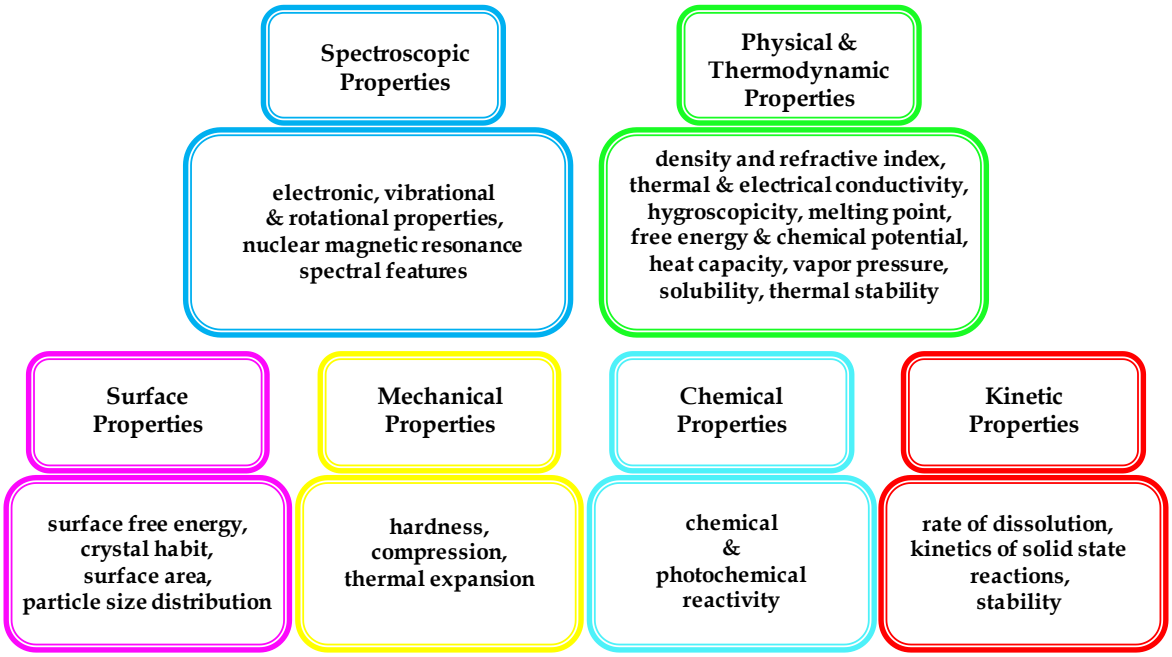

Figure 1.18: Properties that can differ among crystal forms of the same substance.

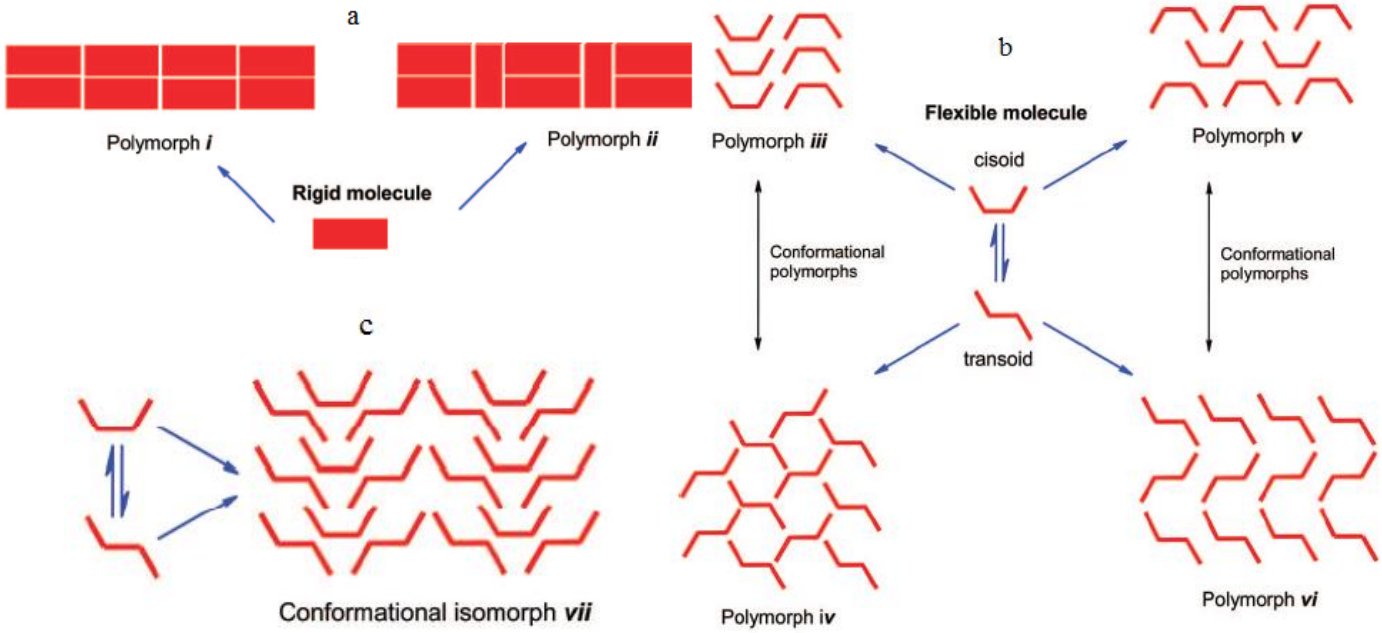

Figure 1.19: Schematic representation of (a) polymorph i and ii for a rigid molecule, (b) Various packing arrangements of a conformationally flexible molecule, (c) Two symmetry-independent molecules in conformational isomorph vii.[52]

The compound 5-methyl-2-[(2-nitrophenyl)amino]-3-thiophenecarbonitrile also known as ROY (red, yellow and orange coloured crystals) currently has seven known polymorphs (Figure 1.20).[75] This compound holds the record for the largest number of polymorphs of known structures in the Cambridge Structural Database.

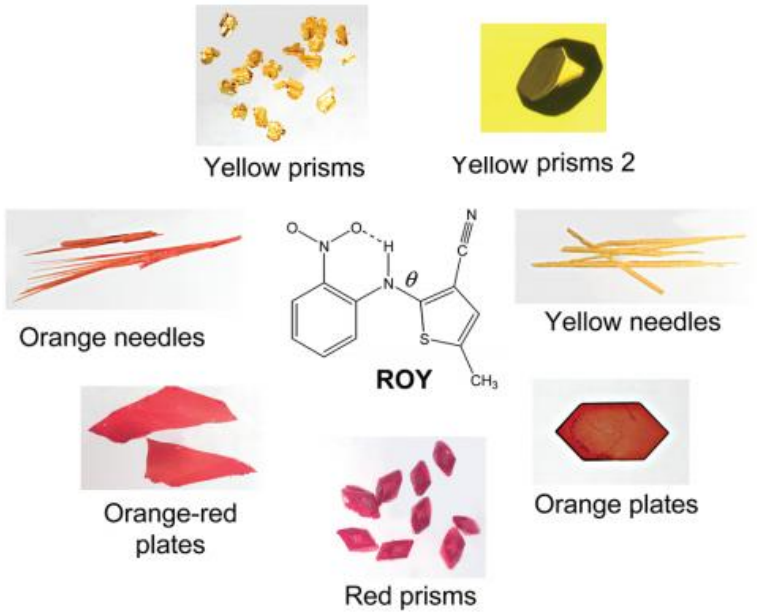

Figure 1.20: The compound ROY with its red, orange, and yellow crystals.[75]

In order to control the crystallization process one has to consider both the thermodynamic and kinetic factors.[76] Under controlled conditions of temperature and pressure only one polymorph is thermodynamically in its stable form (except at the transition point).[4] The thermodynamically stable polymorph has the lowest Gibbs free energy and all other polymorphs are metastable to different degrees.[67] Due to kinetic factors metastable forms can exist or co-exist in the presence of more stable forms.

1.5 Crystals

1.5.1 Crystal Engineering

"The understanding of intermolecular interactions in the context of crystal packing and the utilisation of such understanding in the design of new solids with desired physical and chemical properties"

Gautam R. Desiraju [77]

One area of supramolecular chemistry is molecular crystal engineering. The purpose of crystal engineering is to attain a specific design of a crystalline material with desired physicochemical properties.[78] The Cambridge Structural Database (CSD)[79] contains thousands of crystal structures, this is very useful to crystal engineering studies because information on molecular structural data and intermolecular interaction patterns can be obtained. One can therefore use what is known to establish rules that can be generally applied or considered when synthesising new crystalline compounds.

The existence and function of supermolecules are due to non-covalent interactions.[78] In nature and synthetic systems the hydrogen bond is the most important of supramolecular interactions. In molecular crystal engineering the hydrogen bond is the interaction of choice due to its strength and directionality. These properties make them useful in constructing predictable and replicable structures. Hydrogen bonds and co-ordination bonds are the strategies used in crystal engineering, which are based on the understanding and exploitation of intermolecular interactions.[80]

The concept of viewing a crystal structure as a network proves to be an advantage because we can simplify complex crystalline structural features into easily identifiable network topologies based on chemical and structural information of the constituent molecular building blocks.[81]

1.5.2 Crystal Structure Prediction

"One of the continuing scandals in the physical sciences is that it remains in general impossible to predict the structure of even the simplest crystalline solids from a knowledge of their chemical composition… Solids such as crystalline water (ice) are still thought to lie beyond mortals' ken"

John Maddox [82]

A well defined crystal structure result, allows us to compute non-covalent interactions strengths and directions which hold the structure together. This helps us to predict the behaviour of the solid under various thermodynamic conditions.[23]

The current problem with crystal structure prediction is that the programs employed generally use force-fields based on atom-atom potentials. These tend to yield too many possible solutions, where there will be several possible structures with lattice energies within a few kilojoules of each other. However, recent modifications, in which the low-energy structures are subjected to further refinement by quantum mechanical methods, are proving more successful.[83] The blind tests held by the Cambridge Crystallographic Data Centre (CCDC) shows an improvement in rates of success in predicting the crystal structures over previous blind tests.[83-84]

1.5.3 Disordered Crystal Structure

"A crystal structure in which ions or molecules pack in alternate ways in different unit cells is a disordered structure"

Ashwini Nangia [61]

A crystal structure is an ordered arrangement of ions, atoms or molecules packed together on a lattice to form a crystal.[85]

There are two types of disorders: **Static and Dynamic.**[61]

Static disorder:

In the unit cell, a molecule is located in different orientations or conformations in symmetry-related positions.

Dynamic disorder:

When molecules are fluxional at the same position in the crystal.

If the crystallization process is controlled or the recrystallization solvent is changed then this can improve the quality of a crystal, therefore minimizing or eliminating the disorder found in the crystal structure.[85]

References

1. Lehn, J.M. (1988) Supramolecular Chemistry—Scope and Perspectives Molecules, Supermolecules, and Molecular Devices. *Angewandte Chemie*, 27: 89-112.
2. Lehn, J.M. (2007) From supramolecular chemistry towards constitutional dynamic chemistry and adaptive chemistry. *Chemical Society Reviews*, 36: 151-160.
3. Lehn, J.M. (1995) *Supramolecular Chemistry-Concepts and Perspectives.* VCH, Weinheim.
4. Steed, J.W. & Atwood, J.L. (2009) *Supramolecular Chemistry, 2nd edition*. Singapore: John Wiley & Sons.
5. Lehn, J.M. (2002) Toward complex matter: Supramolecular chemistry and self-organization. *Proceedings of the National Academy of Sciences*, 99: 4763-4768.
6. Steed, J. W. & Atwood, J. L. (2000) *Supramolecular Chemistry*. Singapore: John Wiley & Sons.
7. Dodziuk, H. (2002) *Introduction to Supramolecular Chemistry*. Dordrecht: Kluwer Academic Publishers.
8. Ariga. K. & Kunitake. T. (2006) *Supramolecular Chemistry – Fundamentals and Applications*. Springer-Verlag Berlin Heidelberg.
9. Cragg, P.J. (2010) Supramolecular Chemistry: From Biological Inspiration to Biomedical Applications. Springer Dordrecht Heidelberg London New York.
10. Steed, J. W. (2004) Supramolecular Chemistry: Definition. *Encyclopedia of Supramolecular Chemistry,* 2: 1401-1411. New York, Taylor and Francis.
11. Nassimbeni, L. R. (2004) Inclusion Compounds: Selectivity, Thermal Stability and Kinetics. *Encyclopedia of Supramolecular Chemistry*, 1: 696-703. New York, Taylor and Francis.
12. Cram, D.J. & Cram J.M. (1978) Design of complexes between synthetic hosts and organic guests. *Accounts of Chemical Research*, 11: 8-14.
13. Gdaniec, M. (2004) Channel Inclusion Compounds. *Encyclopedia of Supramolecular Chemistry,* 1: 223-227. New York, Taylor and Francis.
14. Jacobs, A., le Roex, T., Nassimbeni, L.R. & Toda, F. (2006) Inclusion of volatile guests by a tetrapedal host: structure and kinetics. *Organic Biomolecular Chemistry,* 12: 2452–2457.
15. Banerjee, R., Bhatt, P.M. & Desiraju, G.R. (2006) Solvates of Sildenafil saccharinate. A host material. *Crystal Growth & Design*, 6: 1468–1478.
16. Fabbiani, F.P.A., Byrne, L.T., McKinnon, J.J. & Spackman, M.A. (2007) Solvent inclusion in the structural voids of form II carbamazepine: single-crystal X-ray diffraction, NMR spectroscopy and Hirshfeld surface analysis. *CrystEngComm*, 9: 728-731.
17. Sarma, B. & Nangia, A. (2007) Tetrakis(4-sulfophenyl)methane didecahydrate. Reversible and selective water inclusion and release in an organic host. *CrystEngComm*, 9: 628–631.
18. Organo, V.G., Rudkevich, D.M. (2007) Emerging host–guest chemistry of synthetic nanotubes. *Chemical Communications*, 3891–3899.
19. Cabeza, A.J.C., Day, G.M., Motherwell, W.D.S. & Jones, W. (2007) Solvent inclusion in form II of carbamazepine. *Chemical Communications*, 1600–1602.

20. Kumar, T.L., Guleria, P., Vishweshwar, P., Sivalakshmidevi, A. & Babu, J.M. (2010) Host-guest complexes of docetaxel, an anti-cancer drug. *Journal of Inclusion Phenomena and Macrocyclic Chemistry*, 66:261–269.
21. Jacobs, A., Nassimbeni, L. R., Silwana, N., Báthori, N.B. & Weber, E. (2011) Inclusion of 1,4-bis(diphenylhydroxymethyl)benzene with amides: structure and selectivity, *CrystEngComm*, 13: 7014-7018.
22. Thiele, C. Auerbach, D., Jung, G. & Wenz, G. (2011) Inclusion of chemotherapeutic agents in substituted β-cyclodextrin derivatives. *Journal of Inclusion Phenomena and Macrocyclic Chemistry*, 69:303–307.
23. Nassimbeni, L. R. (2003) Physicochemical Aspects of Host-Guest Compounds. *Accounts of Chemical Research*, 36: 631-637.
24. Sarma, J.A.R.P. & Desiraju, G.R. (2002) The Supramolecular Synthon Approach to Crystal Structure Prediction, *Crystal Growth & Design, 2: 93-100.*
25. Ramon, G., Coleman, A.W., Nassimbeni, L.R. & Taljaard, B. (2005) Inclusion of Aromatic Guests by a Xanthenol Host: Structure, Guest Exchange and Desorption Kinetics. *Crystal Growth & Design*, 5: 2331-2335.
26. Jacobs, A., Nassimbeni, L. R., Su, H. & Taljaard, B. (2005) Xanthenol clathrates: structure, thermal stability, guest exchange and kinetics of desolvation, *Organic Biomolecular Chemistry*, 3: 1319-1322.
27. Nassimbeni, L.R., Ramon, G. & Weber, E. (2007) Inclusion by a fluorenyl diol host with substituted pyridines: Structure, selectivity and kinetics of desorption. *Journal of Thermal Analysis and Calorimetry*, 90: 1-8.
28. Tsoucaris, G., Atwood, J.L. & Lipkouwski, J. (1996) *Crystallography of Supramolecular Compounds.* Netherlands: Kluwer Academic Publishers.
29. Dyadin, Y.A. & Terekhova, I.S. (2004) Classical Description of Inclusion Compounds. *Encyclopedia of Supramolecular Chemistry*, 1: 253-260. New York, Taylor and Francis.
30. Steed, J. W., Turner, D. R. & Wallace, K. J. (2007) Core Concepts in Supramolecular Chemistry and Nanochemistry. Singapore: John Wiley & Sons.
31. Schneider, H.J. & Yatsimirsky, A.K. (2008) Selectivity in supramolecular host–guest complexes. *Chemical Society Reviews*, 37:263–277.
32. Báthori, N.B. & Nassimbeni, L.R. (2011) Selectivity of amides by host–guest inclusion. *CrystEngComm*, 13: 3156–3161.
33. Grasselli, R.K. (2004) The Importance of Selectivity in Ammoxidation Catalysis .Harris, K.D.M. & Edwards, P.P. eds. *Turning Points in Solid-State, Material and Surface Science* , 34:577-586. RSC publishing.
34. Schmidtchen, F.P. (2004) Selectivity: Thermodynamic and Kinetic. *Encyclopedia of Supramolecular Chemistry*, 2: 1225-1230. New York, Taylor and Francis.
35. Jacobs, A., Nassimbeni, L.R., Nohako, K.L., Su, H. & Taljaard, J.H. (2008) Inclusion with Mixed Guests: Structure and Selectivity, *Crystal Growth & Design*, 8: 1301-1305.

36. Jacobs, A., Faleni, N., Nassimbeni, L. R. & Taljaard, J.H. (2007) Inclusion by a Xanthenol Host: Relating Structure to the Kinetics of Desolvation and Guest Exchange, *Crystal Growth & Design*, 7: 1003-1006.
37. Korobov, V. I. & Ochkov, V. F. (2011) Chapter 3 – Numerical Solution of the Direct Problem in Chemical Kinetics. *Chemical Kinetics with Mathcad and Maple*. New York: Springer.
38. Báthori, N.B. & Nassimbeni, L.R. (2012) Physico-Chemical Aspects of Inclusion Compounds. Gale, P.A & Steed, J.W. eds. *Supramolecular Chemistry: From Molecules to Nanomaterial*, 3011-3016. John Wiley and Sons.
39. Flynn, J. H. & Wall, L. A. (1966). A Quick, Direct Method for the Determination of Activation Energy from Thermogravimetric Data. *Journal of Polymer Science, Polymer Letters***,** 4: 323-328.
40. Ozawa, T. (1965) A New Method of Analyzing Thermo Gravimetric Data. *Bulletin of the Chemical Society of Japan*, 38(11): 1881-1886.
41. Murthy, P. S. (2006) Molecular Handshake: Recognition through Weak Noncovalent Interactions. *Journal of Chemical Education*, 83: 1010-1013.
42. Dougherty, D.A. (2008). Physical Organic Chemistry on the Brain. *The Journal of Organic Chemistry*, 73: 3667–3673.
43. Arunan, E., Desiraju, G. R., Klein, R. A., Sadlej, J., Scheiner, Alkorta, I., Clary, D.C., Crabtree, R.H., Dannenberg, J.J., Hobza, P., Kjaergaard, H.G., Legon, A.C., Mennucci, B. & Nesbitt, D.J. (2011) Definition of the hydrogen bond(IUPAC Recommendations 2011)*. *Pure* and *Applied Chemistry*, 83: 1637-1641.
44. Desiraju, G.R. (2011) Reflections on the Hydrogen Bond in Crystal Engineering. *Crystal Growth and Design*, 11: 896-898.
45. Long, S. & Li, T. (2009) Controlled Formation of the Acid-Pyridine Heterosynthon over the Acid-Acid Homosynthon in 2-Anilinonicotinic Acids. *Crystal Growth & Design*, 9: 4993-4997.
46. Desiraju, G.R. (2002) Hydrogen Bridges in Crystal Engineering: Interactions without borders. *Accounts of Chemical Research*, 35: 565-573.
47. Desiraju, G. R. (2004) Hydrogen Bonding. *Encyclopedia of Supramolecular Chemistry*, 1: 658-664. New York, Taylor and Francis.
48. Zhu, S., Xing, C., Xu, W., Jin, G. & Li, Z. (2004) Halogen Bonding and Hydrogen Bonding Coexist in Driving Self-Assembly Process. *Crystal Growth & Design*, 4: 53-56.
49. Clyburne, J.A.C., Hamilton, T. & Jenkins, H.A. (2001) The molecular quadrupole moment: solid state architectures containing organic and organometallic molecules. *Crystal Engineering*, 4: 1-9.
50. Boldog, I., Daran, J. C., Chernega, A. N., Rusanov, E. B., Krautscheid, H. & Domasevitch, K. V. (2009) Hydrogen Bonding Patterns and Supramolecular Structure of 4,4′-Bipyrazolium Salts. *Crystal Growth & Design*, 9: 2895-2905.
51. Aakeröy, C.B. (2004) Strong Hydrogen Bonds. *Encyclopedia of Supramolecular Chemistry*, 2: 1379-1386. New York, Taylor and Francis.
52. Nangia, A. (2008) Conformational Polymorphism in Organic Crystals. *Accounts of Chemical Research*, 41: 595-604.

53. Desiraju, R. (2003) *Crystal Design: Structure and Functions- Perspectives in Supramolecular Chemistry*. Singapore: John Wiley & Sons.
54. Nishio, M. (2004) Weak Hydrogen Bonds. *Encyclopedia of Supramolecular Chemistry,* 2: 1576-1585. New York, Taylor and Francis.
55. Schneider, H. J. (2004) Van der Waals Forces. *Encyclopedia of Supramolecular Chemistry*, 2: 1550-1555. New York, Taylor and Francis.
56. Cockroft, S.L., Hunter, C.A., Lawson, K.R., Perkins, J. & Urch, C.J. (2005) Electrostatic Control of Aromatic Stacking Interactions. *Journal of the American Chemical Society*, 127: 8594-8595.
57. Ngola, S.M. & Dougherty, D.A. (1998) Concerning the Effects of Aromatic Ring Fluorination on the Cation- π Interaction and Other Molecular Recognition Phenomena in Aqueous Media. *The Journal of Organic Chemistry*, 63: 4566-4567.
58. Gallivan, J.P. & Dougherty, D.A. (1998) Can Lone Pairs Bind to a π System? The Water···Hexafluorobenzene Interaction. *Organic Lett*ers, 1: 103-105.
59. Dance, B. (2004) π- π interactions: Theory and Scope. *Encyclopedia of Supramolecular Chemistry*, 2: 1076-1092. New York, Taylor and Francis.
60. Keiluweit, M. & Kleber, M. (2009) Molecular-Level Interactions in Soils and Sediments: The Role of Aromatic π-Systems. *Environmental Science & Technology*, 43: 3421–3429.
61. Nangia, A. (2004) Nomenclature in Crystal Engineering . *Encyclopedia of Supramolecular Chemistry*, 2: 967-972. New York, Taylor and Francis.
62. Lee, E.C., Hong, B.H., Lee, J.Y., Kim, J.C., Kim, D., Kim, Y., Tarakeshwar, P. & Kim, K.S. (2005) Substituent Effects on the Edge-to-Face Aromatic Interactions. *Journal of the American Chemical Society*, 127: 4530-4537.
63. Lanzarotti, E,. Biekofsky, R.R., Estrin, D.A., Marti, M.A. & Turjanski, A.G. (2011) Aromatic-Aromatic Interactions in Proteins: Beyond the Dimer. *Journal of Chemical Information and Modeling*, 51: 1623–1633.
64. James, S.L. (2004) π- π Stacking as a Crystal Engineering Tool. *Encyclopedia of Supramolecular Chemistry*, 2: 1093-1099. New York, Taylor and Francis.
65. Bernstein, J. (2002) *Polymorphism in Molecular Crystals.* USA: Oxford University Press.
66. Grepioni, F. (2008) Themed issue: Polymorphism and crystal forms. *New Journal of Chemistry,* 32:1657-1658.
67. Caira, M. R. (2004) Polymorphism. *Encyclopedia of Supramolecular Chemistry*, 2: 1129-1138. New York, Taylor and Francis.
68. Braga, D., Grepioni, F., Maini, L. & Polito, M. (2009) Crystal Polymorphism and Multiple Crystal Forms. Hosseini, M.W. & Mingos, D.M.P. eds. *Molecular Networks*. New York, Springer.
69. Hilfiker, R. (2007) Polymorphism in the Pharmaceutical Industry. *Organic Process Research & Development*, 11:649-650.
70. Kumar, V.S., Sheela, K.C., Nair, V. & Rath, N.P. (2004) Concomitant Polymorphism in a Spirobicyclic Dione. *Crystal Growth & Design,* 4:1245-1247.

71. Bis, J.A., Vishweshwar, P., Middleton, R.A. & Zaworotko, M.J. (2006) Concomitant and Conformational Polymorphism, Conformational Isomorphism, and Phase Relationships in 4-Cyanopyridine·4,4'-biphenol Cocrystals. *Crystal Growth & Design*, 6: 1048:1053.
72. Vujovic, D. & Nassimbeni, L.R. (2006) Methyl Paraben: A New Polymorph? *Crystal Growth & Design*, 6: 1591-1597.
73. Threlfall, T.L. & Gellbrich, T (2007) The Crystal Structure of Methyl Paraben at 118 K Does Not Represent a New Polymorph, *Crystal Growth & Design*, 7:22977.
74. Desiraju, G.R. (2008) Polymorphism: The Same and Not Quite the Same. *Crystal Growth & Design*, 8: 3-5.
75. Yu, L. (2010) Polymorphism in Molecular Solids: An Extraordinary System of Red, Orange, and Yellow Crystals. *Accounts of Chemical Research*, 43:1257-1266.
76. Bernstein, J. (2011) Polymorphism - A Perspective. *Crystal Growth & Design*, 11:632-650.
77. Desiraju, G.M. (1989) *Crystal Engineering, the Design of Organic Solids*. Elsevier: Amsterdam.
78. Braga, D. & Grepioni, F. (2004) Crystal Engineering with Hydrogen Bonds. *Encyclopedia of Supramolecular Chemistry*, 1: 357-362. New York, Taylor and Francis.
79. Cambridge Structural Database (CSD), Version 5.32, November 2010.
80. Burrows, A. D. (2004) Concepts in Crystal Engineering. *Encyclopedia of Supramolecular Chemistry*, 1: 319-324. New York, Taylor and Francis.
81. Sharma, C.V. (2002) Crystal Engineering-Where Do We Go from Here? *Crystal Growth & Design*, 2: 465-474.
82. Maddox, J. (1988) Crystals from first principles. *Nature*, 335, 201. Nature Publishing Group.
83. Kazantsev, A.V., Karamertzanis, P.G., Adjiman, C.S., Pantelides, C.C., Price, S.L., Galek, P.T.A., Day, G.M. & Cruz-Cabeza, A.J. (2011) Successful prediction of a model pharmaceutical in the fifth blind test of crystal structure prediction. *International Journal of Pharmaceutics*, 418: 168-178.
84. Day, G.M., Cooper, T.G., Cruz-Cabeza, A.J., Hejczyk, K.E., Ammon, H.L., Boerrigter, S.X.M., Tan, J.S, Della Valle, R.G., Venuti, E., Jose, J., Gadre, S.R., Desiraju, G.R., Thakur,T.S., van Eijck, B.P., Facelli,J.C., Bazterra,V.E., Ferraro, M.B., Hofmann, D.W.M., Neumann, M.A., Leusen,F.J.J., Kendrick, J., Price,S.L., Misquitta, A.J., Karamertzanis, P.G., Welch,G.W.A., Scheraga, H.A., Arnautova, Y.A., Schmidt, M.U., van de Streek, J., Wolf, A.K. & Schweizer, B. (2009) Significant progress in predicting the crystal structures of small organic molecules - a report on the fourth blind test. *Structural Science*, 65: 107-125.
85. Rissanen, K. (2004) X-Ray Crystallography. *Encyclopedia of Supramolecular Chemistry*, 2: 1586-1591. New York, Taylor and Francis.

CHAPTER 2
TECHNIQUES

2.1 Hot Stage Microscopy

Hot stage microscopy (HSM) is a comprehensive characterization of the physical properties due to its high resolution micrography and image capture.[1] HSM was used to visually monitor changes in the sample during heating and correlate the results obtained from thermal events. Thermal events include melting, recrystallisation, polymorphic transformation, guest desorption and host decomposition.[2] The instrumental setup of the HSM is slightly different to the thermogravimetry (TG) and differential scanning calorimetry (DSC) technique, therefore instrumental differences have to be considered. The samples used are single crystals whereas on the TG and DSC the samples are in powder form. These factors may cause the HSM results to not correlate perfectly with the observed thermal events obtained by TG and DSC.

2.2 Thermal Analysis (TA)

Thermal analysis is a group of techniques in which some change in a physical property of a sample is measured under a controlled temperature programme in a specified atmosphere usually nitrogen gas.[3]

2.2.1 Thermogravimetry (TG)

Thermogravimetry is a thermal analysis method whereby the mass of a sample is continuously measured as a function of temperature or time under a controlled temperature programme in a controlled atmosphere.[4-6] This results in a graph of sample mass loss against temperature and is known as a thermogravimetric curve. A purge gas of nitrogen, argon or helium flows through the balance and creates an atmosphere that is inert.[7] TG is used to achieve accurate host:guest ratios. This is extremely useful because inclusion compounds are not always stoichiometric. The results of the TG experiments can be used to assign site occupancy factors during crystal refinement. The Perkin-Elmer Pyris 6 is a top-loading balance (Figure 2.1) with a temperature range of ambient to 1000°C and heating rates of 0.1-100°C/min.[8]

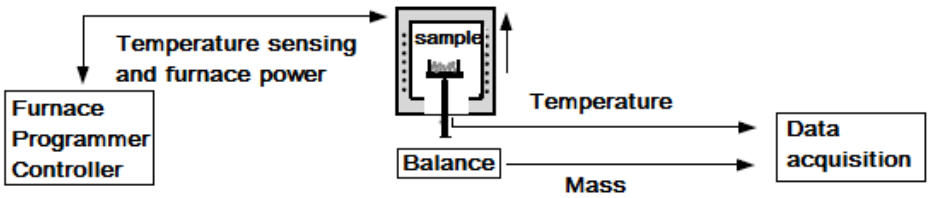

Figure 2.1: Schematic diagram of the general arrangement of components in a top-loading balance. [8]

2.2.2 Differential Scanning Calorimetry (DSC)

Differential scanning calorimetry (**DSC)** is used to monitor energy changes in a sample.[9] DSC is a technique in which the difference in power or heat flow rate to the sample and to the reference is recorded against time while both are subjected to a temperature programme. The sample may undergo endothermic or exothermic processes which would result in a curve recorded against temperature. The area under the curve is directly proportional to the energy change.[9] DSC enthalpy changes can be used to obtain melting points, compound purity, kinetic information, guest loss and phase change onset temperatures. In DSC the endothermic peaks are plotted upwards ($\Delta H>0$) and the exothermic peaks are plotted downwards ($\Delta H<0$).

Power compensation DSC is a measure of the difference in power supplied to the sample and to the reference in order to keep their temperatures the same.[10] The sample and reference have their own heating elements and thermocouples (Figure 2.2). When a change in sample occurs which results in an endothermic process, extra heat will be needed to keep the sample at the same temperature as the reference.[11-12] When a change in sample results in an exothermic process, less heat will be needed to keep the sample at the same temperature as the reference. Either more or less power is supplied to the sample in order to maintain the same temperature as the reference and is plotted as a function of temperature or time.[10,12] The flow of energy is measured in mW or J/s.

The fundamental equation of DSC is [11]

$$\text{DSC signal (W/g)} = \text{Heat capacity [J/(Kg)]} \times \text{Scanning Rate (K/s)}$$

$$dH/dt = dH/dT \times dT/dt$$

"Therefore the raw heat flow signal can be viewed as a form of heat capacity. In practice, it reflects the changes occurring in heat capacity, and the absolute value is obtained when the method used takes into account the contribution of the empty pans and reference together with the scan rate".[11]

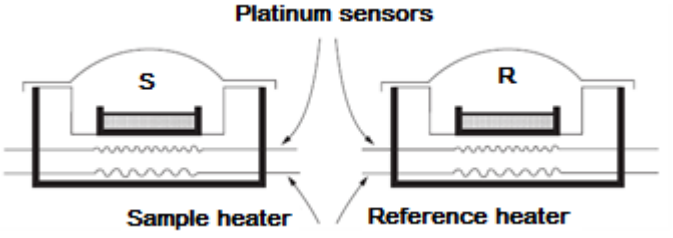

Figure 2.2: Diagram of power compensation DSC.[10]

2.3 Single Crystal X-Ray Crystallography

X-ray studies have four major steps which consist of crystallization, data collection, structure solution and refinement.[13] X-ray crystallography is a technique used to determine the internal crystal structure of a crystalline material.[14] X-ray crystallography has been used to discover structures such as DNA and diamond which can be found in the Cambridge Structural Database (CSD). A crystalline substance has an arrangement of atoms which is periodic in three dimensions.[15] X-ray crystallography exploits the fact that X-rays are diffracted by crystals, therefore making it possible to obtain accurate molecular structures. The crystal should have satisfactory periodicity of the crystal lattice in order to attain sufficient diffraction power.[16] Atoms in the crystal lattice that are heavier and well ordered will produce the best diffraction power.[14] Majority of supramolecular systems consists mainly of hydrogen, carbon, nitrogen and oxygen which are the light elements.[16]

To analyze a sample using X-ray crystallography, a beam of X-rays of uniform wavelength strikes the crystal.[17] A beam of electrons is accelerated by high voltage, usually 50 kV which strikes the metal anode (molybdenum or copper) in the X-ray tube (Figure 2.3).[17] When the target metal is molybdenum (Mo) or copper (Cu), wavelengths of approximately 0.71 Å and 1.54 Å respectively are used. A critical excitation voltage of 20 kV (Mo) or 9 kV (Cu) is required, to enable sufficient bombarding to kick out an inner electron.[18] The range 40-50 kV is typically used to achieve better efficiency.[19]

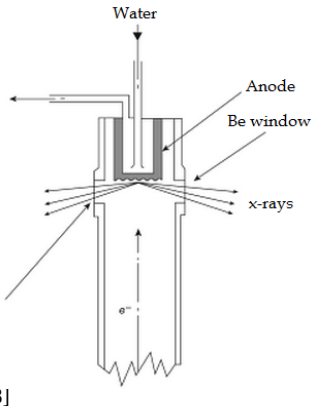

Figure 2.3: Schematic diagram of X-ray tube.[17]

The X-rays are diffracted when striking atoms in the crystal. The X-rays are being absorbed and re-emitted in the form of spherical waves.[20] These waves produced by each atom travel outwards and interact with each other. The pattern known as a diffraction pattern is the resulting pattern of constructive and destructive interferences.[21] From the diffraction pattern the electron density map can be constructed.[21] A compound is then built into the experimental electron density, refined against the data which result in accurate molecular structure (Figure 2.4).

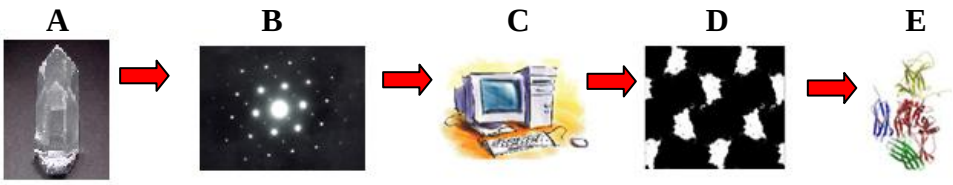

Figure 2.4: A: Crystal; B: Diffraction pattern; C: Computer (Fourier transformation); D: Electron density; E: Molecular structure.

References

1. Vitez, I.M., Newman, A.W., Davidovich, M. & Kiesnowski, C. (1998) The evolution of hot-stage microscopy to aid solid-state characterizations of pharmaceutical solids. *Thermochimica Acta*, 324: 187-196.
2. Munson, E.J. (2009) Analytical Technique in Solid State Characterization. Qiu, Y., Chen, Y., Liu, L. & Geoff, G.Z. eds. *Developing Solid Oral Dosage Forms: Pharmaceutical Theory and Practice*. New York: Elsevier.
3. Warne, S.St.J. (2002) Introduction to Thermal Analysis. *Thermal Analysis-Techniques & Applications*, 1-16. Hartnolls Ltd, Bodmin.
4. Wunderlich, B. (1990) *Thermal Analysis*. Academic Press, INC.
5. Speyer, R.F. (1994) Chapter 5 – Thermogravimetric Analysis. *Thermal Analysis of Materials*, 111-133. New York: Marcel Dekker.
6. Danch, A.L. (2011) Chapter 5 - Basic Role of Thermal Analysis in Polymer Physics. Šesták, J., Mareš, J.J. & Hubík, P. eds. *Glassy, Amorphous and Nano Crystalline Materials - Thermal Physics, Analysis, Structure and Properties, 77-91*. New York: Springer.
7. Bottom, R. (2008) Chapter 3 - Thermogravimetric Analysis. Paul Gabbott, P. ed. *Principles and Applications of Thermal Analysis, 88-118*. Singapore: Blackwell Publishing Ltd.
8. Prime, R.B., Bair, H.E., Vyazovkin, S., Gallagher, P.K. & Riga, A. Chapter 3 - Thermogravimetric Analysis (TGA). Menczel, J.D. & Prime, R.B. eds. *Thermal Analysis of Polymers - Fundamentals and Applications*, 241-318. New Jersey: John Wiley & Sons.
9. Griffin, V.J. (2002). Differential Thermal Analysis and Differential Scanning Calorimetry. *Thermal Analysis-Techniques & Applications*, 17-46. Hartnolls Ltd, Bodmin.
10. Menczel, J.D., Judovits, L., Prime, R.B., Bair, H.E., Reading, M. & Swier, S. (2009) Chapter 2 – Differential Scanning Calorimetry (DSC). Menczel, J.D. & Prime, R.B. eds. *Thermal Analysis of Polymers - Fundamentals and Applications*, 7-240. New Jersey: John Wiley & Sons.
11. Gabbott, P. (2008) Chapter 1- A Practical Introduction to Differential Scanning Calorimetry. Paul Gabbott, P. ed. *Principles and Applications of Thermal Analysis*, 2- 49. Singapore: Blackwell Publishing Ltd.
12. Speyer, R.F. (1994) Chapter 3 – Differential Thermal Analysis. *Thermal Analysis of Materials*, 35-90. New York: Marcel Dekker.
13. Deschamps, J.R. (2010) X-ray crystallography of chemical compounds. *Life Science*, 8:585-589. Elsevier.
14. Rissanen, K. (2004) X-Ray Crystallography. *Encyclopedia of Supramolecular Chemistry*, 2: 1586-1591. New York, Taylor and Francis.
15. Clegg, W. E. (2001) *Crystal Structure: Principles and Practice*. New York: Oxford University Press.
16. Rissanen, K. (2012) Crystallography and Crystal Engineering. Schalley, C.A. ed. *Analytical Methods in Supramolecular Chemistry*, 1:459-498. Germany: Wiley-VCH.
17. Rajput, R.K. (2003) *A Textbook of Electrical Engineering Materials*. New Delhi: Laxmi Publications.
18. Rhodes, G. (2006) *Crystallography Made Crystal Clear: A Guide for Users of Macromolecular Models, 3rd edition*. Canada: Elsevier.

19. Schwalbe, C.H. (2012) Crystallography. Gad, S.C. ed. *Development of Therapeutic Agents Handbook.* 445-462. New Jersey: John Wiley and Sons.

20. Tong, X.C. (2006) *Advanced Materials for Thermal Management of Electronic Packaging*. New York: Springer.

21. Bragg, W. L. (1949) *The Crystalline State: A General Survey.* London: G. Bell and Sons Ltd.

CHAPTER 3
EXPERIMENTAL AND COMPUTATION

3.1 Compounds used in the study

The host compounds were synthesized by Dr. J.H. Taljaard.[1] Tables 3.1 and 3.2 lists the host compounds and solvents used in the study.

A1

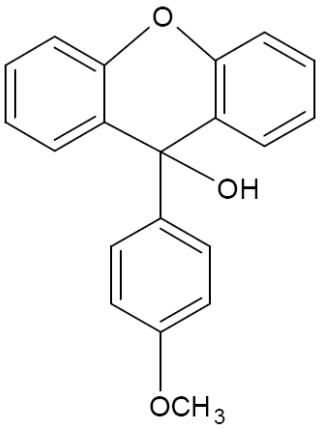

A2

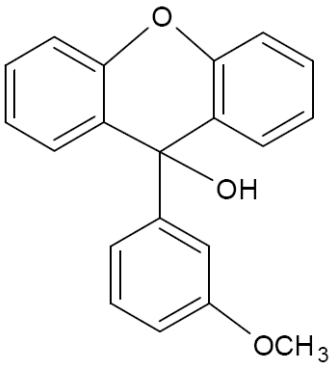

A26

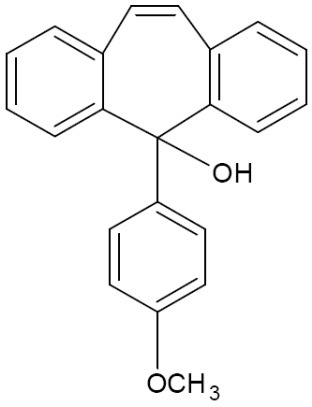

A28

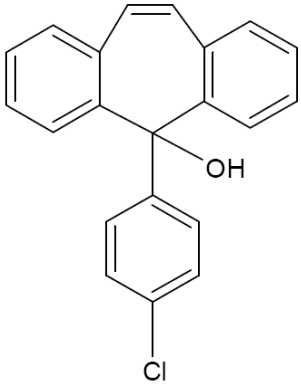

A31

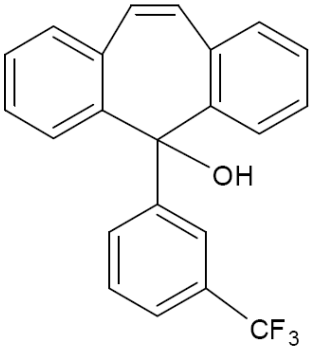

A32

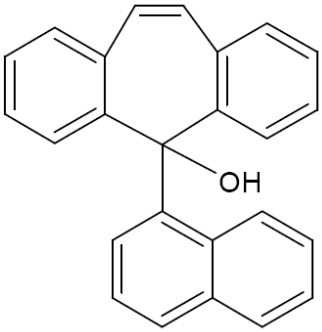

Table 3.1: Host compounds used in the study.

Host	Code	Molecular Formula
9-(4-methoxyphenyl)-9*H*-xanthen-9-ol	**A1**	**$C_{20}H_{16}O_3$**
9-(3-methoxyphenyl)-9*H*-xanthen-9-ol	**A2**	**$C_{20}H_{16}O_3$**
5-(4-methoxyphenyl)-5*H*-dibenzo[a,d]cyclohepten-5-ol	**A26**	**$C_{22}H_{18}O_2$**
5-(4-chlorophenyl)-5*H*-dibenzo[a,d]cyclohepten-5-ol	**A28**	**$C_{21}H_{15}OCl$**
5-[3-(trifluoromethyl)phenyl]-5*H*-dibenzo[a,d]cyclohepten-5-ol	**A31**	**$C_{22}H_{15}OF_3$**
5-(naphthalen-1-yl)-5*H*-dibenzo[a,d]cyclohepten-5-ol	**A32**	**$C_{25}H_{18}O$**

Table 3.2: Solvents used in the study.

Solvents	Code	Molecular Formula
Aniline	**ANI**	**C_6H_7N**
1,4-Dioxane	**DIOX**	**$C_4H_8O_2$**
Morpholine	**MORPH**	**C_4H_9NO**
***N*,*N*-dimethylacetamide**	**DMA**	**C_4H_9NO**
***N*-methylacetamide**	**NMA**	**C_3H_7NO**
***N*-methylformamide**	**NMF**	**C_2H_5NO**
3-Picoline	**3PIC**	**C_6H_7N**
Pyridine	**PYR**	**C_5H_5N**

3.2 Crystal Growth

The host compound was dissolved in excess solvent. The solution was evaporated slowly at ambient temperature until crystals were formed.

Host	Solvent	Compounds
A1	**MORPH**	**A1·MORPH**
A1	**PYR/ANI (a)**	**A1·ANI**
A1	**3PIC**	**A1·3PIC**
A1	**NMA/DMA (a)**	**A1·NMA**
A1	**NMA/DIOX (a)**	**A1·2NMA**
A1	**NMA/ANI (a)**	**2A1·2NMA**
A1	**NMF/DMA (a)**	**A1·NMF·H_2O**
A2	**3PIC**	**APOHOST**
A2	**MORPH**	**A2·MORPH**
A2	**NMA**	**A2·NMA**
A2	**NMF**	**A2·NMF**
A26	**ANI**	**A26·ANI**
A26	**PYR/MORPH (a)**	**A26·MORPH**
A28	**PYR/MORPH (a)**	**A28·MORPH**
A31	**PYR/MORPH (a)**	**A31·MORPH**
A32	**PYR/MORPH (a)**	**A32·MORPH**

(a) Equimolar mixture

3.3 Thermal Analysis

Instrument Parameters (**TG** and **DSC**)

Type : Perkin-Elmer Pyris 6 system

Temperature Programme : 303 – 573K @ 10 K/min

Purge gas : Nitrogen gas @ 20 ml/min

3.3.1 Thermogravimetry (TG): The crystals were removed from the mother liquor and placed on the filter paper where they were blotted, crushed into powder form and placed in open ceramic pans for TG analysis.

3.3.2 Differential Scanning Calorimtery (DSC): The crystals were removed from the mother liquor and placed on the filter paper where they were blotted, crushed (powder form), weighed (3-5 mg) and placed into vented pans for DSC analysis. The DSC was calibrated using indium (T_{on} = 429.8 K).

3.4 Hot Stage Microscopy

Large crystals were selected for HSM, placed on a microscope slide and a drop of silicone oil added to it. The experiments were performed using a Linkam 395/PE hot stage and observed using a Meiji EMZ/8TR microscope which had a Canon camera attached to it. All samples were subjected to a heating rate of 10 K/min. The photographs were captured using the Canon camera.

3.5 Crystal Data Collection

Instrument Parameters

Diffractometer	: Nonius Kappa CCD [2] or Bruker DUO APEX II [3]
Radiation	: Graphite-monochromated Mo-Kα
Data collection temp.(K)	: 298 or 173
Generator	: Nonius FR590
Generator wavelength	: 0.7107 Å
Generator operating parameters	: 53 kV and 23 mA

For all structures, the intensity data were collected by the standard ϕ and ω scans. The data was scaled and reduced using the program *Denzo-SMN*[4] or *SAINT-Plus.*[5] *X-seed*[6] is a graphical interface which is used to run *SHELX,*[7] *POV-RAY,*[8] *LAYER*[9] and *SECTION.*[10] The structures were solved using *SHELXS-97*[11] and refined by full-matrix least squares with *SHELXL-97,*[11] refining F^2. The program *SECTION* was used to obtain cross sections through the unit cell.

The program *PLATON*[12] gives a large variety of standard geometrical calculations, either fully automatic or as specified in detail, such as intramolecular geometry, intermolecular contacts, coordination geometry and MolFit.

3.6 Kinetics of Desolvation

Non-isothermal kinetics of desolvation were studied using the TG technique.[13-14] The crystals were crushed into powder form and blotted dry and placed in open ceramic pans for TG analysis. A series of TG runs were performed at different scan rates over a selected temperature range. A plot of log β vs. 1/T yields a straight line with slope - (0.457Ea)/R.

3.7 Guest Exchange

Crystals of **A26·PYR** were exposed to morpholine vapours in a sealed container at 298 K and the reaction monitored using DSC. The samples were crushed into powder form, blotted dry and placed in crimped but vented pans for DSC analysis.

References

1. Sasol Technologies R&D, Klasie Havenga Road 1, Sasolburg 1947, South Africa.
2. *COLLECT* (1998) Data Collection Software. Nonius, Delft.
3. *APEX 2* (2005) Bruker AXS Inc., Madison, Wisconsin, USA.
4. Otwinowski, Z. & Minor, W. (1997) Methods in Enzymology: Macromolecular Crystallography: Part A. Carter. C. W. & Sweet. R. M., eds, 276: 307-326. New York: Academic Press.
5. *SAINT-Plus* (2004) Bruker AXS Inc., Madison, Wisconsin, USA.
6. Barbour, L. J. (2003) *X-Seed*, Graphical interface for *SHELX* program. *Journal of Supramolecular Chemistry*, 1: 189.
7. Sheldrick, G.M. (2008) Foundations of Crystallography. *Acta Crystallographica Section*, D64:112-122.
8. *POV-RAY* for Windows. (2004) Persistence of Vision Pty. Ltd., Williamstown, Victoria, Australia.
9. Barbour, L. J. (1999) *LAYER*- a computer program for the graphical display of intensity data as simulated precession photographs. *Journal of Applied Crystallography*, 32: 351-352.
10. Barbour, L. J. (1999) *SECTION*- a computer program for the graphic display of cross sections through a unit cell. *Journal of Applied Crystallography*, 32: 353-354.
11. Sheldrick, G. M. (1997) *SHELXS-97* and *SHELXL-97*, Programs for Crystal Structure Determination and Refinement, University of Göttingen: Göttingen, Germany.
12. Spek, A.L. (2009) Structure validation in chemical crystallography. *Acta Crystallographica Section*, D65:148-155.
13. Flynn, J. H. & Wall, L. A. (1966). A Quick, Direct Method for the Determination of Activation Energy from Thermogravimetric Data. *Journal of Polymer Science, Polymer Letters***,** B4(5): 323-328.
14. Ozawa, T. (1965) A New Method of Analyzing Thermo Gravimetric Data. *Bulletin of the Chemical Society of Japan*. 38(11): 1881-1886.

CHAPTER 4
OBJECTIVES AND BACKGROUND

4.1 Objectives

1. Form inclusion compounds using the following hosts:
    - 9-(4-methoxyphenyl)-9*H*-xanthen-9-ol (A1)
    - 9-(3-methoxyphenyl)-9*H*-xanthen-9-ol (A2)
    - 5-(4-methoxyphenyl)-5*H*-dibenzo[a,d]cyclohepten-5-ol (A26)
    - 5-(4-chlorophenyl)-5*H*-dibenzo[a,d]cyclohepten-5-ol (A28)
    - 5-[3-(trifluoromethyl)phenyl]-5*H*-dibenzo[a,d]cyclohepten-5-ol (A31)
    - 5-(naphthalen-1-yl)-5*H*-dibenzo[a,d]cyclohepten-5-ol (A32)

Characterise resultant inclusion compounds using:

- Thermogravimetry (TG)
- Differential scanning calorimetry (DSC)
- Single crystal X-ray diffraction

2. Competition experiments will be performed to establish selectivity profiles of these hosts with pairs of guests.
3. Kinetics of decomposition of selected inclusion compounds will be performed.

4.2 Background to Study

The inclusion ability of a series of hydroxyl hosts with a general formula shown in Scheme 1, will be investigated in this study.

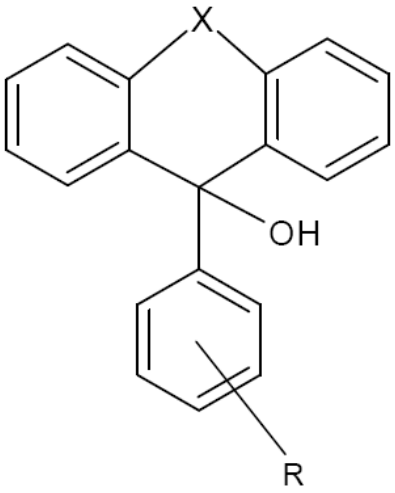

X = O, CH=CH

R (*o*- , *m*- , *p*-) = -OCH_3, -Cl , -CF_3, -C_6H_5

Scheme 1: a molecular diagram for a series of hydroxyl host compounds.[1]

The ability of a host compound to include a guest is largely dependent on its molecular structure. These host compounds conform to Weber's rules for host design because they are bulky, rigid, and have hydroxyl moieties that can act as hydrogen-bonding donors. In some cases the hosts possess electronegative moieties at X, which act as hydrogen bond acceptors. A number of xanthenol (X=oxygen) hosts have been studied and found to form inclusion compounds with a variety of guests.

4.2.1 Host A1

The host compound 9-(4-methoxyphenyl)-9*H*-xanthen-9-ol features in five international journals, which includes CrystEngComm,[2] Cryst.Growth Des.,[3] Org.Biomol.Chem.[4] and New J.Chem.,[5] according to the data obtained from the Cambridge Structural Database.[6] Host A1 formed inclusion compounds with 17 different guests (aniline,[2] cyclohexane,[3] 1,4-dioxane,[3] *N*,*N*-dimethylformamide,[3] *p*-xylene,[4] benzene,[4] *o*-xylene,[4] *m*-xylene,[4] acridine,[5] 8-hydroxyquinoline,[5] 1-naphthylamine,[5] triethylenediamine,[5] naphthalene,[7] anthracene,[7] phenanthrene,[7] pyrene[7] and β-naphthol[7]).

4.2.2 Host A2

The host molecule 9-(3-methoxyphenyl)-9*H*-xanthen-9-ol has not been extensively studied. The two isomeric xanthenol host compounds (A1 and A2) have been found to form inclusion compounds with aniline.[2]

4.2.3 Host A26

The host molecule 5-(4-methoxyphenyl)-5*H*-dibenzo[a,d]cyclohepten-5-ol forms inclusion compounds with aromatic solvents such as pyridine, *p*-xylene, chlorobenzene, bromobenzene and benzene.[8]

4.2.4 Hosts A28, A31 and A32

According to the CSD there are currently no structures involving these host compounds.

References

1. Ramon, G., Coleman, A.W., Nassimbeni, L.R. & Taljaard, B. (2006) Inclusion Compounds from a Host Mixture: A Cautionary Tale. *Supramolecular Chemistry*, 18: 59-65.

2. Jacobs, A., Nassimbeni, L. R. & Taljaard, J.H. (2006) Inclusion compounds of isomeric xanthenol hosts with aniline. *CrystEngComm*, 7: 731-734.

3. Jacobs, A., Faleni, N., Nassimbeni, L. R. & Taljaard, J.H. (2007) Inclusion by a Xanthenol Host: Relating Structure to the Kinetics of Desolvation and Guest Exchange, *Crystal Growth & Design*, 7: 1003-1006.

4. Jacobs, A., Nassimbeni, L. R., Su, H. & Taljaard, B. (2005) Xanthenol clathrates: structure, thermal stability, guest exchange and kinetics of desolvation. *Organic Biomolecular Chem*istry, 3: 1319-1322.

5. Jacobs, A., Nassimbeni, L.R., Nohako, K.L., Ramon, G. & Taljaard, J.H. (2009) Enclathration by a xanthenol host via solid–solid reactions: structures and kinetics, *New Journal of Chemistry*, 33: 1960-1964.

6. Cambridge Structural Database (CSD), Version 5.33, November 2011.

7. Curtis, E., Nassimbeni, L.R., Su, H. & Taljaard, J.H. (2006) Xanthenol Clathrates: Structures and Solid−Solid Reactions, *Crystal Growth & Design*, 6: 2716–2719.

8. Nassimbeni, L.R., Ramon, G. & Taljaard, J.H. (2009) Selectivity profiles of 5-(4-methoxyphenyl)-5*H*-dibenzo [a,d]cyclohepten-5-ol with aromatic solvents and conformational polymorphism of 10,11-dihydro-5-(4-methoxyphenyl)-5*H*-dibenzo[a,d]cyclohepten-5-ol. *Crystal Growth & Design*, 9(1): 88-94.

CHAPTER 5
RESULTS AND DISCUSSION

PART ONE :

The host 9-(4-methoxyphenyl)-9*H*-xanthen-9-ol forms inclusion compounds with aniline, 3-picoline, morpholine, *N*-methylacetamide and *N*-methylformamide.

A1

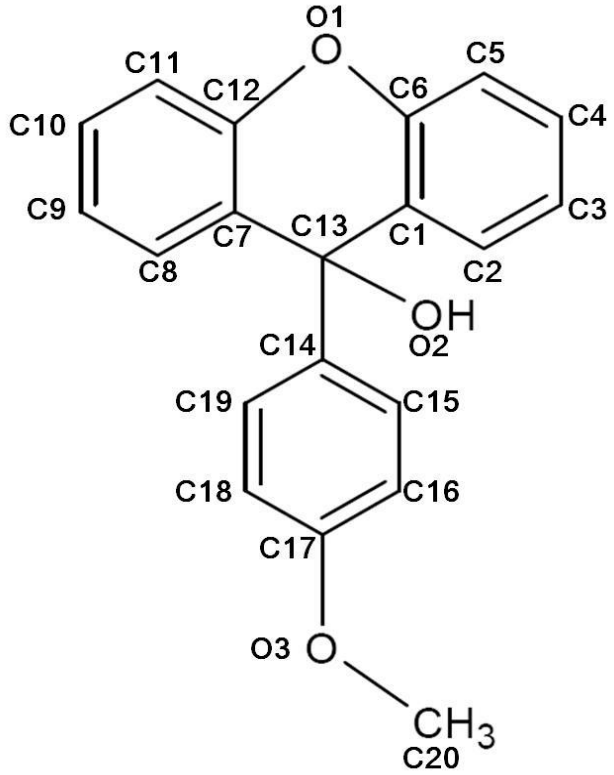

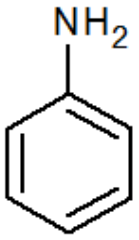

Aniline

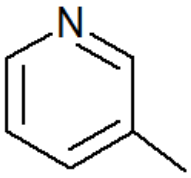

3-Picoline

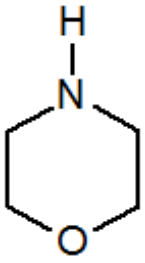

Morpholine

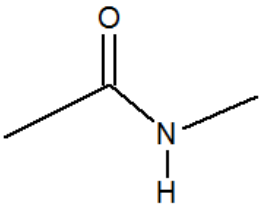

***N*-Methylacetamide**

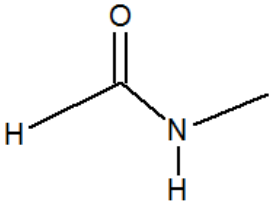

***N*-Methylformamide**

5.1 Guest: Aniline

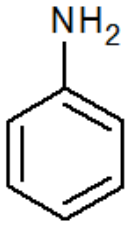

Table 5.1: Properties of aniline.

Guest	ANI
Molecular formula	**C_6H_7N**
Molar mass (g/mol)	**93.13**
Boiling Point (K)	**457**

5.1.1 Thermal Analysis

The thermal analysis results are shown in Figure 5.1. A two step mass loss is observed for the **A1·ANI** inclusion compound. The total mass loss of 13.0 % corresponds to a 1:½ host-guest ratio. In the DSC curve two endotherms are observed for the release of the guest followed by dissolution of the host. A summary of the thermal data is given in Table 5.2.

Table 5.2: Thermal analysis data for **A1·ANI.**

Compound	A1·ANI
Host: Guest ratio	**1:½**
TG calculated % mass loss	**13.3**
TG experimental % mass loss	**13.0**
DSC Endo$_1$ (T_{onset}, K)	**357.2**
DSC Endo$_2$ (T_{onset}, K)	**364.4**
DSC Host (T_{onset}, K)	**395.3**

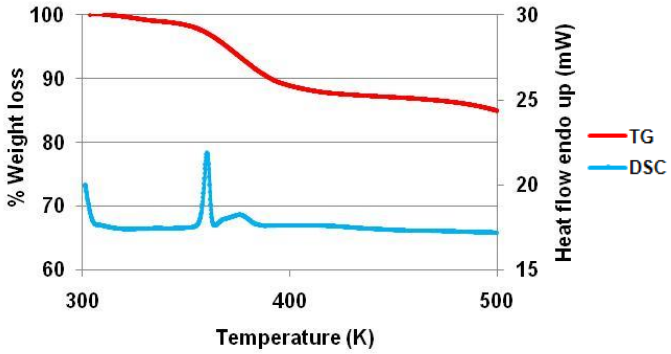

Figure 5.1: TGA and DSC curves obtained for **A1·ANI.**

5.1.2 Hot Stage Microscopy

(a) The crystals are immersed in silicone oil.
(b) The crystals become opaque upon guest release.
(c) The crystal begins to melt.
(d) The host melt is complete.

(a) 298K **(b) 357K** **(c) 365 K** **(d) 382 K**

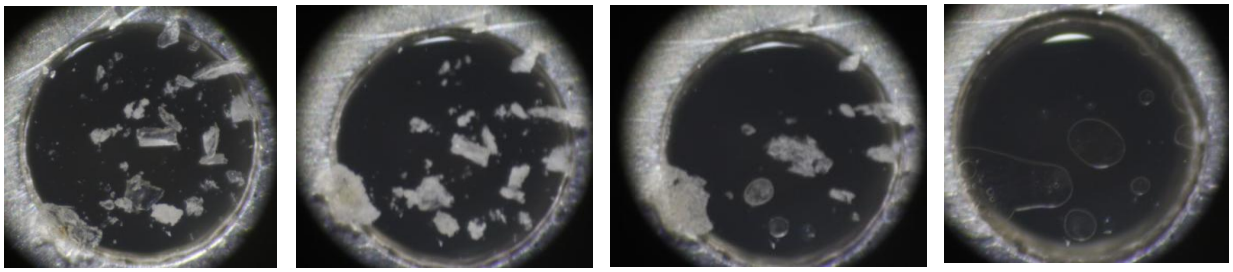

Figure 5.2 : HSM photographs of **A1·ANI**

5.1.3 Structure Refinement

All non-hydrogen atoms were found by direct methods and refined anisotropically. The host hydroxyl hydrogen was first located in the difference electron density map and then refined with a simple bond length constraint dependent on the O···O distance.[1] The nitrogen atom of aniline was assigned a site occupancy factor of 0.5. The amine hydrogen was located in the difference electron density map. The structure refined to R_1= 0.0540 with wR_2= 0.1290. The crystal data of **A1·ANI** is reported in Table 5.3.

Table 5.3: Crystal data of **A1·ANI.**

Compound	**A1•ANI**
Structural Formula	$C_{20}H_{16}O_3 \cdot ½C_6H_7N$
Host-Guest ratio	**1:½**
Molecular Mass (g.mol^{-1})	**350.89**
Data collection temp (K)	**173**
Crystal system	**Monoclinic**
Space group	***P*2$_1$/*c***
a (Å)	**13.238(3)**
b (Å)	**9.6516(19)**
c (Å)	**15.945(3)**
β (°)	**119.62(3)**
Volume (Å^3)	**1771.1(6)**
Z	**4**
μ/ mm^{-1}	**0.087**
F(000)	**740**
No. of reflections collected	**10566**
No. of unique reflection	**4413**
No. of reflections with I>2σ(I)	**3391**
D_c, Calculated density (g.cm^{-3})	**1.316**
Index range	**h: -16 to 17,** **k: -12 to 11,** **l: -21 to 14**
θ range	**1.77-28.35**
Goodness of fit, S	**1.035**
Final R indices [I>2σ(I)]	**R_1= 0.0540 ; wR_2= 0.1290**
R indices (all data)	**R_1= 0.0714; wR_2= 0.1409**
Largest diff peak and hole (eÅ^{-3})	**0.53 ; -0.53**

5.1.4 Discussion

The structure of **A1·½ANI** which crystallises in $P\bar{1}$ with Z=2, has previously been reported.[2] The two inclusion compounds obtained are polymorphs. The asymmetric unit contains a host and half a guest molecule with structural formula of $C_{20}H_{16}O_3 \cdot ½C_6H_7N$ (Figure 5.3). The structure of **A1·ANI** crystallises in the monoclinic space group $P2_1/c$ with one host molecule located in general positions and the aniline guest located on a centre of inversion at Wyckoff position *a*. The aniline is therefore disordered with each amino group having a site occupancy factor of 0.5 (Figure 5.4).

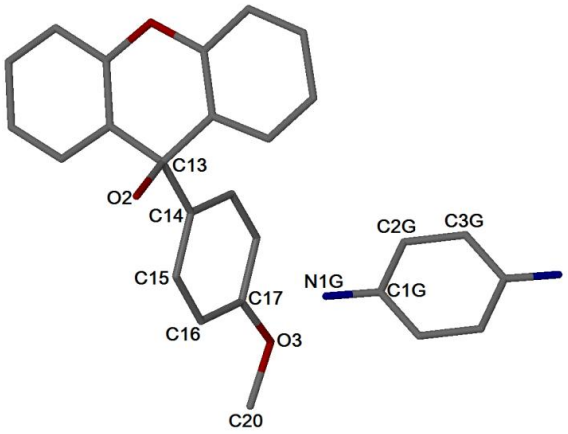

Figure 5.3: Asymmetric unit of **A1·ANI**.

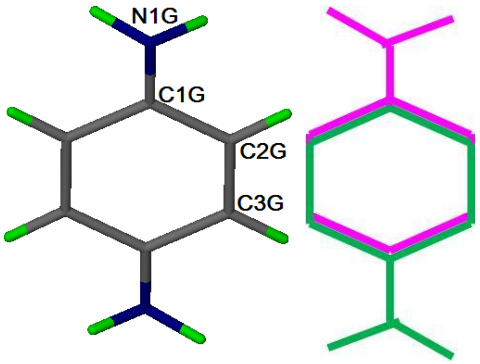

Figure 5.4: Aniline guest.

Selected torsion angles of the host are provided in Table 5.4. When the value for the torsion angles τ_1 and τ_2 are close to zero, the methoxy group takes a *cis*-configuration with respect to the hydroxyl moiety.[3] Torsion angles of τ_1= 16.3(2)° and τ_2= 11.1(2)° are observed for **A1•ANI.** This leads to the conformation of the host molecules hydroxyl group in a *cis* configuration with respect to the methoxy group (Figure 5.5).

Table 5.4: Conformation parameters of host molecule in **A1·ANI.**

τ_1= O2-C13-C14-C15/°	τ_2= C20-O3-C17-C16/°	Host conformation
16.3(2)	**11.1(2)**	***Cis* conformation**

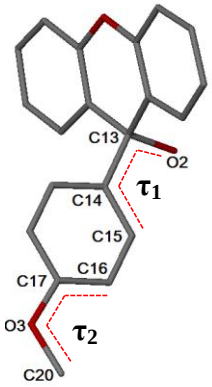

Figure 5.5: Torsion angles used in **A1.**

The structure is stabilised by (Host)-OH···O-(Host) hydrogen bonds with an O···O distance of 2.880(2) Å, shown in Figure 5.6. The host hydrogen bonds via the hydroxyl moiety of one molecule to the methoxy oxygen of a second molecule, forming anti-parallel chains running in the [001] direction. The hydrogen bonding observed can be characterized as $C_1^1(3)$.[4]

Table 5.5: Hydrogen bond parameters of **A1·ANI**.

Donor(D)-H	Acceptor(A)	D···A (Å)	D-H (Å)	H···A (Å)	D-H···A (°)
O2-H1	**O3 [x, -y+1/2, z+1/2]**	**2.880(2)**	**0.955(1)**	**1.931(4)**	**173(2)**

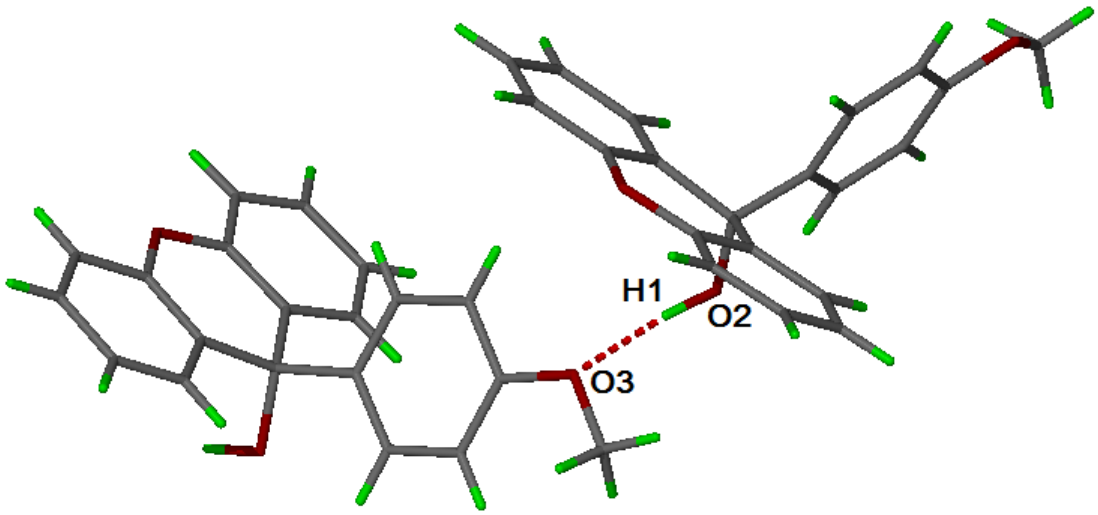

Figure 5.6: Hydrogen bonding between two host molecules.

Pairs of host molecules display edge-to-face and face-to-face π-π interactions. These dimers are further strengthened by (Host)-C19-H···O1-(Host) hydrogen bonds. The **A1·ANI** is further stabilised by weaker C-H···π and N-H···π interactions**,** shown in Figure 5.7. The C-H···π parameters are provided in Table 5.6. Also a N1G-H···π interaction is observed with a N···π distance of 3.263 Å and angle of 132°. The C-H···π parameters are listed in Table 5.6.

Table 5.6: C-H···π parameters of **A1·ANI.**

C-H···π	C···π (Å)	H···π(Å)	C-H-π (°)	Symmetry Operator
C4-H···π	**4.205**	**3.309**	**158**	**x , -1+y , z**
C18-H···π	**3.608**	**2.661**	**175**	**x , ½-y , -½+z**
C20-H···π	**4.099**	**3.281**	**142**	**x , ½-y , -½+z**

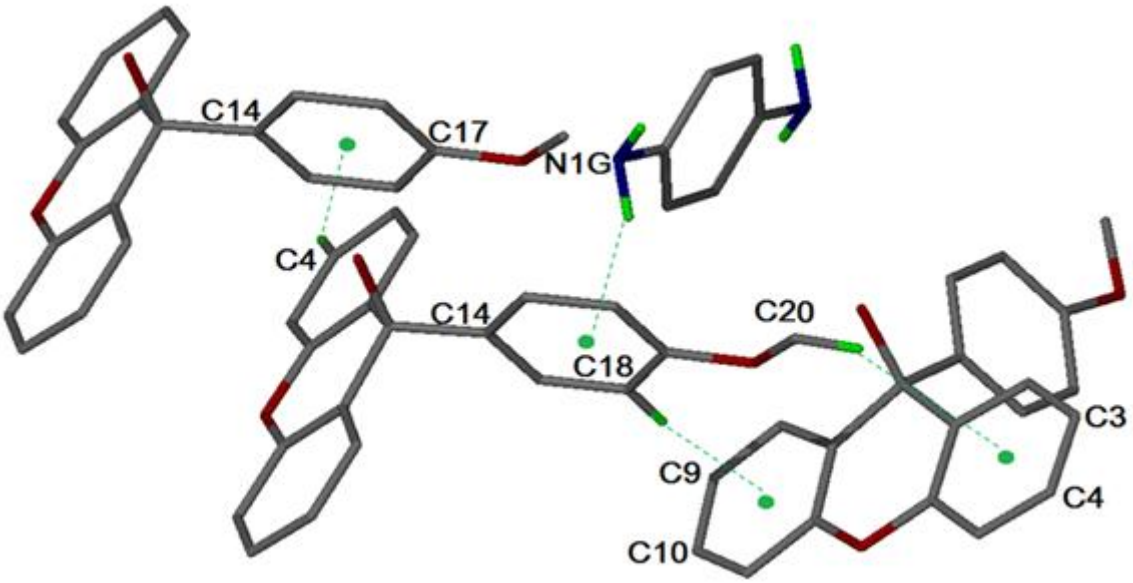

Figure 5.7: C-H···π and N-H···π interaction in **A1·ANI**. The C-H···π and N-H···π interactions are indicated by green dotted lines.

The packing diagram of **A1·ANI** viewed along [010] with hydrogen bonds shown in Figure 5.8. The aniline guests are situated in cavities shown in Figure 5.9.[5] **A1·ANI** is a clathrate.

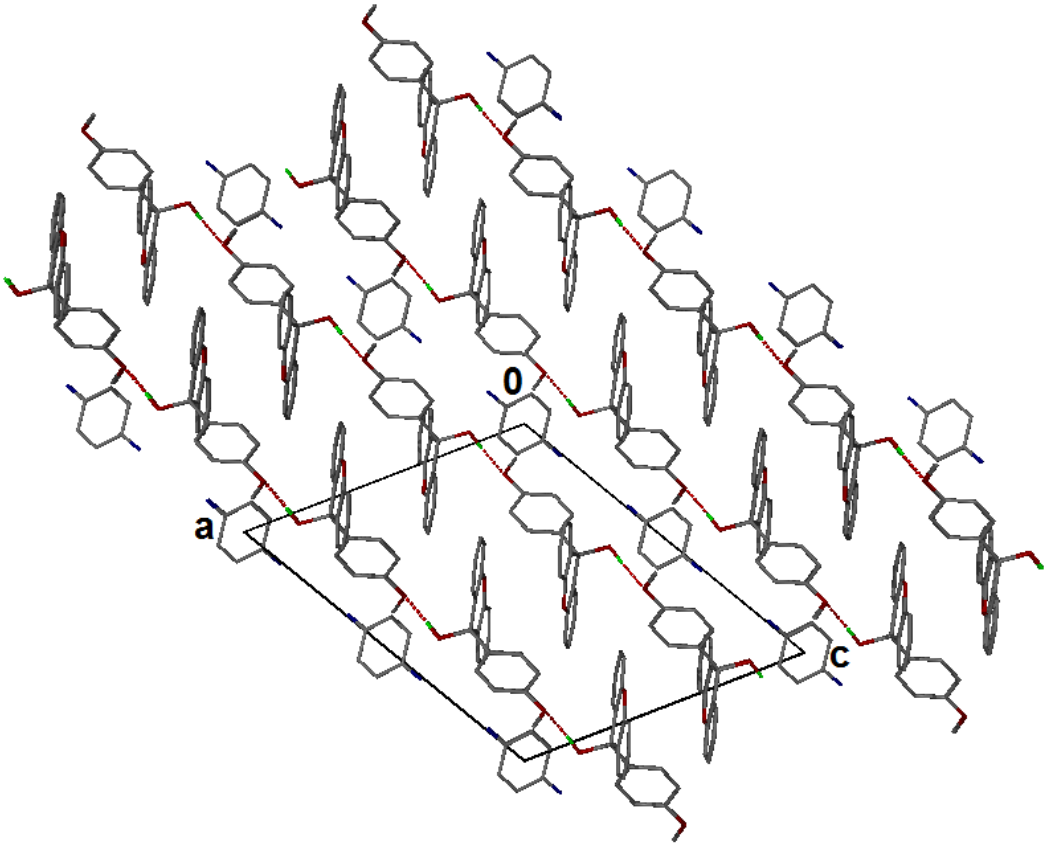

Figure 5.8: Packing diagram of **A1·ANI** viewed along [010] direction.
All hydrogen atoms are omitted except the hydroxyl hydrogen. Hydrogen bonding is also displayed.

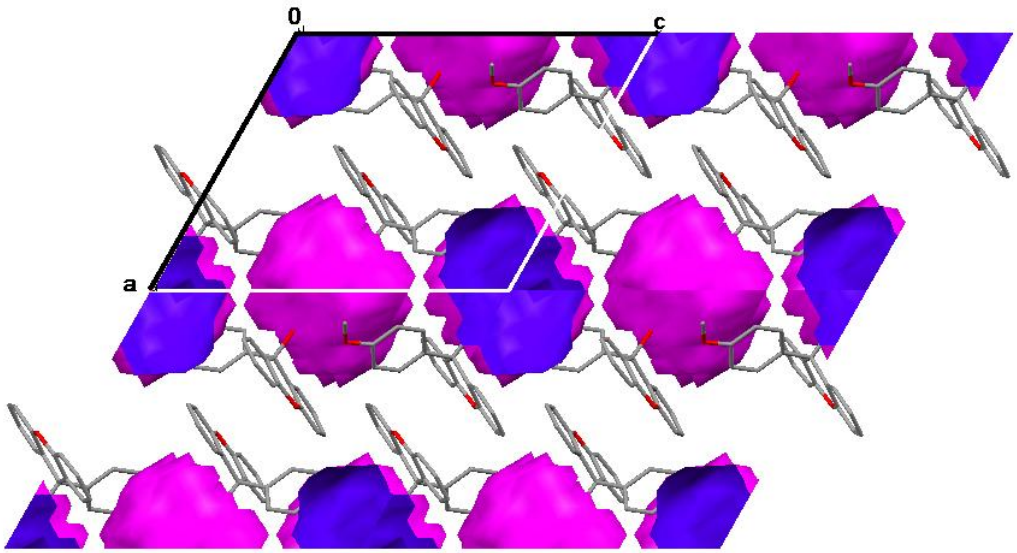

Figure 5.9: The cavities in which the aniline guests are located.

The program *SECTION*[6] was used to map the cavities in which the guests are located at different section heights shown in Figure 5.10. The program *PLATON*[7] was used to calculate the total potential solvent accessible volume and was found to be 314.5Å^3.

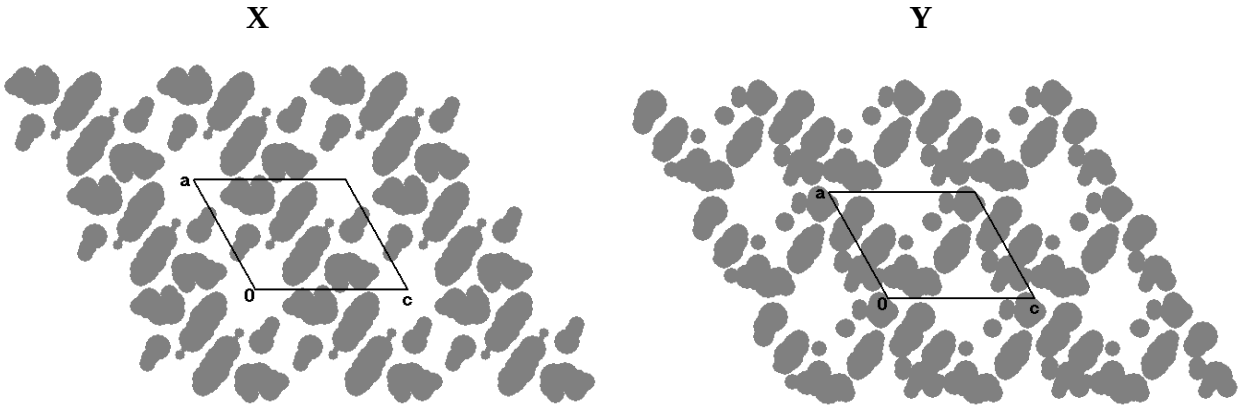

Figure 5.10: Section plot of **A1·ANI** along [010]. X = section height @ 0.00 Å ; Y = section height @ 4.00Å.

5.2 Guest: 3-Picoline

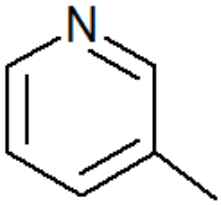

Table 5.7: Properties of 3-Picoline.

Guest	3-Picoline
Molecular formula	C_6H_7N
Molar mass (g/mol)	93.1
Boiling Point (K)	417

5.2.1 Thermal Analysis

The TG experimental and calculated percentage mass losses are in good correlation with one another. The thermal analysis results are listed in Table 5.8. The TG curve shows a single mass loss of 23.2 % which corresponds to the loss of the guest. The host-guest ratio was determined from the TG results and found to be 1:1. A single endotherm is observed which corresponds to dissolution of the host upon release of the guest. The thermal analysis results are shown in Figure 5.11.

Table 5.8: Thermal analysis data for **A1·3PIC.**

Compound	A1•3PIC
Host: Guest ratio	1:1
TG calculated % mass loss	23.5
TG experimental % mass loss	23.2
DSC $Endo_1$ (T_{onset}, K)	339.3
DSC Host (T_{onset}, K)	395.3

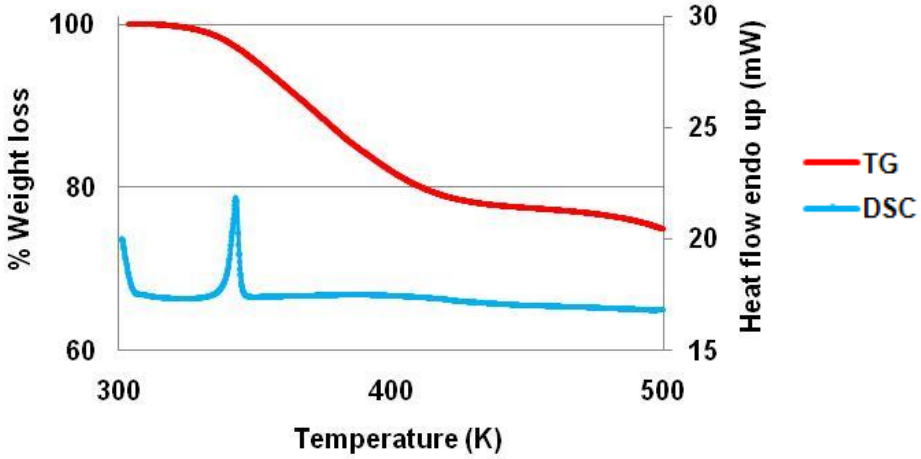

Figure 5.11: TGA and DSC curves obtained for **A1·3PIC.**

5.2.2 Structure Refinement

The inclusion compound **A1·3PIC** structure refined successfully to R_1= 0.0424 with wR_2= 0.1046. All non-hydrogen atoms were located by direct methods in the difference electron density map and refined anisotropically. The hydroxyl hydrogen was located in the difference electron density map. The nitrogen atom of the guest was identified by the highest peak magnitude in the aromatic ring. The crystal data is given in Table 5.9.

Table 5.9: Crystal data of **A1·3PIC.**

Compound	**A1•3PIC**
Structural Formula	$C_{20}H_{16}O_3 \cdot C_6H_7N$
Host-Guest ratio	**1:1**
Molecular Mass (g.mol^{-1})	**397.45**
Data collection temp (K)	**173**
Crystal system	**Triclinic**
Space group	$P\bar{1}$
a (Å)	**8.7298(10)**
b (Å)	**11.1494(12)**
c (Å)	**12.3866(14)**
α (°)	**64.473(2)**
β (°)	**82.426(2)**
γ (°)	**73.784(2)**
Volume (Å^3)	**1044.6(2)**
Z	**2**
μ/ mm^{-1}	**0.082**
F(000)	**420**
No. of reflections collected	**8219**
No. of unique reflection	**5171**
No. of reflections with I>2σ(I)	**3974**
D_c, Calculated density (g.cm^{-3})	**1.264**
Index range	**h: -11 to 11,** **k: -7 to 14,** **l: -11 to 16**
θ range	**1.82-28.39**
Goodness of fit, S	**1.033**
Final R indices [I>2σ(I)]	**R_1= 0.0424 ; wR_2= 0.1046**
R indices (all data)	**R_1= 0.0583; wR_2= 0.1140**
Largest diff peak and hole (eÅ^{-3})	**0.30 ; -0.19**

5.2.3 Discussion

The structure crystallises in the triclinic space group $P\bar{1}$ with Z=2, and the host and guest molecules are located in general positions. The asymmetric unit of **A1·3PIC** consists of a host and guest molecule which gives a host-guest ratio of 1:1 (Figure 5.12).

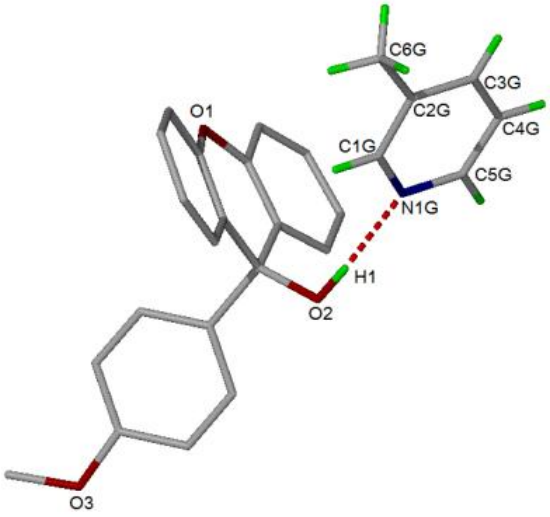

Figure 5.12: Hydrogen bonding in the asymmetric unit of **A1·3PIC**.

Selected torsion angles of the host are provided in Table 5.10. In **A1·3PIC**, the host molecule's hydroxyl group is said to be in a *trans* configuration with respect to the methoxy group shown in Figure 5.13.

Table 5.10: Conformation parameters of host molecule in **A1·3PIC.**

τ_1= O2-C13-C14-C15/°	τ_2= C20-O3-C17-C16/°	Host conformation
-16.7(1)	-178.8(1)	*Trans* conformation

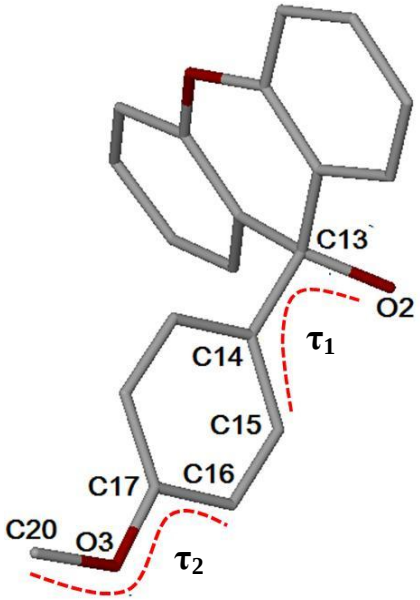

Figure 5.13: Torsion angles used in **A1.**

The hydroxyl group of the host interacts with the nitrogen of the guest. A (Host)-OH···N-(Guest) hydrogen bond stabilises the **A1·3PIC** structure with a bond distance of 2.799(1) Å shown in Figure 5.14. The O-H-N angle is 176(1)°. The hydrogen bonding parameters are provided in Table 5.11.

Table 5.11: Hydrogen bond parameters of **A1·3PIC**.

Donor(D)-H	Acceptor(A)	D···A (Å)	D-H (Å)	H···A (Å)	D-H···A (°)
O2-H1	**N1G**	**2.799(1)**	**0.840(1)**	**1.960(1)**	**176(1)**

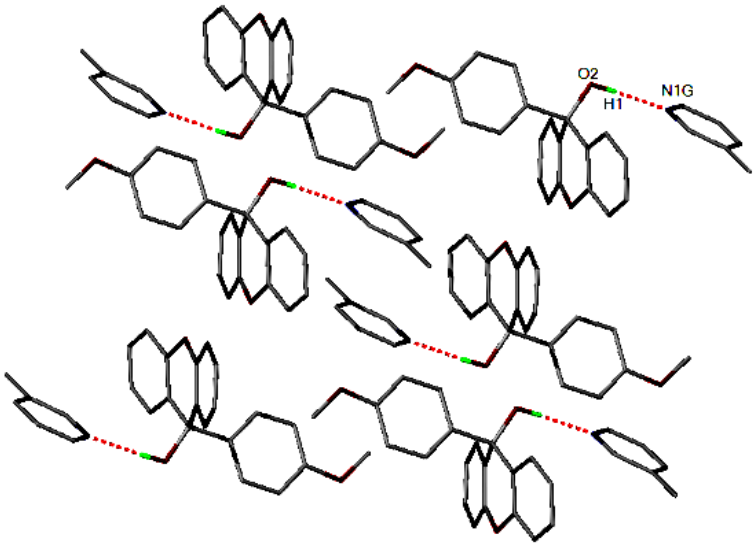

Figure 5.14: Hydrogen bonding in **A1·3PIC.**

The distance between the ring centroids of two guest molecules is 3.843 Å, which occurs between a pair of neighbouring guest molecules shown in Figure 5.15. The shortest C···π distance has C20···π and H···π distances of 3.647 Å and 2.755 Å respectively, with a C-H-π angle of 148° shown in Figure 5.16. C-H···π interactions between host and guest molecules are also observed. Pairs of host molecules form dimers which are strengthened by (Host)-C19-H···O1-(Host) hydrogen bonds.

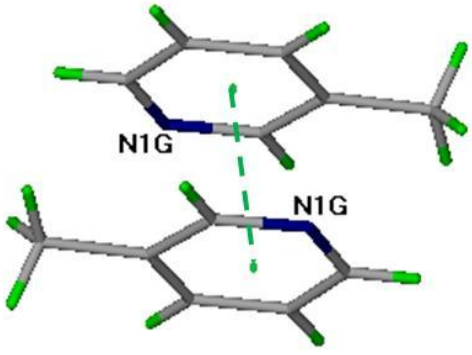

Figure 5.15: Off-set face-to-face π- π stacking of neighbouring guest molecules. The distance between the centroids is indicated by green dotted lines.

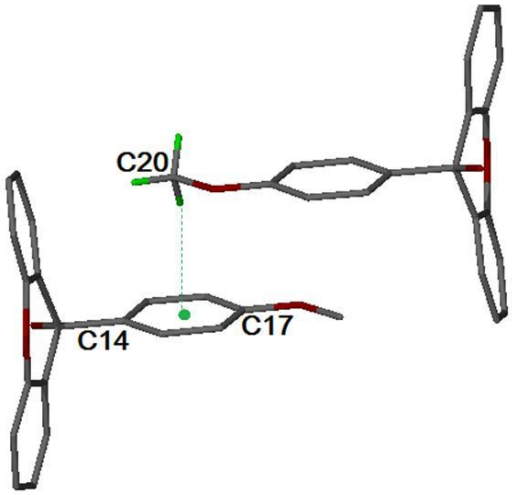

Figure 5.16: C-H···π interaction of neighbouring host molecules. The C-H···π interaction is indicated by green dotted lines.

The packing diagram of **A1·3PIC** along [100] is shown in Figure 5.17. The guests reside in open channels down [100] shown in Figure 5.18.[5]

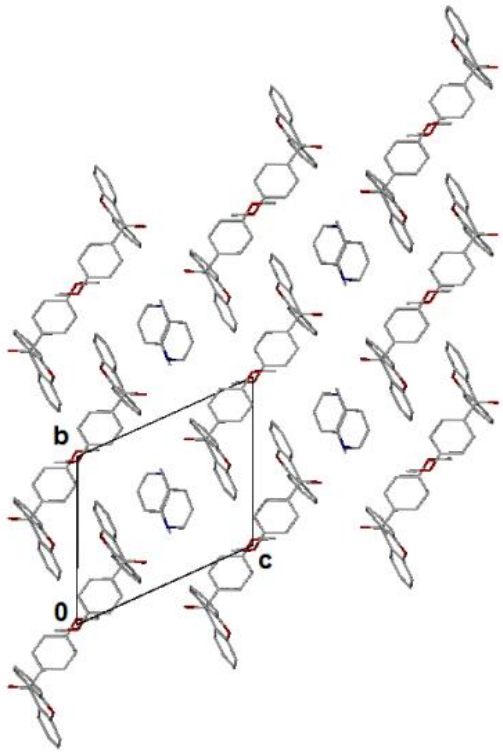

Figure 5.17: Packing diagram of **A1·3PIC** viewed along [100] direction. All hydrogen atoms are omitted.

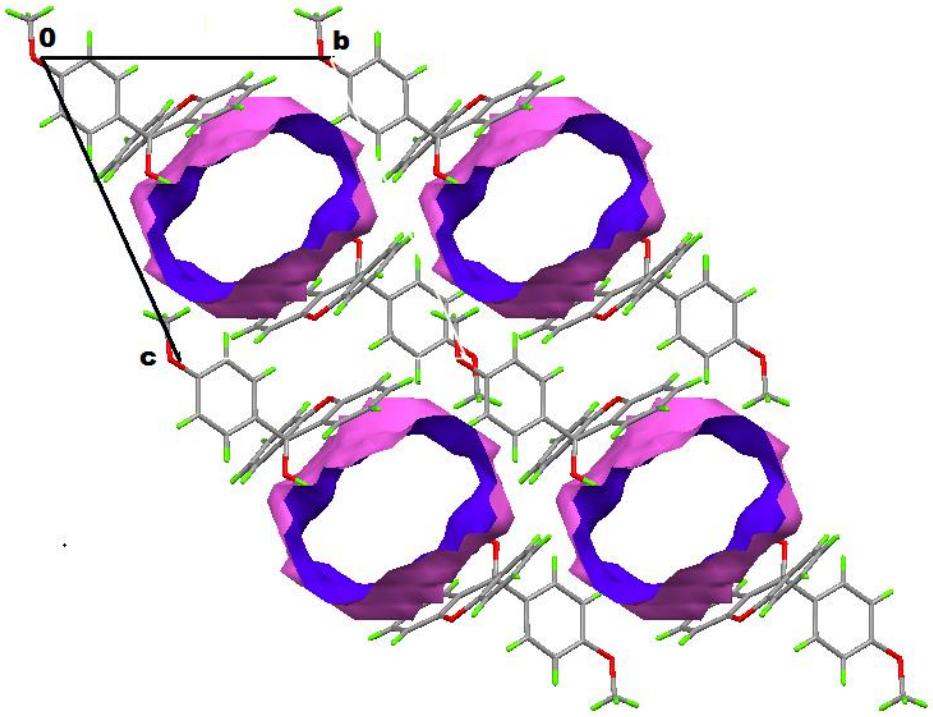

Figure 5.18: Open channels viewed down [100].

5.2.4 Non-isothermal Kinetics

The non-isothermal method was used to study the desolvation of **A1·3PIC**. [8-9] TG mass loss curves using heating rates of 7, 13, 18 and 24 K/min were recorded (Figure 5.19). Ramped TG experiments at selected scan rates gave a series of –log β *vs* 1000/T curves, where β is the heating rate (Figure 5.20). The series gave an activation energy range of 42 to 63 kJ/mol.

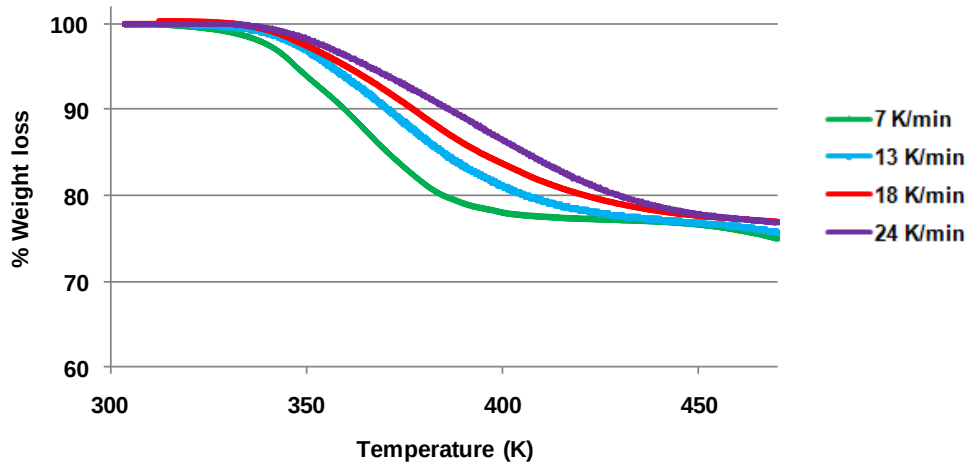

Figure 5.19: TG curves indicating the desolvation of **A1·3PIC** at 7, 13, 18 and 24 K/min.

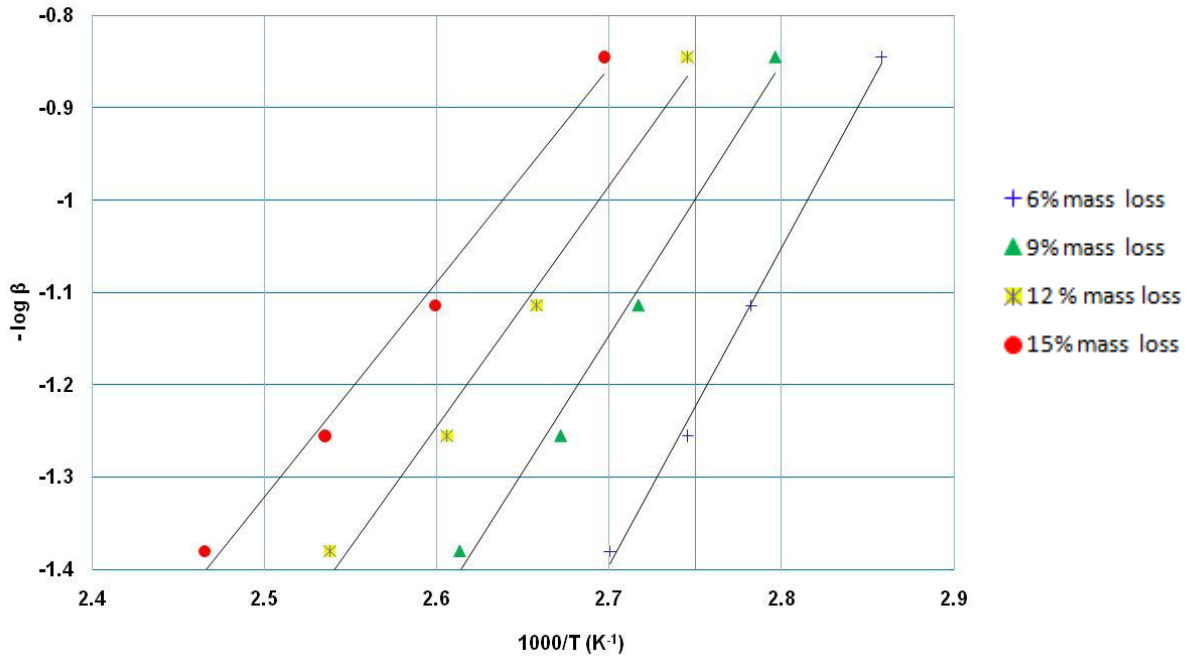

Figure 5.20: Plot of –log β vs 1000/T.

5.3 Guest: Morpholine

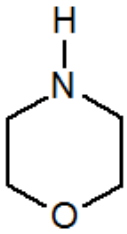

Table 5.12: Properties of morpholine.

Guest	MORPH
Molecular formula	C_4H_9NO
Molar mass (g/mol)	87.1
Boiling Point (K)	401

5.3.1 Thermal Analysis

The thermal analysis data is given in Table 5.13. A single mass loss step of 13.1 % was observed in the TG curve which corresponds to a 1:½ host-guest ratio. A single endotherm was observed in the DSC curve which corresponds to dissolution of the host upon release of the guest. The thermal analysis results are shown in Figure 5.21.

Table 5.13: Thermal analysis data for **A1·MORPH.**

Compound	A1•MORPH
Host: Guest ratio	1:½
TG calculated % mass loss	12.5
TG experimental % mass loss	13.1
DSC $Endo_1$ (T_{onset}, K)	350.9
DSC Host (T_{onset}, K)	395.3

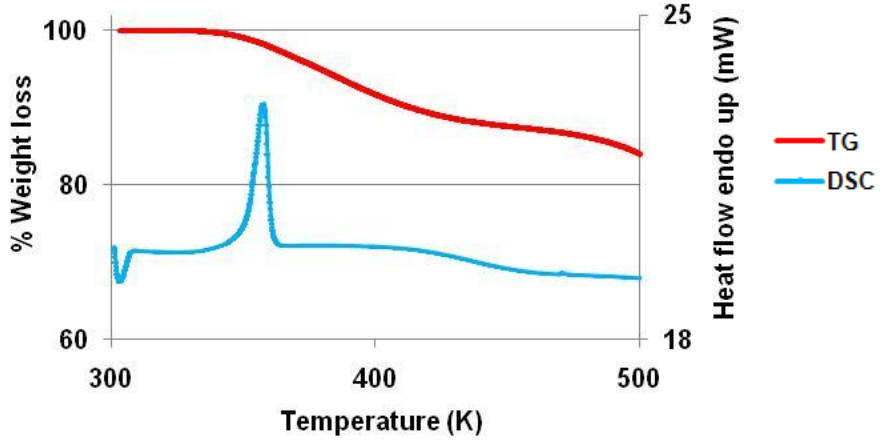

Figure 5.21: TGA and DSC curves obtained for **A1·MORPH.**

5.3.2 Structure Refinement

Direct methods yielded all host and guest non-hydrogen atoms and these were refined anisotropically. The secondary amine hydrogen was located in the difference electron density map. A bond length constraint of 0.94 Å was assigned to the NH bond of the guest. The NH bond refined to 0.89(1) Å. The crystal data is reported in Table 5.14.

Table 5.14: Crystal data of **A1·MORPH.**

Compound	**A1•MORPH**
Structural Formula	**$C_{20}H_{16}O_3 \cdot ½C_4H_9NO$**
Host-Guest ratio	**1:½**
Molecular Mass (g.mol^{-1})	**347.89**
Data collection temp (K)	**173**
Crystal system	**Monoclinic**
Space group	***P*2$_1$/*c***
a (Å)	**8.9358(6)**
b (Å)	**15.0970(10)**
c (Å)	**13.1591(9)**
β (°)	**101.253(2)**
Volume (Å^3)	**1741.1(2)**
Z	**4**
μ/ mm^{-1}	**0.089**
F(000)	**736**
No. of reflections collected	**13233**
No. of unique reflection	**4319**
No. of reflections with I>2σ(I)	**3683**
D$_c$, Calculated density (g.cm^{-3})	**1.327**
Index range	**h: -11 to 8,** **k: -18 to 20,** **l: -17 to17**
θ range	**2.08-28.33**
Goodness of fit, S	**1.052**
Final R indices [I>2σ(I)]	**R_1= 0.0419;** **wR_2= 0.1128**
R indices (all data)	**R_1= 0.0494;** **wR_2= 0.1186**
Largest diff peak and hole (eÅ^{-3})	**0.37 ; -0.21**

5.3.3 Discussion

The **A1·MORPH** structure crystallised in the monoclinic space group $P2_1/c$ with Z = 4. The asymmetric unit contains one host and half a guest molecule with structural formula of $C_{20}H_{16}O_3 \cdot \frac{1}{2}C_4H_9NO$. The morpholine guest is situated on a centre of inversion at Wyckoff position *a* and is therefore disordered (Figure 5.22). The nitrogen and oxygen of the morpholine guest atoms occupies the same position each with site occupancy factors of 0.5.

The host molecule's hydroxyl group is said to be in a *trans* configuration with respect to the methoxy group. Selected torsion angles of the host are listed in Table 5.15. The structure is stabilised by hydrogen bonding between the host and the morpholine guest (Figure 5.23). The hydrogen bond parameters are provided in Table 5.16.

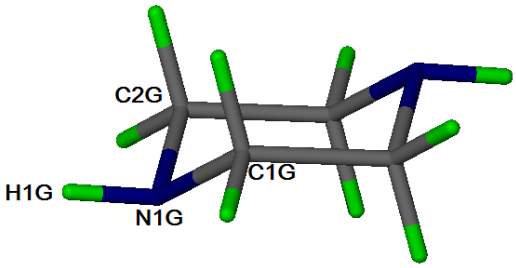

Figure 5.22: Morpholine guest.

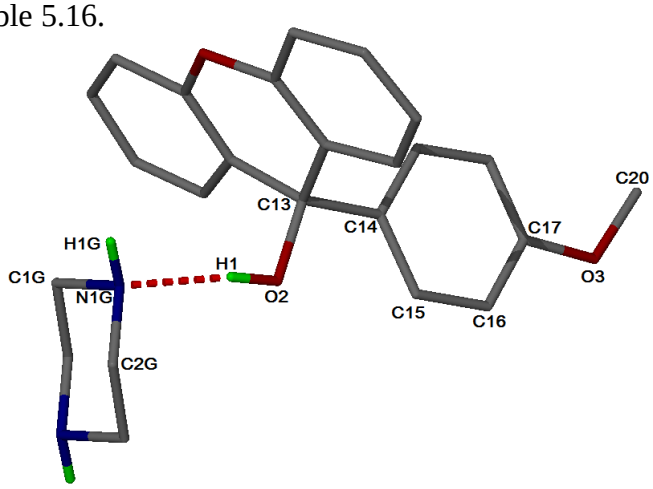

Figure 5.23: Hydrogen bonding in **A1·MORPH.**

Table 5.15: Conformation parameters of host molecule in **A1·MORPH.**

τ_1= O2-C13-C14-C15/°	τ_2= C20-O3-C17-C16/°	Host conformation
-5.9(1)	-177.3(1)	*Trans* conformation

Table 5.16: Hydrogen bond parameters of **A1· MORPH.**

Donor(D)-H	Acceptor(A)	D···A (Å)	D-H (Å)	H···A (Å)	D-H···A (°)
O2-H1	N1G	2.775(1)	0.840(1)	1.944(1)	170(1)

The structure is further stabilised by weaker C-H···π interactions. The host molecules display off-set face-to-face and edge-to-face π- π interactions. Pairs of host molecules form dimers which are strengthened by (Host)-C19-H···O1-(Host) hydrogen bonds (Figure 5.24). C-H···π interactions between host and guest molecules are shown in Figure 5.25. The C-H···π associations between host molecules are shown in Figure 5.26. The closest contact of this type between host molecules is C11···π = 3.422 Å.

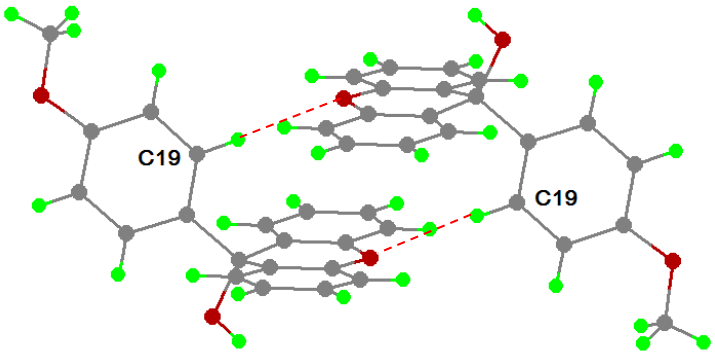

Figure 5.24: Pairs of host molecules form dimers which are strengthened by C-H···O hydrogen bonds.

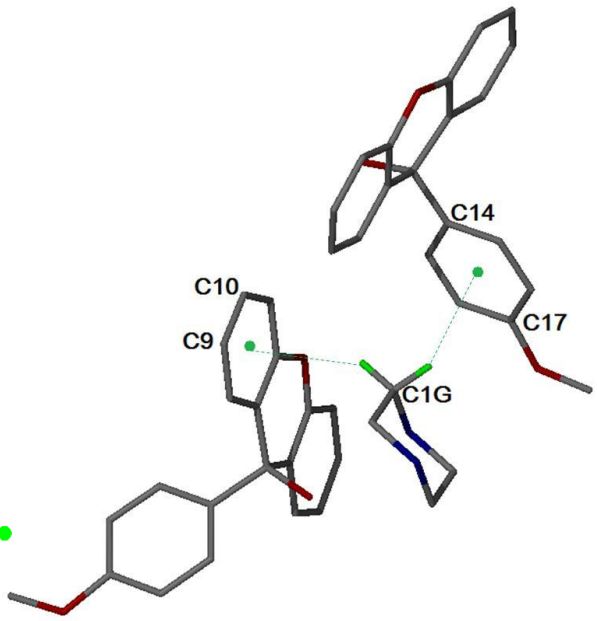

Figure 5.25: C-H···π interactions between host and guest molecules. The C-H···π interactions are indicated by green dotted lines.

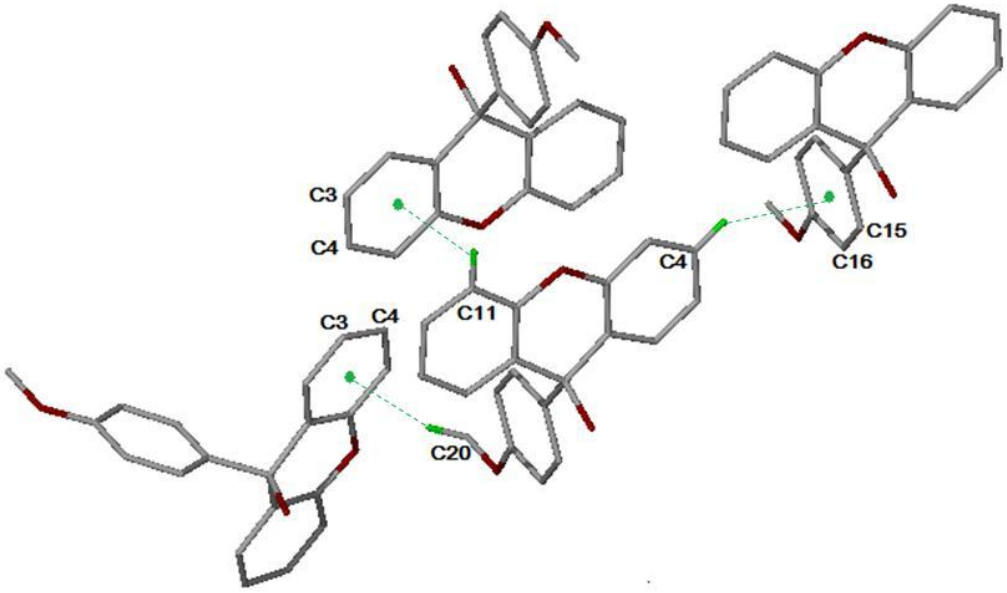

Figure 5.26: C-H···π interaction between host molecules. The C-H···π interactions are indicated by green dotted lines.

The packing diagrams down [100] and [010] are shown in Figure 5.27. The location of the *p*-methoxy phenyl moieties as well as the xanthenol fragments is such that they encapsulate the morpholine guest that lies on a centre of symmetry. The cavities in which the guests are located are shown in Figure 5.28.[5]

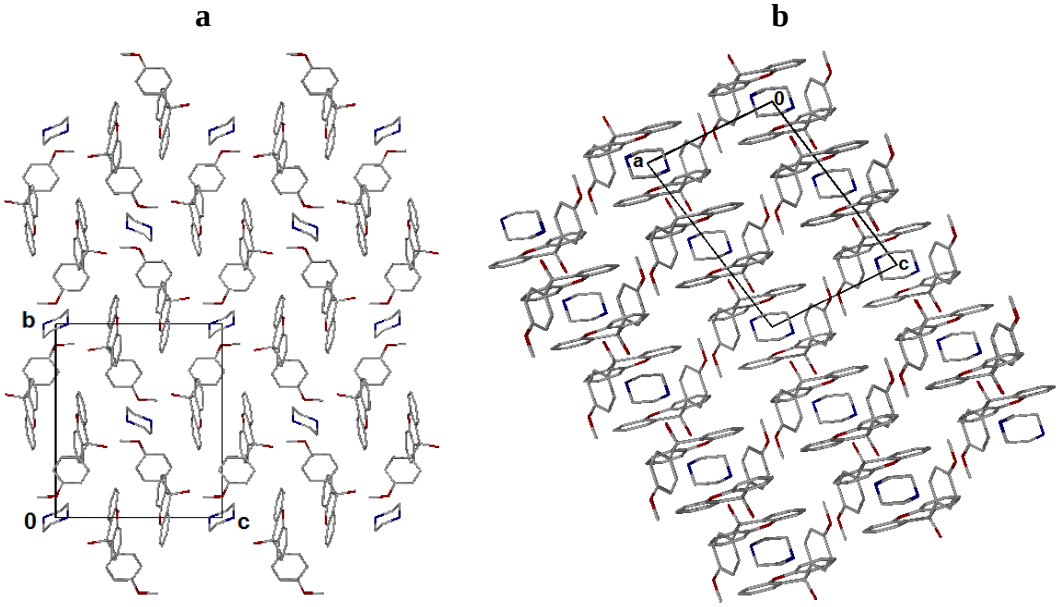

Figure 5.27: Packing diagram of **A1·MORPH**. All hydrogen atoms are omitted. (a) along [100] direction. (b) along [010] direction.

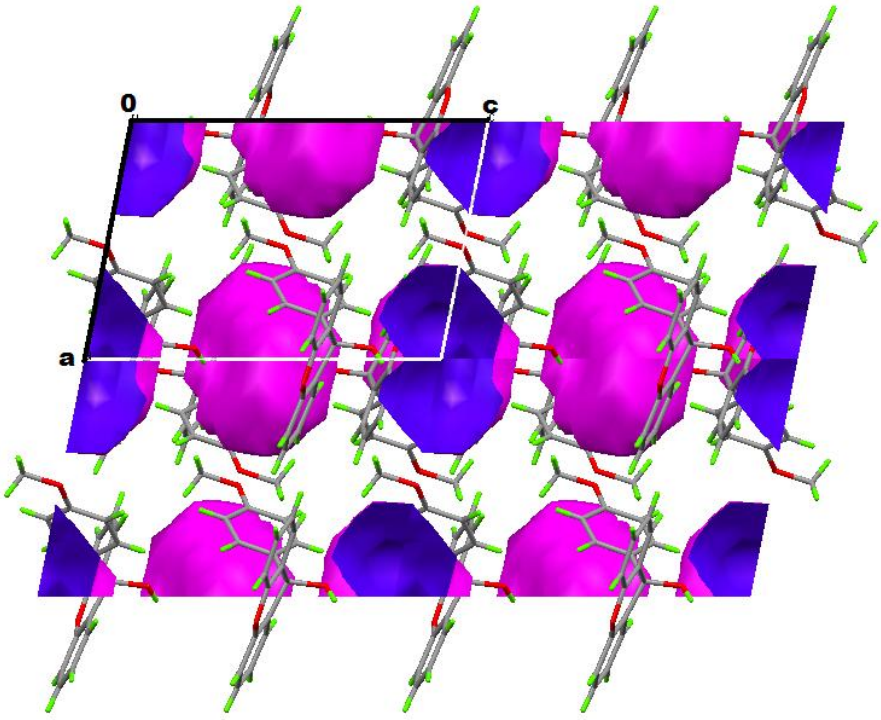

Figure 5.28: The cavities in which the morpholine guests are located.

The cavities in which the guests reside were mapped using the program *SECTION*[6] shown in Figure 5.29. The program *PLATON*[7] was used to calculate the total potential solvent accessible volume and was found to be 247.4 Å^3.

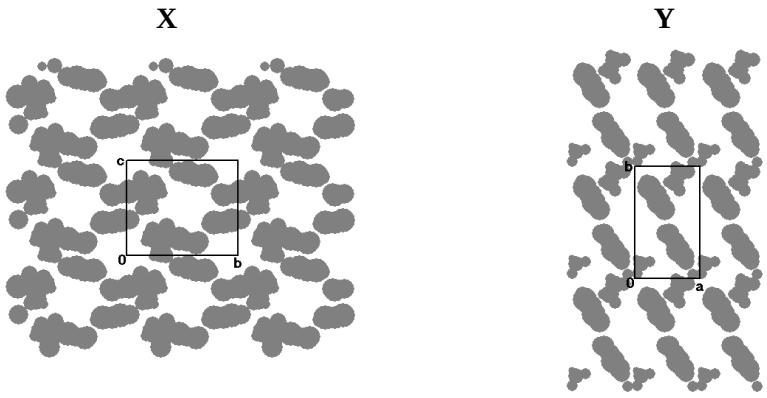

Figure 5.29: Section plot of **A1·MORPH.**
X = View along [100] with section height = 7.60 Å ; Y=View along [001] with section height = 6.25Å.

5.3.4 Non-isothermal Kinetics

TG mass loss curves for **A1·MORPH** using heating rates of 10, 15 and 30 K/min were recorded (Figure 5.30). A plot of –log β *vs* 1/T where β=scan rate and T=temperature is shown in Figure 5.31. The activation energy range was found to be 49 to 72 kJ/mol.

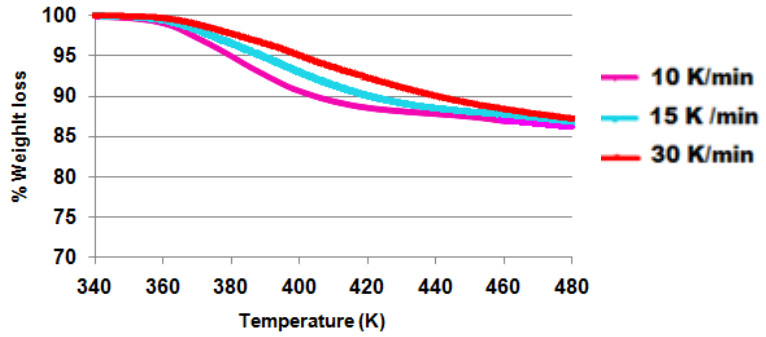

Figure 5.30: TG curves at heating rates of 10, 15 and 30 K/min.

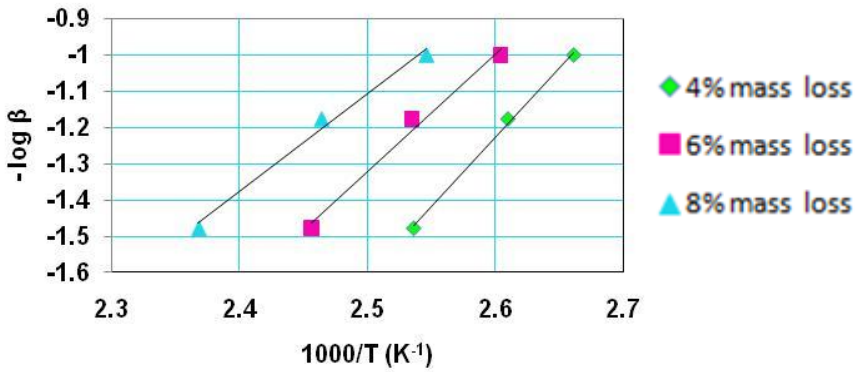

Figure 5.31: Plot of –log β *vs* 1000/T for **A1·MORPH.**

5.4 Guest: N-methylacetamide

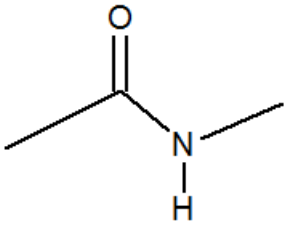

Table 5.17: Properties of *N*-methylacetamide.

Guest	NMA
Molecular formula	**C_3H_7NO**
Molar mass (g/mol)	**73.1**
Boiling Point (K)	**479**

5.4.1 Thermal Analysis

The thermal analysis results are listed in Table 5.18. A single mass loss of 19.6 % was observed in the TG curve which corresponds to a 1:1 host-guest ratio. The DSC shows two endotherms at T_{on}=356.1 K and T_{on}=389.8 K. The first endotherm is a sharp peak which is due to guest release. The second broad endotherm is due to the host melting. The thermal analysis results are shown in Figure 5.32.

Table 5.18: Thermal analysis data for **A1·NMA.**

Compound	A1·NMA
Host: Guest ratio	**1:1**
TG calculated % mass loss	**19.4**
TG experimental % mass loss	**19.6**
DSC Endo$_1$ (T_{onset}, K)	**356.1**
DSC Endo$_2$ (T_{onset}, K)	**389.8**
DSC Host (T_{onset}, K)	**395.3**

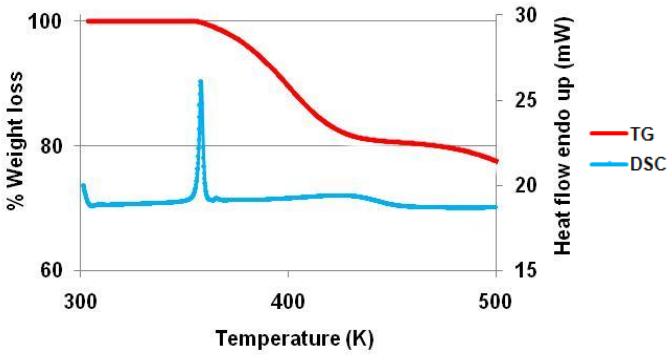

Figure 5.32: TGA and DSC curves obtained for **A1·NMA.**

5.4.2 Hot Stage Microscopy

(a) The crystal is immersed in silicone oil.
(b) The crystal breaks into pieces upon guest release.
(c) The crystal begins to melt.
(d) The host melt is complete.

(a) 298 K **(b) 358 K** **(c) 375 K** **(d) 380 K**

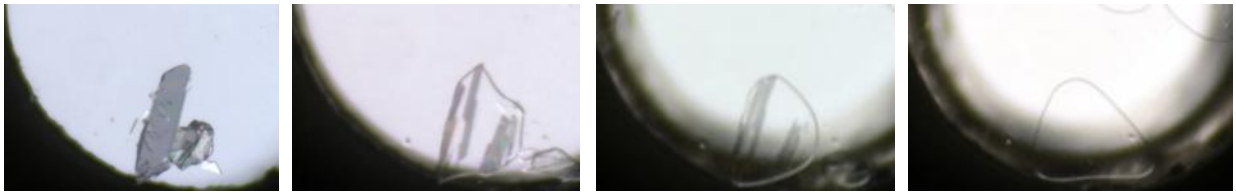

Figure 5.33: HSM photographs of **A1·NMA.**

5.4.3 Structure Refinement

All non-hydrogen atoms were located by direct methods in the difference electron density map and were refined anisotropically. The hydroxyl hydrogen of the host was located in the difference electron density map and refined with simple bond length constraints based on the relationship between O–H and O···O distances.[1] The disordered guest was solved by parts (part 1=GA and part 2=GB). The structure refined successfully to R_1= 0.0477 with wR_2= 0.1028. The crystal data is given in Table 5.19.

Table 5.19: Crystal data of **A1·NMA.**

Compound	**A1·NMA**
Structural Formula	**$C_{20}H_{16}O_3 \cdot C_3H_7NO$**
Host-Guest ratio	**1:1**
Molecular Mass (g.mol^{-1})	**377.42**
Data collection temp (K)	**173**
Crystal system	**Monoclinic**
Space group	***P*2$_1$/*n***
a (Å)	**11.1072(10)**
b (Å)	**9.3922(8)**
c (Å)	**18.6654(14)**
β (°)	**92.706(2)**
Volume (Å^3)	**1945.0(3)**
Z	**4**
μ/ mm^{-1}	**0.088**
F(000)	**800**
No. of reflections collected	**15083**
No. of unique reflection	**4846**
No. of reflections with I>2σ(I)	**2916**
D_c, Calculated density (g.cm^{-3})	**1.289**
Index range	**h: -14 to 13, k: -12 to 12, l: -24 to 12**
θ range	**2.09-28.35**
Goodness of fit, S	**0.950**
Final R indices [I>2σ(I)]	**R_1= 0.0477 ; wR_2= 0.1028**
R indices (all data)	**R_1= 0.0946; wR_2= 0.1219**
Largest diff peak and hole (eÅ^{-3})	**0.19 ; -0.22**

5.4.4 Discussion

The structure was solved successfully in the monoclinic space group $P2_1/n$ with Z=4. The asymmetric unit contains a host and a guest molecule in general positions (Figure 5.34). The NMA guest is disordered over two positions shown in Figure 5.35. The disordered NMA guest has suffixes GA and GB which have site occupancy factors of 0.49 and 0.51 respectively. The host molecule's methoxy group has a *trans* configuration with respect to the hydroxyl moiety. The conformation parameters of the host molecule are reported in Table 5.20.

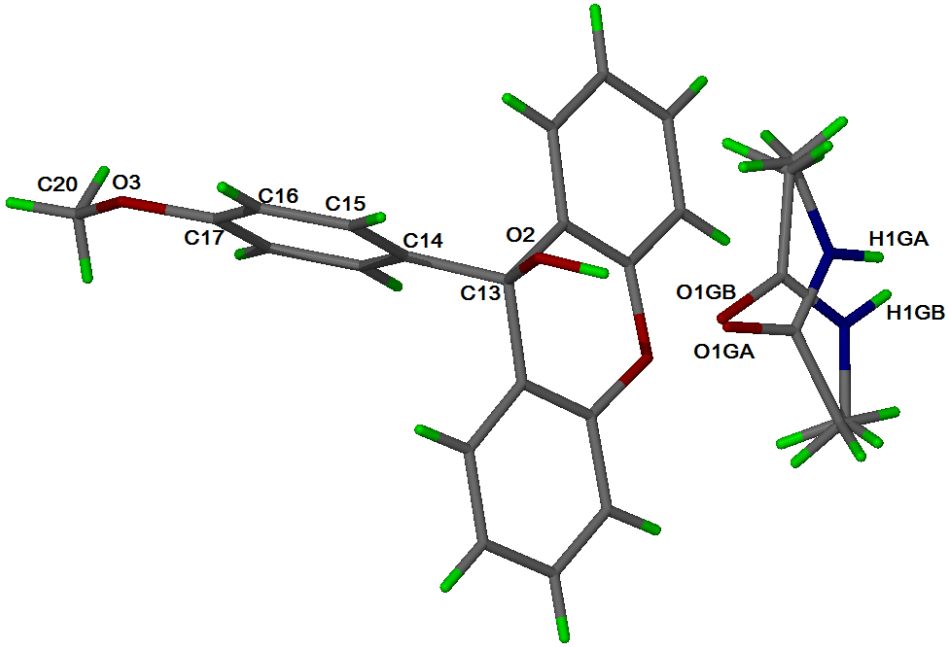

Figure 5.34: Asymmetric unit of **A1·NMA.**

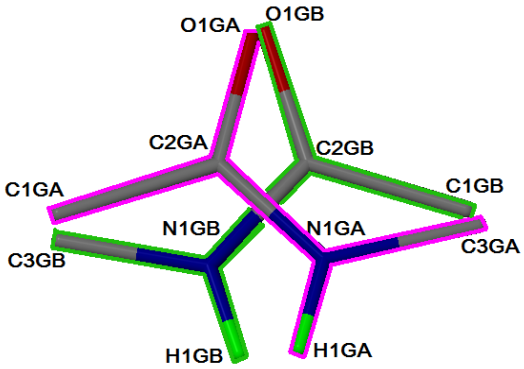

Figure 5.35: Disordered NMA guest.

Table 5.20: Conformation parameters of host molecule in **A1·NMA**.

τ_1= O2-C13-C14-C15/°	τ_2= C20-O3-C17-C16/°	Host conformation
-5.3 (2)	-179.1(2)	*Trans* conformation

The structure is stabilised by (Host)-OH···O-(Guest) and (Guest)-NH···O-(Guest) hydrogen bonds (Figure 5.36). The metrics of the hydrogen bonds are given in Table 5.21. The hydrogen bonding between hosts and major guests are shown in Figure 5.37. The hydrogen bonding pattern may be described as $C_2^2(7)$ according to Etter's graphical notation.[4]

Table 5.21: Hydrogen bond parameters of **A1·NMA**.

Donor(D)-H	Acceptor(A)	D···A (Å)	D-H (Å)	H···A (Å)	D-H···A (°)
O2-H1	**O1GA**	**2.893(7)**	**0.965(1)**	**1.94(1)**	**168(3)**
O2-H1	**O1GB**	**2.779(5)**	**0.965(1)**	**1.823(1)**	**170(3)**
N1GA-H1GA	**O1GA[½-x, y-½, ½- z]**	**3.08(6)**	**0.880(1)**	**2.203(1)**	**176(1)**
N1GB-H1GB	**O1GB[½-x, y-½, ½- z]**	**2.91(6)**	**0.880(1)**	**2.097(1)**	**154(1)**

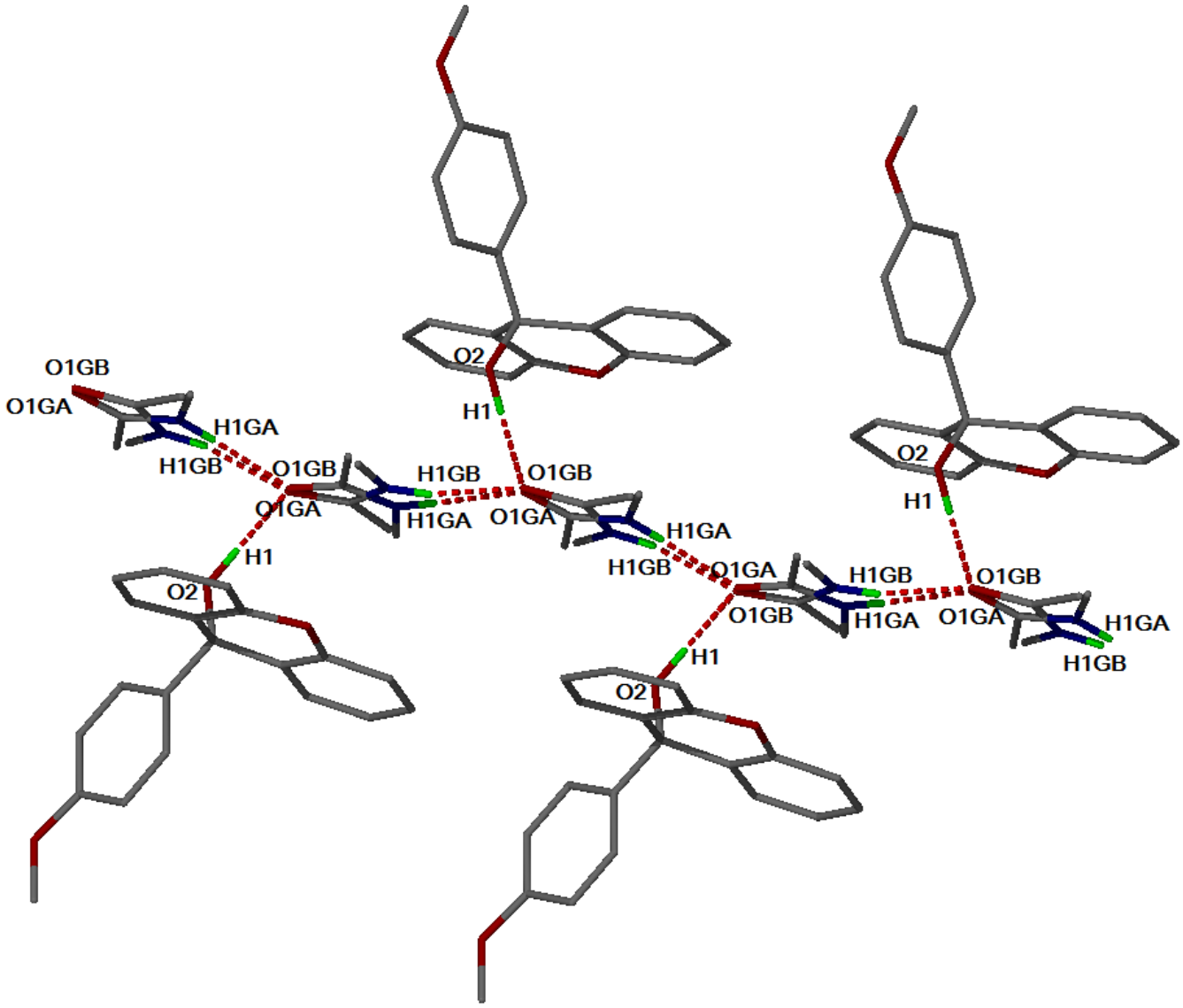

Figure 5.36: Hydrogen bonding in **A1·NMA.** The disordered guests are shown.

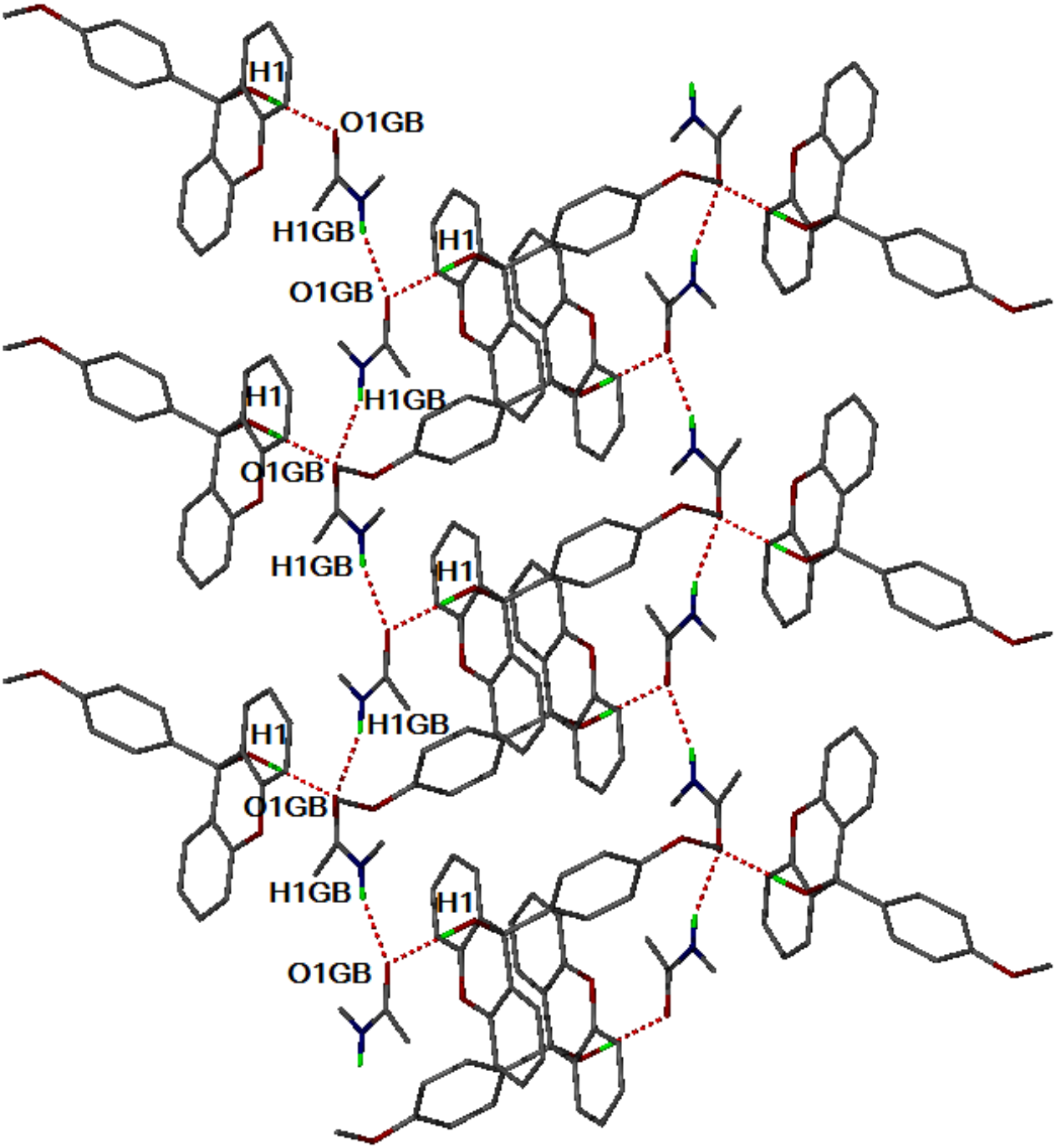

Figure 5.37: Hydrogen bonding in **A1·NMA.** Only the major guest is shown.

The C-H···π interaction between the host and guest molecules has a C···π (centroid) distance of 3.432 Å (Figure 5.38). The only C-H···π interaction between host molecules has a C···π distance of 4.213 Å with a C-H-π angle of 150°, shown in Figure 5.39.

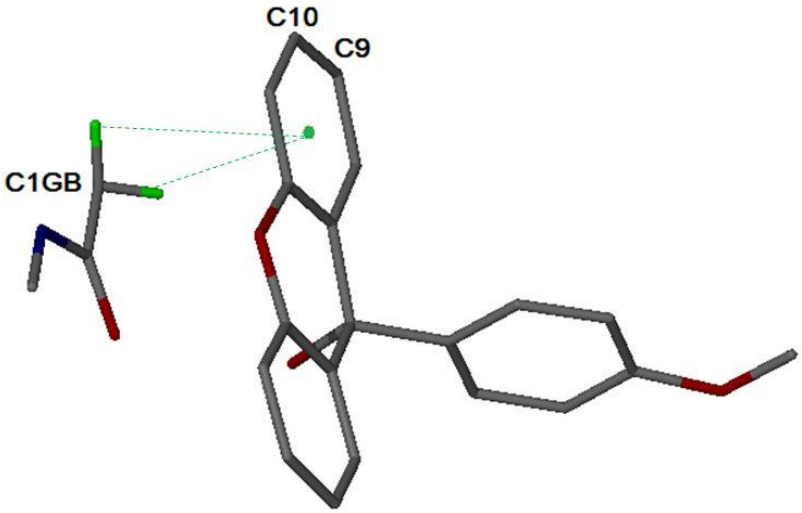

Figure 5.38: C-H···π interaction between a host and guest molecule. The C-H···π interactions are indicated by a green dotted line.

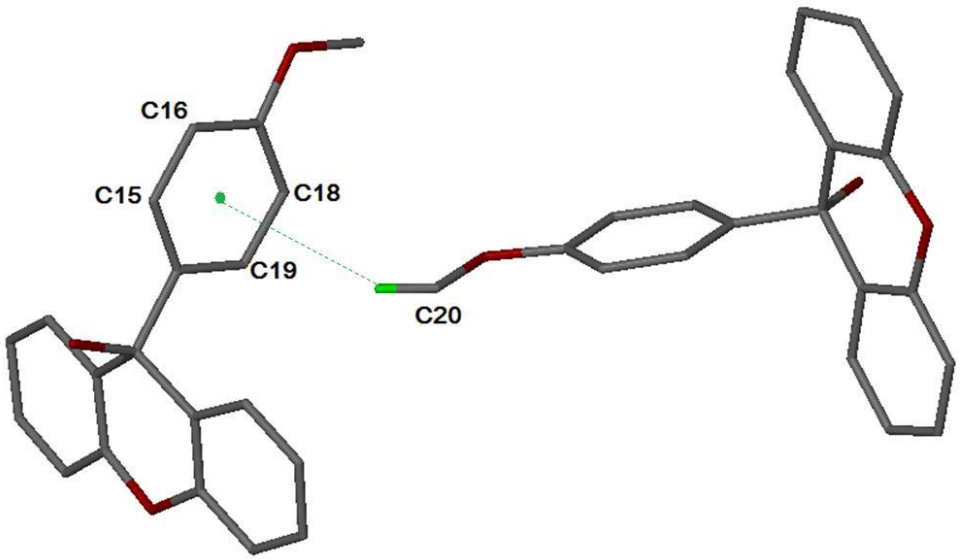

Figure 5.39: C-H···π interaction between host molecules. The C-H···π interaction is indicated by a green dotted line.

The packing diagrams of **A1·NMA** along the [010] direction are shown in Figure 5.40(a). Two host molecules form a dimer which is strengthend by (Host)-C19-H···O1-(Host) hydrogen bonds. The host molecules exhibit a zigzag arrangement shown in Figure 5.40(b). The host molecules pack around a centre of symmetry at Wyckoff position *a*. The guest molecules are located in zigzag channels down [010] shown in Figure 5.41. The zigzag channels are shown in Figure 5.42.[5]

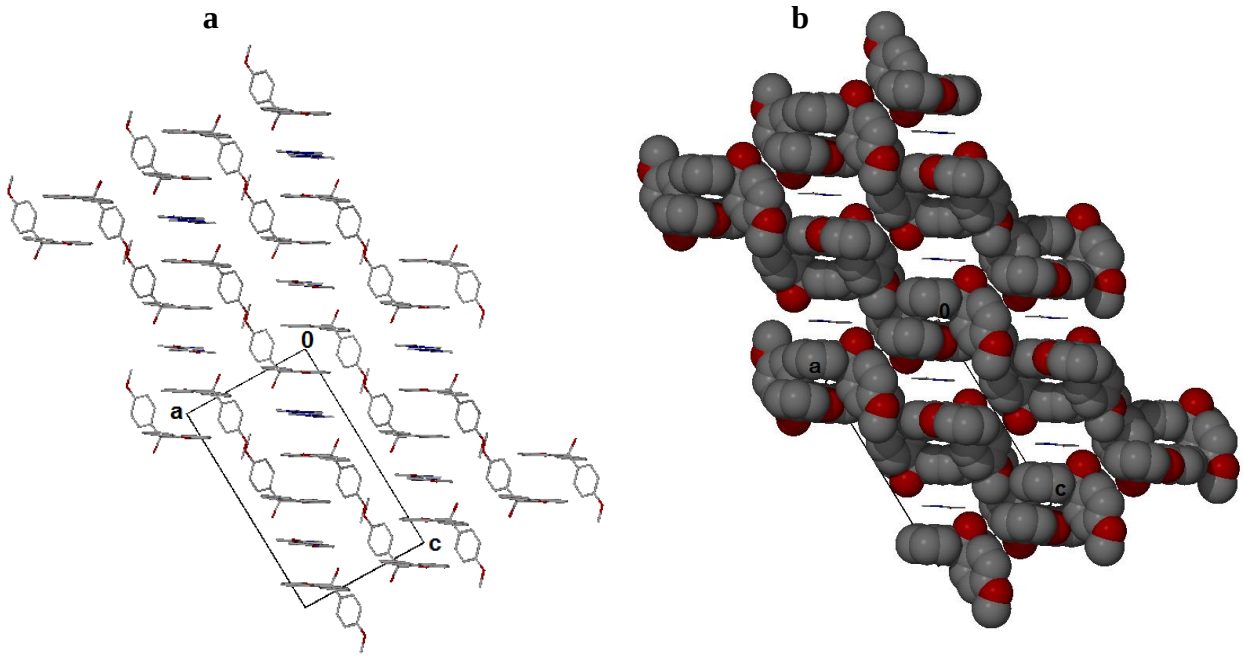

Figure 5.40: Packing diagram of **A1·NMA** viewed along [010] direction. All hydrogen atoms are omitted. (a) Packing diagram of host and guest. (b) The host molecules are shown as van der Waals radii and the guest molecules as sticks.

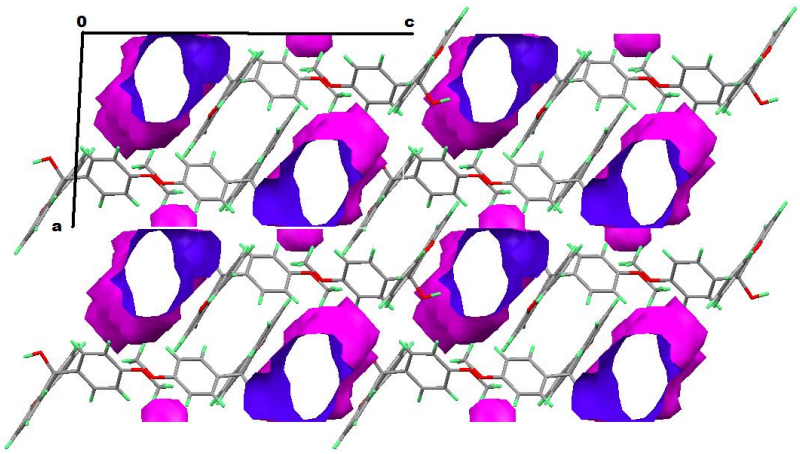

Figure 5.41: Channels down [010].

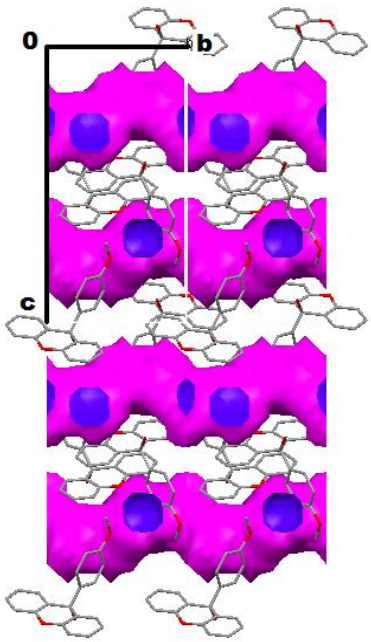

Figure 5.42: Zigzag channel.

5.5 Guest: N-methylacetamide

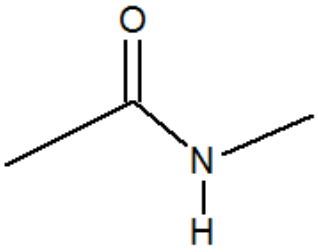

Table 5.22: Properties of *N*-methylacetamide.

Guest	NMA
Molecular formula	**C_3H_7NO**
Molar mass (g/mol)	**73.1**
Boiling Point (K)	**479**

5.5.1 Thermal Analysis

The thermal analysis results are listed in Table 5.23. The TG curve shows a single mass loss step of 32.2 %. The thermal analysis results are shown in Figure 5.43. The host-guest ratio was determined from the TG results and found to be 1:2. The DSC shows two endotherms at T_{on}=350.2 K and T_{on}=399.2 K. The first endotherm is a sharp peak which is due to guest release. The second peak (T_{on}=399.2 K) was assigned to the melting of the host.

Table 5.23: Thermal analysis data for **A1·2NMA.**

Compound	A1·2NMA
Host: Guest ratio	**1:2**
TG calculated % mass loss	**32.5**
TG experimental % mass loss	**32.2**
DSC $Endo_1$ (T_{onset}, K)	**350.2**
DSC $Endo_2$ (T_{onset}, K)	**399.2**
DSC Host (T_{onset}, K)	**395.3**

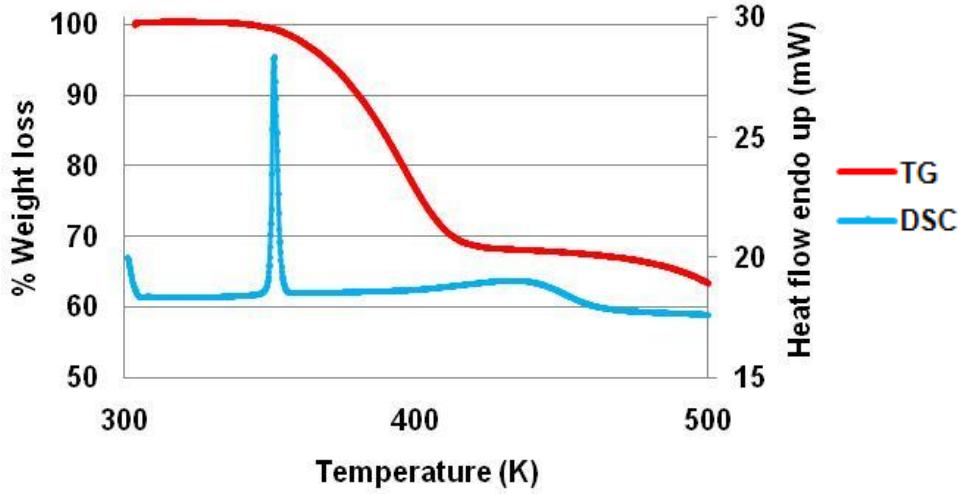

Figure 5.43: TGA and DSC curves obtained for **A1·2NMA.**

5.5.2 Structure Refinement

All non-hydrogen atoms were located by direct methods in the difference electron density map for both host molecules. All non-hydrogen atoms were refined anisotropically. The host hydroxyl hydrogen was first located in the difference electron density map and then refined with a simple bond length constraint dependent on the O···O distance[1] (major guest). Both NMA guests are disordered and were solved by parts (part 1=GA, part 2=GB, part 3=GC and part 4=GD). The crystal data is given in Table 5.24. The structure refined successfully to R_1= 0.0533 with wR_2= 0.1119.

Table 5.24: Crystal data of **A1·2NMA.**

Compound	**A1·2NMA**
Structural Formula	**$C_{20}H_{16}O_3 \cdot 2C_3H_7NO$**
Host-Guest ratio	**1:2**
Molecular Mass (g.mol^{-1})	**450.52**
Data collection temp (K)	**173**
Crystal system	**Triclinic**
Space group	**$P\bar{1}$**
a (Å)	**9.1195(8)**
b (Å)	**9.8215(9)**
c (Å)	**14.7418(12)**
α (°)	**87.010(2)**
β (°)	**89.262(2)**
γ (°)	**64.417(2)**
Volume (Å^3)	**1189.24(18)**
Z	**2**
μ/ mm^{-1}	**0.087**
F(000)	**480**
No. of reflections collected	**10688**
No. of unique reflection	**5956**
No. of reflections with I>2σ(I)	**3337**
D_c, Calculated density (g.cm^{-3})	**1.285**
Index range	**h: -11 to 12, k: -13 to 13, l: -16 to 19**
θ range	**1.38-28.41**
Goodness of fit, S	**0.970**
Final R indices [I>2σ(I)]	**R_1= 0.0533 ; wR_2= 0.1119**
R indices (all data)	**R_1= 0.1132; wR_2= 0.1433**
Largest diff peak and hole (eÅ^{-3})	**0.22 ; -0.26**

5.5.3 Discussion

The structure was solved in the triclinic space group $P\bar{1}$ with Z=2. The asymmetric unit of **A1·2NMA** contains a host and two disordered guest molecules located in general positions shown in Figure 5.44, and has a structural formula of $C_{20}H_{16}O_3 \cdot 2C_3H_7NO$. Both NMA guests are disordered over two positions (Figure 5.45). The major NMA guests have suffixes GB and GC with site occupancy factors of 0.63 and 0.81 respectively. The host's hydroxyl and methoxyl groups have a *trans* configuration with respect to one another. Selected torsion angles of the host molecule are given in Table 5.25.

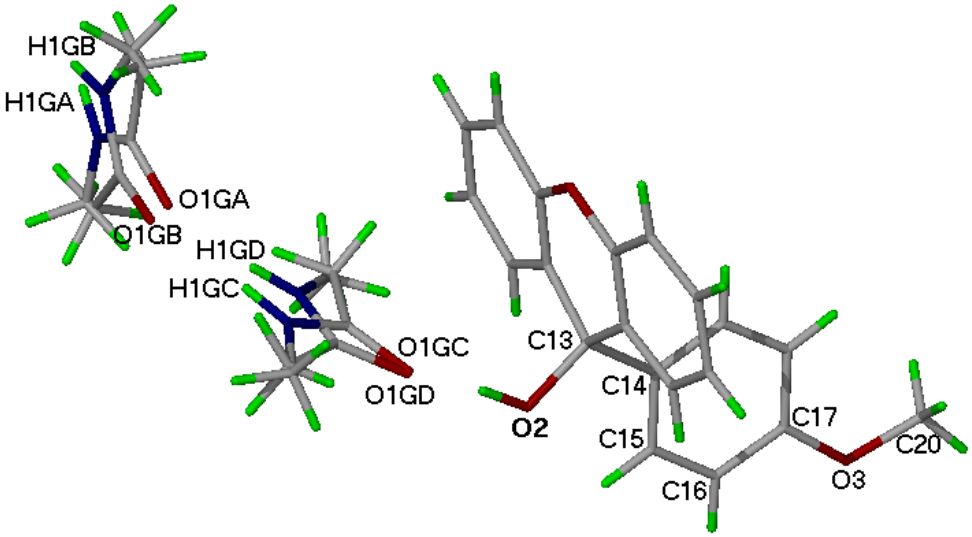

Figure 5.44: Asymmetric unit of **A1·2NMA.**

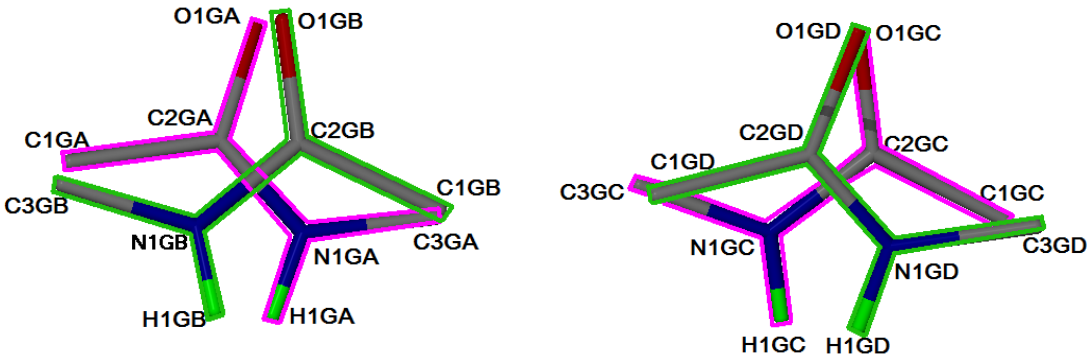

Figure 5.45: Disordered NMA guests.

Table 5.25: Conformation parameters of host molecule in **A1·2NMA**.

τ_1= O2-C13-C14-C15/°	τ_2= C20-O3-C17-C16/°	Host conformation
0.2(2)	-171.8(2)	*Trans* conformation

The structure is stabilised by (Host)-OH···O-(Guest) and (Guest)-NH···O-(Guest) hydrogen bonds. The hydrogen bonding parameters are provided in Table 5.26. The hydrogen bonding between hosts and disordered guests are shown in Figure 5.46. The hydrogen bonding between hosts and major guests are shown in Figure 5.47. The hydrogen bonding pattern may be described as $C_3^3(11)$ according to Etter's graph set notation.[4]

Table 5.26: Hydrogen bond parameters of **A1·2NMA**.

Donor(D)-H	Acceptor(A)	D···A (Å)	D-H (Å)	H···A (Å)	D-H···A (°)
O2-H1	**O1GC**	**2.760(4)**	**0.960(1)**	**1.810(1)**	**170(2)**
O2-H1	**O1GD**	**2.76(2)**	**0.960(1)**	**1.81(3)**	**169(2)**
N1GD-H1GD	**O1GA**	**2.68(4)**	**0.880(1)**	**1.802(1)**	**173(1)**
N1GC-H1GC	**O1GA**	**2.76(4)**	**0.880(1)**	**1.883(1)**	**172 (1)**
N1GD-H1GD	**O1GB**	**2.78(3)**	**0.880(1)**	**1.905(1)**	**172(1)**
N1GC-H1GC	**O1GB**	**2.81(2)**	**0.880(1)**	**1.939(1)**	**176(1)**
N1GA-H1GA	**O1GC [1+x, y, z]**	**2.94(1)**	**0.880(1)**	**2.086(1)**	**163(1)**
N1GA-H1GA	**O1GD [1+x, y, z]**	**2.92(3)**	**0.880(1)**	**2.065(1)**	**162(1)**
N1GB-H1GB	**O1GC [1+x, y, z]**	**2.929(7)**	**0.880(1)**	**2.051(1)**	**174(1)**
N1GB-H1GB	**O1GD [1+x, y, z]**	**2.92(3)**	**0.880(1)**	**2.036(1)**	**176(1)**

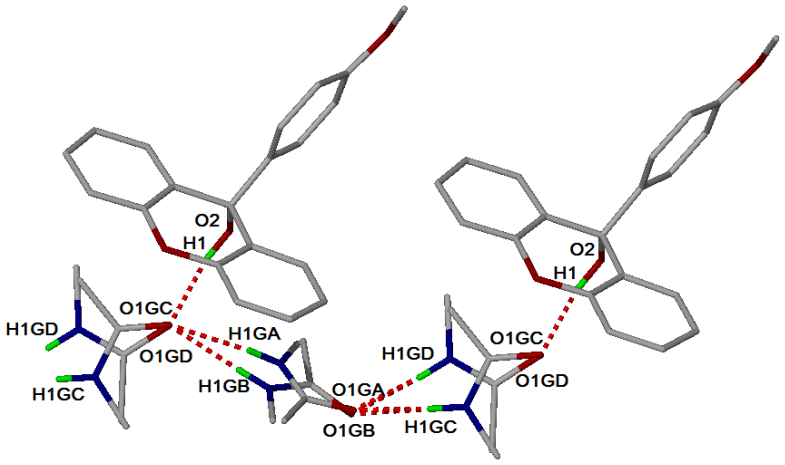

Figure 5.46: Hydrogen bonding in **A1·2NMA.** The disordered guests are shown.

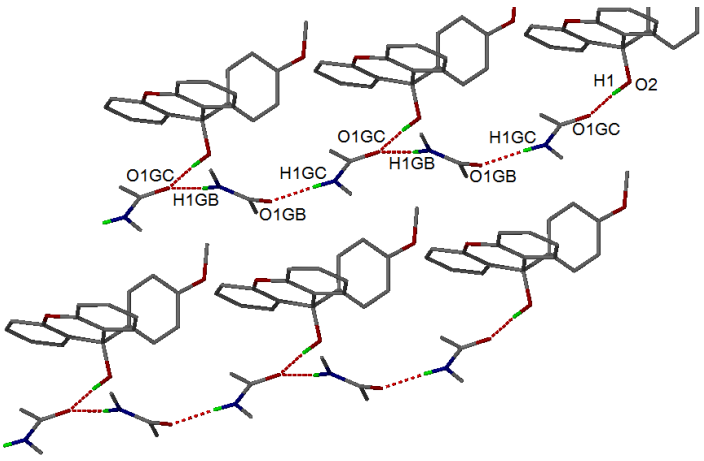

Figure 5.47: Hydrogen bonding in **A1·2NMA.** Only the major guest is shown.

Only the major guests (GB and GC) display C-H···π interactions with the host. The shortest C···π distance of the C-H···π interactions between host and guest molecules is 3.484 Å [C(1GC)···π(centroid)], shown in Figure 5.48. Edge-to-face π- π interactions are observed between hosts. The C-H···π interactions between host molecules have C···π distances of C10···π = 3.698 Å and C20···π = 3.708 Å, with C-H-π angles of 143° and 147° respectively, shown in Figure 5.49.

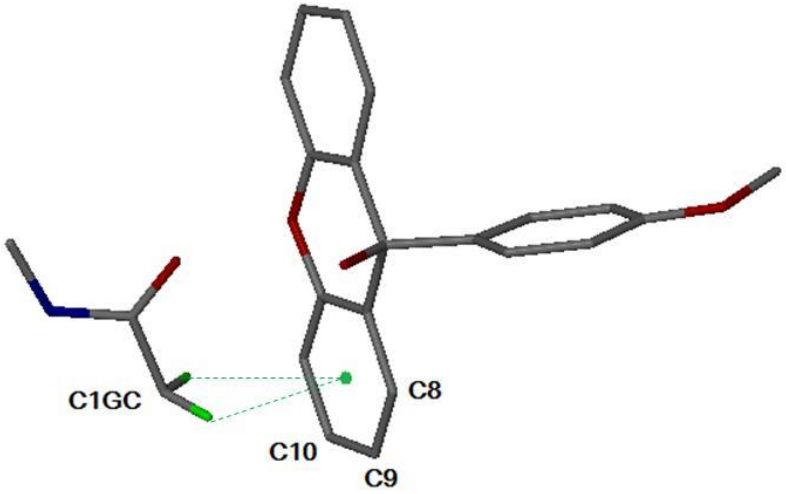

Figure 5.48: C-H···π interaction between a host and guest molecule. The C-H···π interactions are indicated by a green dotted line.

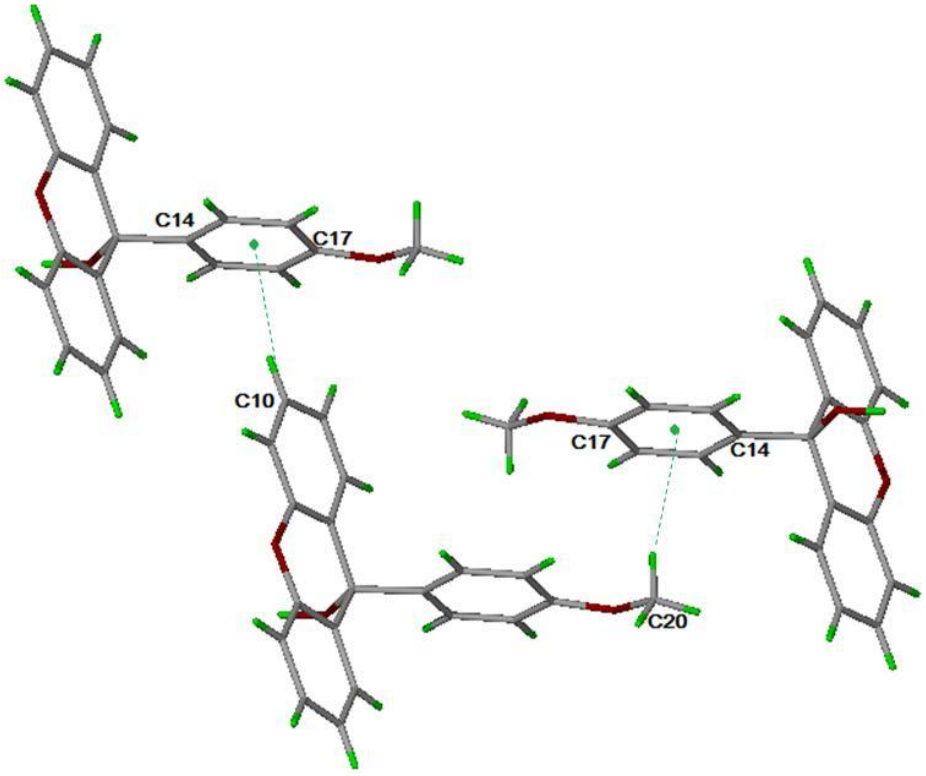

Figure 5.49: C-H···π interaction between host molecules. The C-H···π interactions are indicated by green dotted lines.

The packing diagrams of **A1·2NMA** along [100] are shown in Figure 5.50. Both guests occupy the same channel down [100] as shown in Figure 5.50(b). When viewed along the [100] direction, as space fill representation, the host molecules exhibit an S shape arrangement. The guest molecules are located in open channels down [100], illustrated in Figure 5.51.[5] The shape of the open channels is shown in Figure 5.52.

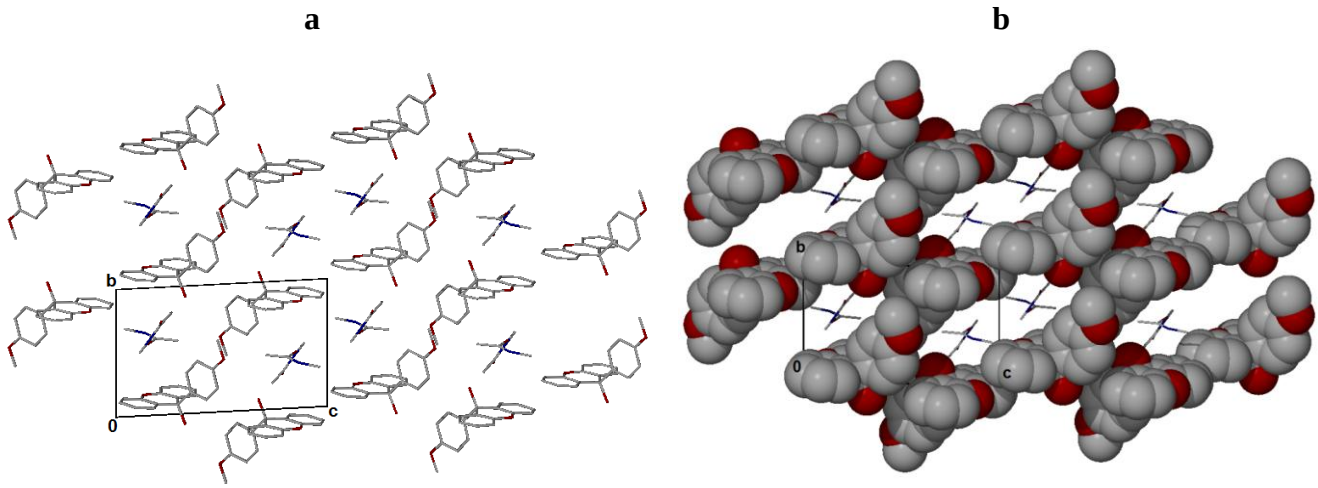

Figure 5.50: Packing diagram of **A1·2NMA** viewed along [100] direction. All hydrogen atoms are omitted. (a) Packing diagram of host and guest. (b) The host molecules are shown as van der Waals radii and the guest molecules as sticks.

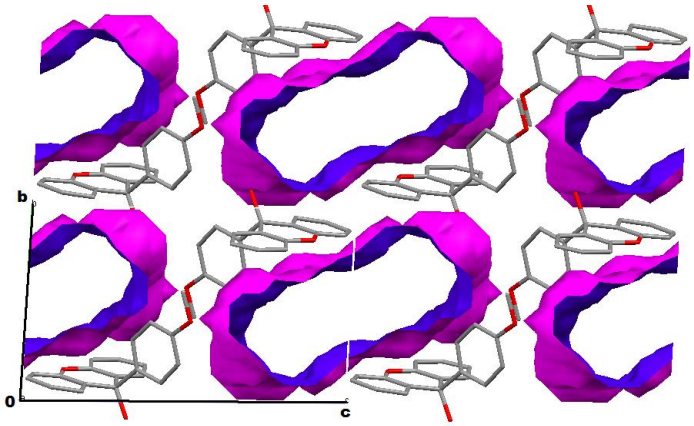

Figure 5.51: Open channels down [100].

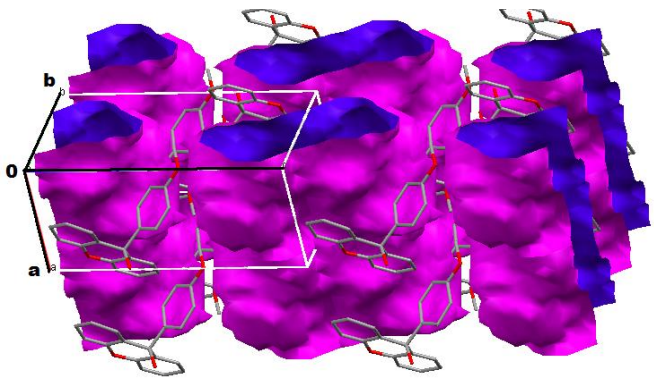

Figure 5.52: Shape of the channels.

5.6 Guest: N-methylacetamide

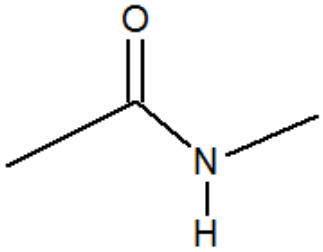

Table 5.27: Properties of *N*-methylacetamide.

Guest	NMA
Molecular formula	**C_3H_7NO**
Molar mass (g/mol)	**73.1**
Boiling Point (K)	**479**

5.6.1 Thermal Analysis

The thermal analysis data is given in Table 5.28. A single step mass loss of 19.4 % was observed in the TG curve which corresponds to a 1:1 host-guest ratio. Two endotherms are observed for the **2A1·2NMA** inclusion compound. The first endotherm (T_{on}=333.4 K) is due to the loss of the guest. The peak at T_{on} =394.5 K corresponds to the melting point of the host. The thermal analysis results are shown in Figure 5.53.

Table 5.28: Thermal analysis data for **2A1·2NMA.**

Compound	2A1·2NMA
Host: Guest ratio	**1:1**
TG calculated % mass loss	**19.4**
TG experimental % mass loss	**19.4**
DSC Endo$_1$ (T_{onset}, K)	**333.4**
DSC Endo$_2$ (T_{onset}, K)	**394.5**
DSC Host (T_{onset}, K)	**395.3**

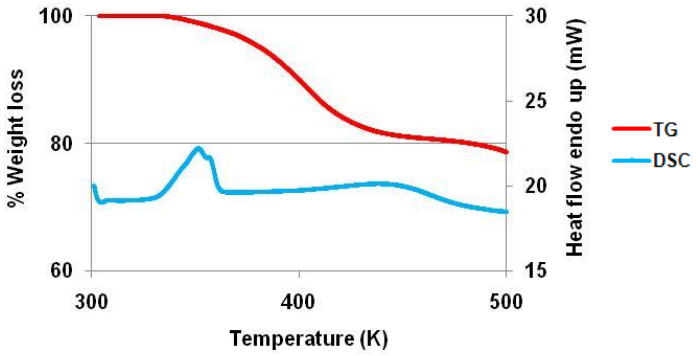

Figure 5.53: TGA and DSC curves obtained for **2A1·2NMA.**

5.6.2 Hot Stage Microscopy

(a) The crystals are immersed in silicone oil.
(b) The crystals become clear and bubbles appear as the guest is released.
(c) The crystals begin to melt.
(d) The host melt is complete.

(a) 298 K **(b) 331 K** **(c) 361 K** **(d) 378 K**

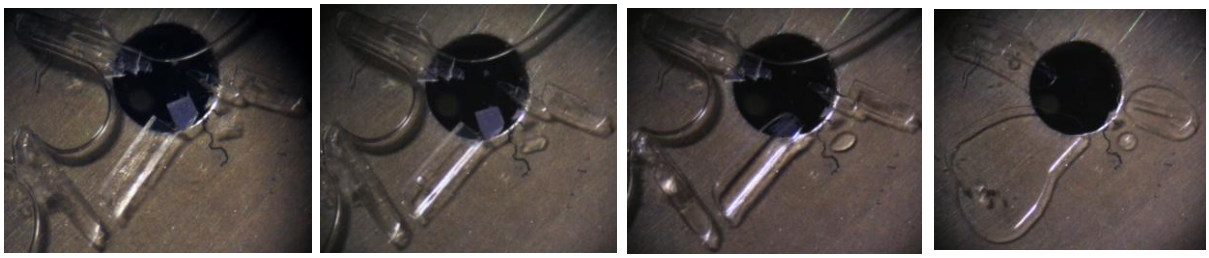

Figure 5.54: HSM photographs of **2A1·2NMA.**

5.6.3 Structure Refinement

All non-hydrogen atoms were located by direct methods in the difference electron density map. All non-hydrogen atoms were refined anisotropically except for the disordered guest atoms which were refined isotropically. The hydroxyl hydrogen of the hosts was located in the difference electron density map and then refined with a simple bond length constraint dependent on the O···O distance[1] (major guest). The guest hydrogen (H1G) was found in the electron density map. The disordered guests were solved by parts (part 1=GA and part 2=GB). The inclusion compound **2A1·2NMA** refined successfully to R_1= 0.0485 with wR_2= 0.1233. The crystal data is given in Table 5.29.

Table 5.29: Crystal data of **2A1·2NMA.**

Compound	**2A1·2NMA**
Structural Formula	**$2C_{20}H_{16}O_3 \cdot 2C_3H_7NO$**
Host-Guest ratio	**1:1**
Molecular Mass (g.mol^{-1})	**754.85**
Data collection temp (K)	**173**
Crystal system	**Triclinic**
Space group	**$P\bar{1}$**
a (Å)	**9.4556(19)**
b (Å)	**11.632(2)**
c (Å)	**18.736(4)**
α (°)	**84.15(3)**
β (°)	**76.15(3)**
γ (°)	**78.14(3)**
Volume (Å^3)	**1955.0(7)**
Z	**2**
μ/ mm^{-1}	**0.088**
F(000)	**800**
No. of reflections collected	**7403**
No. of unique reflection	**7403**
No. of reflections with I>2σ(I)	**4281**
D_c, Calculated density (g.cm^{-3})	**1.282**
Index range	**h: 0 to 11, k: -13 to 14, l: -21 to 22**
θ range	**1.12-25.69**
Goodness of fit, S	**1.059**
Final R indices [I>2σ(I)]	**R_1= 0.0485 ; wR_2= 0.1233**
R indices (all data)	**R_1= 0.1097; wR_2= 0.1716**
Largest diff peak and hole (eÅ^{-3})	**0.38 ; -0.38**

5.6.4 Discussion

The inclusion compound of **2A1·2NMA** has a structural formula of $2C_{20}H_{16}O_3 \cdot 2C_3H_7NO$ with a host-guest ratio of 1:1. The structure was solved in the triclinic space group $P\bar{1}$. The asymmetric unit contains two independent host and two independent guest molecules located in general postions shown in Figure 5.55. One NMA guest is disordered over two positions shown in Figure 5.56. The disordered NMA guests GA and GB have site occupancy factors of 0.26 and 0.74 respectively. The host molecule's methoxy group has a *trans* configuration with respect to the hydroxyl moiety in both host molecules. Selected torsion angles of the host molecule are given in Table 5.30.

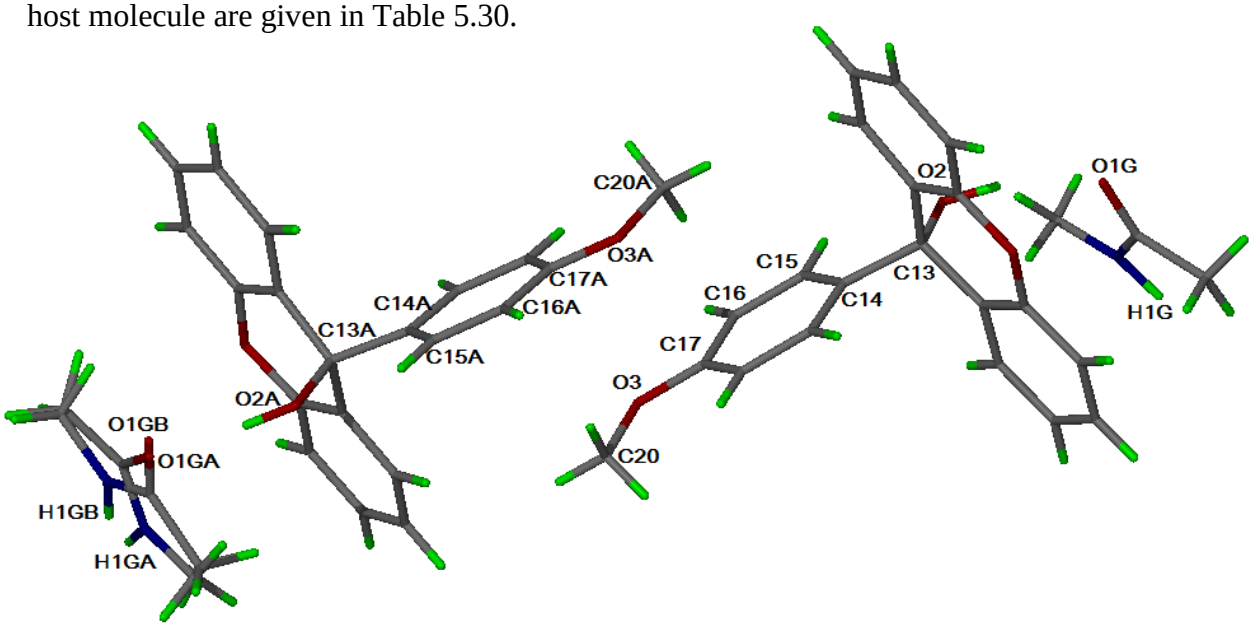

Figure 5.55: Asymmetric unit of **2A1·2NMA.**

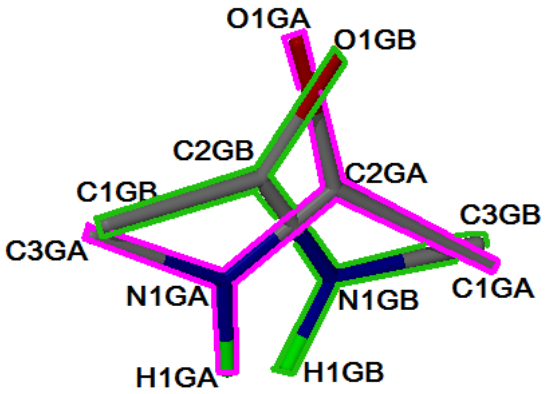

Figure 5.56: Disordered **NMA** guest.

Table 5.30: Conformation parameters of host molecule in **2A1·2NMA**.

Suffix	τ_1= O2-C13-C14-C15/°	τ_2= C20-O3-C17-C16/°	Host conformation
-	-1.6(3)	177.7(2)	*Trans* conformation
A	-7.0(3)	-172.6(2)	*Trans* conformation

The structure is stabilised by (Host)-OH···O-(Guest) and (Guest)-NH···O-(Guest) hydrogen bonds. The hydrogen bonding parameters are provided in Table 5.31. The hydrogen bonding between the host and guest molecules are depicted in Figures 5.57 and 5.58. The hydrogen bonding pattern may be described as $C_4^2(11)$ according to Etter's graph set notation.[4]

Table 5.31: Hydrogen bond parameters of **2A1·2NMA**.

Donor(D)-H	Acceptor(A)	D···A (Å)	D-H (Å)	H···A (Å)	D-H···A (°)
O2-H1	**O1G**	**2.790(2)**	**0.960(1)**	**1.879(1)**	**157(6)**
O2A-H1A	**O1GA**	**2.812(8)**	**0.965(1)**	**1.849(8)**	**175(2)**
O2A-H1A	**O1GB**	**2.833(3)**	**0.965(1)**	**1.881(1)**	**168(1)**
N1GA-H1GA	**O1G[x, y, z-1]**	**3.028(1)**	**0.880(1)**	**2.159(1)**	**169(1)**
N1GB-H1GB	**O1G[x, y, z-1]**	**2.844(4)**	**0.880(1)**	**2.024(1)**	**155(1)**
N1G-H1G	**O1GA[x-1, y, z+1]**	**3.016(9)**	**0.880(1)**	**2.11(5)**	**150(4)**
N1G-H1G	**O1GB[x-1, y, z+1]**	**2.906(4)**	**0.880(1)**	**2.02(5)**	**146(4)**

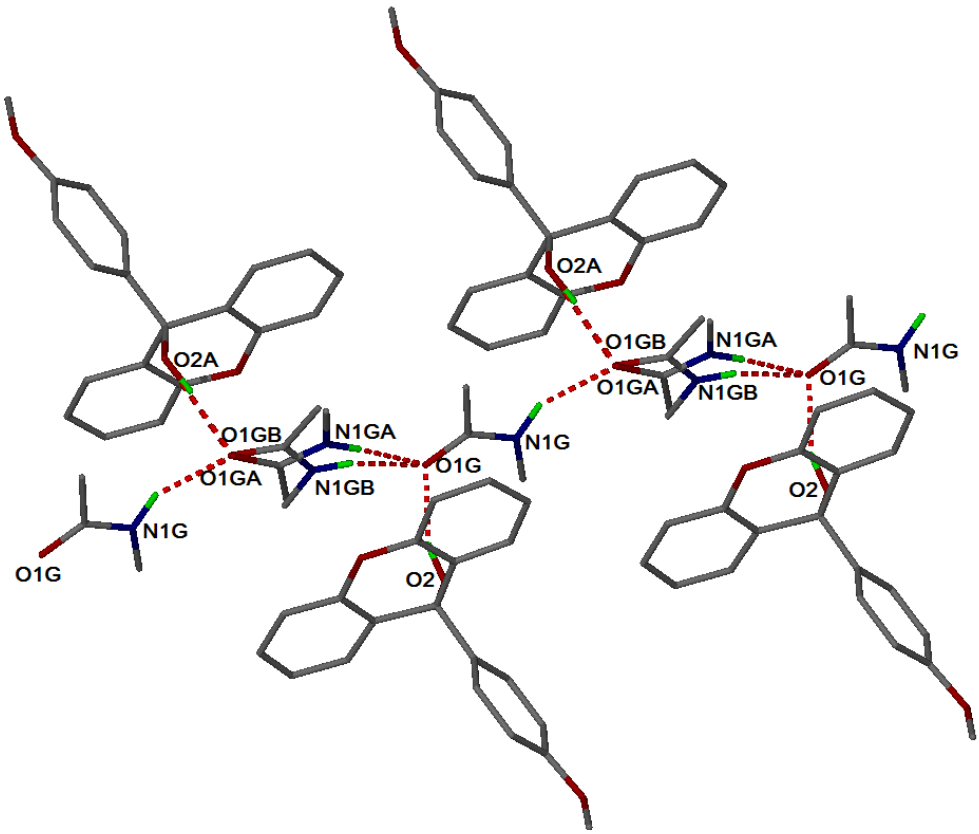

Figure 5.57: Hydrogen bonding in **2A1·2NMA.** The disordered guests are shown.

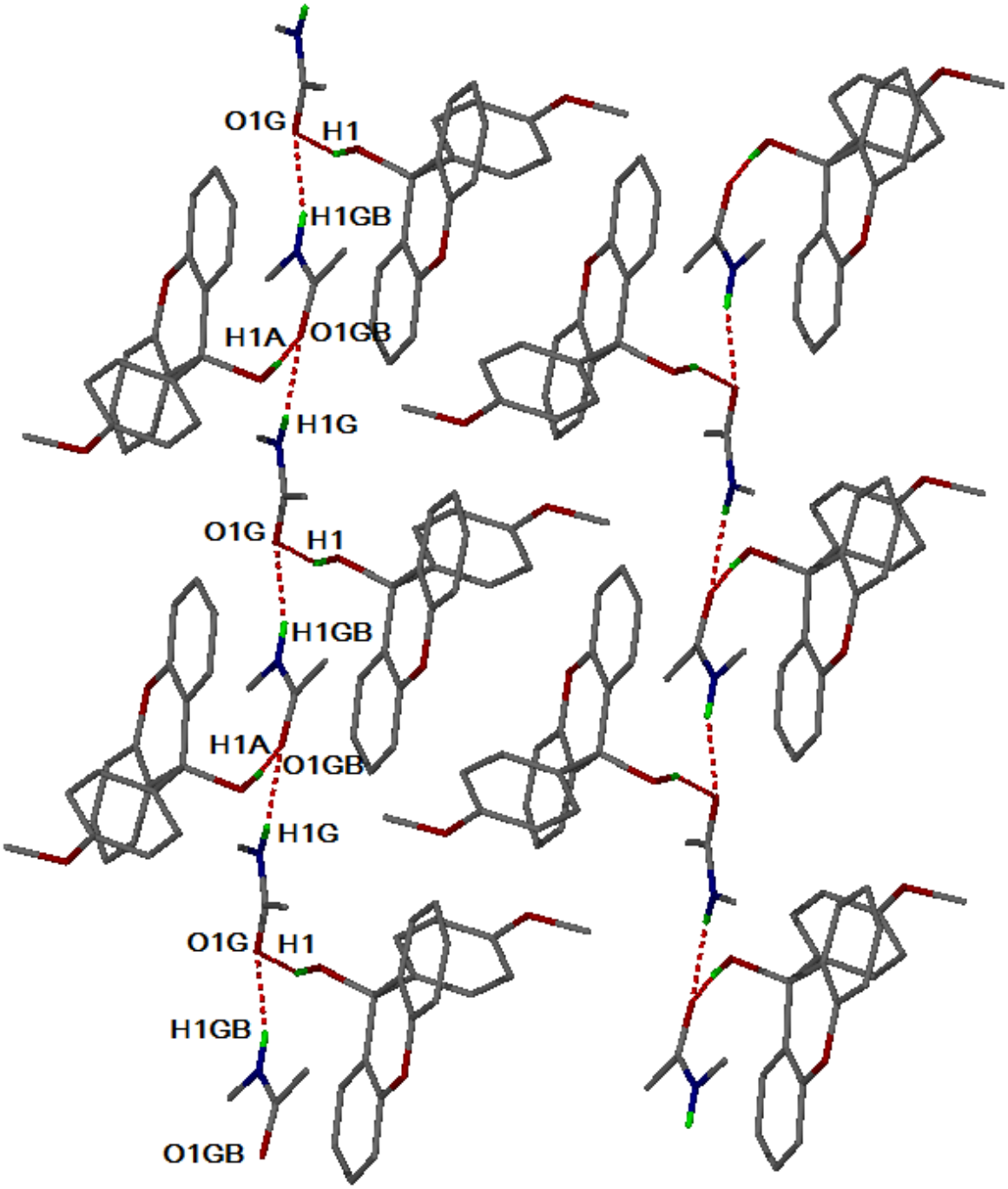

Figure 5.58: Hydrogen bonding in **2A1·2NMA.** Only the major guest is shown.

A number of C-H···π interactions are observed in this structure. The shortest C···π distance between the host and the guest molecule is 3.464 Å with a C-H-π angle of 149°, shown in Figure 5.59. The shortest C···π distance between a pair of host molecules is 3.774 Å with a C-H-π angle of 137°, shown in Figure 5.60. The host molecule displays edge-to-face π- π interactions. Pairs of host molecules form dimers which are strengthened by (Host)-C19-H···O1-(Host) hydrogen bonds.

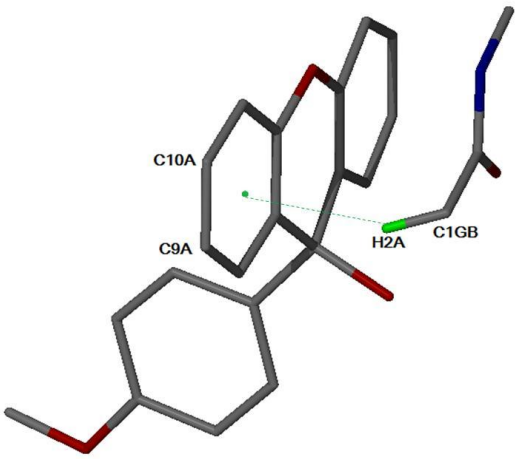

Figure 5.59: C-H···π interaction between a host and guest molecule. The C-H···π interaction is indicated by a green dotted line.

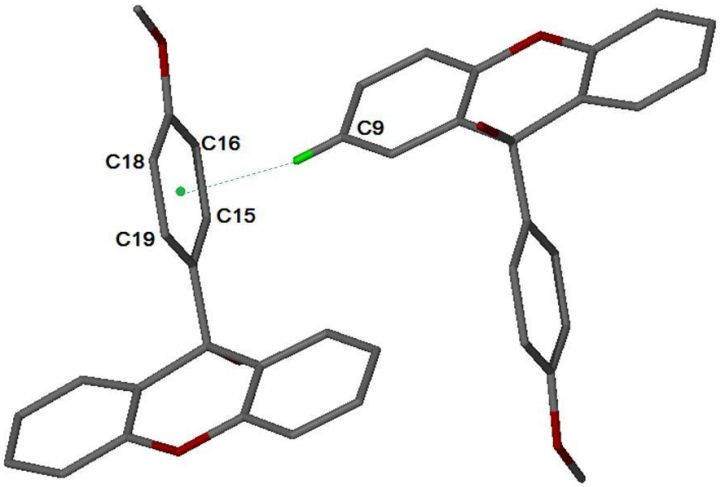

Figure 5.60: C-H···π interaction between host molecules. The C-H···π interaction is indicated by a green dotted line.

The packing diagrams of **2A1·2NMA** viewed along the [100] direction are shown in Figure 5.61(a). When shown in space fill representation, the host molecules exhibits a zigzag arrangement shown in Figure 5.61(b). The constricted channels in which the guests are located are parallel to [100] shown in Figure 5.62.[5]

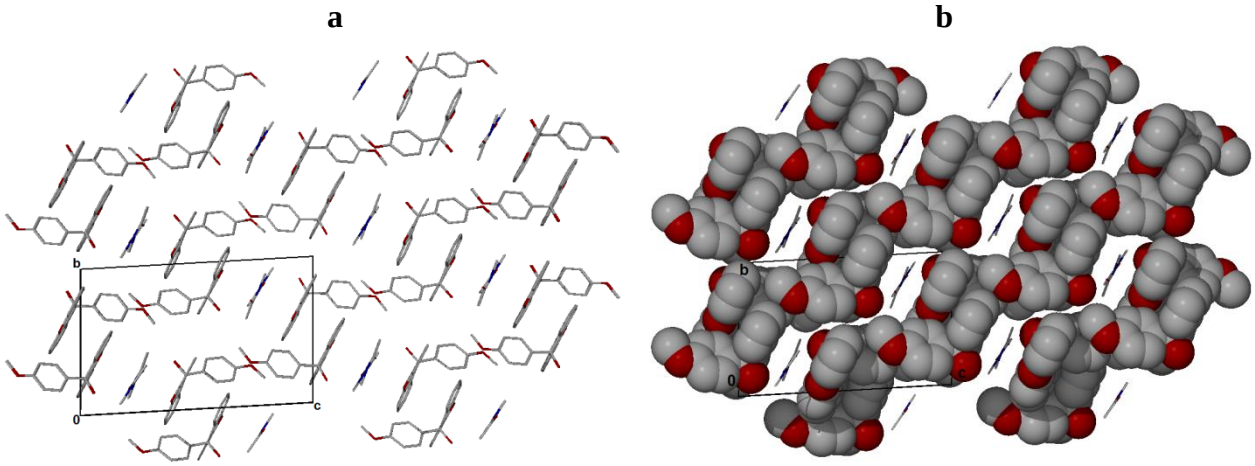

Figure 5.61: Packing diagram of **2A1·2NMA** viewed along the [100] direction. All hydrogen atoms are omitted. (a) Packing diagram of host and guest. (b) The host molecules are shown as van der Waals radii and the guest molecules as sticks.

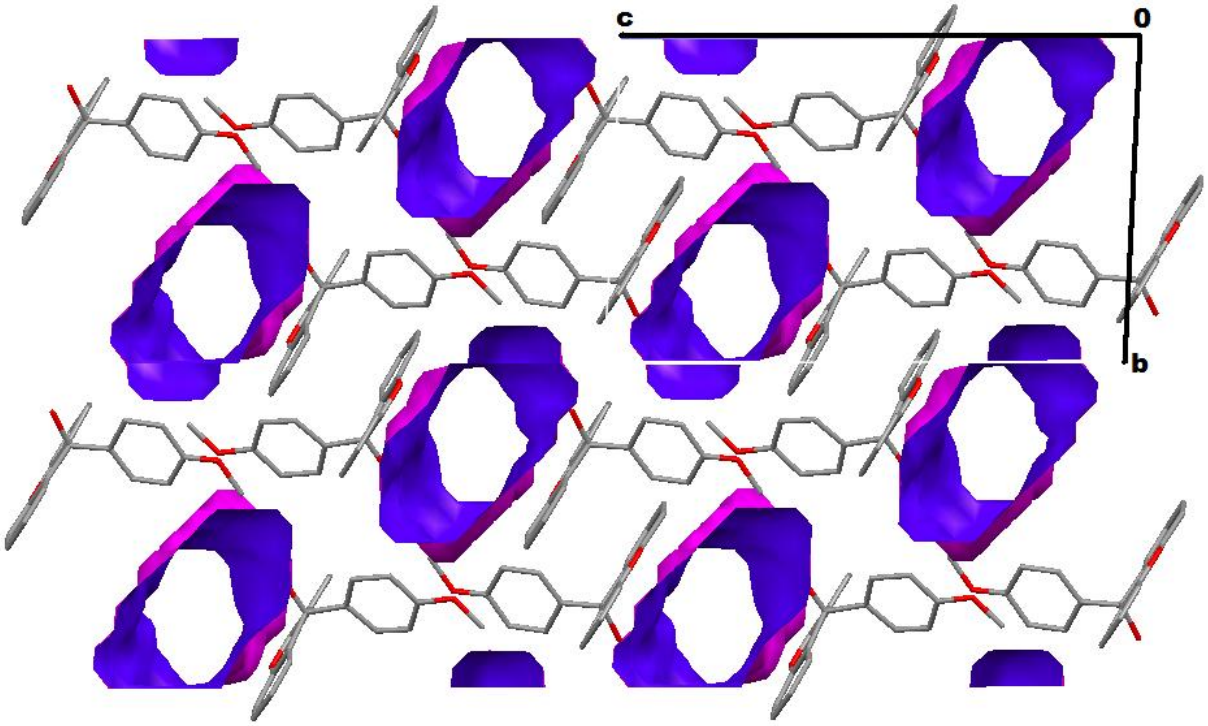

Figure 5.62: Channels down [100].

5.7 Guest: N-methylformamide

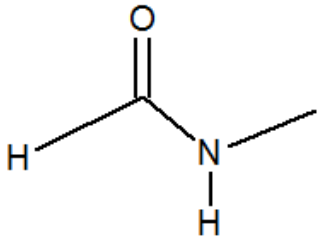

Table 5.32: Properties of *N*-methylformamide.

Guest	NMF
Molecular formula	**C_2H_5NO**
Molar mass (g/mol)	**59.1**
Boiling Point (K)	**453-458**

5.7.1 Thermal Analysis

The TG curve shows a two-step mass loss. The thermal analysis results are shown in Figure 5.63. The first step is 4.6 % which corresponds to the loss of a water molecule. The second mass loss is 15.2 % which corresponds to the loss of the NMF guest. The total mass loss for the two steps corresponds to the loss of both guests. The host-guest ratio was determined from the TG results and found to be 1:1. On the DSC trace, the first endotherm (T_{on}=334.1 K) is complex because it is due to the loss of water and NMF. The second broad endotherm (T_{on}=402.7 K) is due to the melt of the host compound. The thermal analysis data is given in Table 5.33.

Table 5.33: Thermal analysis data for **A1·NMF·H_2O.**

Compound	A1·NMF·H_2O
Host: Guest ratio	**1:1**
TG calculated % mass loss	**20.2**
TG experimental % mass loss	**19.8**
DSC Endo$_1$ (T_{onset}, K)	**334.1**
DSC Endo$_2$ (T_{onset}, K)	**402.7**
DSC Host (T_{onset}, K)	**395.3**

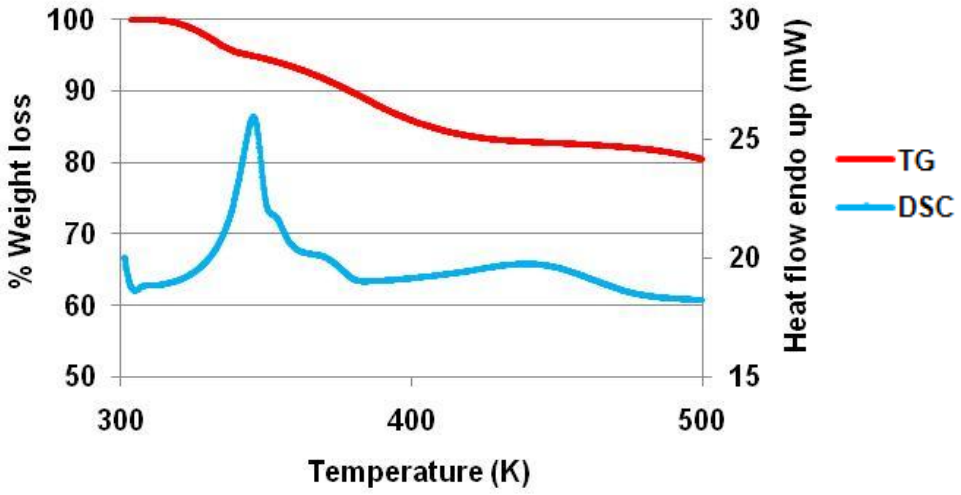

Figure 5.63: TGA and DSC curves obtained for **A1·NMF·H_2O.**

5.7.2 Structure Refinement

All non-hydrogen atoms were found by direct methods in the difference electron density map and refined anisotropically. The hydroxyl hydrogen was first located in the difference electron density map and then refined with a simple bond length constraint dependent on the O···O distance.[1] The hydrogen atoms attached to the water molecule were found in the difference electron density map and then the OH distances were geometrically constrained. The structure refined successfully to R_1= 0.0489 with wR_2= 0.1160. The crystal data is given in Table 5.34.

Table 5.34: Crystal data of **A1·NMF·H_2O.**

Compound	**A1·NMF·H_2O**
Structural Formula	**$C_{20}H_{16}O_3$ ·C_2H_5NO·H_2O**
Host-Guest ratio	**1(host):1(guest 1):1(guest 2)**
Molecular Mass (g.mol^{-1})	**381.41**
Data collection temp (K)	**173**
Crystal system	**Triclinic**
Space group	**$P\bar{1}$**
a (Å)	**9.0578(18)**
b (Å)	**9.6575(19)**
c (Å)	**12.644(3)**
α (°)	**102.32(3)**
β (°)	**108.68(3)**
γ (°)	**100.49(3)**
Volume (Å^3)	**985.4(3)**
Z	**2**
μ/ mm^{-1}	**0.091**
F(000)	**404**
No. of reflections collected	**4490**
No. of unique reflection	**4490**
No. of reflections with I>2σ(I)	**3282**
D_c, Calculated density (g.cm^{-3})	**1.285**
Index range	**h: 0 to 11, k: -12 to 12, l: -16 to 15**
θ range	**1.78-27.48**
Goodness of fit, S	**1.129**
Final R indices [I>2σ(I)]	**R_1= 0.0489 ; wR_2= 0.1160**
R indices (all data)	**R_1= 0.0794; wR_2= 0.1426**
Largest diff peak and hole (eÅ^{-3})	**0.34 ; -0.30**

5.7.3 Discussion

The **A1·NMF·H_2O** structure was solved in the triclinic space group $P\bar{1}$ with Z=2. The asymmetric unit contains A1, NMF and a water molecule in general positions with structural formula of $C_{20}H_{16}O_3 \cdot C_2H_5NO \cdot H_2O$. The hydrogen bonding in the asymmetric unit of **A1·NMF·H_2O** is illustrated in Figure 5.64.

The torsion angles observed for **A1·NMF·H_2O** are provided in Table 5.35. These values are close to zero which implies that the conformation of the methoxyl group of the host molecule is *cis* with respect to the hydroxyl moiety.

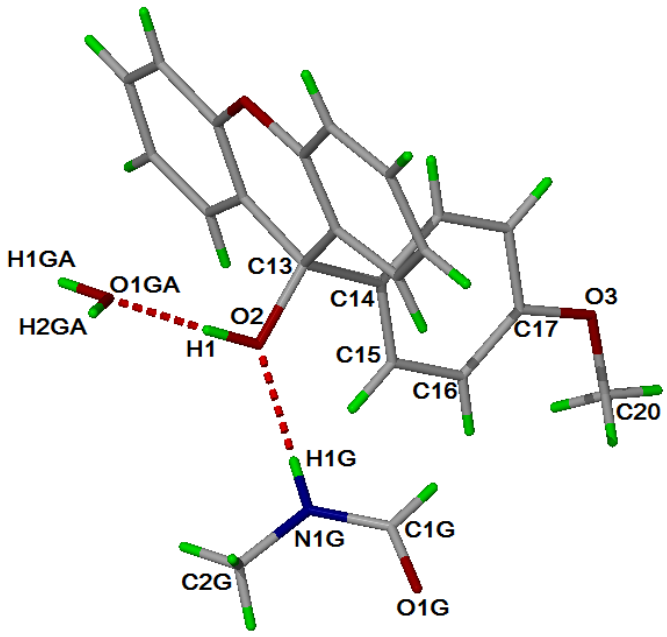

Figure 5.64: Hydrogen bonding in asymmetric unit of **A1·NMF·H_2O.**

Table 5.35: Conformation parameters of host molecule in **A1·NMF·H_2O**.

τ_1= O2-C13-C14-C15/°	τ_2= C20-O3-C17-C16/°	Host conformation
6.6(2)	**2.8(3)**	***Cis* conformation**

The structure is stabilised by OH···O and NH···O hydrogen bonds, shown in Figure 5.65. The hydrogen bond parameters are provided in Table 5.36. The hydrogen bond pattern consists of repeating NMF and water molecules forming a cyclic pattern which may be described as $R_4^2(8)$.[4] Another hydrogen bond pattern is observed between the host, NMF and water molecules and can be described as $R_6^6(16)$.

Table 5.36: Hydrogen bond parameters of **A1·NMF·H_2O**.

Donor(D)-H	Acceptor(A)	D···A (Å)	D-H (Å)	H···A (Å)	D-H···A (°)
O2-H1	**O1GA**	**2.665(2)**	**0.985(1)**	**1.680(1)**	**177(2)**
N1G-H1G	**O2**	**2.932(2)**	**0.904(3)**	**2.033(3)**	**173(2)**
O1GA-H1GA	**O1G[x-1, y, z]**	**2.784(2)**	**0.963(1)**	**1.831(5)**	**170(2)**
O1GA-H2GA	**O1G[-x-1, -y, -z]**	**2.803(2)**	**0.965(1)**	**1.844(5)**	**172(3)**

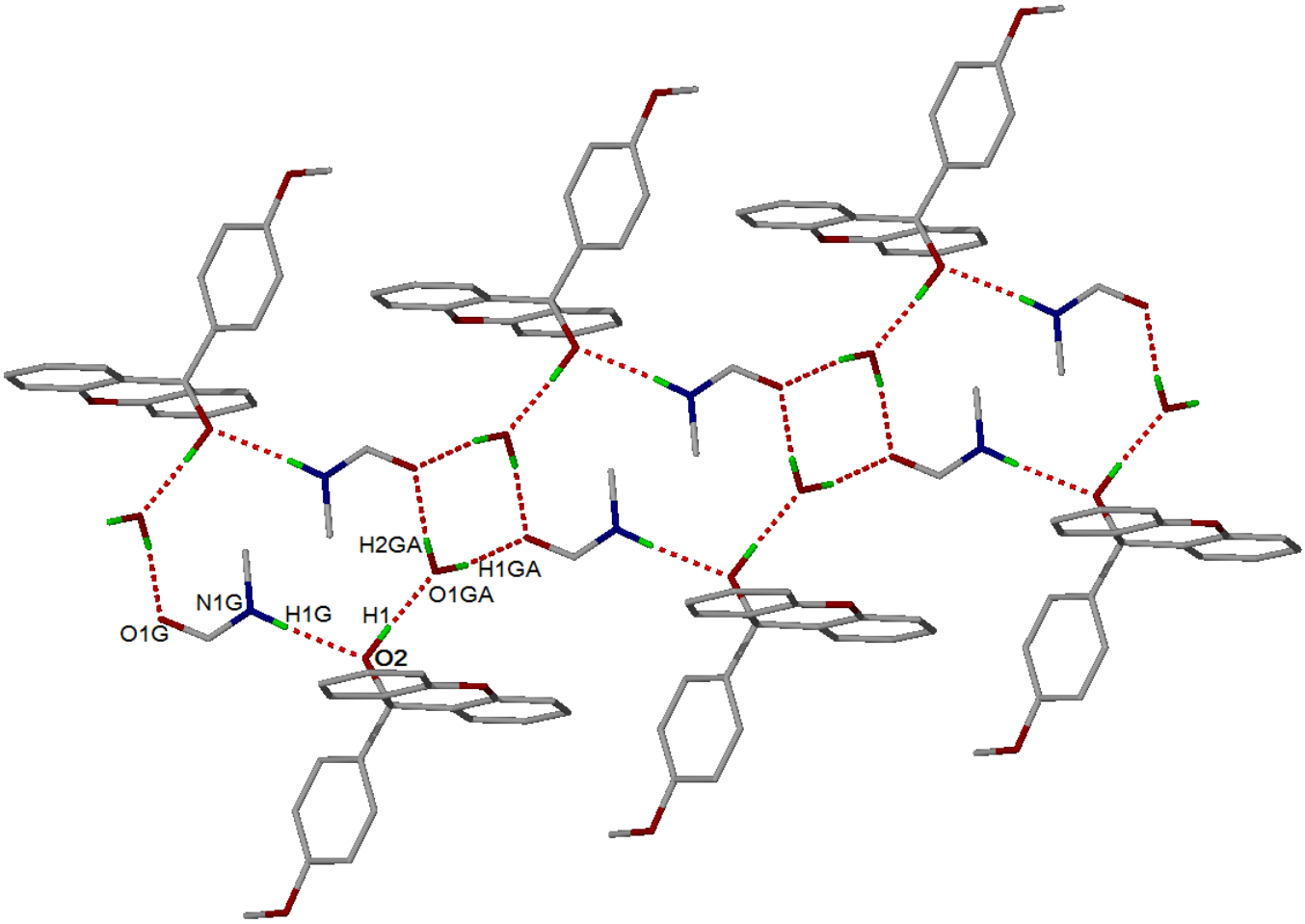

Figure 5.65: Hydrogen bonding in **A1·NMF·H_2O.** All hydrogen atoms were omitted except those involved in hydrogen bonding.

The C-H···π interactions observed for **A1·NMF·H_2O** are shown in Figures 5.66 and 5.67. The C-H···π parameters are provided in Table 5.37.

Table 5.37: C-H···π parameters of **A1·NMF·H_2O.**

C-H···π	C···π (Å)	H···π(Å)	C-H-π (°)	Symmetry Operator
C2G-H···π	**3.920**	**3.178**	**133**	**x , y , z**
C10-H···π	**3.609**	**2.705**	**159**	**-1+x , y , z**

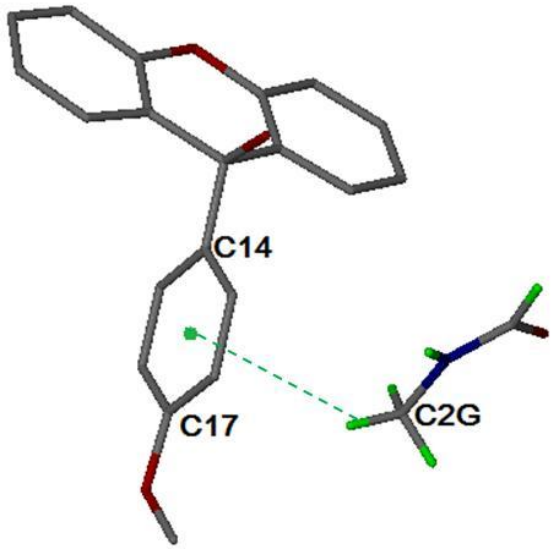

Figure 5.66: C-H···π interaction between a host and guest molecule. The C-H···π interaction is indicated by a green dotted line.

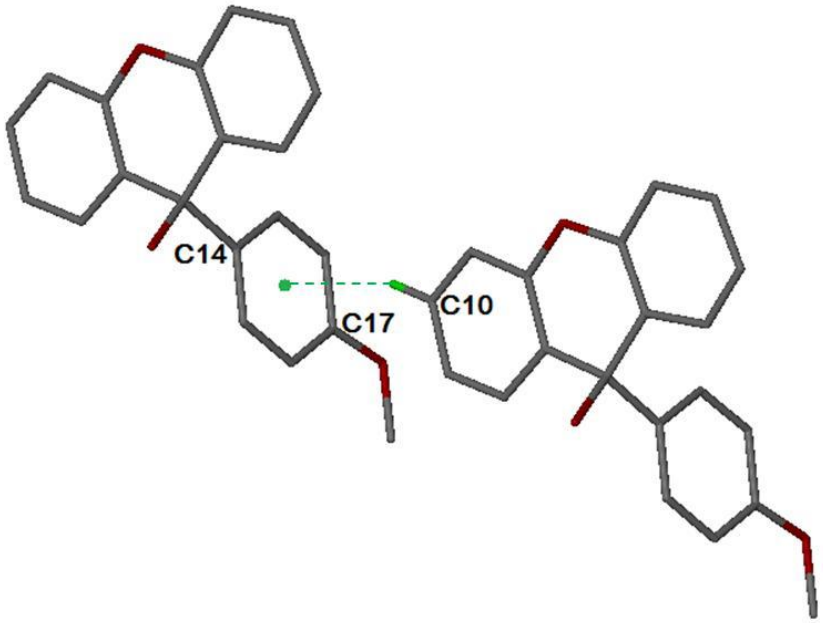

Figure 5.67: C-H···π interaction between a pair of host molecules. The C-H···π interaction is indicated by a green dotted line.

The packing diagram of **A1·NMF·H_2O** along [100] is shown in Figure 5.68(a). The NMF and water molecules are located in constricted channels viewed down [100] shown in Figure 5.69. The constricted channels can be clearly seen in Figure 5.70. The host molecules pack in bilayers parallel to the (001) plane with the xanthene rings facing each other. Pairs of host molecules form dimers which are strengthened by (Host)-C19-H···O1-(Host) hydrogen bonds.

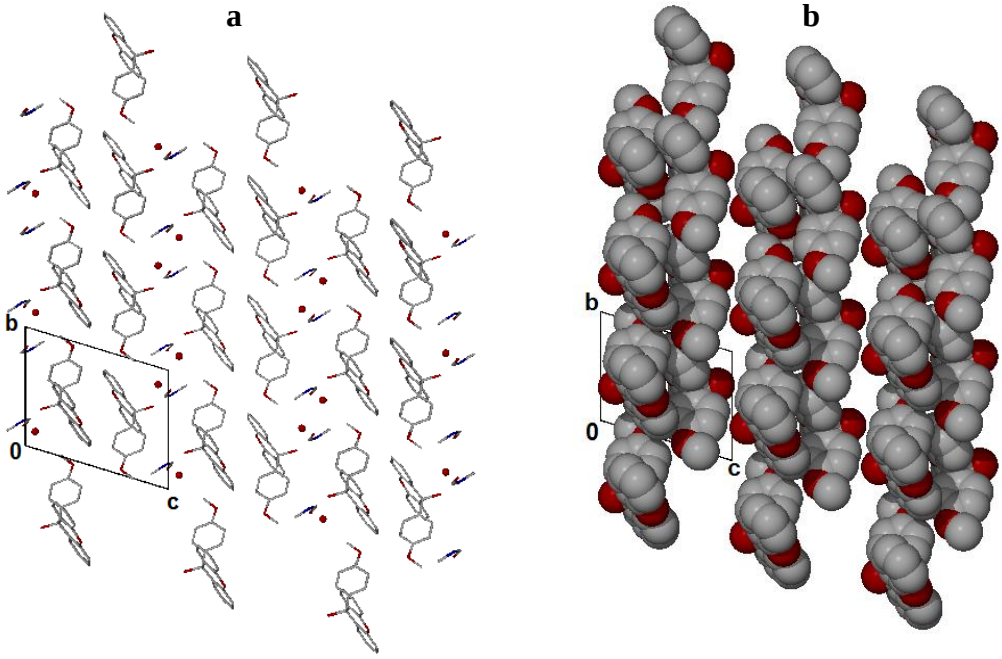

Figure 5.68: Packing diagram of **A1·NMF·H_2O** viewed along [100]. All hydrogen atoms are omitted. (a) Packing diagram with the host, NMF and water molecules. (b) The host molecules are shown as van der Waals radii with guest molecules omitted.

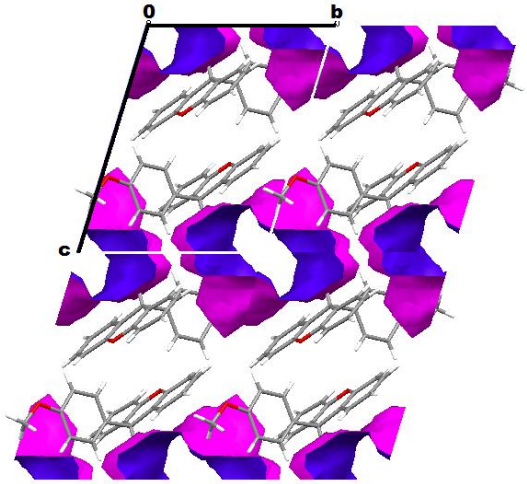

Figure 5.69: Channels down [100].

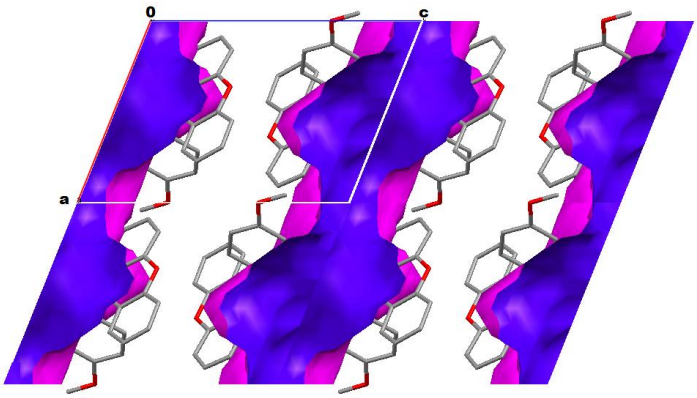

Figure 5.70: Constricted channels.

5.8 Structure Comparisons

The host compound 9-(4-methoxyphenyl)-9*H*-xanthen-9-ol forms inclusion compounds with the cyclic guest's aniline, 3-picoline and morpholine. The inclusion compounds **A1·MORPH** and **A1·ANI** were successfully solved in $P2_1/c$, whereas **A1·3PIC** was solved in $P\bar{1}$. The location of the *p*-methoxy phenyl moieties is such that they encapsulate the morpholine guest that lies on a centre of inversion at Wyckoff position *a*. The aniline guests are situated on a centre of inversion at Wyckoff position *a* in highly constricted channels. The host and guest molecules in **A1·3PIC** are located in general positions. For the **A1·ANI** structure the host molecules are found in general positions, with (Host)-OH···O-(Host) hydrogen bonding observed. The packing of **A1·3PIC** and **A1·MORPH** is characterized by host-guest hydrogen bonding.

The model free non-isothermal method was used to study the desolvation of **A1·3PIC** and **A1·MORPH** which gave activation energy ranges of 42-63 and 49-72 kJ/mol respectively. The higher activation energy for **A1·MORPH** is consistent with a higher onset temperature value observed in the DSC results and with the observation that for **A1·MORPH** the guests are trapped in cavities whereas for **A1·3PIC** the guest lies in channels.

The structures **A1·2NMA, 2A1·2NMA** and **A1·NMF·H$_2$O** were successfully solved in the triclinic space group $P\bar{1}$. **A1·NMA** was solved in the monoclinic space group $P2_1/n$. **A1·NMA** and **2A1·2NMA** are polymorphs with a host-guest ratio of 1:1. The packing of **A1·NMA, A1·2NMA** and **2A1·2NMA** are characterized by (Host)-OH···O-(Guest) and (Guest)-NH···O-(Guest) hydrogen bonds, which gives a hydrogen bonding pattern $C_2^2(7)$, $C_3^3(11)$ and $C_4^2(11)$ respectively. The **A1·NMF·H$_2$O** hydrogen bond pattern consists of repeating NMF and water molecules forming a cyclic pattern which may be described as $R_4^2(8)$. Another hydrogen bonding pattern is observed between the host, NMF and water molecules and can be described as $R_6^6(16)$. In the structures **A1·2NMA, 2A1·2NMA** and **A1·NMF·H$_2$O,** the host molecules pack to form channels along [100] in which the guests reside. For the **A1·NMA** structure the guest molecules are located in zigzag channels down [010]. The NMA guests were found disordered in all the structures.

Selected torsion angles of **A1** are shown in Figure 5.71, which can be used to describe the conformation of the host molecule. The selected torsion angles of the host molecules are listed in Table 5.39.

Table 5.38: Torsion angles for **A1.**

Torsion angles
τ_1= O2-C13-C14-C15/°
τ_2= C20-O3-C17-C16/°
τ_3= C1-C13-C14-C15/°
τ_4= C7-C13-C14-C19/°

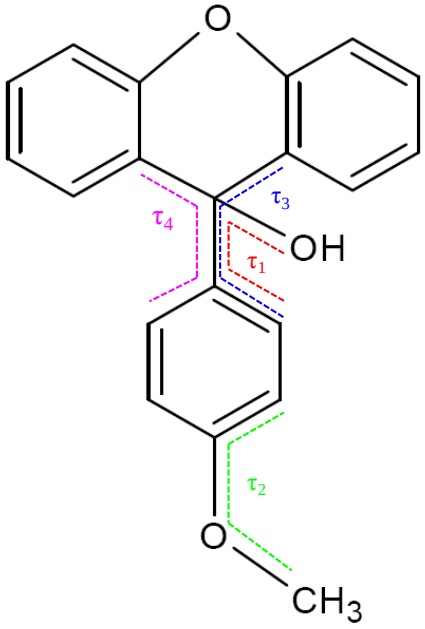

Figure 5.71: Schematic diagram indicating torsion angles for **A1**.

Table 5.39: Comparison of selected torsion angles for **A1**.

Torsion angles of A1					
Compound	**Suffix**	**τ_1**	**τ_2**	**τ_3**	**τ_4**
A1·ANI	-	16.3(2)	11.1(2)	135(2)	75.4(2)
A1·3PIC	-	-16.7(1)	-178.8(1)	103.2(1)	144.7(1)
A1·MORPH	-	-5.9(1)	-177.3(1)	112.4(1)	56.8(1)
A1·NMA	-	-5.3(2)	-179.1(2)	114.0(2)	56.6(2)
A1·2NMA	-	0.2(2)	-171.8(2)	119.4(2)	63.1(2)
2A1·2NMA	-	-1.6(3)	177.7(2)	117.9(2)	57.6(3)
	A	-7.0(3)	-172.6(2)	112.3(2)	56.2(2)
A1·NMF·H_2O	-	6.6(2)	2.8(3)	125.9(2)	65.8(2)

When the value for the torsion angles τ_1 and τ_2 are close to zero, the methoxy group takes a *cis*-configuration with respect to the hydroxyl moiety.[3]

Table 5.40: Summary of the Host conformations.

Compound	Suffix	Host conformation
A1·ANI	-	***cis***
A1·3PIC	-	***trans***
A1·MORPH	-	***trans***
A1·NMA	-	***trans***
A1·2NMA	-	***trans***
2A1·2NMA	-	***trans***
	A	***trans***
A1·NMF·H_2O	-	***cis***

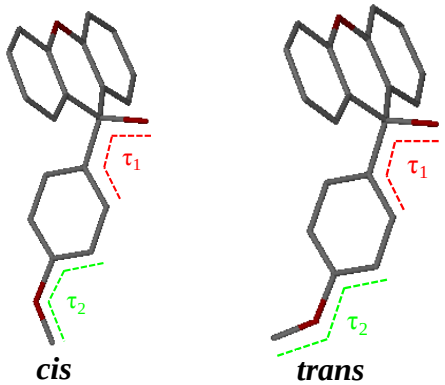

Figure 5.72: Schematic diagram of the host's methoxy group with respect to the hydroxyl moiety.

CHAPTER 5
RESULTS AND DISCUSSION

PART TWO :

The host 9-(3-methoxyphenyl)-9*H*-xanthen-9-ol forms inclusion compounds with morpholine, *N*-methylacetamide and *N*-methylformamide.

A2

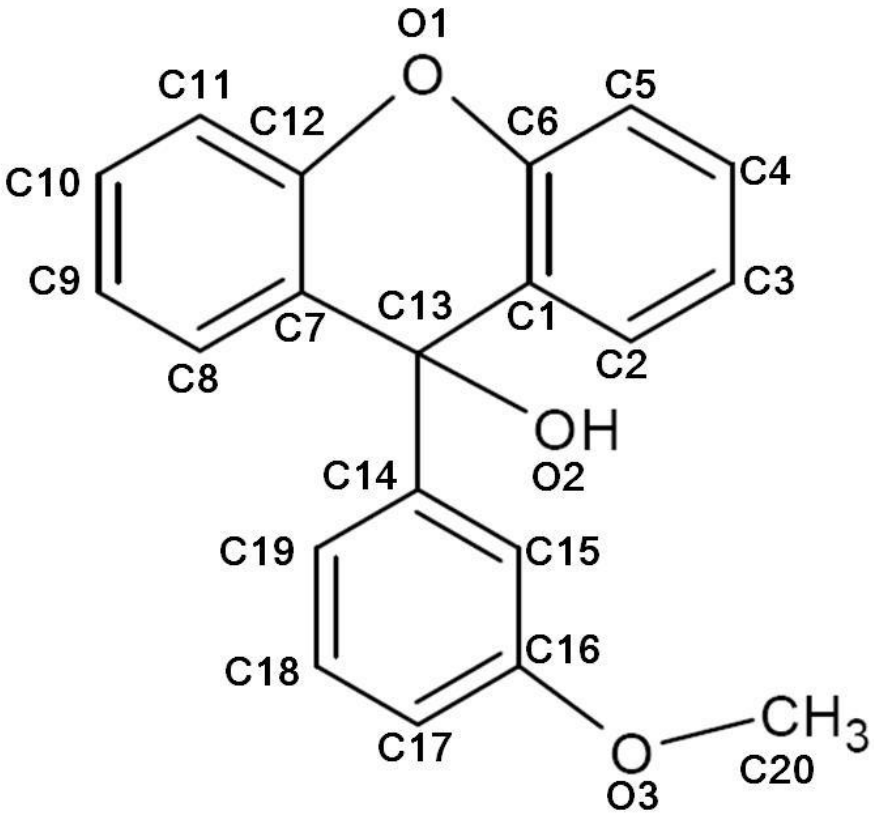

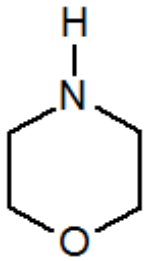

Morpholine

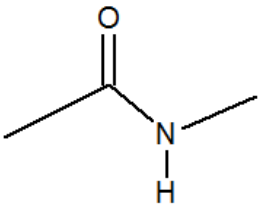

***N*-Methylacetamide**

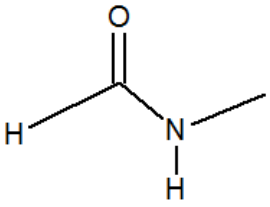

***N*-Methylformamide**

5.9 Host: 9-(3-methoxyphenyl)-9*H*-xanthen-9-ol

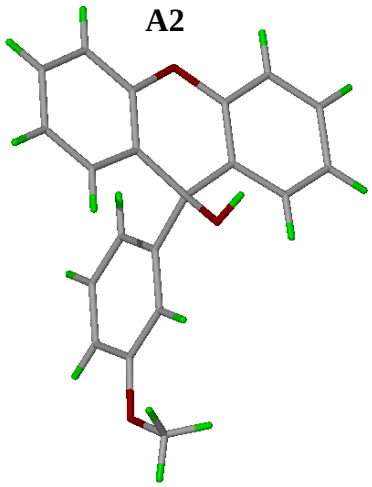

5.9.1 Thermal Analysis

The DSC curve shows a sharp peak, shown in Figure 5.73, at an onset temperature of 394.1 K which is the host melting point. The properties of **A2** are given in Table 5.41.

Table 5.41: Properties of **A2.**

Compound	A2
DSC Endo$_1$ (T_{onset}, K)	394.1
Molecular formula	$C_{20}H_{16}O_3$
Molar mass (g/mol)	304.33

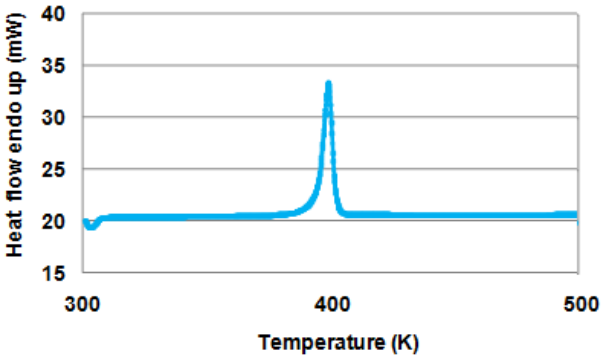

Figure 5.73: DSC curve obtained for **A2.**

5.9.2 *Hot Stage Microscopy*

(a) The crystal is immersed in silicone oil.
(b) The crystal of the apohost begins to melt.
(c) The apohost melt is complete.

(a) 298 K **(b) 395 K** **(c) 401 K**

Figure 5.74: HSM photographs of **A2.**

5.9.3 Structure Refinement

The crystal structure of the apohost refined successfully in the orthorhombic crystal system to R_1= 0.0444 with wR_2= 0.1131. All non-hydrogen atoms were found by direct methods in the difference electron density map and refined anisotropically. All the crystal data and experimental conditions are given in Table 5.42.

Table 5.42: Crystal data of **A2.**

Compound	**A2**
Structural Formula	**$C_{20}H_{16}O_3$**
Molecular Mass (g.mol^{-1})	**304.33**
Data collection temp (K)	**173**
Crystal system	**Orthorhombic**
Space group	**P*bca***
a (Å)	**6.5073(13)**
b (Å)	**21.194(4)**
c (Å)	**21.940(4)**
α (°)	**90**
β (°)	**90**
γ (°)	**90**
Volume (Å^3)	**3025.7(10)**
Z	**8**
μ/ mm^{-1}	**0.089**
F(000)	**1280**
No. of reflections collected	**3477**
No. of unique reflection	**3477**
No. of reflections with I>2σ(I)	**2432**
D_c, Calculated density (g.cm^{-3})	**1.336**
Index range	**h: 0 to 8, k: 0 to 27, l: 0 to28**
θ range	**1.92-27.53**
Goodness of fit, S	**1.074**
Final R indices [I>2σ(I)]	**R_1= 0.0444 ; wR_2= 0.1131**
R indices (all data)	**R_1= 0.0718 ; wR_2= 0.1355**
Largest diff peak and hole (eÅ^{-3})	**0.24 ; -0.22**

5.9.4 Discussion

The host compound **A2** crystallises in the space group P*bca*, and the asymmetric unit contains one host molecule. A thermal ellipsoid plot of the host **A2** at 50 % probability is shown in Figure 5.75. The packing diagram down [100] is shown in Figure 5.76.

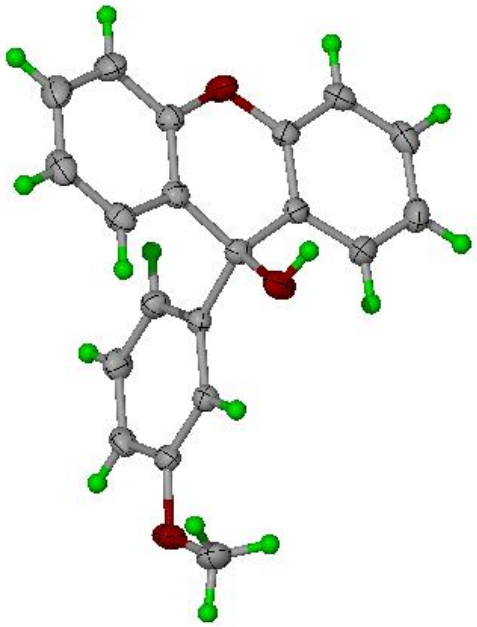

Figure 5.75: Atom displacement ellipses shown at the 50% probability level.

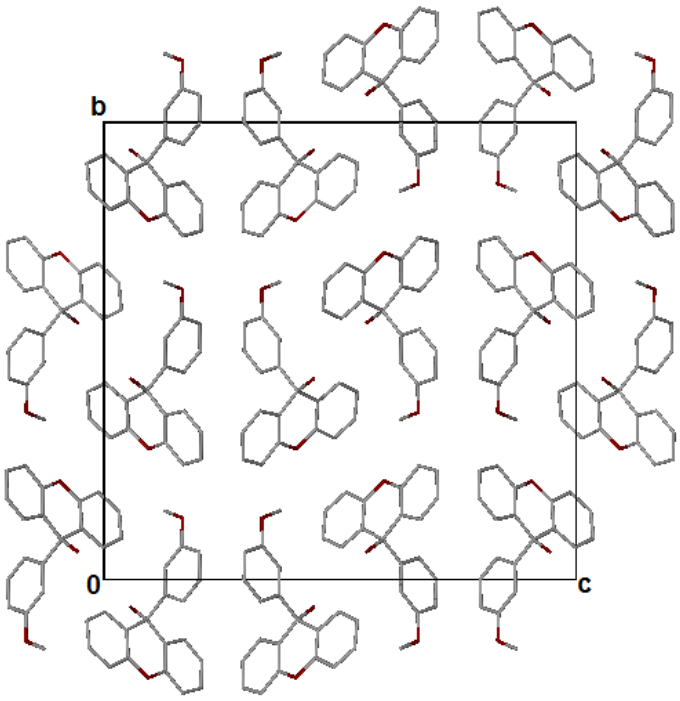

Figure 5.76: Packing diagram of **A2** viewed down [100].

The C-H···π interactions of **A2** are listed in Table 5.43. The C-H···π interactions between host molecules are shown in Figure 5.77. The C-H···π parameters are provided in Table 5.43. The closest C···π distance of neighbouring host molecules is 3.522 Å. A single O-H···π interaction is also observed with a O···π distance of 3.770 Å and O-H-π angle of 141°.

Table 5.43: C-H···π parameters of **A2.**

C-H-···π	C···π (Å)	H···π(Å)	C-H-π (°)	Symmetry Operator
C3-H···π	**3.522**	**2.641**	**154**	**-½+x , y , ½-z**
C9-H···π	**3.717**	**2.802**	**161**	**1-x , 1-y , -z**
C18-H···π	**3.609**	**2.756**	**149**	**½+x , y , ½-z**
C19-H···π	**3.023**	**2.631**	**105**	**x , y , z**
C20-H···π	**3.715**	**3.148**	**118**	**-x , 1-y , -z**

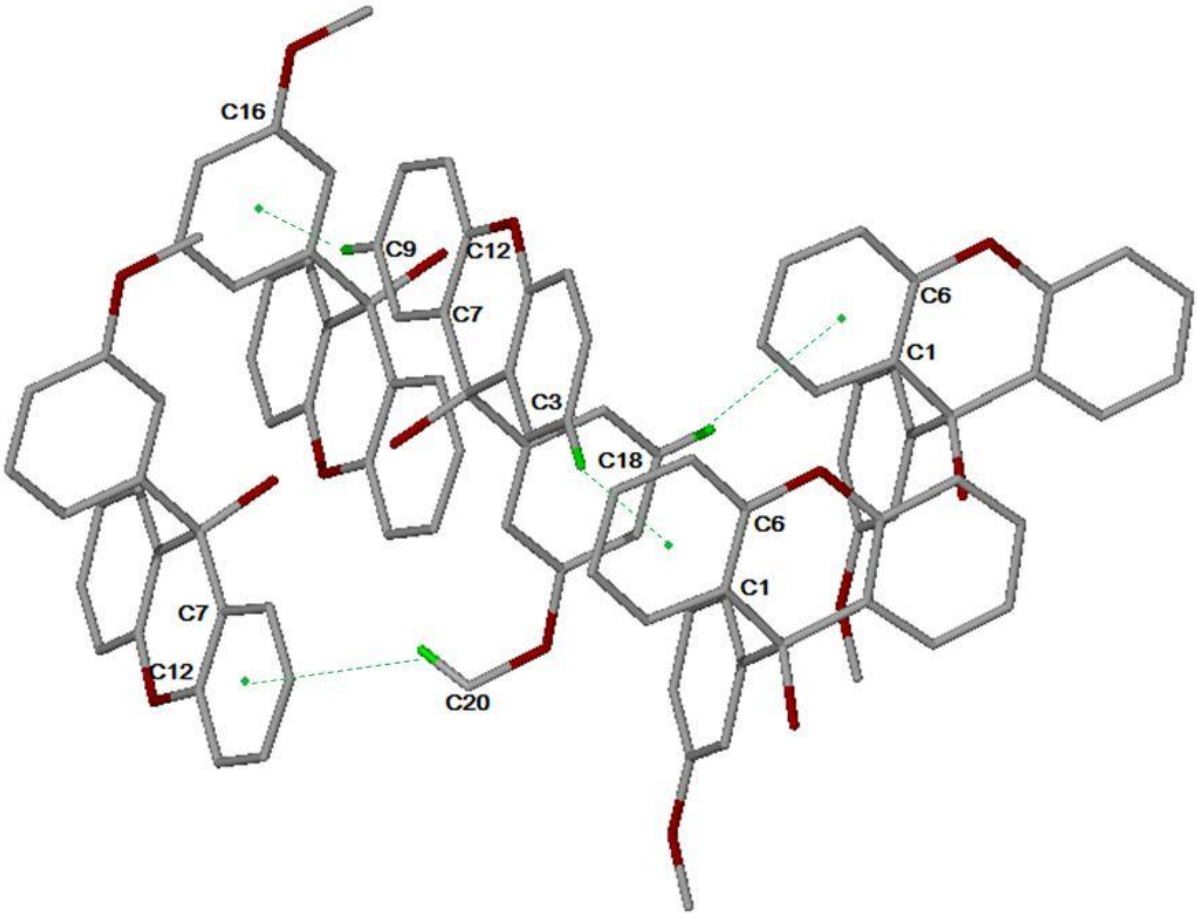

Figure 5.77: C-H···π interaction between host molecules. The C-H···π interactions are indicated by green dotted lines. Only the hydrogens involved in hydrogen bonding are shown.

5.10 Guest: Morpholine

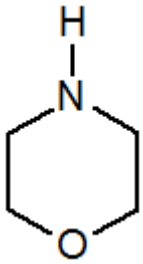

Table 5.44: Properties of morpholine.

Guest	MORPH
Molecular formula	C_4H_9NO
Molar mass (g/mol)	87.1
Boiling Point (K)	401

5.10.1 Thermal Analysis

The thermal analysis results are shown in Figure 5.78. The TGA curve shows a two-step mass loss. The first mass loss step is 8.0 % and the second step is 13.8%, the combined percentage mass loss of 21.8 % corresponds to a 1:1 host-guest ratio. The thermal analysis data is given in Table 5.45. An endotherm (T_{on}=345.5 K) is observed in the DSC curve which is due to dissolution of the host upon release of the guest.

Table 5.45: Thermal analysis data for **A2·MORPH.**

Compound	A2•MORPH
Host: Guest ratio	1:1
TG calculated % mass loss	22.2
TG experimental % mass loss	21.8
DSC $Endo_1$ (T_{onset}, K)	345.5

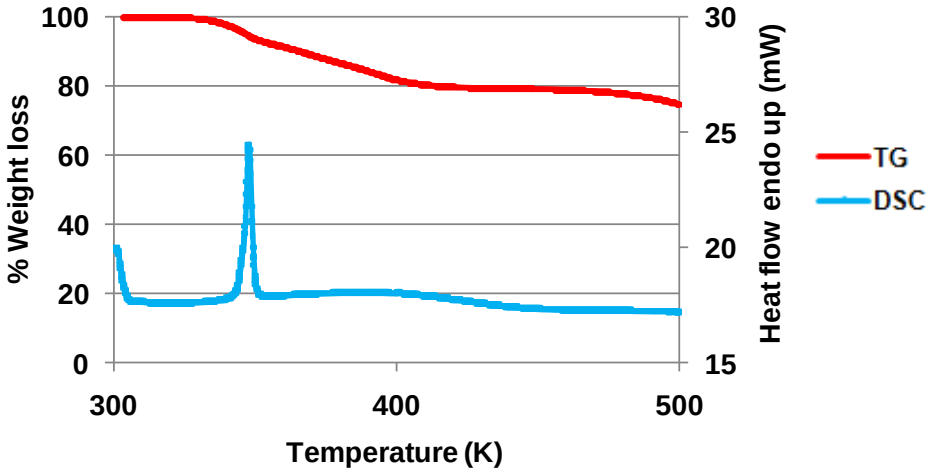

Figure 5.78: TGA and DSC curves obtained for **A2·MORPH.**

5.10.2 Structure Refinement

Direct methods yielded all host and guest non-hydrogen atoms which were refined anisotropically. The host hydroxyl hydrogen was located in the difference electron density map. The amine hydrogen atoms (H1G and H1GA) were located in the difference electron density map. The structure refined successfully to R_1= 0.0444 with wR_2= 0.1185. The crystal data is reported in Table 5.46.

Table 5.46: Crystal data of **A2·MORPH.**

Compound	**A2•MORPH**
Structural Formula	**$2C_{20}H_{16}O_3 \cdot 2C_4H_9NO$**
Host-Guest ratio	**1:1**
Molecular Mass (g.mol^{-1})	**782.90**
Data collection temp (K)	**173**
Crystal system	**Triclinic**
Space group	**$P\bar{1}$**
a (Å)	**8.9784(18)**
b (Å)	**12.595(3)**
c (Å)	**18.932(4)**
α (°)	**77.78(3)**
β (°)	**88.78(3)**
γ (°)	**72.22(3)**
Volume (Å^3)	**1990.3(7)**
Z	**2**
μ/ mm^{-1}	**0.089**
F(000)	**832**
No. of reflections collected	**9867**
No. of unique reflection	**9867**
No. of reflections with I>2σ(I)	**7401**
D_c, Calculated density (g.cm^{-3})	**1.306**
Index range	**h: 0 to 11,** **k: -15 to 16,** **l: -25 to25**
θ range	**1.10-28.30**
Goodness of fit, S	**1.024**
Final R indices [I>2σ(I)]	**R_1= 0.0444 ; wR_2= 0.1185**
R indices (all data)	**R_1= 0.0675 ; wR_2= 0.1376**
Largest diff peak and hole (eÅ^{-3})	**0.28 ; -0.25**

5.10.3 Discussion

The inclusion compound of **A2·MORPH** has a structural formula of $2C_{20}H_{16}O_3 \cdot 2C_4H_9NO$ with a host-guest ratio of 1:1. The structure was solved in the triclinic crystal system, space group $P\bar{1}$. The asymmetric unit contains two independent host and two independent guest molecules located in general positions, shown in Figure 5.79. The guest molecules exhibit a chair conformation (Figure 5.80).

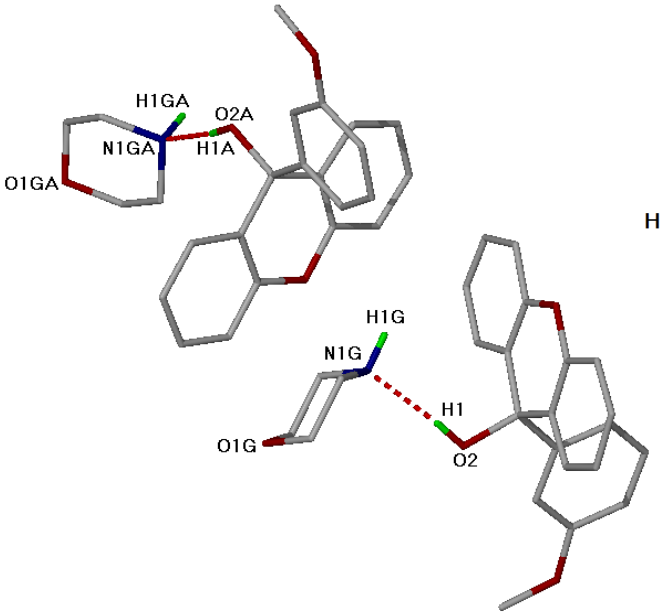

Figure 5.79: Hydrogen bonding in the asymmetric unit of **A2·MORPH.**

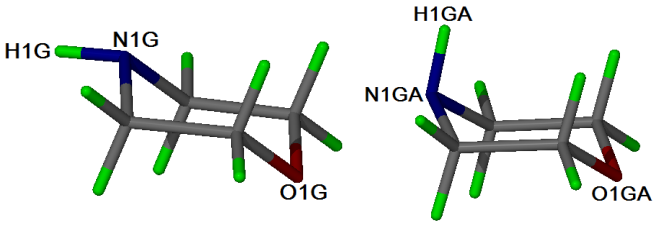

Figure 5.80: Guest molecules in the asymmetric unit.

The structure is stabilised by (Host)-OH···N-(Guest) hydrogen bonds with the hydrogen bond parameters provided in Table 5.47. In addition there exists a weaker (Guest)-N-H···$O_{methoxy}$-(Host) hydrogen bond with an N···O distance of 3.509(2) Å.

Table 5.47: Hydrogen bond parameters of **A2·MORPH**.

Donor(D)	Acceptor(A)	D···A (Å)	D-H (Å)	H···A (Å)	D-H···A(Å)
O2	**N1G**	**2.836(2)**	**0.840(1)**	**2.004 (1)**	**170(1)**
O2A	**N1GA**	**2.777(2)**	**0.840(1)**	**1.940(1)**	**175(1)**

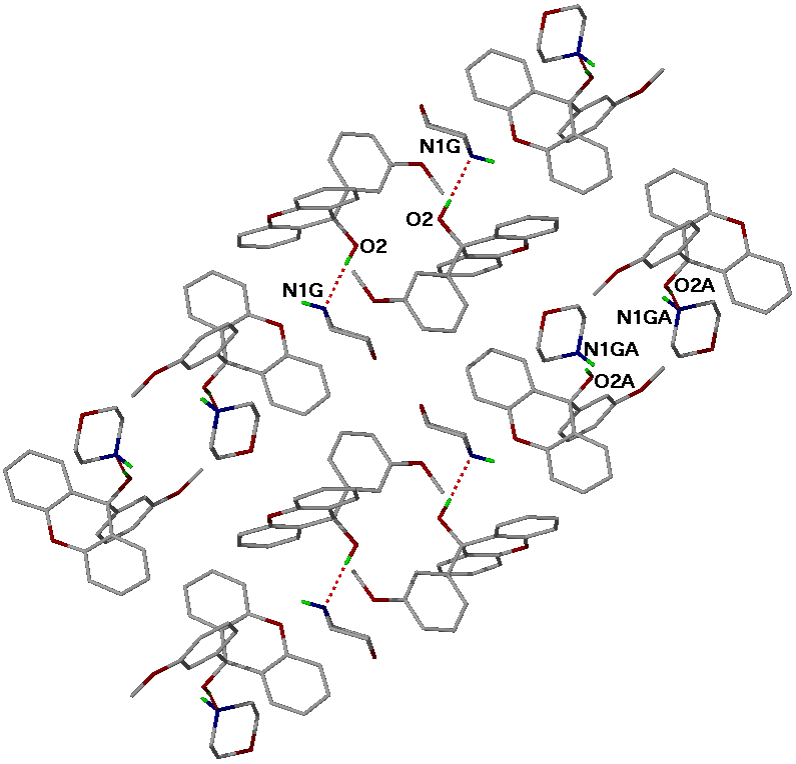

Figure 5.81: Hydrogen bonding in **A2·MORPH**.

The structure was further analysed using the program *PLATON*,[7] which listed the weak C-H···π and N-H···π interactions. The shortest C···π contact between host and guest molecules is 3.631 Å with a C-H-π angle of 118° shown in Figure 5.82. Another noteworthy interaction is the N-H···π interaction, which is observed between a host and a guest molecule with a distance of 3.833Å and an N-H-π angle of 128° (Figure 5.83). The shortest C···π distance listed between host molecules is 3.509 Å with angle of 116° shown in Figure 5.84.

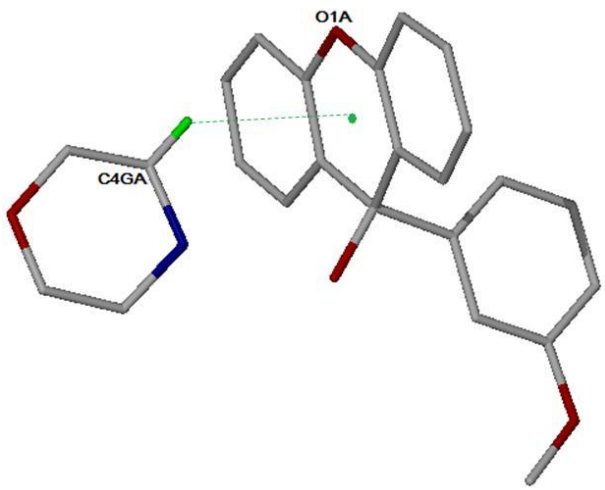

Figure 5.82: C-H···π interaction between a host and guest molecule. The C-H···π interaction is indicated by a green dotted line.

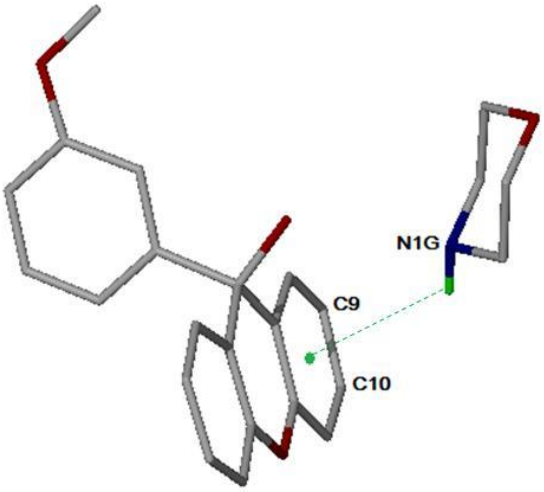

Figure 5.83: N-H···π interaction between a host and guest molecule. The N-H···π interaction is indicated by a green dotted line.

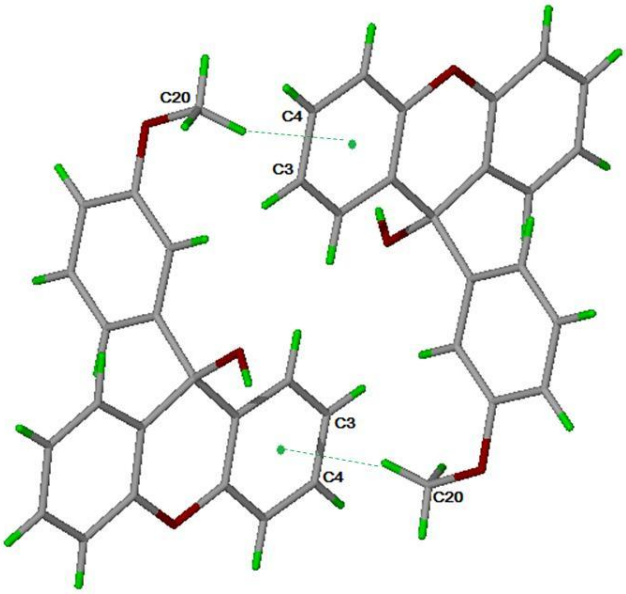

Figure 5.84: C-H···π interaction between host molecules.
The C-H···π interaction is indicated by a green dotted line.

The packing diagram of **A2·MORPH** along [100] direction is shown in Figure 5.85. The guests lie within corrugated channels down [001] (Figure 5.86).[5]

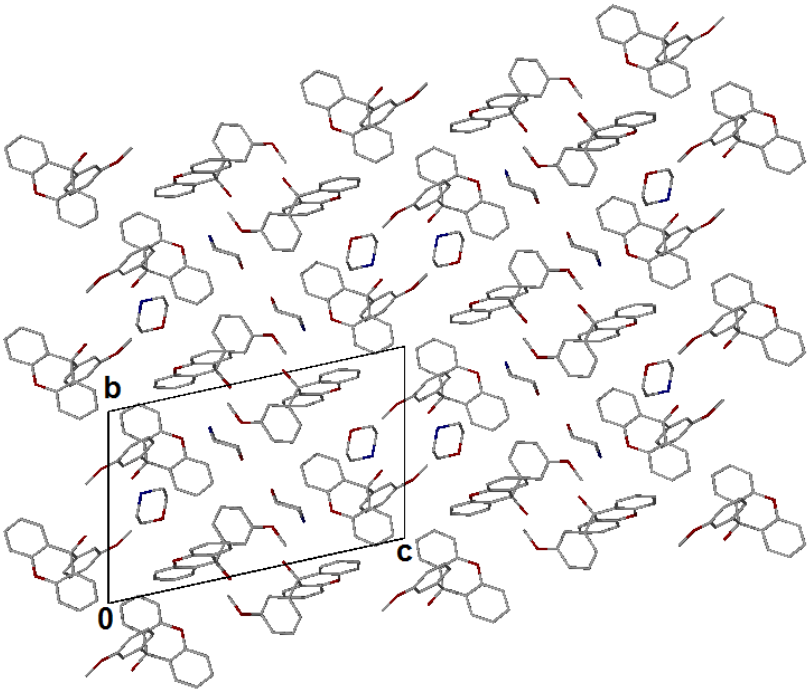

Figure 5.85: Packing diagram of **A2·MORPH** viewed along [100] direction.
All hydrogen atoms are omitted.

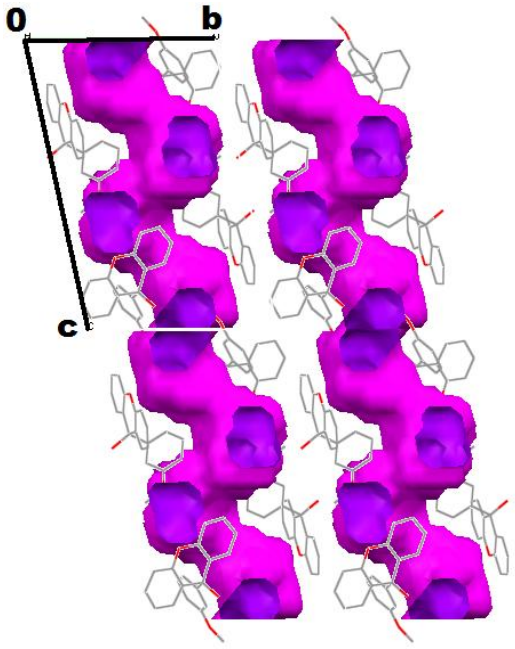

Figure 5.86: Corrugated channels.

5.11 Guest: N-methylacetamide

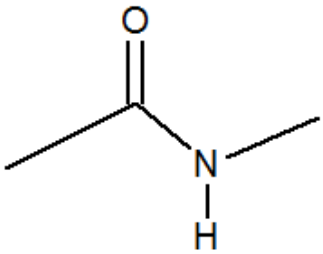

Table 5.48: Properties of *N*-methylacetamide.

Guest	NMA
Molecular formula	**C_3H_7NO**
Molar mass (g/mol)	**73.1**
Boiling Point (K)	**479**

5.11.1 Thermal Analysis

The thermal analysis results are shown in Figure 5.87. A single mass loss step of 20.1 % is observed in the TG curve which corresponds to a 1:1 host-guest ratio. A sharp peak is observed in the DSC (T_{on}=382.4 K) which corresponds to the desolvation which is followed by simultaneous melt and dissolution of the host. The thermal analysis data is given in Table 5.49.

Table 5.49: Thermal analysis data for **A2·NMA.**

Compound	A2•NMA
Host: Guest ratio	**1:1**
TG calculated % mass loss	**19.4**
TG experimental % mass loss	**20.1**
DSC Endo$_1$ (T_{onset}, K)	**382.4**

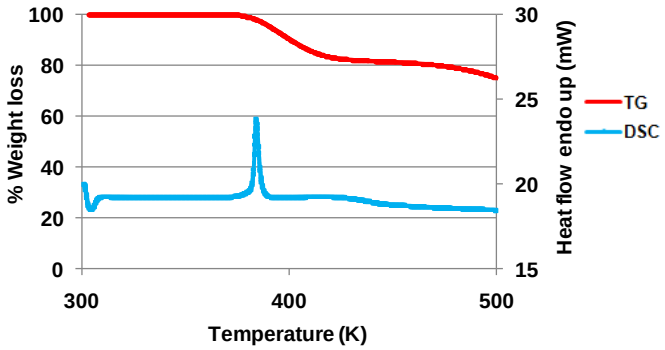

Figure 5.87: TGA and DSC curves obtained for **A2·NMA.**

5.11.2 Hot Stage Microscopy

(a) The crystals are immersed in silicone oil.
(b) The crystal begins to melt due to dissolution of the host upon release of the guest.
(c) Shows further melting of crystals.
(d) The host melt is complete.

(a) 298 K **(b) 383 K** **(c) 384 K** **(d) 385 K**

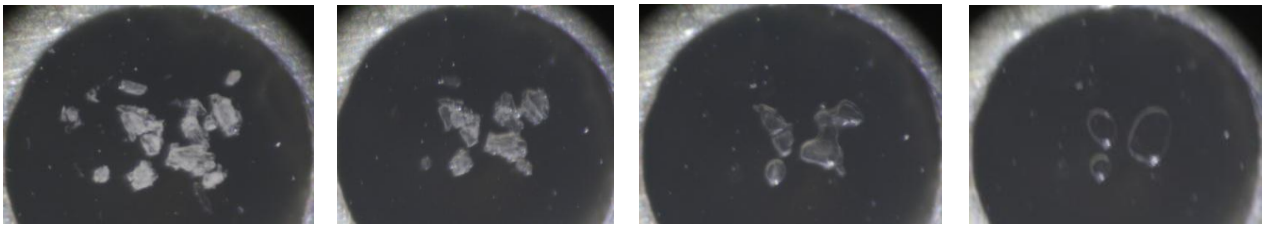

Figure 5.88: HSM photographs of **A2·NMA.**

5.11.3 Structure Refinement

The data collection of **A2·NMA** was attempted at lower temperatures but the crystal cracked, therefore data collection was carried out at 298 K. All non-hydrogen atoms were found by direct methods in the difference electron density map and refined anisotropically. The hydroxyl hydrogen was first located in the difference electron density map and then refined with a simple bond length constraint dependent on the O···O distance.[1] The structure refined successfully to R_1= 0.0767 with wR_2= 0.1963. The crystal data is given in Table 5.50.

Table 5.50: Crystal data of **A2·NMA.**

Compound	**A2•NMA**
Structural Formula	**$C_{20}H_{16}O_3 \cdot C_3H_7NO$**
Host-Guest ratio	**1:1**
Molecular Mass (g.mol^{-1})	**377.42**
Data collection temp (K)	**298**
Crystal system	**Monoclinic**
Space group	***P*2$_1$/*n***
a (Å)	**11.274(2)**
b (Å)	**9.5079(19)**
c (Å)	**18.330(4)**
β (°)	**91.11(3)**
Volume (Å^3)	**1964.4(7)**
Z	**4**
μ/ mm^{-1}	**0.087**
F(000)	**800**
No. of reflections collected	**6886**
No. of unique reflection	**3597**
No. of reflections with I>2σ(I)	**1554**
D_c, Calculated density (g.cm^{-3})	**1.276**
Index range	**h: -13 to 13, k: -11 to 11, l: -22 to22**
θ range	**2.10-25.33**
Goodness of fit, S	**1.002**
Final R indices [I>2σ(I)]	**R_1= 0.0767 ; wR_2= 0.1963**
R indices (all data)	**R_1= 0.1967 ; wR_2= 0.2619**
Largest diff peak and hole (eÅ^{-3})	**0.39 ; -0.24**

5.11.4 Discussion

A2·NMA crystallises in the monoclinic space group $P2_1/n$ with Z=4. The asymmetric unit contains a host and guest molecule with structural formula of $C_{20}H_{16}O_3 \cdot C_3H_7NO$, shown in Figure 5.89. The host molecules are situated in general positions around a centre of symmetry at Wyckoff position *d*.

The structure is stabilised by (Host)-OH···O-(Guest) and (Guest)-NH···O-(Guest) hydrogen bonds which can be described using the graph set notation $C_2^2(7)$ shown in Figure 5.90.[4] The metrics of the hydrogen bonds are reported in Table 5.51.

Table 5.51: Hydrogen bond parameters of **A2·NMA.**

Donor(D)-H	Acceptor(A)	D···A (Å)	D-H (Å)	H···A (Å)	D-H···A (Å)
O2-H1	O1G	2.758(4)	0.965(1)	1.806(1)	168(2)
N1G-H1G	O1G[½ -x, ½+y, ½-z]	3.044(6)	0.880(1)	2.166(1)	176(1)

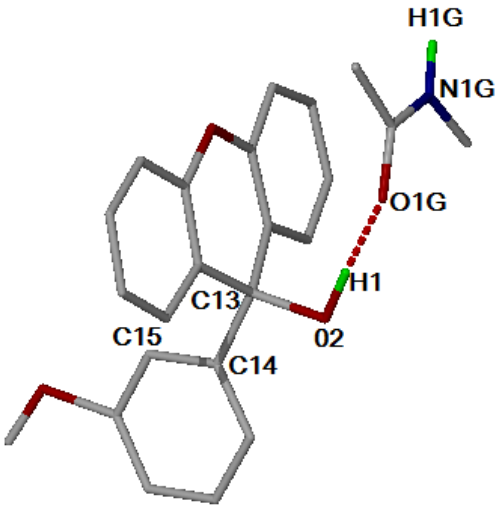

Figure 5.89: Asymmetric unit of **A2·NMA.**

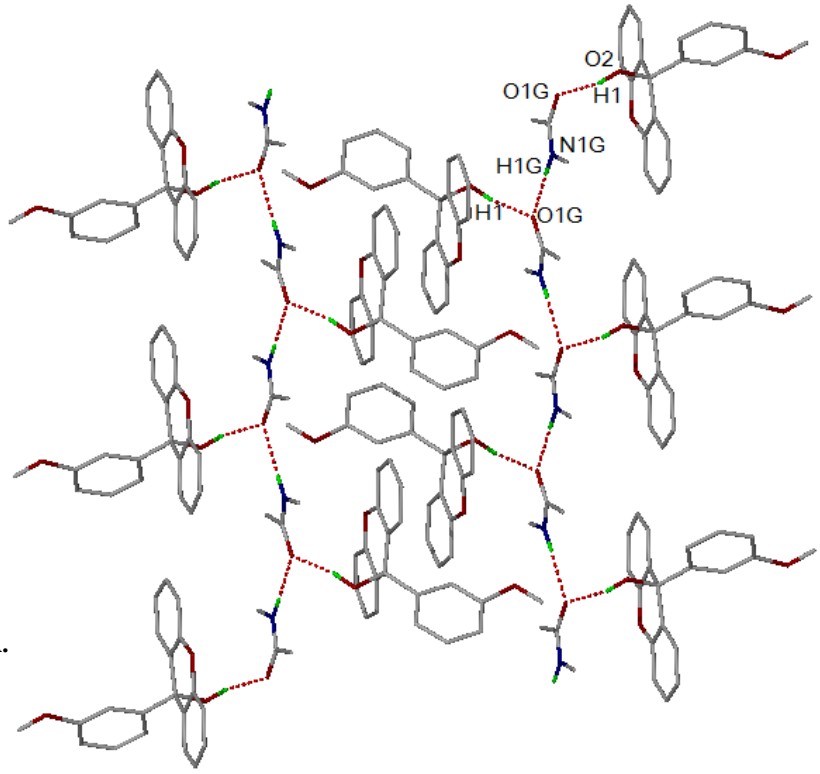

Figure 5.90: Hydrogen bonding in **A2·NMA**.

The only C-H···π interaction between the host and guest molecule is C(3G)···π(centroid) = 3.541 Å, with a C-H-π angle of 137° (Figure 5.91). The edge-to-face C-H···π interaction has H···π = 3.332 Å and C9···π = 4.006 Å distances, with C-H- π angle of 129° (Figure 5.92). Pairs of host molecules form dimers which are strengthened by (Host)-C15-H···O1-(Host) hydrogen bonds.

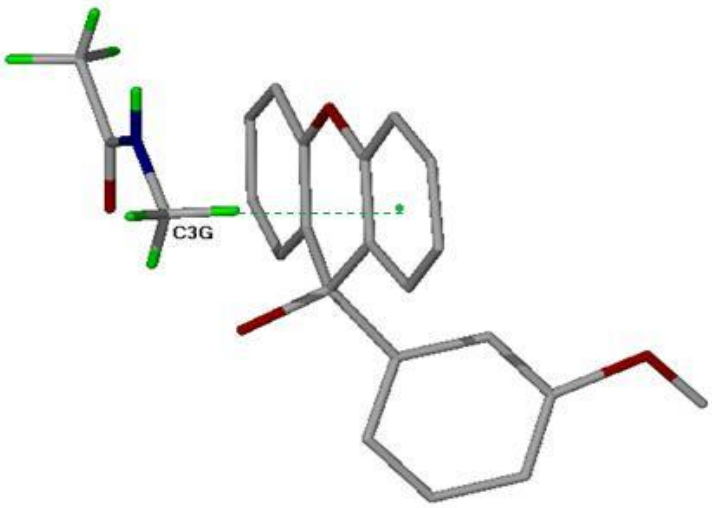

Figure 5.91: C-H···π interaction is indicated by a green dotted line, between a host and guest molecule.

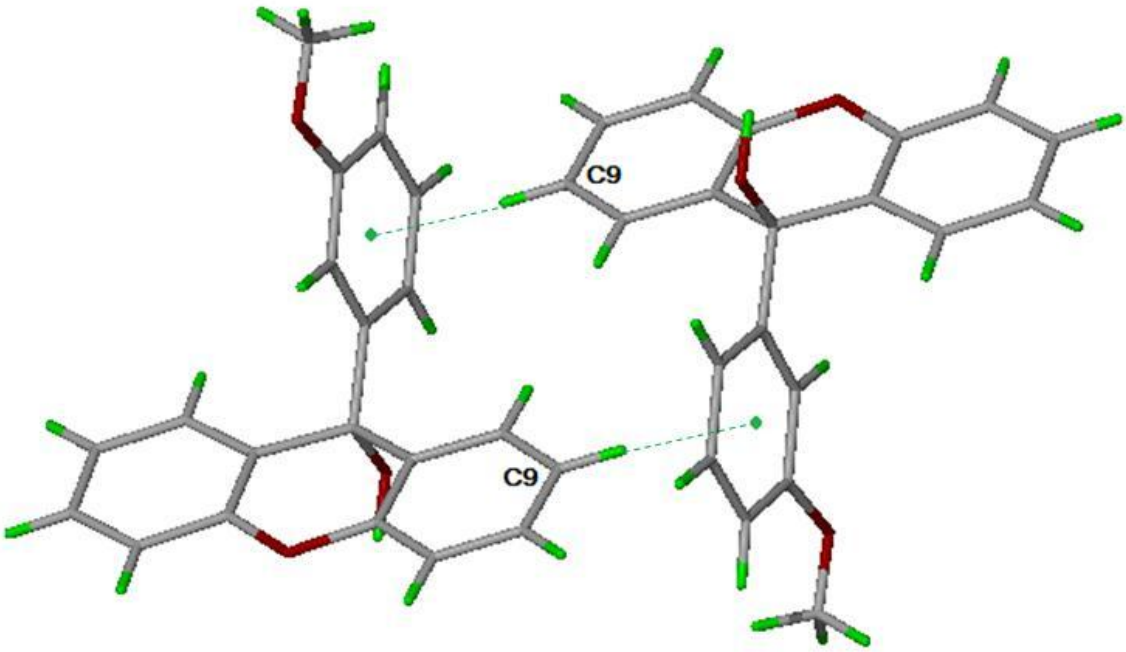

Figure 5.92: Edge-to-face π -π interaction of neighbouring host molecules. The C-H···π interactions are indicated by green dotted lines.

The packing diagrams of **A2·NMA** down [100] and [010] are shown in Figures 5.93 and 5.94(a) respectively. When viewed along the [010] direction the host molecules exhibits a zigzag arrangement (Figure 5.94). The channels are down [010], shown in Figure 5.95.[5]

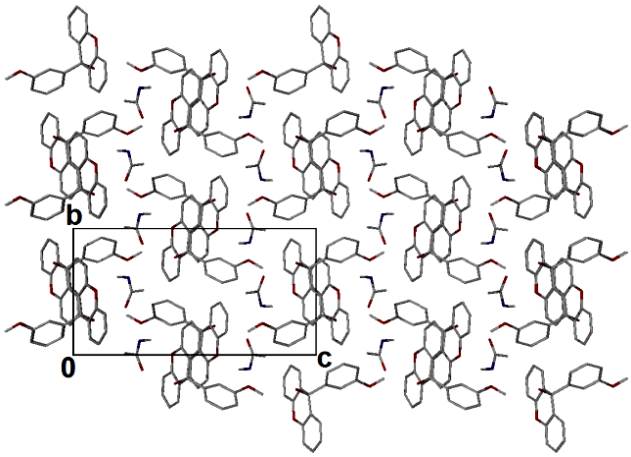

Figure 5.93: Packing diagram of **A2·NMA** viewed along [100]. All hydrogen atoms are omitted.

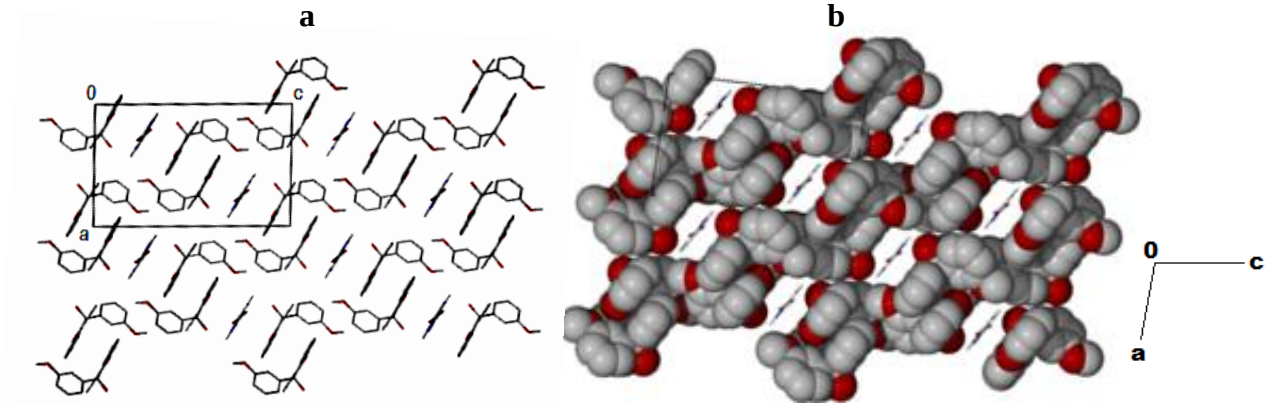

Figure 5.94: Packing diagram of **A2·NMA** down [010]. All hydrogen atoms are omitted. (a) Packing diagram of host and guest. (b) The host molecules are shown as van der Waals radii and the guest molecules as sticks.

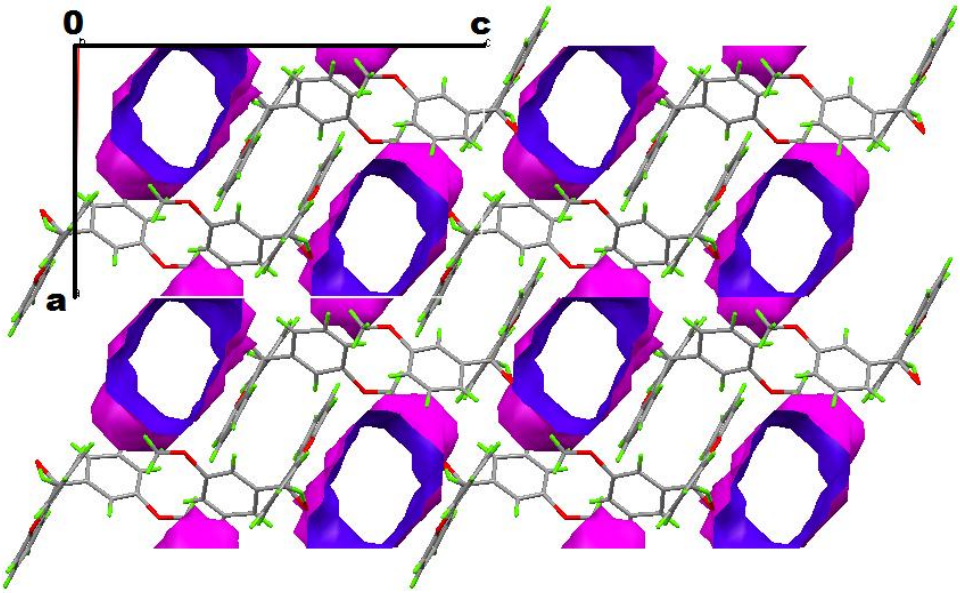

Figure 5.95: Channels down [010].

The section plots confirm that the channels the guest resides in are parallel to [010]. This is illustrated in Figure 5.96.

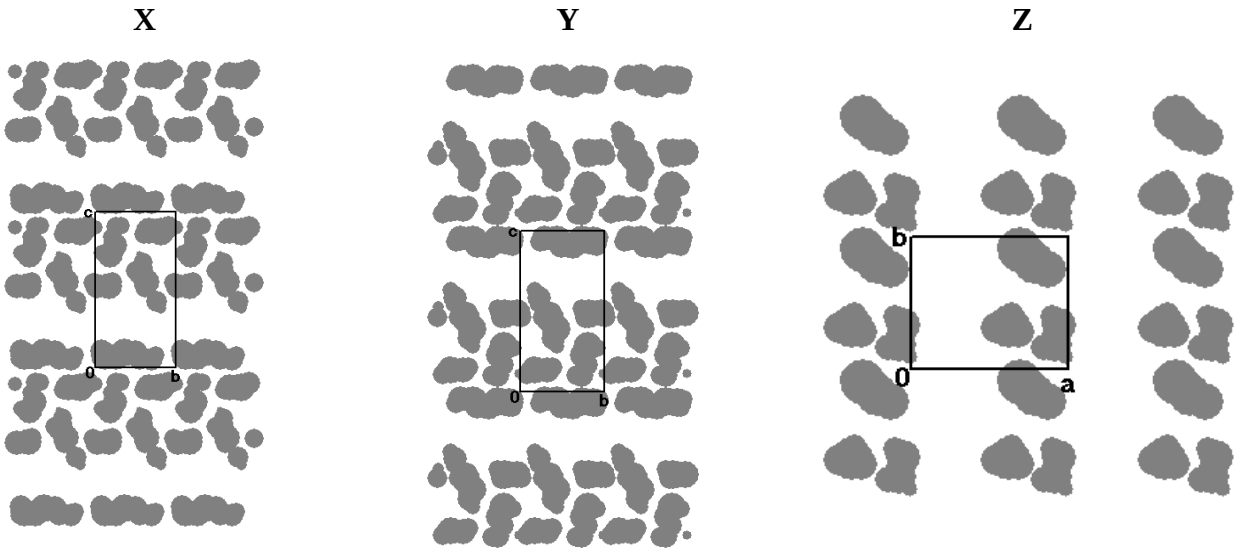

Figure 5.96: Section plot of **A2·NMA.**

X = View along [100] direction at section height 1.00 Å.

Y = View along [100] direction at section height 10.00 Å.

Z = View along [001] direction at section height 3.5 Å.

5.12 Guest: N-methylformamide

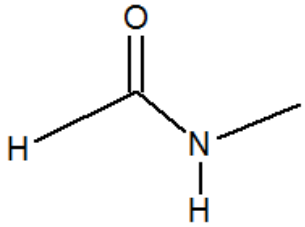

Table 5.52: Properties of *N*-methylformamide.

Guest	NMF
Molecular formula	**C_2H_5NO**
Molar mass (g/mol)	**59.1**
Boiling Point (K)	**453-458**

5.12.1 Thermal Analysis

The TG curve shows two mass loss steps which is confirmed by the DSC endotherms (T_{on}=309.2 K and 382.9 K). The thermal analysis results are shown in Figure 5.97. The combined percentage mass loss is 15.5 % which is due to the loss of the guest. These results suggest that **A2·NMF** undergoes a complex mechanism for thermal decomposition. The thermal data is given in Table 5.53.

Table 5.53: Thermal analysis data for **A2·NMF.**

Compound	A2•NMF
Host: Guest ratio	**1:1**
TG calculated % mass loss	**16.3**
TG experimental % mass loss	**15.5**
DSC Endo$_1$ (T_{onset}, K)	**309.2**
DSC Endo$_2$ (T_{onset}, K)	**382.9**
DSC Endo$_3$ (T_{onset}, K)	**402.8**

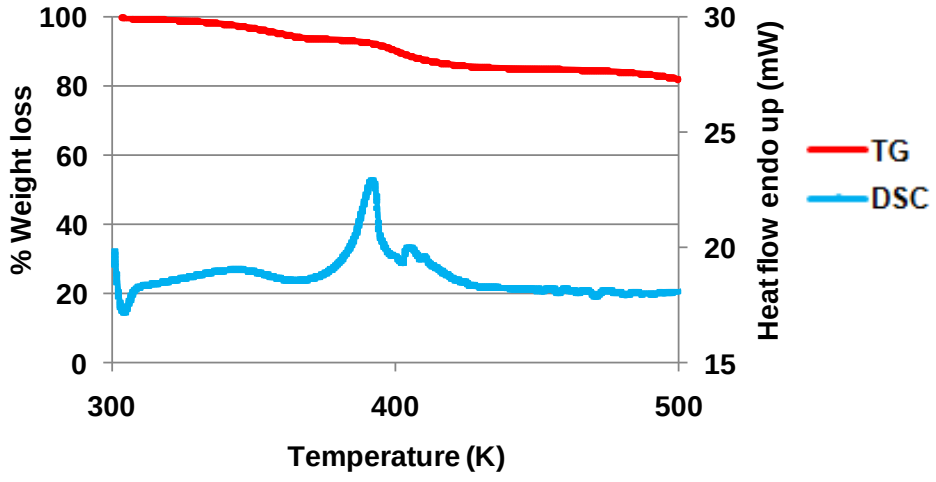

Figure 5.97: TGA and DSC curves obtained for **A2·NMF.**

5.12.2 Structure Refinement

All non-hydrogen atoms were found by direct methods in the difference electron density map and were refined anisotropically. The host hydroxyl hydrogen was first located in the difference electron density map and then refined with a simple bond length constraint dependent on the O···O distance.[1] The NMF guest is disordered and the hydrogen atoms on the guest was neither placed nor found in the electron density map, and therefore omitted from the final model. The site occupancy factors of the guest atoms were calculated according to Scheme 1 and assigned as follows, O1G=0.34, C1G=0.5, C2G=0.83 and C3G=0.5. The crystal data is reported in Table 5.54.

Table 5.54: Crystal data of **A2·NMF.**

Compound	**A2•NMF**
Structural Formula	**$C_{20}H_{16}O_3 \cdot C_2H_5NO$**
Host-Guest ratio	**1:1**
Molecular Mass (g.mol^{-1})	**363.40**
Data collection temp (K)	**173**
Crystal system	**Triclinic**
Space group	**$P\bar{1}$**
a (Å)	**8.9609(7)**
b (Å)	**9.0911(8)**
c (Å)	**11.5784(9)**
α (°)	**67.6320(10)**
β (°)	**84.786(2)**
γ (°)	**72.355(2)**
Volume (Å^3)	**830.90(12)**
Z	**2**
μ/ mm^{-1}	**0.100**
F(000)	**384**
No. of reflections collected	**7881**
No. of unique reflection	**4152**
No. of reflections with I>2σ(I)	**3129**
D_c, Calculated density (g.cm^{-3})	**1.452**
Index range	**h: -11 to 11, k: -12 to 10, l: -15 to15**
θ range	**1.90-28.44**
Goodness of fit, S	**1.052**
Final R indices [I>2σ(I)]	**R_1= 0.0571; wR_2= 0.1654**
R indices (all data)	**R_1= 0.0764 ; wR_2= 0.1815**
Largest diff peak and hole (eÅ^{-3})	**0.52 ; -0.32**

5.12.3 Discussion

The structure **A2·NMF** crystallises in the triclinic space group $P\bar{1}$ with Z=2. The guest molecule is disordered and the hydrogen atoms were not located. The host molecules are in general positions and the guest molecules are situated on a centre of symmetry at Wyckoff position *d*. The structure is stabilised by hydrogen bonding with the hydrogen bond parameters provided in Table 5.55. The hydrogen bonding interaction between host and guest is illustrated in Figure 5.98. Figure 5.99 displays the NMF guest which is disordered. The different positions that the NMF guest can occupy is shown in Scheme 1.

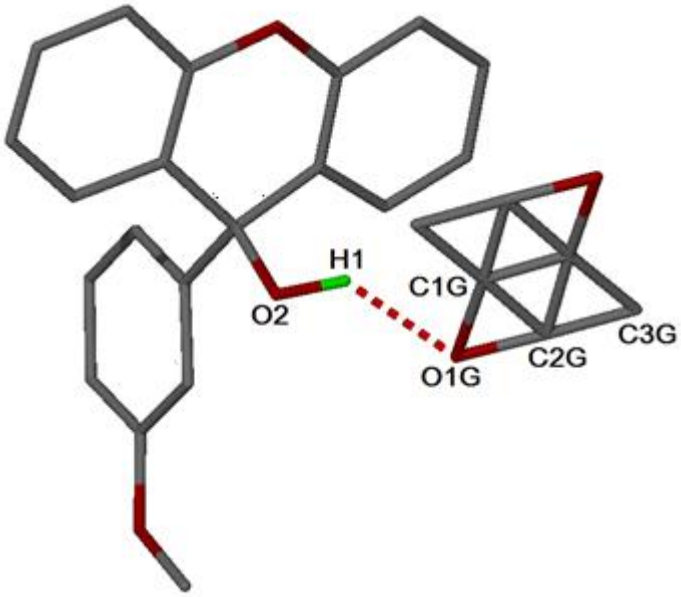

Figure 5.98: Asymmetric unit of **A2·NMF.**

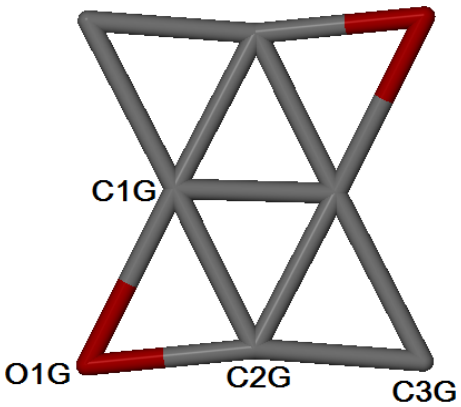

Figure 5.99: Disordered NMF guest.

Table 5.55: Hydrogen bond parameters of **A2·NMF**.

Donor(D)-H	Acceptor(A)	D···A (Å)	D-H (Å)	H···A (Å)	D-H···A (Å)
O2-H1	**O1G**	**2.663(8)**	**0.98(1)**	**1.880(6)**	**135(2)**

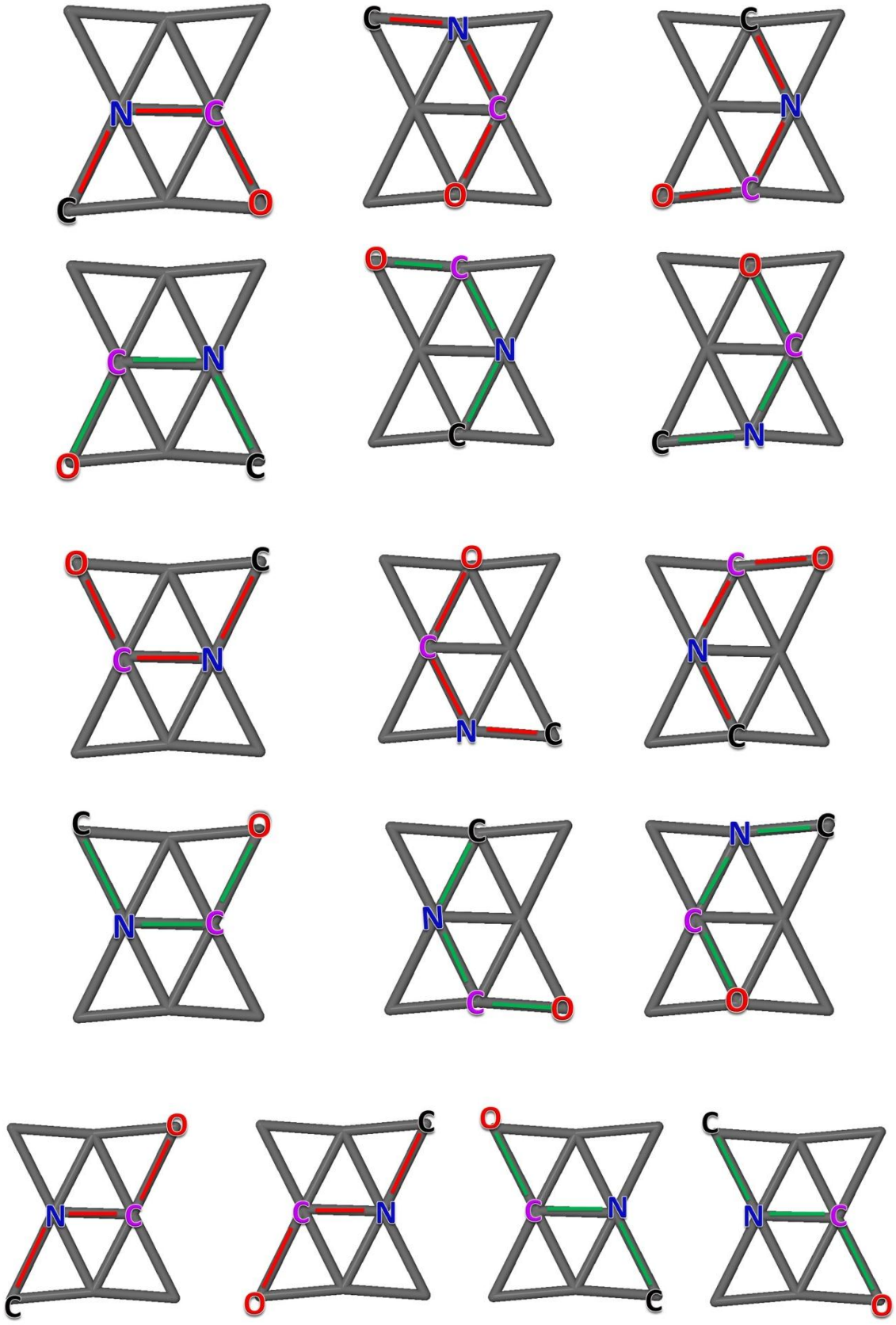

Scheme 1: Different positions that the NMF guest can occupy.

The program *PLATON*[7] was used to identify all C-H···π interactions in the inclusion compound (Figure 5.100). The shortest C18···π distances is 3.502 Å with C-H-π = 172°.

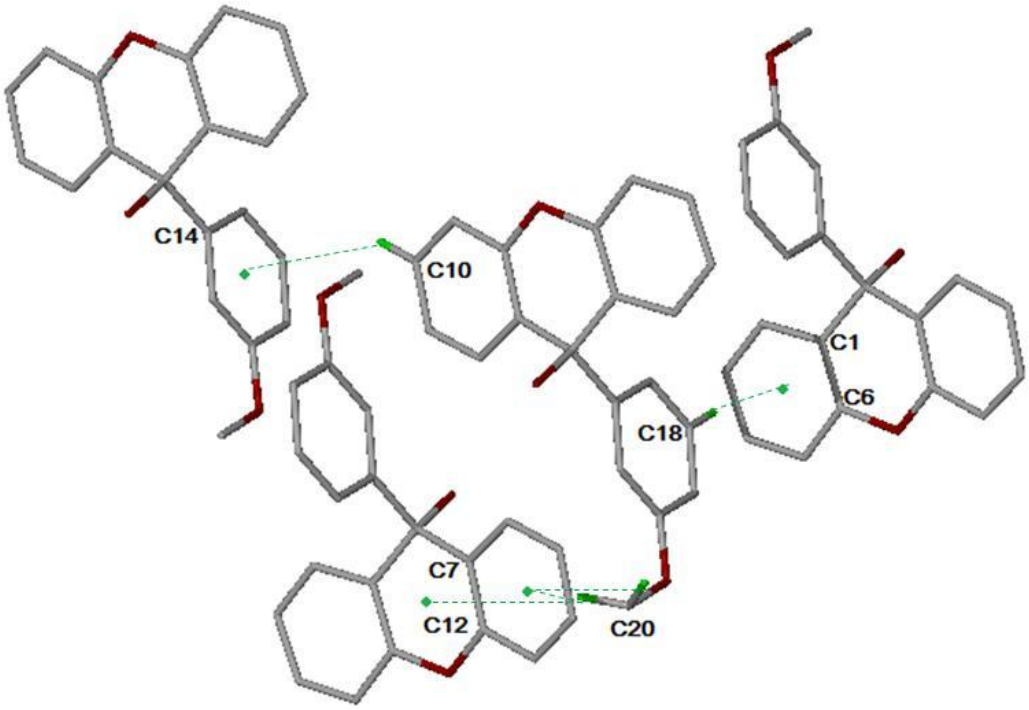

Figure 5.100: C-H···π interactions of neighbouring host molecules. The C-H···π interactions are indicated by green dotted lines.

The packing diagrams of **A2·NMF** along [100] direction are shown in Figure 5.101. The host molecules pack in such a manner that they encapsulate the guests (Figure 5.102).

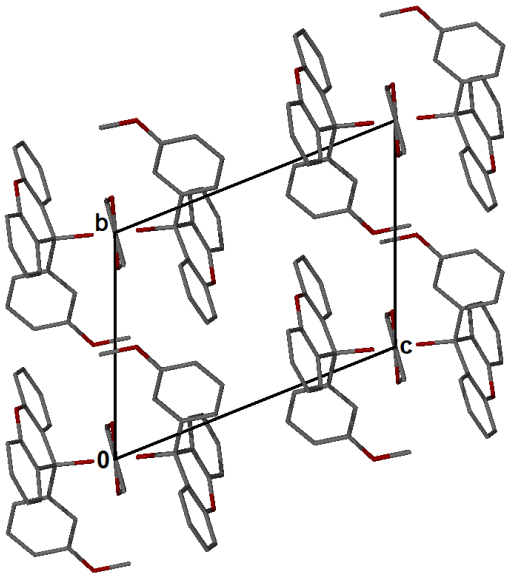

Figure 5.101: Packing diagram of **A2·NMF** down [100].

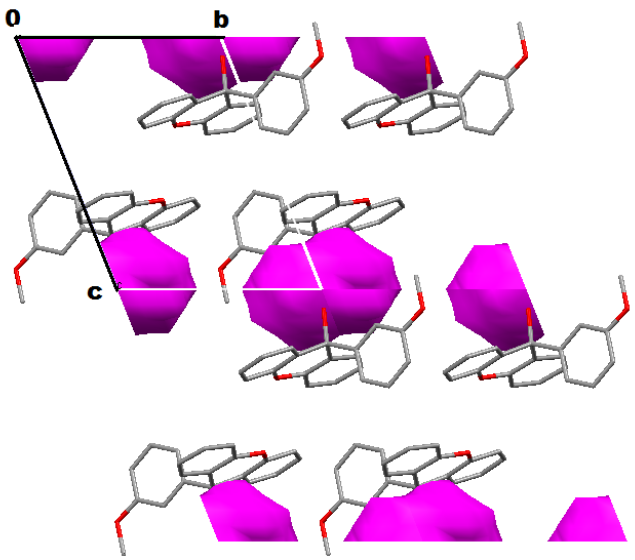

Figure 5.102: The cavities in which the guest resides.

The program *SECTION*[6] was used to map the cavities in which the guests are located (Figure 5.103). The program *PLATON*[7] was used to calculate the total potential solvent accessible volume and was found to be 89.2 Å^3.

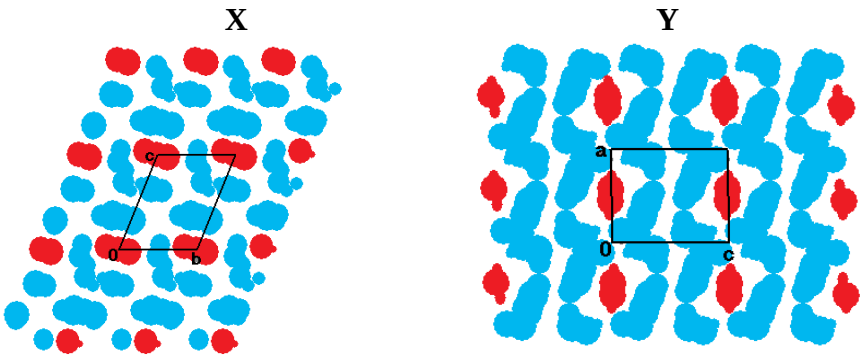

Figure 5.103: Section plot of **A2·NMF.** Host molecules are displayed in blue and guest molecules in red. X = View along [100] direction at section height 3.60 **Å**. Y = View along [010] direction at section height 0.00 **Å**.

5.13 Structure Comparison

The host 9-(3-methoxyphenyl)-9*H*-xanthen-9-ol forms inclusion compounds with morpholine, *N*-methylacetamide and *N*-methylformamide. Thermogravimetry results confirmed that all inclusion compounds have a host-guest ratio of 1:1. The crystal structure of the apohost (**A2**) refined successfully in the orthorhombic crystal system. **A2** crystallises in the space group *Pbca* with Z=8, and the asymmetric unit contains one host molecule. The melting point is 394.1 K with a density of 1.336 g/cm^3 which has been calculated.

The structures of **A2·MORPH** and **A2·NMF** were solved in the triclinic crystal system, space group $P\bar{1}$ with Z=2. The packing of **A2·MORPH** is stabilised by (Host)-OH···N-(Guest) hydrogen bonds. In addition there exists a weaker (Guest)-N-H···O-(Host) hydrogen bond with an N···O distance of 3.509(2) Å. The **A2·NMF** structure is stabilised by (Host)-OH···O-(Guest) hydrogen bonds. In this case the host molecules are in general positions with the guests disordered at Wyckoff position *d*. **A2·NMA** crystallises in the monoclinic space group $P2_1/n$ with Z=4, with the host and guest molecules in general positions. The structure is stabilised by (Host)-OH···O-(Guest) and (Guest)-NH···O-(Guest) hydrogen bonds with the Etter notation $C_2^2(7)$. Both the morpholine and the *N*-methylacetamide guests occupy channels, whereas the *N*-methylformamide guest is situated in cavities.

Selected torsion angles of **A2** are displayed in Figure 5.104, which can be used to describe the conformation of the host molecule. The torsion angles of the host molecules for **A2, A2·MORPH, A2·NMA** and **A2·NMF** are listed in Table 5.57.

Table 5.56: Torsion angles for **A2.**

Torsion angles
τ_1= O2-C13-C14-C15/°
τ_2= C20-O3-C16-C15/°
τ_3= C1-C13-C14-C15/°
τ_4= C7-C13-C14-C19/°

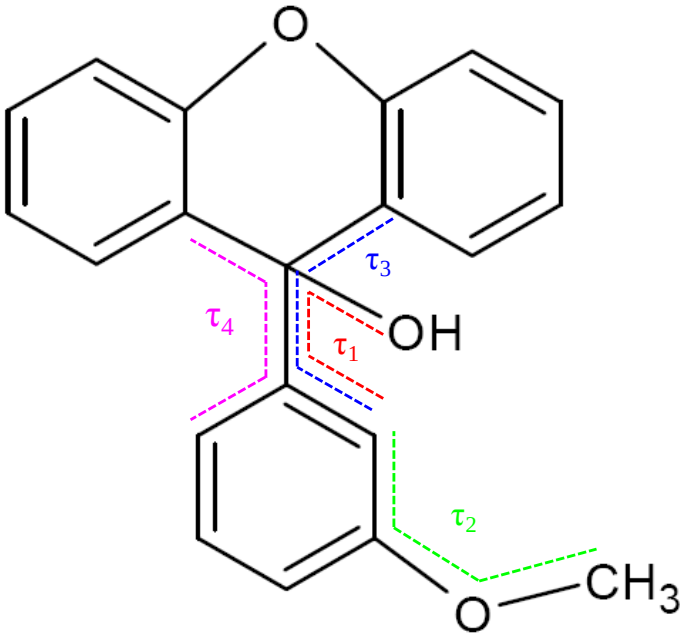

Figure 5.104: Schematic diagram of torsion angles in **A2**.

Table 5.57: Comparison of selected torsion angles for **A2**.

Torsion angles of A2					
Compound	**Suffix**	τ_1	τ_2	τ_3	τ_4
Apohost	-	0.5(2)	-0.2(2)	119.9(1)	60.7(2)
A2·MORPH	-	-2.5(2)	-0.5(2)	117.3(1)	57.1(2)
A2·NMA	-	-174.3(4)	-175.0(7)	-55.7(5)	-112.2(4)
A2·NMF	-	-4.3(2)	3.4(3)	113.6(2)	56.3(2)

CHAPTER 5
RESULTS AND DISCUSSION

***PART THREE* :**

The host 5-(4-methoxyphenyl)-5*H*-dibenzo[a,d]cyclohepten-5-ol forms inclusion compounds with aniline and morpholine.

A26

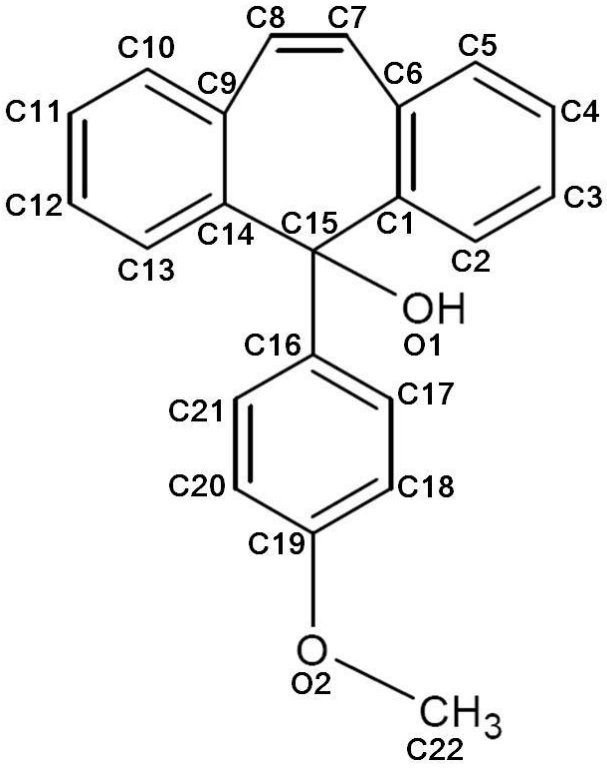

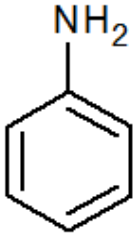

Aniline

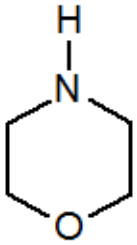

Morpholine

5.14 Guest: Aniline

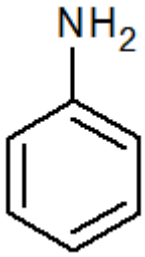

Table 5.58: Properties of aniline.

Guest	ANI
Molecular formula	**C_6H_7N**
Molar mass (g/mol)	**93.13**
Boiling Point (K)	**457**

5.14.1 Thermal Analysis

The thermal analysis results are shown in Figure 5.105. A single step mass loss of 12.9 % was observed in the TG curve which corresponds to a 1:½ host-guest ratio. The DSC shows two endotherms at T_{on}=371.3 K and T_{on}=391.9 K. The first endotherm is a sharp peak which is due to guest release. The second endotherm is due to the host melting. The thermal analysis results are listed in Table 5.59.

Table 5.59: Thermal analysis data for **A26·ANI.**

Compound	A26·ANI
Host: Guest ratio	**1:½**
TG calculated % mass loss	**12.9**
TG experimental % mass loss	**13.8**
DSC Endo$_1$ (T_{onset}, K)	**371.3**
DSC Endo$_2$ (T_{onset}, K)	**391.9**
DSC Host (T_{onset}, K)	**400.6**

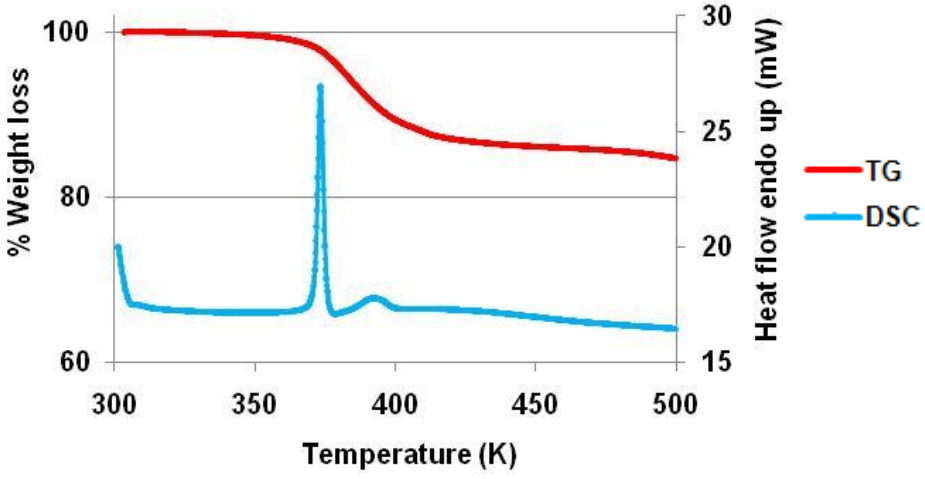

Figure 5.105: TGA and DSC curves obtained for **A26·ANI.**

5.14.2 Structure Refinement

All non-hydrogen atoms were found by direct methods in the difference electron density map and refined anisotropically. The hydroxyl hydrogen was first located in the difference electron density map and then refined with a simple bond length constraint dependent on the O···O distance.[1] The aniline guest is disordered and the hydrogen atoms on the guest was neither placed nor found in the electron density map, and therefore omitted from the final model. The carbon atoms (C1G, C2G and C4G) of the guest were assigned site occupancy factors of 0.5, whereas C3G=1.0. The nitrogen and carbon atom of the guest occupy the same position, therefore a site occupancy factor of 1.0 was assigned to the nitrogen atom. The structure refined successfully to R_1= 0.0568 with wR_2= 0.1568. The crystal data is given in Table 5.60.

Table 5.60: Crystal data of **A26·ANI.**

Compound	**A26·ANI**
Structural Formula	$C_{22}H_{18}O_2 \cdot ½C_6H_7N$
Host-Guest ratio	**1:½**
Molecular Mass (g.mol^{-1})	**360.93**
Data collection temp (K)	**296(2)**
Crystal system	**Triclinic**
Space group	$P\bar{1}$
a (Å)	**7.7475(12)**
b (Å)	**9.3914(14)**
c (Å)	**14.357(2)**
α (°)	**105.177(3)**
β (°)	**93.510(3)**
γ (°)	**106.494(3)**
Volume (Å^3)	**956.3(2)**
Z	**2**
μ/ mm^{-1}	**0.079**
F(000)	**382**
No. of reflections collected	**8151**
No. of unique reflection	**4728**
No. of reflections with I>2σ(I)	**3402**
D_c, Calculated density (g.cm^{-3})	**1.254**
Index range	**h: -10 to 10,** **k: -12 to 10,** **l: -19 to 14**
θ range	**1.49-28.40**
Goodness of fit, S	**0.910**
Final R indices [I>2σ(I)]	**R_1= 0.0568 ; wR_2= 0.1568**
R indices (all data)	**R_1= 0.0794; wR_2= 0.1789**
Largest diff peak and hole (eÅ^{-3})	**0.45 ; -0.38**

5.14.3 Discussion

The structure was solved in the triclinic space group $P\bar{1}$ with a structural formula of $C_{22}H_{18}O_2 \cdot ½C_6H_7N$. The asymmetric unit contains a host and guest molecule shown in Figure 5.106. The aniline guest is disordered over two positions as shown in Figure 5.107. The packing of the structure is characterized by host dimers that are hydrogen bonded via pairs of (Host)-O···$O_{methoxy}$-(Host) bonds. This is illustrated in Figure 5.108. The location of the *p*-methoxy phenyl moieties is such that they encapsulate the aniline guest that lies on a centre of symmetry at Wyckoff position *d*. The metrics of the hydrogen bonds are given in Table 5.61.

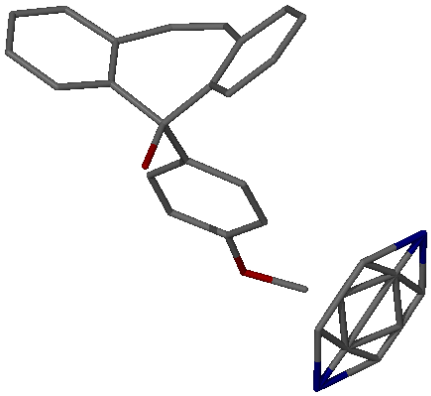

Figure 5.106: Asymmetric unit of **A26·ANI**.

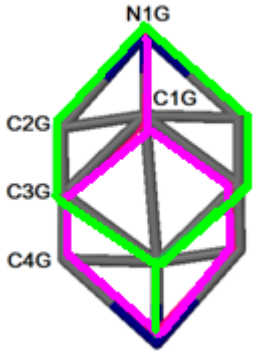

Figure 5.107: Disordered aniline.

Table 5.61: Hydrogen bond parameters of **A26·ANI.**

Donor(D)-H	Acceptor(A)	D···A (Å)	D-H (Å)	H···A (Å)	D-H···A (°)
O1-H1	O2 [-x , -y+1, -z]	2.812(2)	0.960(1)	1.872(1)	165(7)

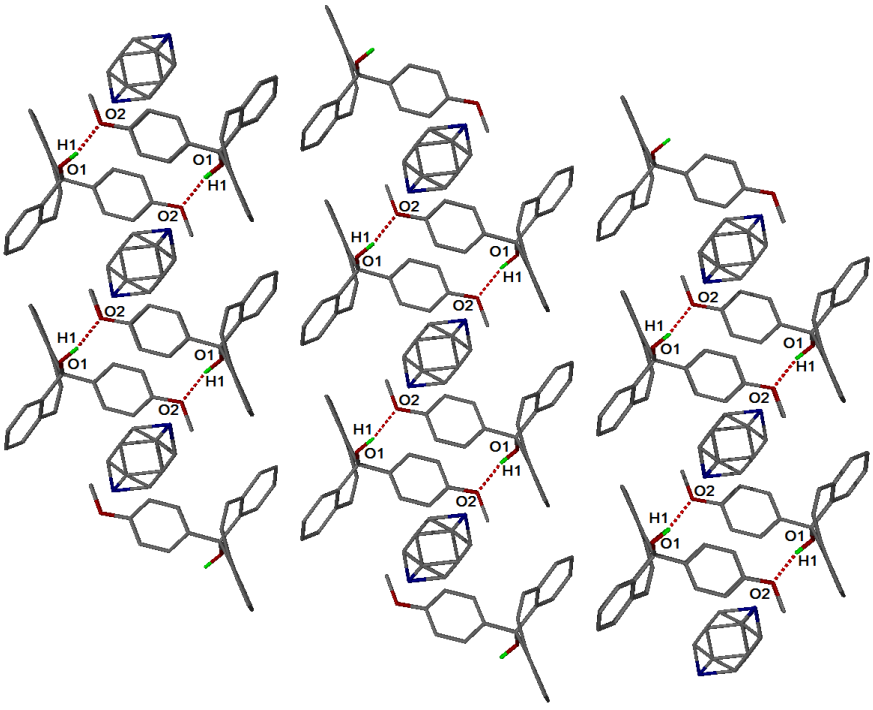

Figure 5.108: Hydrogen bonding in **A26·ANI.**

Pairs of host molecules display off-set face-to-face π-π interactions, with a shortest distance between two ring centroids of 3.726 Å (Figure 5.109). The shortest C···π distance of the C-H···π interactions listed is 3.540 Å with a C-H-π angle of 155° (Figure 5.110).

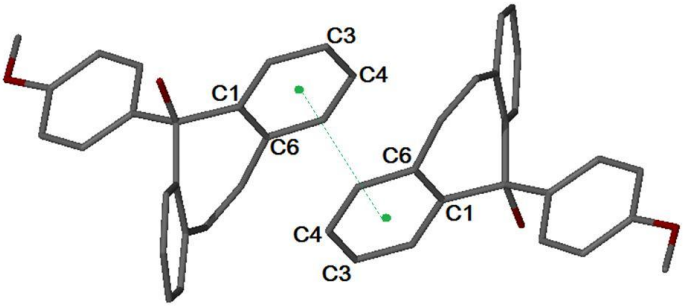

Figure 5.109: Off-set face-to-face π- π stacking of neighbouring host molecules. The distance between the centroids is indicated by green dotted lines. All hydrogen atoms were omitted for clarity.

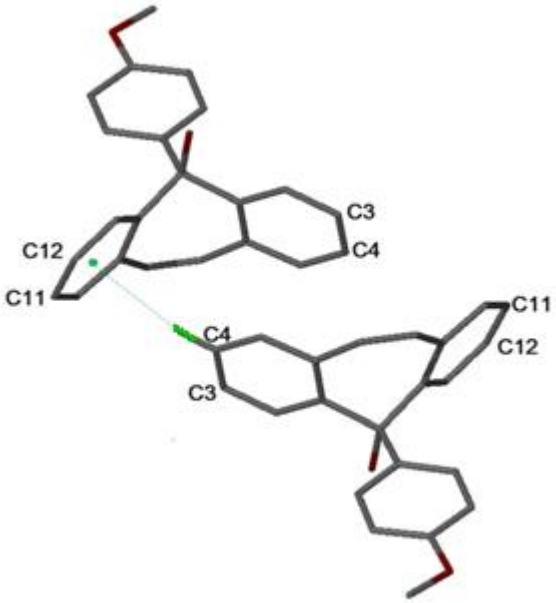

Figure 5.110: C-H···π interaction of neighbouring host molecules. The C-H···π interaction is indicated by a green dotted line.

The packing is shown in Figure 5.111, which displays a host-guest ratio of 1:½, and the guests are located in cavities (Figure 5.112).[5]

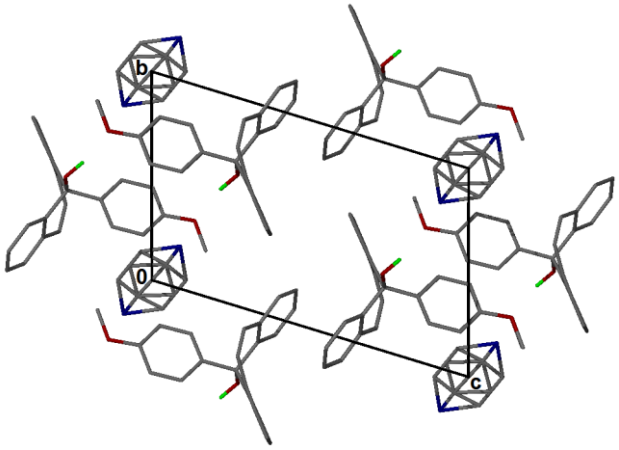

Figure 5.111: The packing diagram of **A26·ANI** down [100].

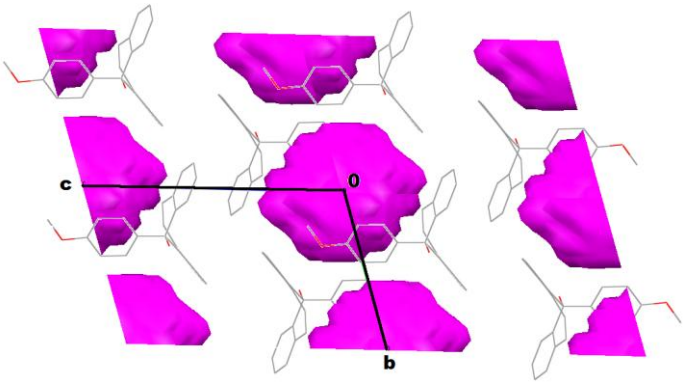

Figure 5.112: The cavities in which the guests are located.

5.15 Guest: Morpholine

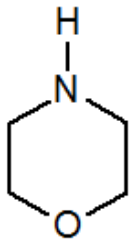

Table 5.62: Properties of morpholine**.**

Guest	MORPH
Molecular formula	**C_4H_9NO**
Molar mass (g/mol)	**87.1**
Boiling Point (K)	**401**

5.15.1 Thermal Analysis

The thermal data is given in Table 5.63. In the TG curve the percentage mass loss of 8.9 % corresponds to a host-guest ratio of 1:⅓. A single endotherm is observed for the DSC curve which corresponds to simultaneous dissolution of the host upon release of the guest. The thermal analysis results are shown in Figure 5.113.

Table 5.63: Thermal analysis data for **A26·MORPH.**

Compound	A26•MORPH
Host: Guest ratio	**3:1**
TG calculated % mass loss	**8.5**
TG experimental % mass loss	**8.9**
DSC $Endo_1$ (T_{onset}, K)	**403.7**
DSC Host $Endo_1$ (T_{onset}, K)	**400.6**

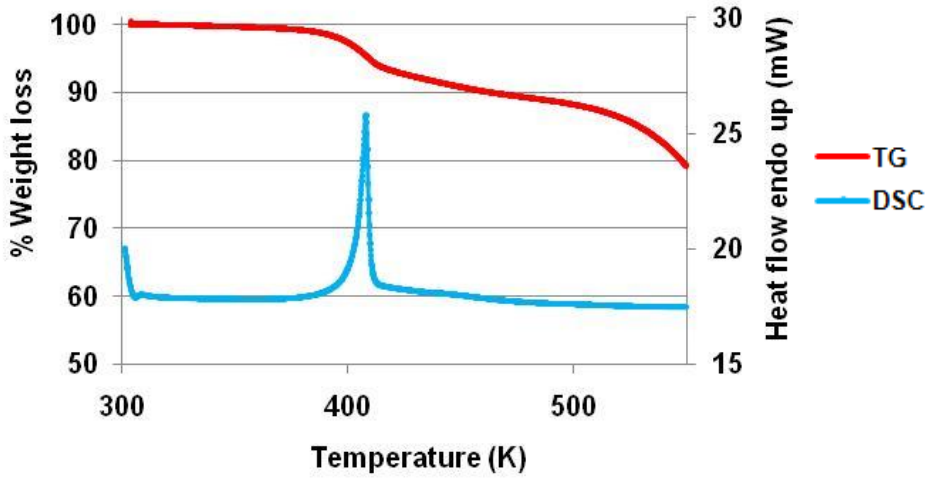

Figure 5.113: TGA and DSC curves obtained for **A26·MORPH.**

5.15.2 Structure Refinement

All non-hydrogen atoms were found by direct methods in the difference electron density map and refined anisotropically. The hydroxyl hydrogen (H1A) was first located in the difference electron density map and then refined with a simple bond length constraint dependent on the O···O distance.[1] One morpholine guest was found disordered and was solved by parts (part 1 = GA and part 2 = GB). The disordered morpholine non-hydrogen atoms was refined anisotropically, but the refinement was unstable. The disordered guest (GB) was therefore refined isotropically. The structure refined successfully to R_1= 0.0715 with wR_2= 0.1559. The crystal data is reported in Table 5.64.

Table 5.64: Crystal data of **A26·MORPH.**

Compound	**A26·MORPH**
Structural Formula	**$6C_{22}H_{18}O_2 \cdot 2\ C_4H_9NO$**
Host-Guest ratio	**3:1**
Molecular Mass (g.mol^{-1})	**2060.43**
Data collection temp (K)	**173**
Crystal system	**Monoclinic**
Space group	***Pc***
a (Å)	**9.9800(6)**
b (Å)	**22.6606(13)**
c (Å)	**23.6337(15)**
β (°)	**92.5100(10)**
Volume (Å^3)	**5339.7(6)**
Z	**2**
μ/ mm^{-1}	**0.082**
F(000)	**2184**
No. of reflections collected	**32481**
No. of unique reflection	**17297**
No. of reflections with I>2σ(I)	**9969**
D_c, Calculated density (g.cm^{-3})	**1.282**
Index range	**h: -12 to 13, k: -22 to 30, l: -12 to 31**
θ range	**1.72-28.30**
Goodness of fit, S	**1.027**
Final R indices [I>2σ(I)]	**R_1= 0.0715 ; wR_2= 0.1559**
R indices (all data)	**R_1= 0.1399; wR_2= 0.1888**
Largest diff peak and hole (eÅ^{-3})	**0.61 ; -0.44**

5.15.3 Discussion

The asymmetric unit of **A26·MORPH** contains six independent host and two independent guest molecules, which gives a structural formula of $6C_{22}H_{18}O_2 \cdot 2C_4H_9NO$ (Figure 5.114). The host and guest molecules are located in general positions. One of the morpholine guests is disordered over two positions and has site occupancy factors of 0.62 (GA) and 0.38 (GB) (Figure 5.115). The morpholine guests exhibits a chair conformation. The structure is stabilised by (Host)-OH···O-(Host) hydrogen bonding shown in Figure 5.116. The hydrogen bonding parameters are provided in Table 5.65.

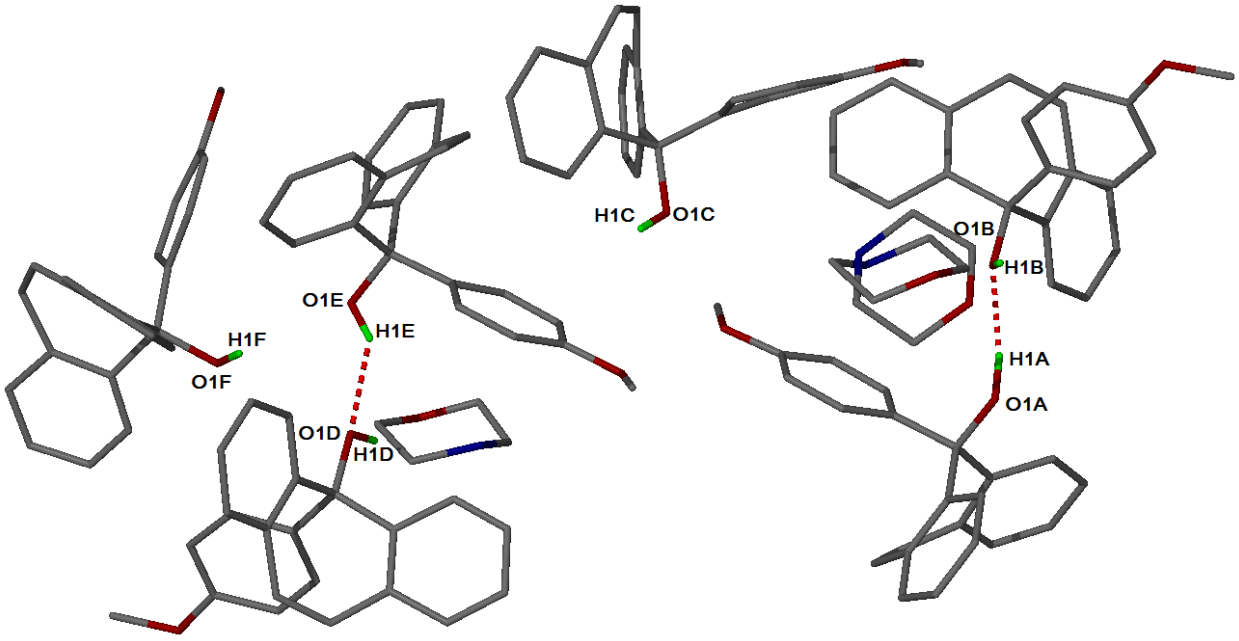

Figure 5.114: Hydrogen bonding in asymmetric unit of **A26·MORPH.** The disordered guest is shown.

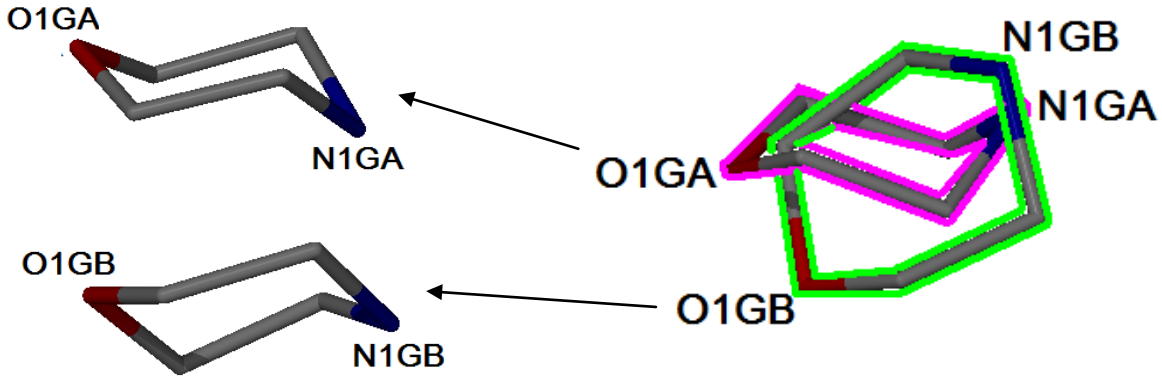

Figure 5.115: Disordered morpholine guests.

Table 5.65: Hydrogen bond parameters of **A26·MORPH.**

Donor(D)-H	Acceptor(A)	D···A (Å)	D-H (Å)	H···A (Å)	D-H···A (°)
O1A-H1A	**O1B**	**2.80(1)**	**0.961(3)**	**1.887(2)**	**159(3)**
O1E-H1E	**O1D**	**2.81(1)**	**0.851(1)**	**2.023(1)**	**154(1)**

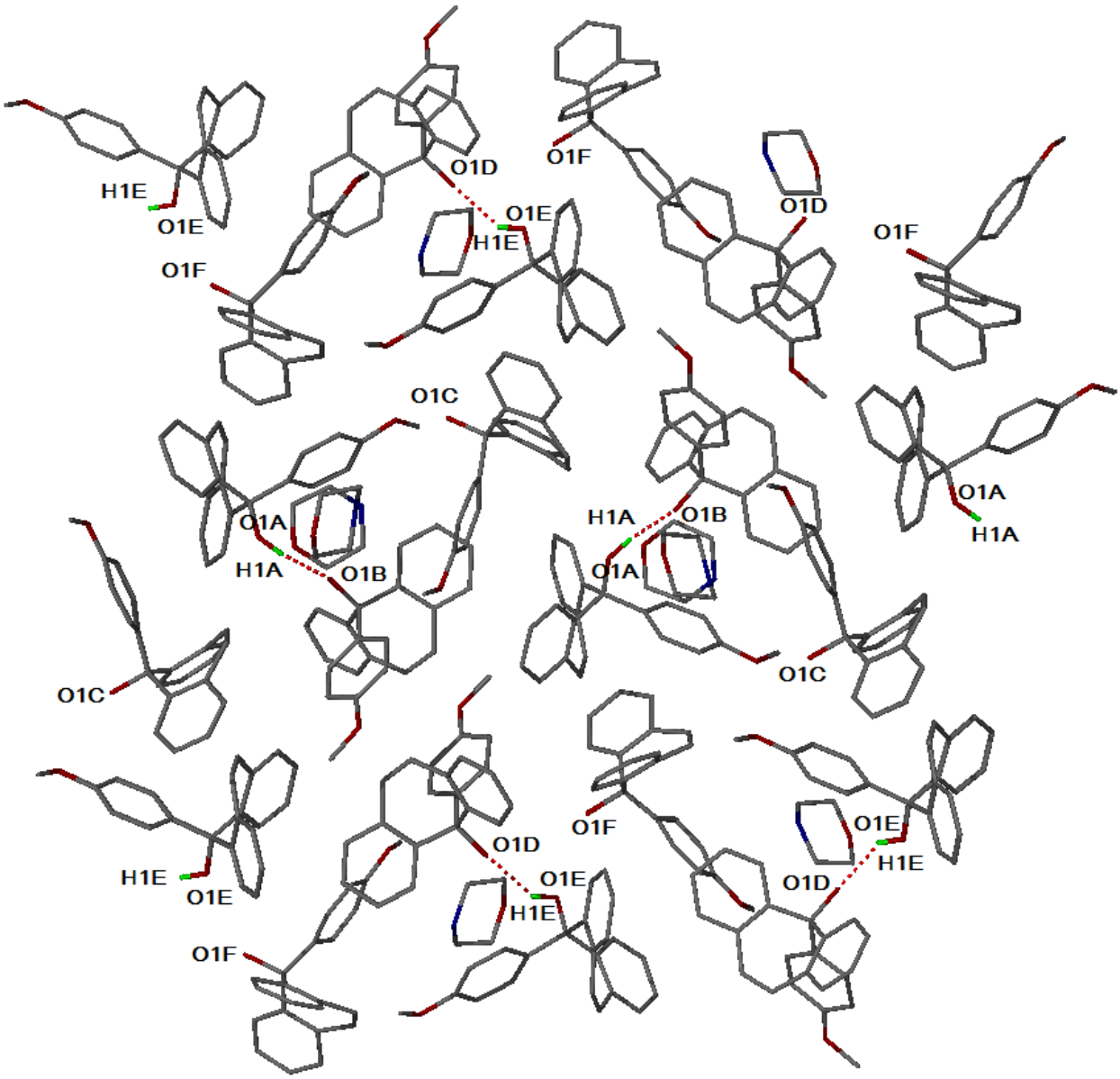

Figure 5.116: Hydrogen bonding in **A26·MORPH.** The disordered guest is shown.

The only C···π distance between a host and guest molecule has a C···π and H···π distance of 3.735 Å and 3.071 Å respectively, with angle of 125° (Figure 5.117). The shortest C···π distance between a pair of host molecules is 3.473 Å with a C-H-π angle of 151° shown in Figure 5.118.

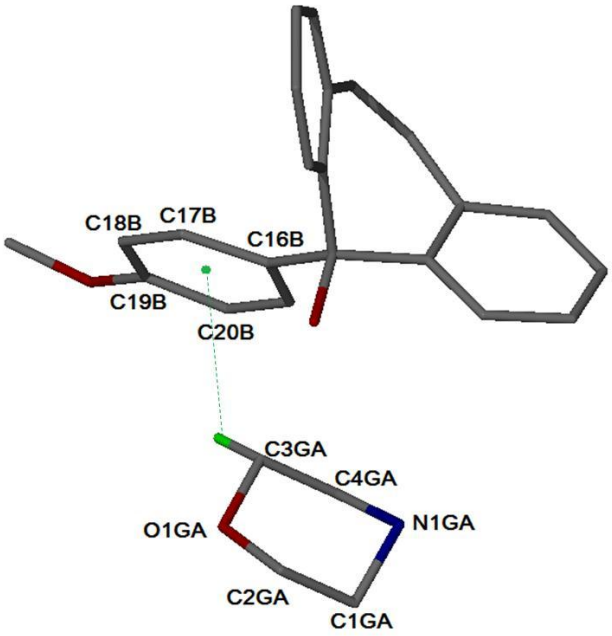

Figure 5.117: C-H···π interaction between a host and guest molecule. The C-H···π interaction is indicated by a green dotted line.

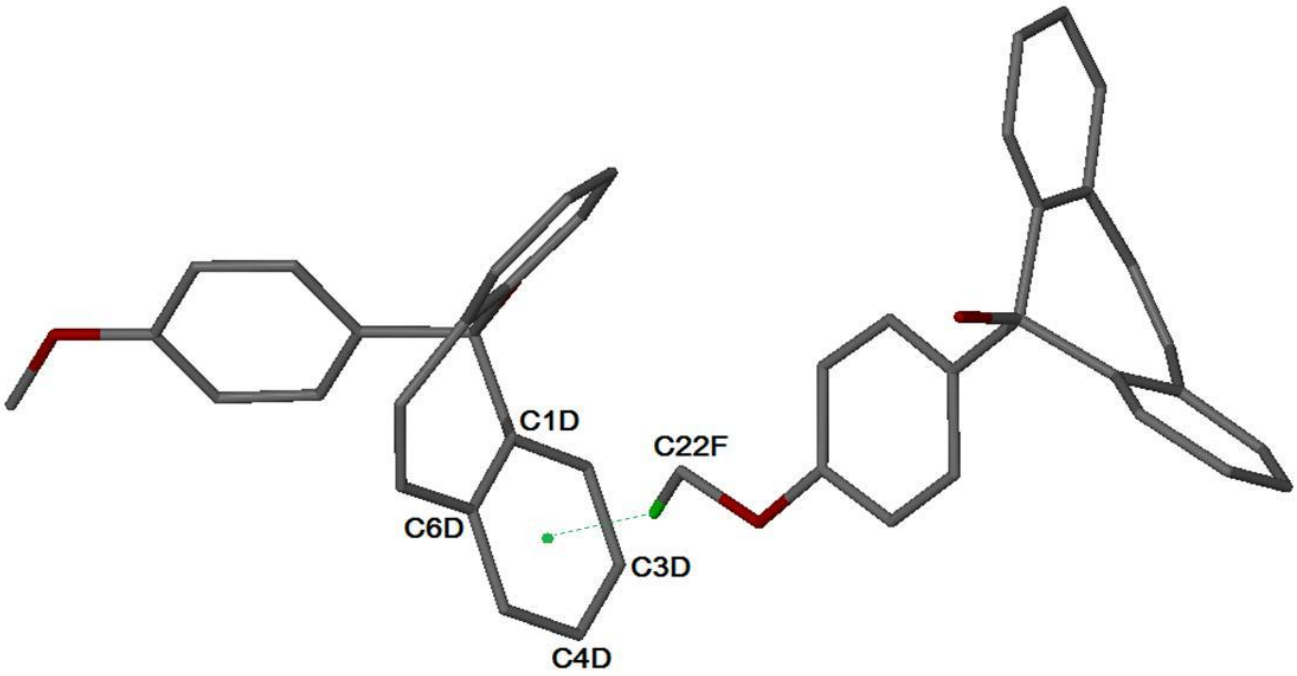

Figure 5.118: C-H···π interaction between a pair of host molecules. The C-H···π interaction is indicated by a green dotted line.

The packing diagram viewed down [100] is shown in Figure 5.119. The morpholine guests effectively lie in cavities, making this a true clathrate structure. The cavities in which the guests are located are shown in Figure 5.120.[5]

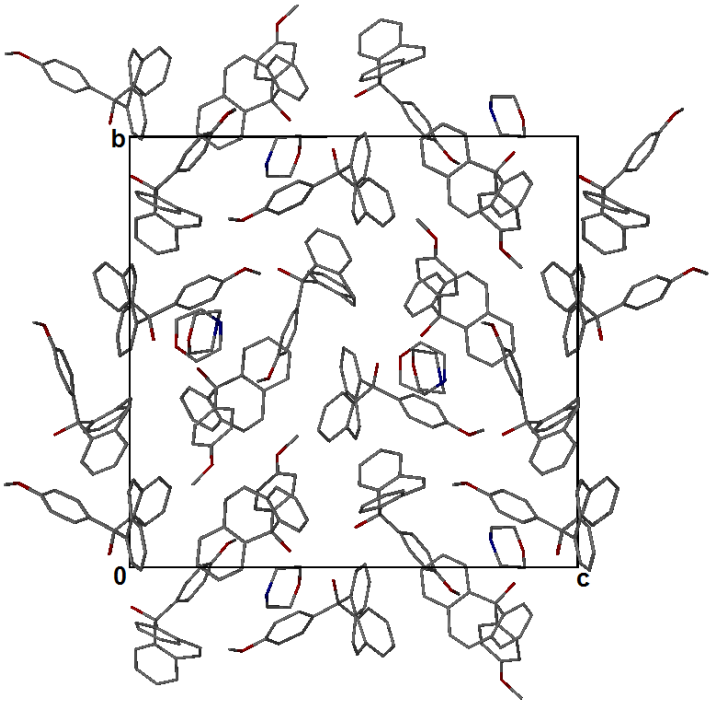

Figure 5.119: Packing diagram of **A26·MORPH** along [100]. All hydrogen atoms are omitted.

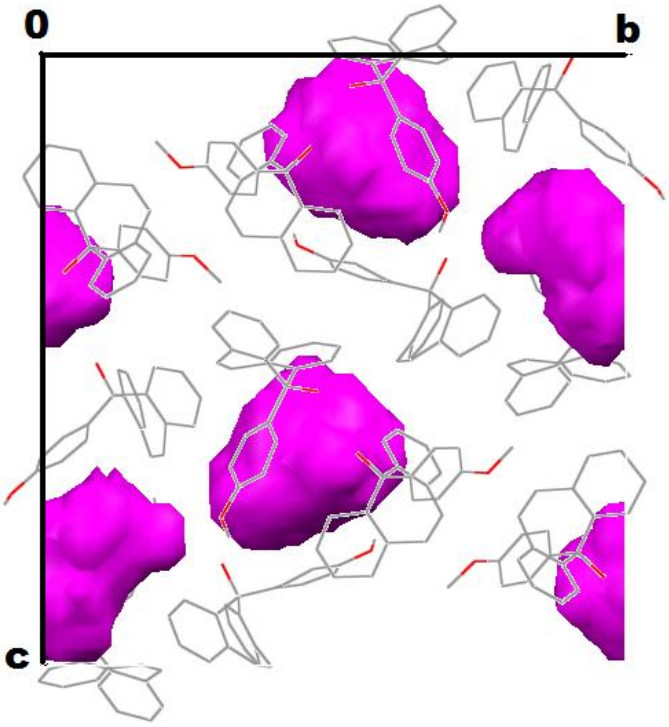

Figure 5.120: The cavities in which the morpholine guests are located.

5.15.4 Guest Exchange

A guest exchange experiment was conducted to determine whether **A26·PYR** could convert to **A26·MORPH** via exposure to the vapour of the morpholine guest. The crystals were exposed to the vapour of morpholine for 200 minutes and the progress of the exchange reaction was monitored using DSC. At the start of the experiment (t=0 min) two endotherms are present. The first endotherm is the desorption of the pyridine from the inclusion compound and the second is the melt of the host compound. As the exchange reaction proceeds the first endotherm diminishes due to loss of the pyridine guest and the peak due to the host compound melt disappears. The reaction is complete at t=200 min, when only the **A26·MORPH** is detected. The vapour pressures (in mmHg@20°C) of morpholine and pyridine are 7.44 and 15.65 respectively.[10] A TG experiment was performed on the crystals at t=200 minutes and showed a single mass loss step of 8.9 %, which corresponds to the TG curve of **A26·MORPH.** The paucity of **A26** prohibited further guest exchange experiments.

Guest exchange reaction : A26•PYR$_{(s)}$ + MORPH$_{(vap)}$ → A26•MORPH$_{(s)}$ + PYR$_{(vap)}$

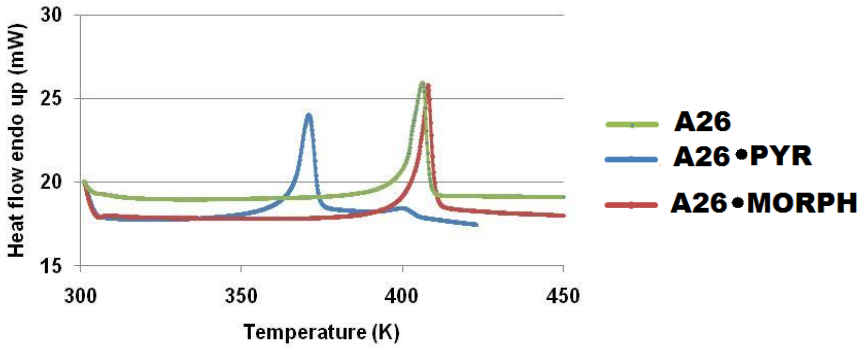

Figure 5.121: DSC curves of **A26**, **A26·PYR** and **A26·MORPH**.

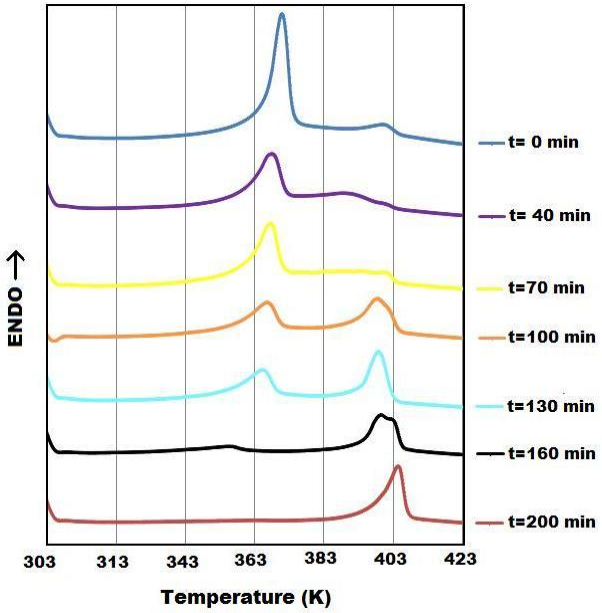

Figure 5.122: DSC curves of crystals (**A26·PYR**) exposed to morpholine vapour at t=0, t=40, t=70, t=100, t=130, t=160 and t=200 minutes.

5.16 Structure Comparison

The host 5-(4-methoxyphenyl)-5*H*-dibenzo[a,d]cyclohepten-5-ol forms inclusion compounds with aniline and morpholine. The **A26·MORPH** structure crystallises in the spacegroup *Pc* with a structural formula of $6C_{22}H_{18}O_2 \cdot 2C_4H_9NO$, with the host and guest molecules in general positions. **A26·ANI** was solved in the space group $P\bar{1}$ with a structural formula of $C_{22}H_{18}O_2 \cdot ½C_6H_7N$, while the aniline guest lies on a centre of symmetry at Wyckoff position *d*. Both structures are stabilised by (Host)-OH···O-(Host) hydrogen bonding. The morpholine and aniline guests are located in cavities, therefore **A26·MORPH** and **A26·ANI** are clathrates. The packing of the **A26·ANI** structure is characterized by host dimers that are hydrogen bonded to one another.

A guest exchange experiment was successfully conducted, the reaction was as follows:

$$\mathbf{A26{\bullet}PYR_{(s)} + MORPH_{(vap)} \rightarrow A26{\bullet}MORPH_{(s)} + PYR_{(vap)}}$$

Selected torsion angles of **A26** are listed in Table 5.66, which can be used to describe the conformation of the host molecule. The torsion angles of the host molecules for **A26·ANI** and **A26·MORPH** are listed in Table 5.67.

Table 5.66: Torsion angles for **A26.**

Torsion angles
τ_1= O1-C15-C16-C17/°
τ_2= C18-C19-O2-C22/°
τ_3= C1-C15-C16-C17/°
τ_4= C14-C15-C16-C21/°
τ_5= C7-C6-C1-C15/°
τ_6= C8-C9-C14-C15/°
τ_7= C6-C7-C8-C9/°

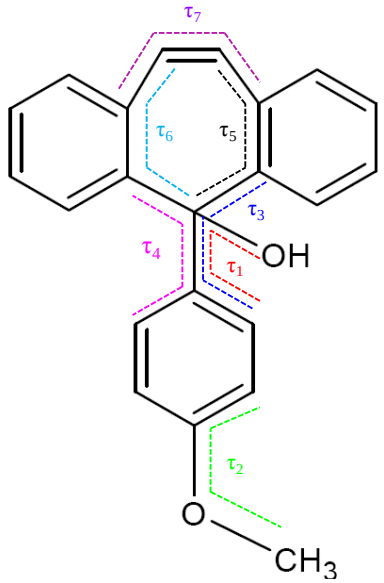

Figure 5.123: Schematic diagram indicating torsion angles for **A26.**

Table 5.67: Comparison of selected torsion angles for **A26**.

Torsion angles of A26								
Compound	**Suffix**	**τ_1**	**τ_2**	**τ_3**	**τ_4**	**τ_5**	**τ_6**	**τ_7**
A26·ANI	**-**	**-79(1)**	**-11(2)**	**38(2)**	**-27(2)**	**4(2)**	**-10(2)**	**2(3)**
A26·MORPH	**A**	**-87(1)**	**-178(1)**	**32(1)**	**-30(1)**	**4(2)**	**-7(2)**	**-1(2)**
	B	**77(1)**	**4(1)**	**-162(1)**	**143(1)**	**7(1)**	**-6(2)**	**-1(2)**
	C	**-88(1)**	**8(2)**	**28(2)**	**-25(2)**	**5(2)**	**-6(2)**	**-1(2)**
	D	**-76(1)**	**1(1)**	**40(1)**	**-23(1)**	**8(1)**	**-7(2)**	**-2(2)**
	E	**83(1)**	**171(1)**	**-157(1)**	**150(1)**	**9(2)**	**-4(1)**	**1(2)**
	F	**-89(1)**	**174(1)**	**158(1)**	**-148(1)**	**-5(2)**	**6(2)**	**-1(2)**

CHAPTER 5
RESULTS AND DISCUSSION

***PART FOUR*:**

The hosts 5-(4-chlorophenyl)-5*H*-dibenzo[a,d]cyclohepten-5-ol (A28), 5-[3(trifluoromethyl)phenyl]-5*H*-dibenzo[a,d]cyclohepten-5-ol (A31) and 5-(naphthalen-1-yl)-5*H*-dibenzo[a,d]cyclohepten-5-ol (A32) form inclusion compounds with morpholine.

A28

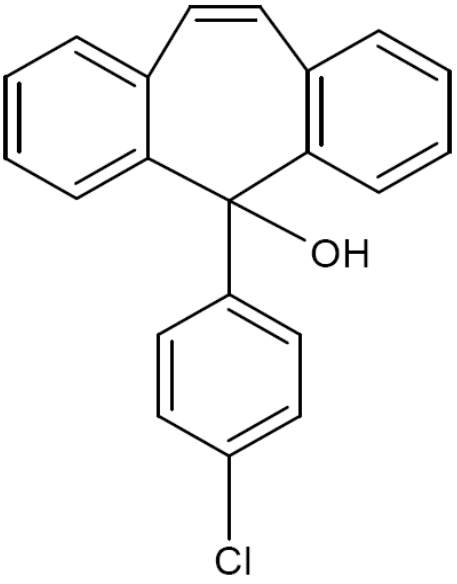

A31

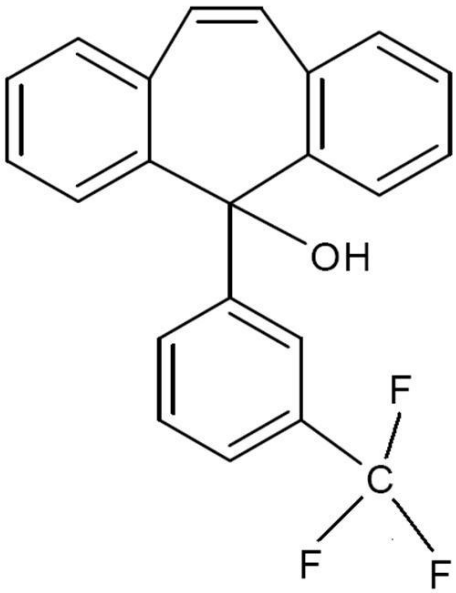

A32

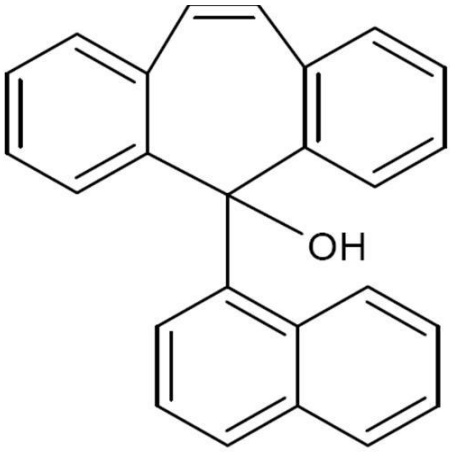

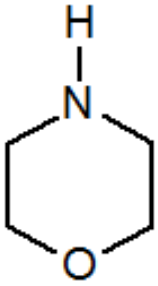

Morpholine

5.17 Host: 5-(4-chlorophenyl)-5*H*-dibenzo[a,d]cyclohepten-5-ol

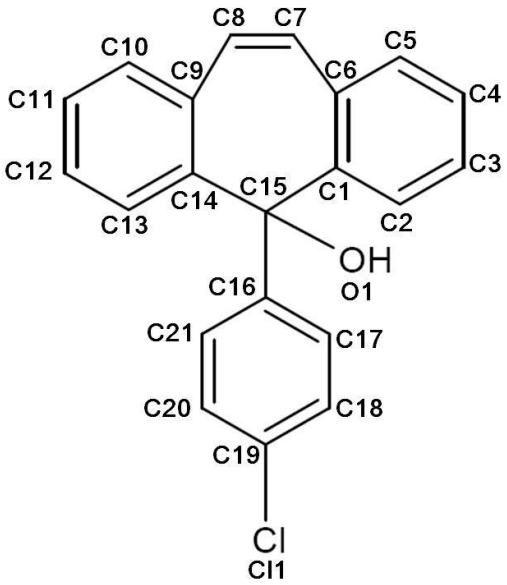

Figure 5.124: Atomic numbering of **A28.**

5.17.1 Guest: Morpholine

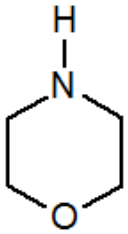

Table 5.68: Properties of morpholine**.**

Guest	MORPH
Molecular formula	**C_4H_9NO**
Molar mass (g/mol)	**87.1**
Boiling Point (K)	**401**

5.17.2 Thermal Analysis

The thermal analysis results are shown in Figure 5.125. The TG curve shows two mass loss steps, the first and second step corresponds to 11.5 % and 10.6 % respectively. The combined percentage mass loss is 22.1 % which corresponds to the host-guest ratio 1:1. These results suggest that **A28·MORPH** undergoes a complex mechanism for thermal decomposition. This is confirmed by the DSC results which gave four endotherms. The thermal analysis results are listed in Table 5.69.

Table 5.69: Thermal analysis data for **A28·MORPH.**

Compound	A28•MORPH
Host: Guest ratio	**1:1**
TG calculated % mass loss	**21.5**
TG experimental % mass loss	**22.1**
DSC Endo$_1$ (T_{onset}, K)	**317.2**
DSC Endo$_2$ (T_{onset}, K)	**378.9**
DSC Endo$_3$ (T_{onset}, K)	**384.5**
DSC Endo$_4$ (T_{onset}, K)	**413.9**
DSC Host (T_{onset}, K)	**397.8**

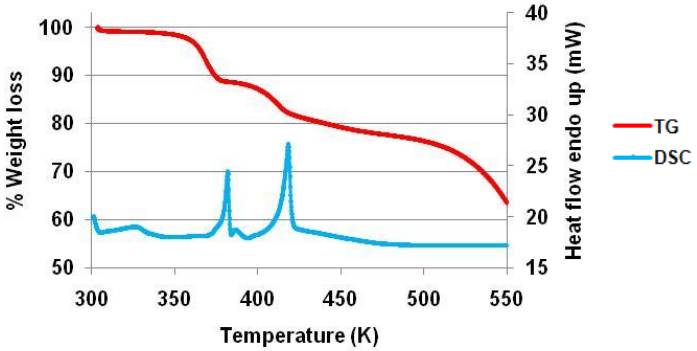

Figure 5.125: TGA and DSC curves obtained for **A28·MORPH.**

5.17.3 Structure Refinement

All non-hydrogen atoms were found by direct methods in the difference electron density map and refined anisotropically. The hydroxyl hydrogens of the host were located in the difference electron density map. The secondary amine hydrogens (N1G and N1GA) were located in the difference electron density map. One morpholine guest was found disordered and was solved by parts (part 1 = GA and part 2 = GB). The structure refined successfully to R_1= 0.0380 with wR_2= 0.1013. The crystal data is given in Table 5.70.

Table 5.70: Crystal data of **A28·MORPH.**

Compound	**A28·MORPH**
Structural Formula	**$2C_{21}H_{15}OCl \cdot 2C_4H_9NO$**
Host-Guest ratio	**1:1**
Molecular Mass (g.mol^{-1})	**811.80**
Data collection temp (K)	**173**
Crystal system	**Triclinic**
Space group	**$P\bar{1}$**
a (Å)	**10.283(4)**
b (Å)	**13.724(6)**
c (Å)	**15.069(6)**
α (°)	**87.226(9)**
β (°)	**86.777(8)**
γ (°)	**73.953(10)**
Volume (Å^3)	**2039.3(14)**
Z	**2**
μ/ mm^{-1}	**0.209**
F(000)	**856**
No. of reflections collected	**16032**
No. of unique reflection	**7201**
No. of reflections with I>2σ(I)	**5663**
D_c, Calculated density (g.cm^{-3})	**1.322**
Index range	**h: -12 to 12, k: -15 to 16, l: -17 to 17**
θ range	**1.35-25.20**
Goodness of fit, S	**1.042**
Final R indices [I>2σ(I)]	**R_1= 0.0380; wR_2= 0.1013**
R indices (all data)	**R_1= 0.0536 ; wR_2= 0.1105**
Largest diff peak and hole (eÅ^{-3})	**0.49 ; -0.30**

5.17.4 Discussion

The structure was solved in the triclinic space group $P\bar{1}$ with Z=2. The asymmetric unit of **A28·MORPH** contains two independent host and two independent guest molecules in general positions, which gives a structural formula of $2C_{21}H_{15}OCl{\cdot}2C_4H_9NO$ (Figure 5.126). One of the morpholine guests is disordered and has site occupancy factors of 0.56 (GA) and 0.44 (GB) shown in Figure 5.127. The morpholine guests exhibit a chair conformation.

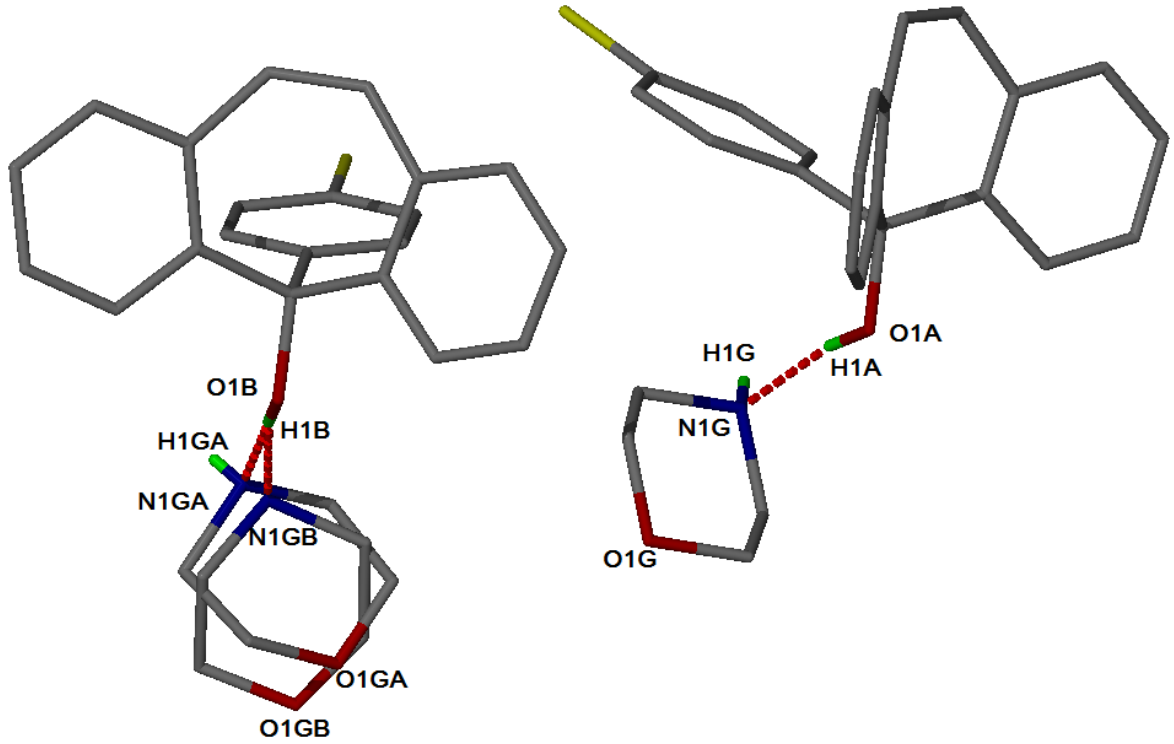

Figure 5.126: Hydrogen bonding in the asymmetric unit of **A28·MORPH.** The disordered guest is shown.

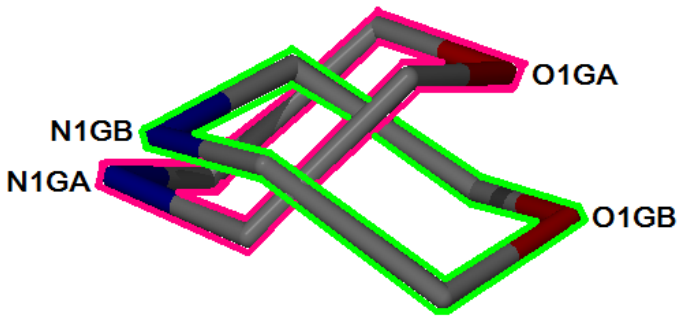

Figure 5.127: Disordered morpholine guests.

The structure is stabilised by (Host)-OH···N-(Guest) hydrogen bonds. The hydrogen bonding parameters are provided in Table 5.71. The hydrogen bonding between host and disordered guest is shown in Figure 5.128.

Table 5.71: Hydrogen bond parameters of **A28·MORPH.**

Donor(D)-H	Acceptor(A)	D···A (Å)	D-H (Å)	H···A (Å)	D-H···A (°)
O1A-H1A	**NIG**	**2.726(2)**	**0.87(3)**	**1.87(3)**	**166(3)**
O1B-H1B	**N1GA**	**2.748(7)**	**0.88(3)**	**1.87(3)**	**173(3)**
O1B-H1B	**N1GB**	**2.69(1)**	**0.88(3)**	**1.84(3)**	**164(3)**

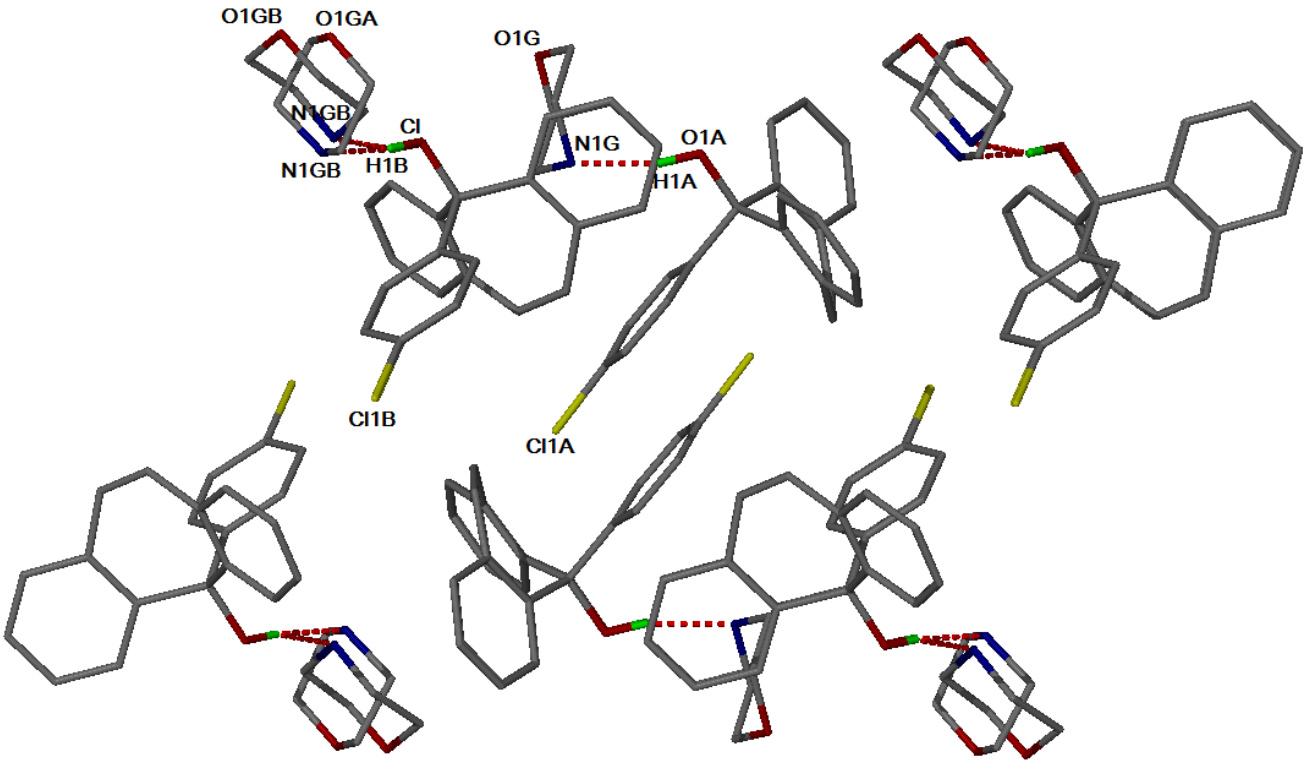

Figure 5.128: Hydrogen bonding in **A28·MORPH.** The disordered guests are shown.

The shortest C···π distance between a host and guest molecule is 3.470 Å [C(1GA)···π], with an angle of 142°, shown in Figure 5.129.

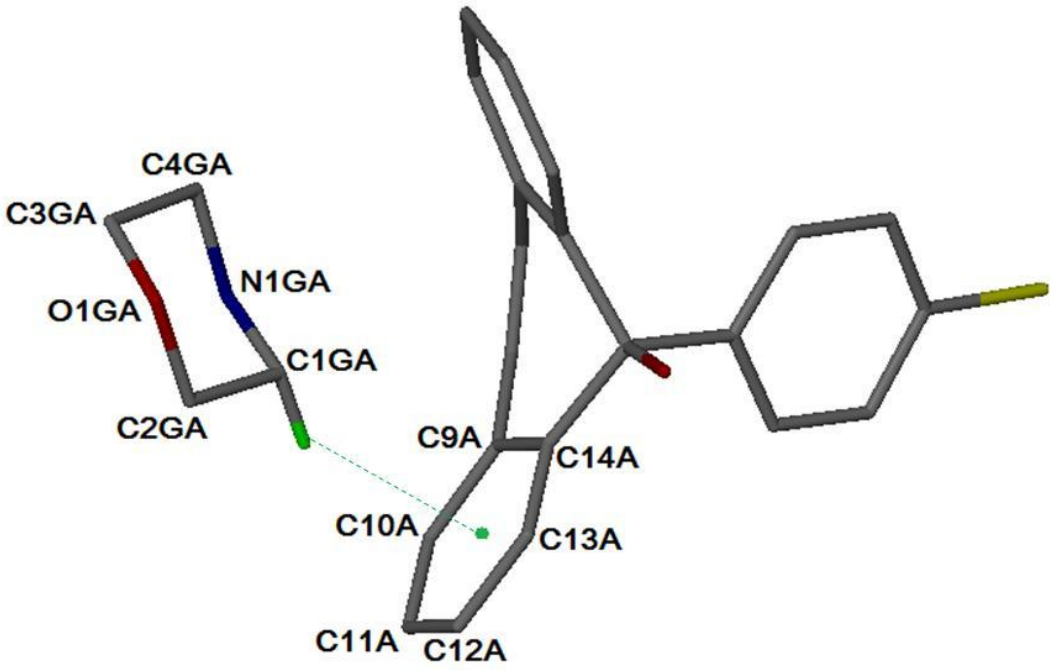

Figure 5.129: C-H···π interaction between a host and guest molecule.
The C-H···π interaction is indicated by a green dotted line.

The guest molecules are located in intersecting channels viewed down [100] and [010] shown in Figure 5.130. The channels are constricted shown in Figure 5.130(b). In Figure 5.131 the intersecting channels can be seen when viewed down [001].

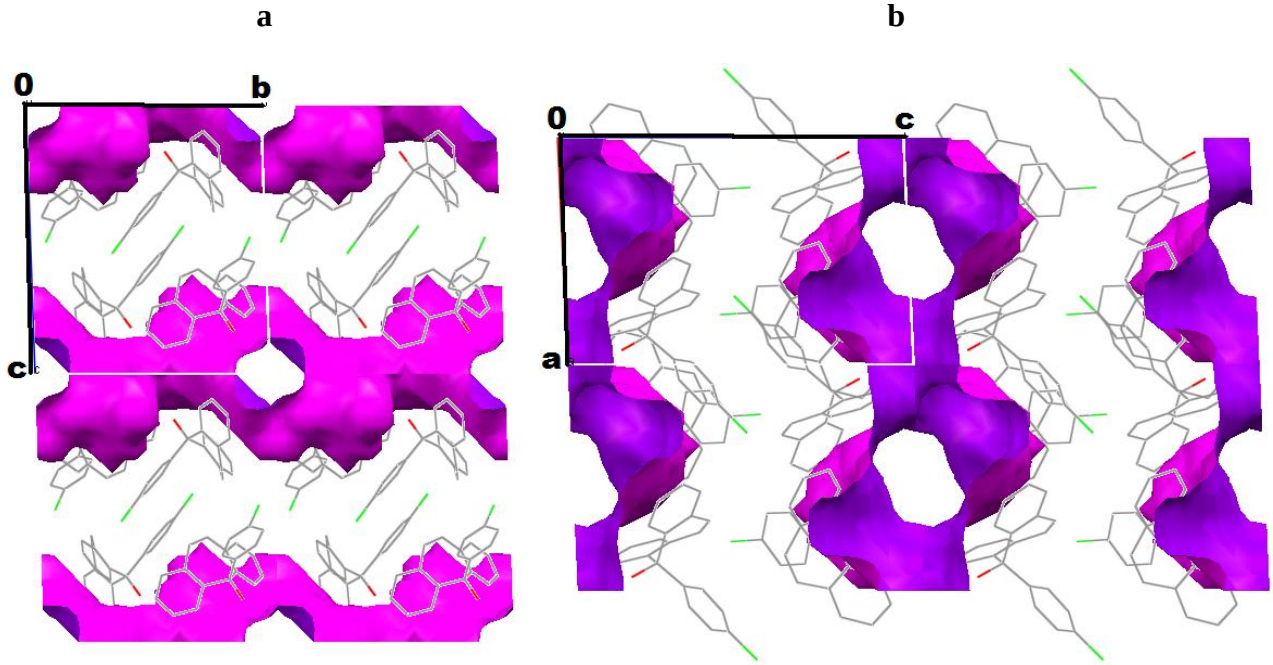

Figure 5.130: Channels down (a) [100] (b) [010].

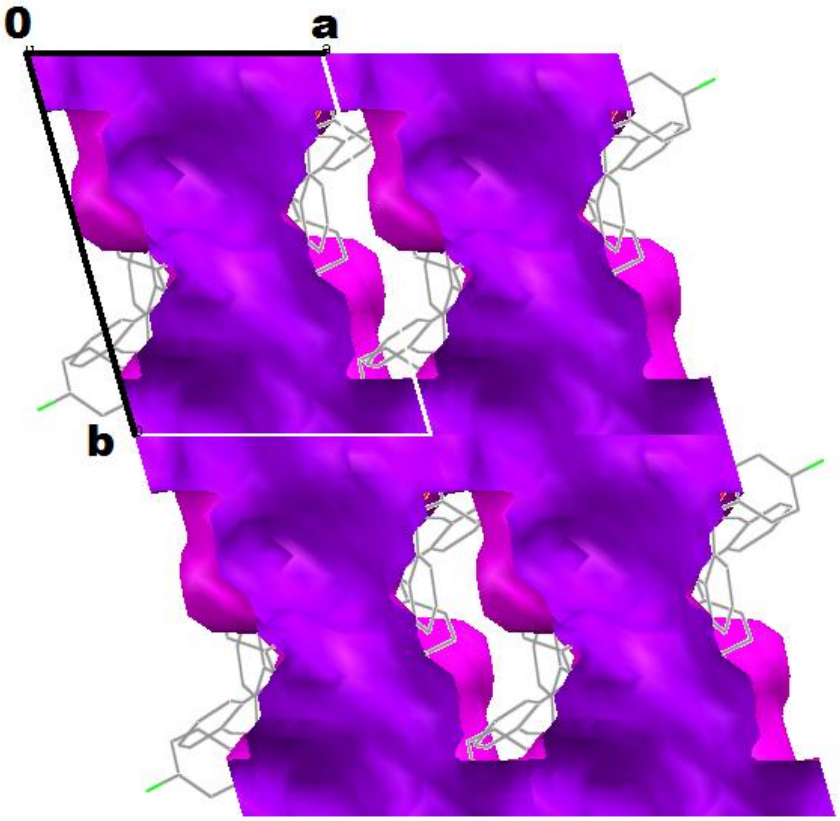

Figure 5.131: Intersecting channel, view down [001].

5.18 Host: 5-[3(trifluoromethyl)phenyl]-5*H*-dibenzo[a,d]cyclohepten-5-ol

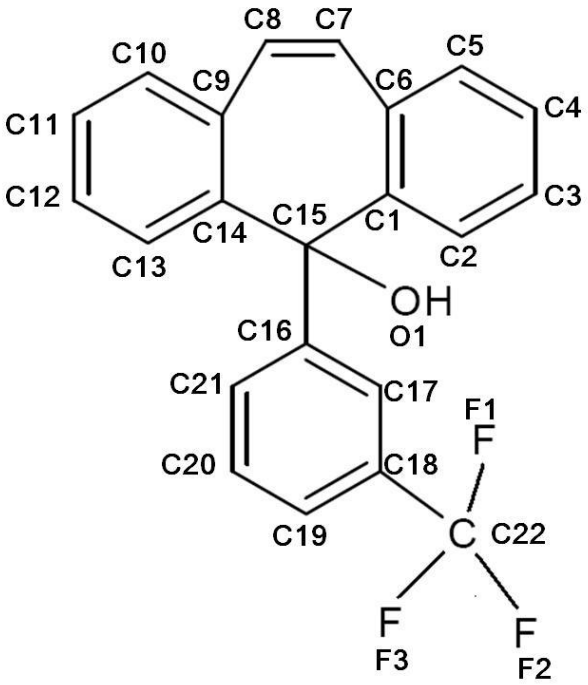

Figure 5.132: Atomic numbering of **A31**.

5.18.1 Guest: Morpholine

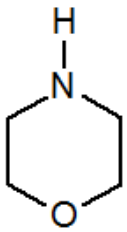

Table 5.72: Properties of morpholine.

Guest	MORPH
Molecular formula	C_4H_9NO
Molar mass (g/mol)	87.1
Boiling Point (K)	401

5.18.2 Thermal Analysis

The thermal analysis results are shown in Figure 5.133. A single mass loss step of 10.7 % was observed in the TG curve which is due to loss of half a guest. A single endotherm in the DSC curve corresponds to dissolution of the host upon release of the guest. The thermal data is given in Table 5.73.

Table 5.73: Thermal analysis data for **A31·MORPH.**

Compound	A31•MORPH
Host: Guest ratio	1:½
TG calculated % mass loss	11.0
TG experimental % mass loss	10.7
DSC Endo$_1$ (T_{onset}, K)	376.3
DSC Host (T_{onset}, K)	405.1

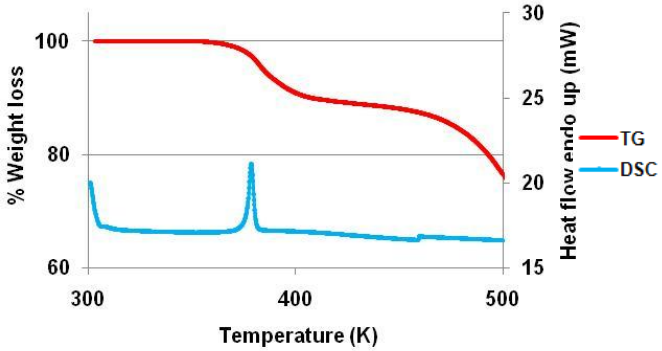

Figure 5.133: TGA and DSC curves obtained for **A31·MORPH.**

5.18.3 Structure Refinement

The structure solved successfully in $P\bar{1}$ and refined to R_1= 0.0523 with wR_2= 0.1184. All non-hydrogen atoms were found in the electron density map by direct methods and refined anisotropically. A bond length constraint of 0.94 Å was assigned to the NH bond of the guest. The host was found to be partially disordered and therefore the fluorine atoms were solved by parts (part 1 = A and part 2 =B). The crystal data is given in Table 5.74.

Table 5.74: Crystal data of **A31·MORPH.**

Compound	**A31•MORPH**
Structural Formula	**$C_{22}H_{15}OF_3$· ½C_4H_9NO**
Host-Guest ratio	**1:½**
Molecular Mass (g.mol^{-1})	**395.90**
Data collection temp (K)	**173**
Crystal system	**Triclinic**
Space group	**$P\bar{1}$**
a (Å)	**8.2882(16)**
b (Å)	**9.8236(18)**
c (Å)	**12.166(2)**
α (°)	**95.026(4)**
β (°)	**94.722(4)**
γ (°)	**104.991(4)**
Volume (Å^3)	**947.5(3)**
Z	**2**
μ/ mm^{-1}	**0.106**
F(000)	**412**
No. of reflections collected	**9059**
No. of unique reflection	**4718**
No. of reflections with I>2σ(I)	**3123**
D_c, Calculated density (g.cm^{-3})	**1.388**
Index range	**h: -10 to 11, k: -13 to 11, l: -16 to16**
θ range	**1.69-28.40**
Goodness of fit, S	**0.980**
Final R indices [I>2σ(I)]	**R_1= 0.0523 ; wR_2= 0.1184**
R indices (all data)	**R_1= 0.0872 ; wR_2= 0.1359**
Largest diff peak and hole (eÅ^{-3})	**0.30 ; -0.27**

5.18.4 Discussion

The structure was solved successfully in the triclinic space group $P\bar{1}$ with Z=2. The asymmetric unit contains the host molecule and half a guest molecule with a structural formula of $C_{22}H_{15}OF_3 \cdot \frac{1}{2}C_4H_9NO$. The morpholine guest is situated on a centre of inversion at Wyckoff position *h* and is therefore disordered. The nitrogen and oxygen of the morpholine guest atoms occupies the same position each with site occupancy factors of 0.5. The host molecule is partially disordered (Figures 5.134). The fluorine atoms with suffixes A and B have site occupancy factors of 0.79 and 0.21 respectively shown in Figure 5.135. The disordered guest is shown in Figure 5.136. The structure is stabilised by hydrogen bonding (Figure 5.137). The hydrogen bond parameters are given in Table 5.75.

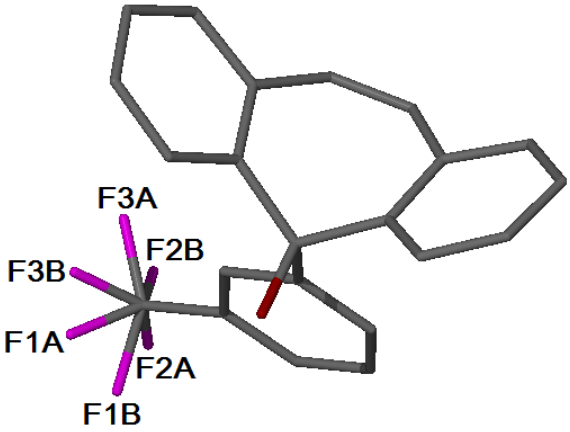

Figure 5.134: The host **A31** with disordered fluorine atoms.

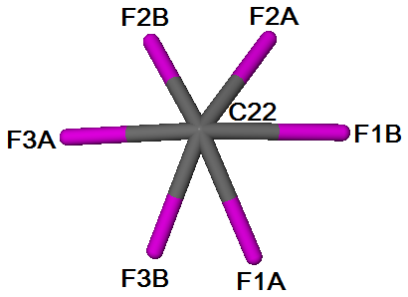

Figure 5.135: Disordered CF_3 of the host.

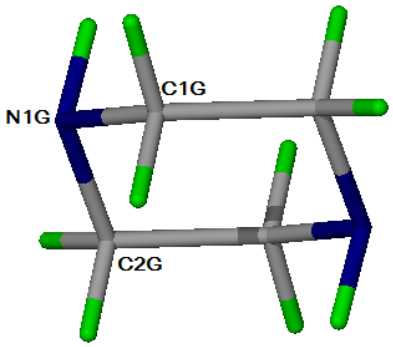

Figure 5.136: Disordered morpholine.

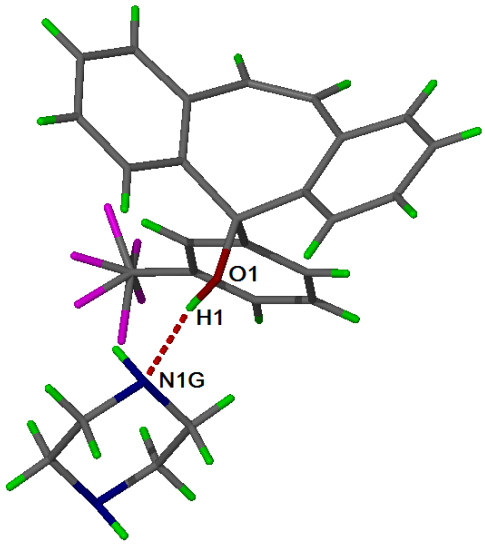

Figure 5.137: Hydrogen bonding in asymmetric unit of **A31·MORPH.**

Table 5.75: Hydrogen bond parameters of **A31· MORPH**.

Donor(D)-H	Acceptor(A)	D···A (Å)	D-H (Å)	H···A (Å)	D-H···A (°)
O1-H1	N1G	2.850(2)	0.90(3)	1.96(3)	167(2)

A pair of host molecules display off-set face-to-face π-π interactions with the shortest distance between two ring centroids = 3.647 Å shown in Figure 5.138. The only C-H···π interaction between a host and guest molecule has a C···π = 3.441 Å and C-H- π = 137° (Figure 5.139). The C-H···π interactions between host molecules has C···π distances of 3.549 Å(C4··· π), 3.821 Å(C7···π) and 3.666 Å(C20···π) with angles of 154°, 139° and 151° respectively (Figure 5.140).

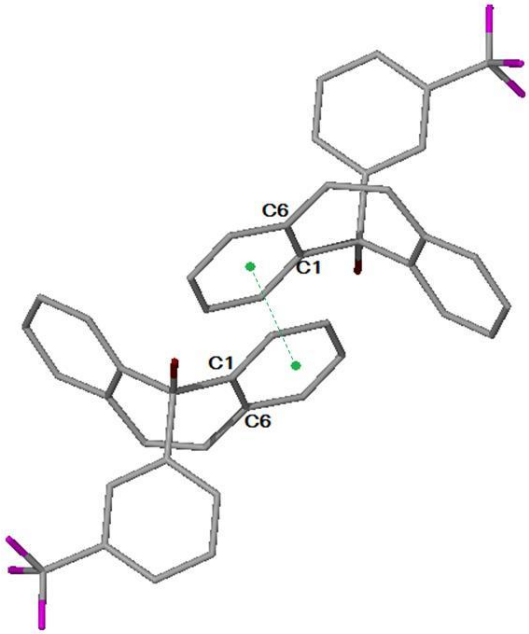

Figure 5.138: Off-set face-to-face π-π stacking of neighbouring host molecules. The distance between the centroids is indicated by green dotted lines. All hydrogen atoms were omitted for clarity.

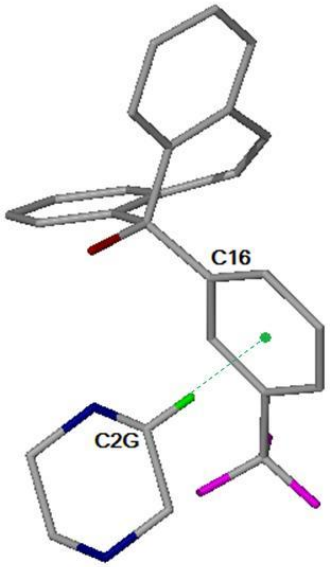

Figure 5.139: C-H···π interaction between a host and guest molecule. The C-H···π interaction is indicated by a green dotted line.

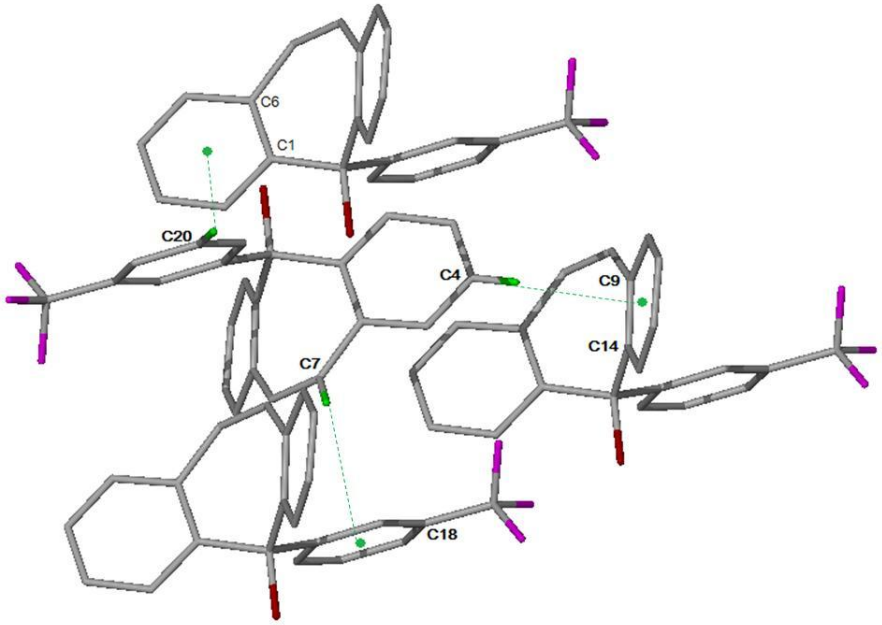

Figure 5.140: C-H···π interaction between host molecules. The C-H···π interactions are indicated by green dotted lines.

In the packing diagrams it can be seen that the host molecules surround the guest molecule when viewed along [100], [010] and [001]. The guest molecules reside in cavities making **A31·MORPH** a clathrate (Figure 5.144).[5]

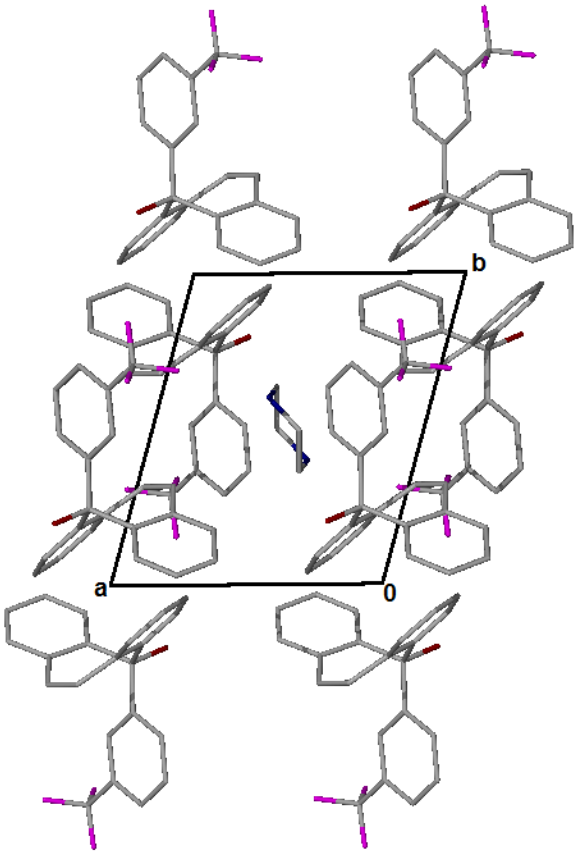

Figure 5.141: Packing diagram of **A31·MORPH** down [001].

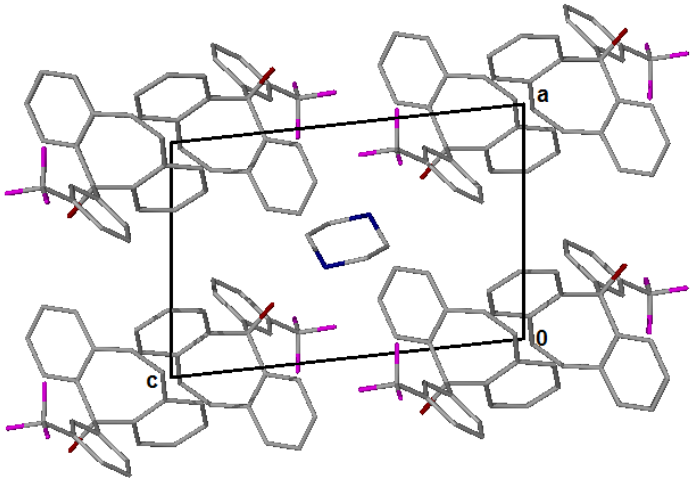

Figure 5.142: Packing diagram of **A31·MORPH** down [010].

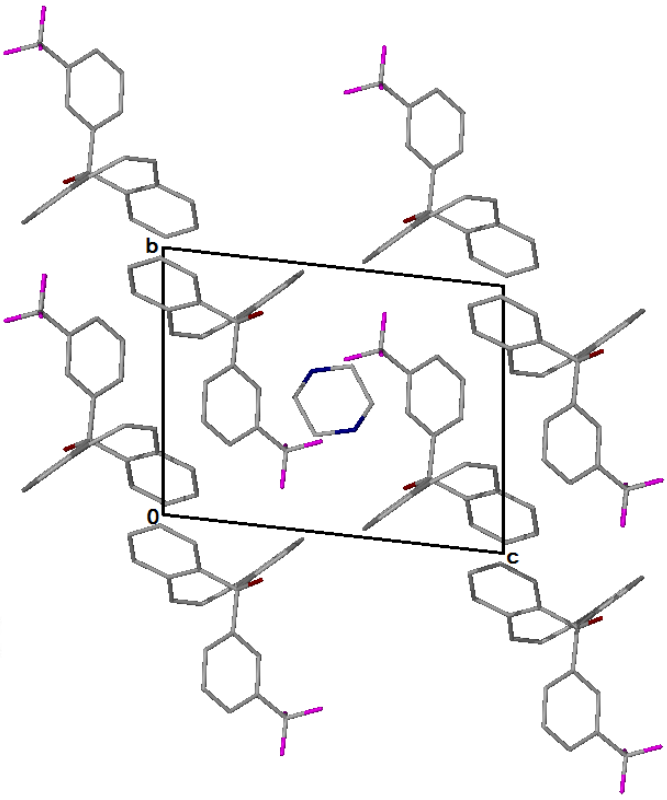

Figure 5.143: Packing diagram of **A31·MORPH** down [100].

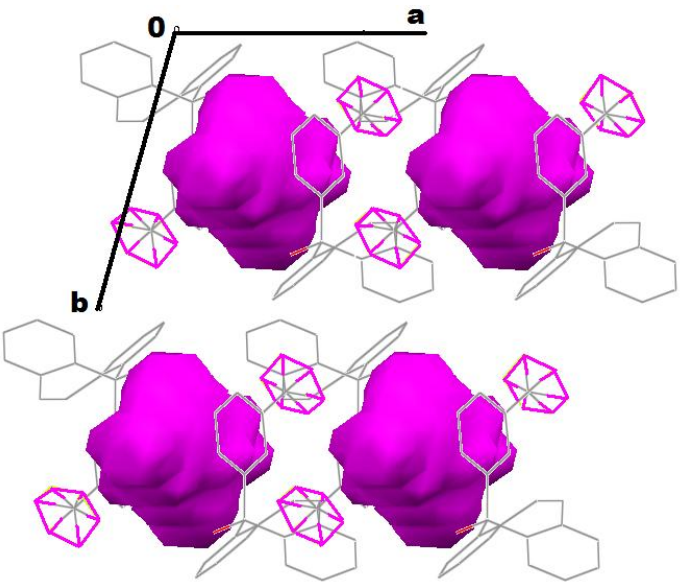

Figure 5.144: The cavities in which the guests are located.

The program *SECTION*[6] was used to map the cavities in which the guests are located as shown in Figure 5.145. The program *PLATON*[7] was used to calculate the total potential solvent accessible volume and was found to be 150.8 Å^3.

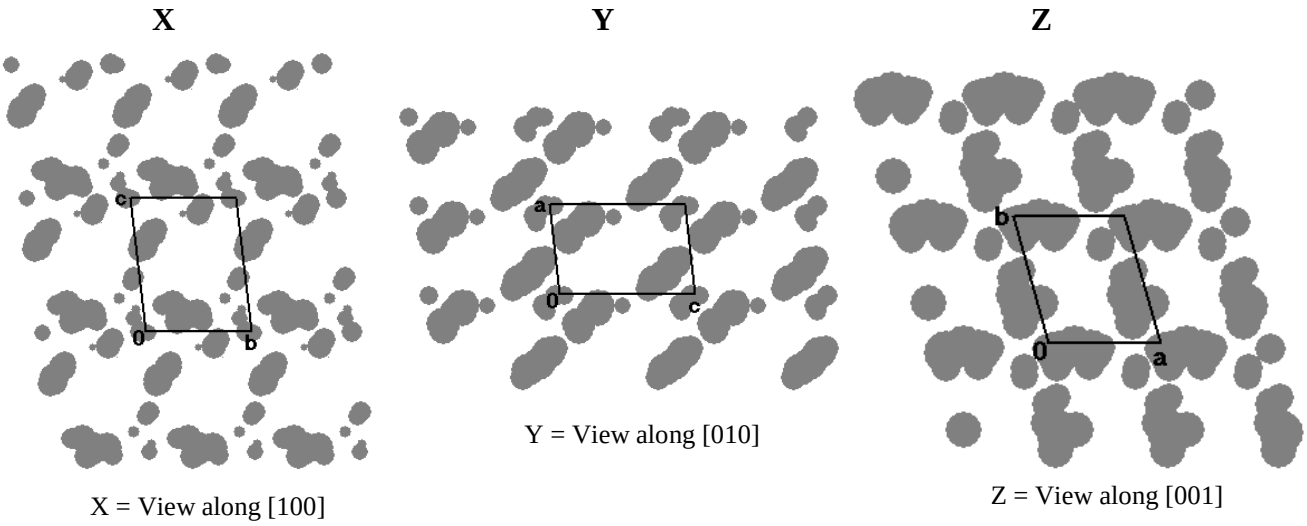

Figure 5.145: Section plot of **A31·MORPH** at section height =4.50 Å.

5.19 Host: 5-(naphthalen-1-yl)-5*H*-dibenzo[a,d]cyclohepten-5-ol

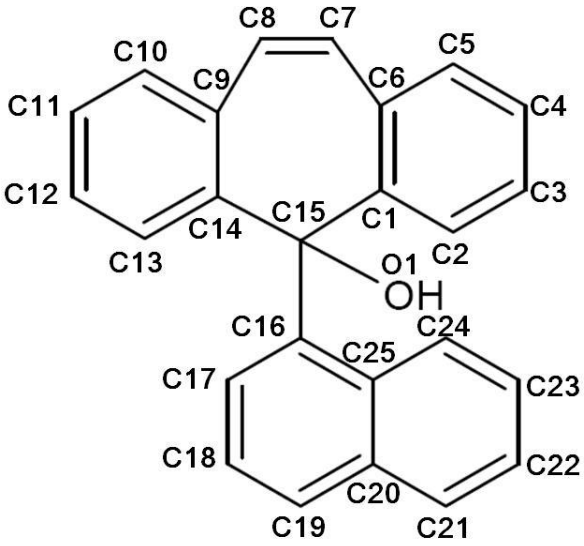

Figure 5.146: Atomic numbering of **A32**.

5.19.1 Guest: Morpholine

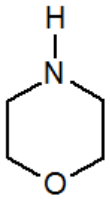

Table 5.76: Properties of morpholine**.**

Guest	MORPH
Molecular formula	**C_4H_9NO**
Molar mass (g/mol)	**87.1**
Boiling Point (K)	**401**

5.19.2 Thermal Analysis

The thermal data is given in Table 5.77. The TG curve shows a two step mass loss, total = 12.0 %, which corresponds to a host-guest ratio of 1:½. The endotherm observed in the DSC curve corresponds to the simultaneous dissolution of the host upon release of the guest. The thermal analysis results are shown in Figure 5.147.

Table 5.77: Thermal analysis data for **A32·MORPH.**

Compound	A32•MORPH
Host: Guest ratio	**1:½**
TG calculated % mass loss	**11.5**
TG experimental % mass loss	**12.0**
DSC Endo$_1$ (T_{onset}, K)	**412.9**
DSC Host Endo$_1$ (T_{onset}, K)	**353.3**
DSC Host Endo$_2$ (T_{onset}, K)	**425.8**

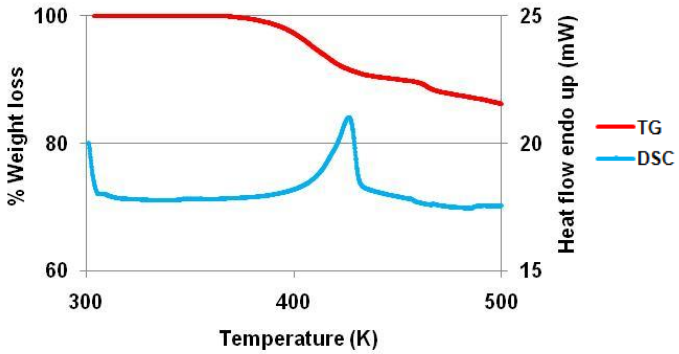

Figure 5.147: TGA and DSC curves obtained for **A32·MORPH.**

5.19.3 Structure Refinement

All non-hydrogen atoms were found by direct methods in the difference electron density map and refined anisotropically. The hydroxyl hydrogens were located in the difference electron density map. The nitrogen atom in both morpholine guests was identified by the highest peak magnitude. The secondary amine hydrogens were located in the difference electron density map. A bond length constraint of 0.94 Å was assigned to the N1GA-H1GA bond of the secondary amine. The NH bond refined to 0.92(1) Å. The crystal data is reported in Table 5.78.

Table 5.78: Crystal data of **A32·MORPH.**

Compound	**A32·MORPH**
Structural Formula	**$2C_{25}H_{18}O{\cdot}1C_6H_7N$**
Host-Guest ratio	**1:½**
Molecular Mass ($g.mol^{-1}$)	**755.91**
Data collection temp (K)	**173**
Crystal system	**Triclinic**
Space group	**$P\bar{1}$**
a (Å)	**9.6407(8)**
b (Å)	**14.6797(13)**
c (Å)	**15.0331(13)**
α (°)	**98.781(2)**
β (°)	**99.806(2)**
γ (°)	**105.038(2)**
Volume ($Å^3$)	**1980.9(3)**
Z	**2**
μ/ mm^{-1}	**0.077**
F(000)	**800**
No. of reflections collected	**20995**
No. of unique reflection	**11798**
No. of reflections with I>2σ(I)	**8017**
D_c, Calculated density ($g.cm^{-3}$)	**1.267**
Index range	**h: -13 to 13, k: -20 to 18, l: -21 to 21**
θ range	**1.47-30.52**
Goodness of fit, S	**1.034**
Final R indices [I>2σ(I)]	**R_1= 0.0595 ; wR_2= 0.1545**
R indices (all data)	**R_1= 0.0929; wR_2= 0.1753**
Largest diff peak and hole ($eÅ^{-3}$)	**0.52 ; -0.20**

5.19.4 Discussion

The **A32·MORPH** structure crystallises in the triclinic crystal system in the space group $P\bar{1}$ with Z=2. The asymmetric unit contains two independent host molecules and two independent half guest molecules. Both morpholine guests lie on centres of inversion at Wyckoff position *d* and *g* and are therefore disordered. The nitrogen and oxygen atoms of the morpholine guest molecules occupy the same position each with site occupancy factors of 0.5. The structure is stabilised by hydrogen bonding. The hydrogen bond metrics are provided below.

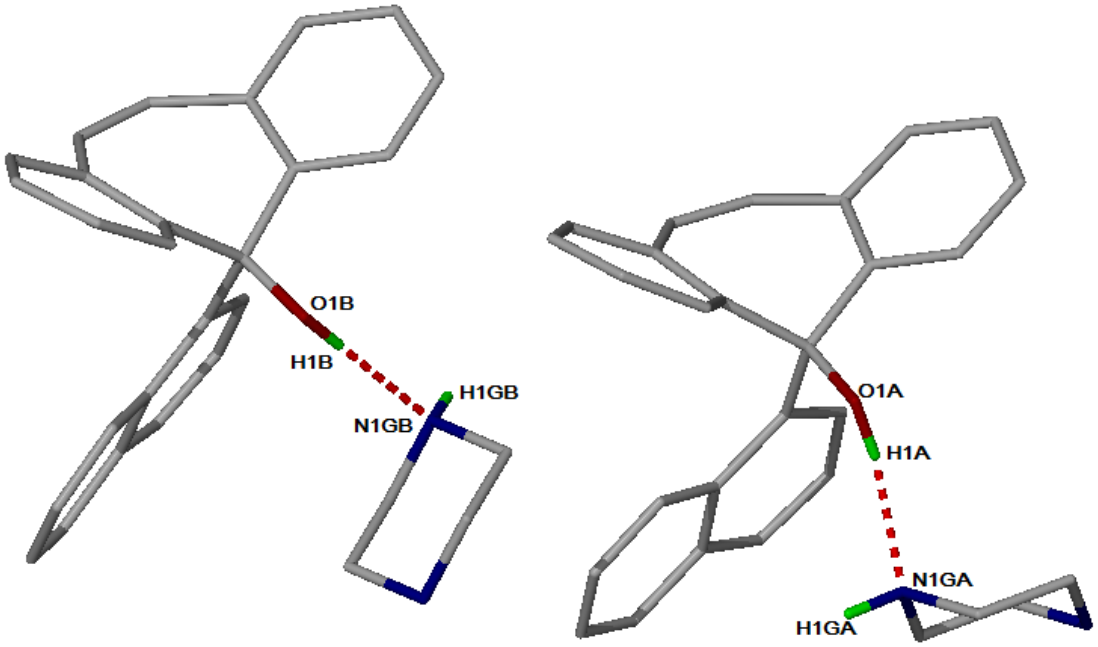

Figure 5.148: Hydrogen bonding in **A32·MORPH.**

Table 5.79: Hydrogen bond parameters of **A32·MORPH**.

Donor(D)-H	Acceptor(A)	D···A (Å)	D-H (Å)	H···A (Å)	D-H···A (°)
O1A-H1A	**N1GA**	**2.821(2)**	**0.87(2)**	**1.99(2)**	**158(2)**
O1B-H1B	**N1GA**	**2.777(2)**	**0.82(2)**	**1.96(2)**	**169(2)**

The program *PLATON*[7] was used to generate all the C-H···π interactions found in the inclusion compound. The shortest C···π distance between a host and a guest molecule is 3.450 Å with a C-H- π angle = 141° (Figure 5.149). The shortest C···π distance between a pair of host molecules is 3.697 Å with a C-H- π angle = 173° shown in Figure 5.150.

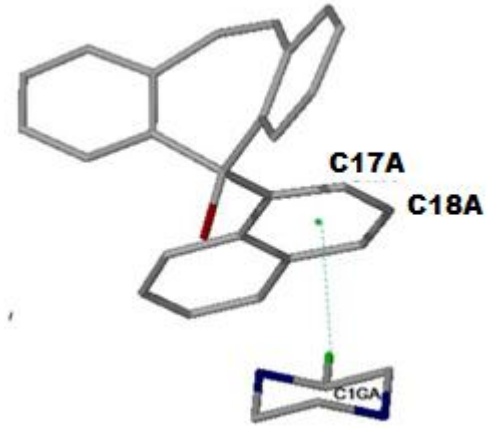

Figure 5.149: C-H···π interaction between a host and guest molecule. The C-H···π interaction is indicated by a green dotted line.

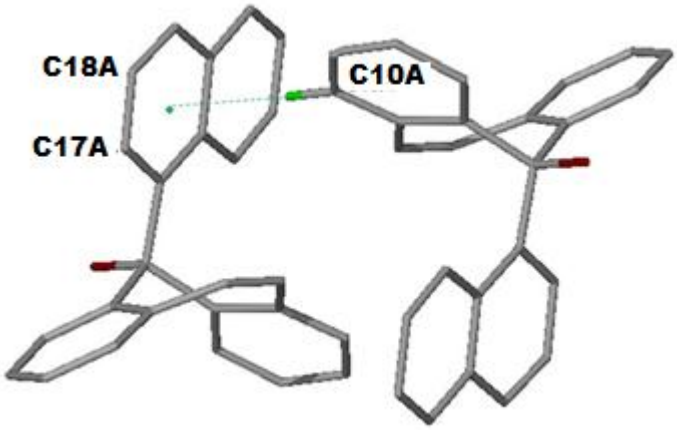

Figure 5.150: C-H···π interaction between host molecules. The C-H···π interaction is indicated by a green dotted line.

In the packing diagram down [100] and [001], the host molecules pack in such a manner that they encapsulate the morpholine guest. The guest molecules are situated in cavities and therefore **A32·MORPH** is a clathrate (Figure 5.152).[5]

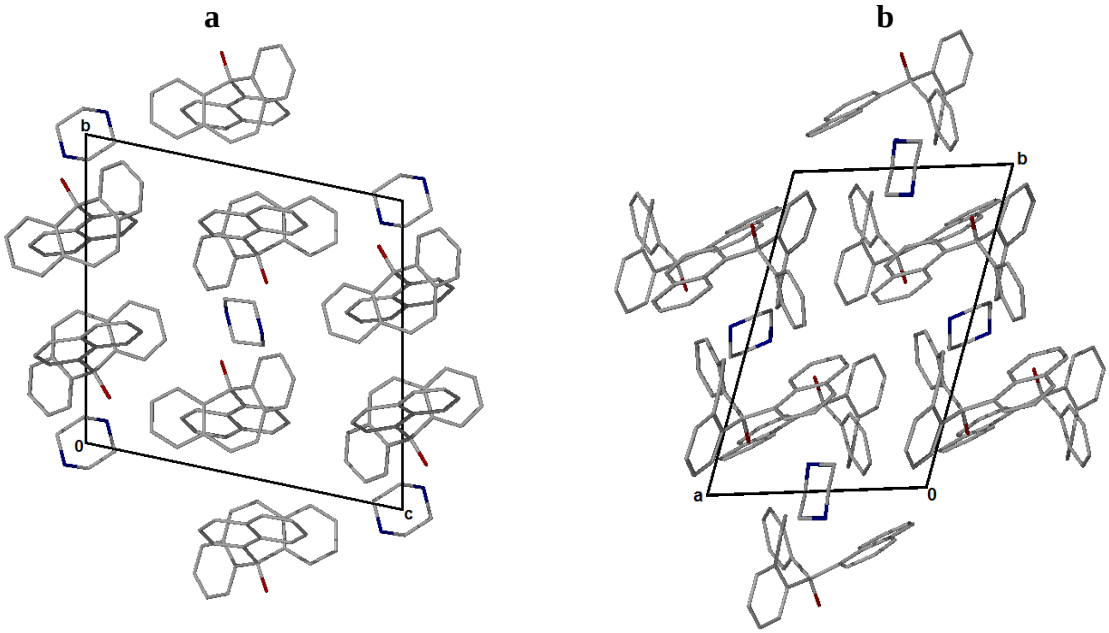

Figure 5.151: Packing diagram of **A32·MORPH.** (a) down [100] (b) down [001]. All hydrogen atoms are omitted.

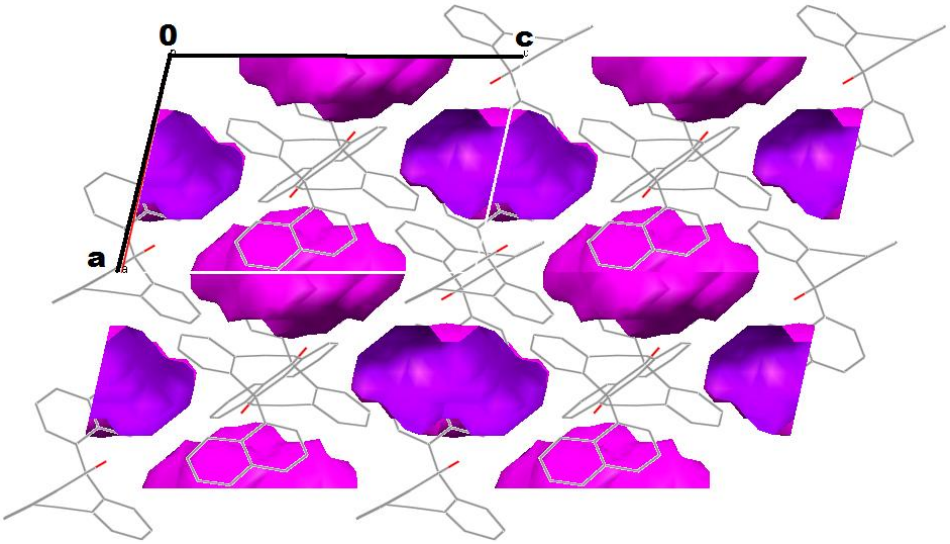

Figure 5.152: The cavities in which the guests are located.

The cavities in which the guests reside were mapped using the program *SECTION*.[6] The program *PLATON*[7] was used to calculate the total potential solvent accessible area volume which is 287.7 $Å^3$.

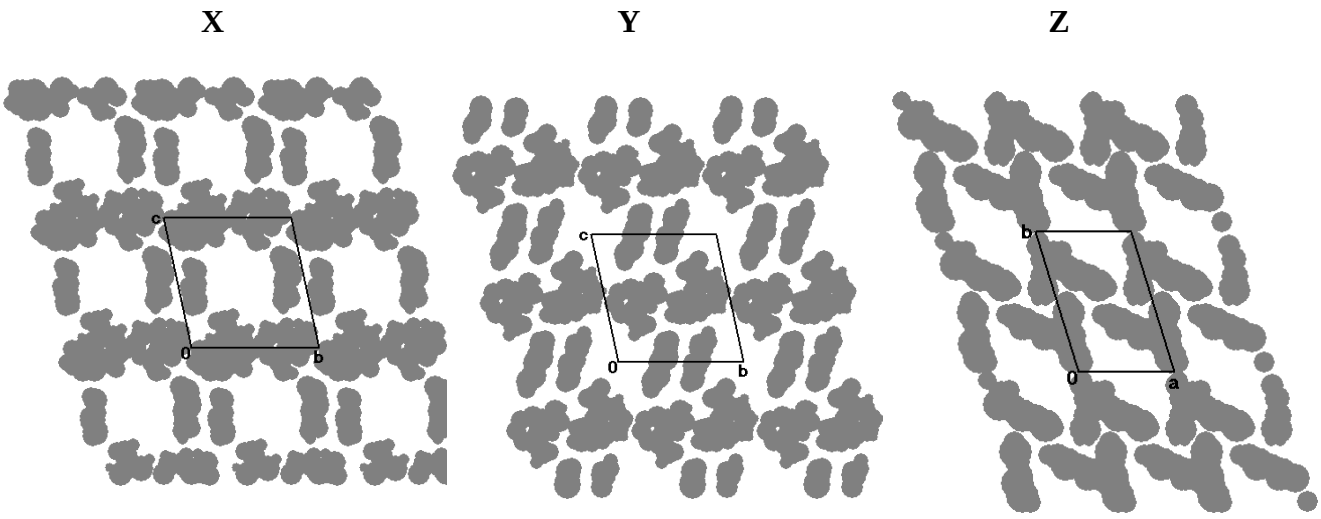

Figure 5.153: Section plot of **A32·MORPH.**

X = View along [100] with a section height = 0 Å ;

Y=View along [100] with a section height = 5.00 Å ;

Z=View along [001] with a section height = 0 Å.

5.20 Structure Comparison

The host compounds 5-(4-chlorophenyl)-5*H*-dibenzo[a,d]cyclohepten-5-ol, 5-[3(trifluoromethyl)phenyl]-5*H*-dibenzo[a,d]cyclohepten-5-ol and 5-(naphthalen-1-yl)-5*H*-dibenzo[a,d]cyclohepten-5-ol form inclusion compounds with morpholine. All three structures were solved successfully in the triclinic space group $P\bar{1}$ with the host molecules hydrogen bonded to the morpholine guests. The structural formulas for **A28·MORPH**, **A31·MORPH** and **A32·MORPH** are $2C_{21}H_{15}OCl{\cdot}2C_4H_9NO$, $C_{22}H_{15}OF_3{\cdot}½C_4H_9NO$ and $2C_{25}H_{18}O{\cdot}1C_6H_7N$. For the **A28·MORPH** structure the guest molecules are located in intersecting channels down [100] and [010]. In **A31·MORPH** and **A32·MORPH** the guest molecules reside in cavities, therefore these structures are clathrates.

References

1. Olovsson, I & Jönsson, P. (1975) *The Hydrogen Bond-Structure and Spectroscopy.* Schuster, P., Zundel, G. & Sardify, C., eds. USA: North Holland Publishing Company.

2. Jacobs, A., Nassimbeni, L.R. & Taljaard, J.H. (2005) Inclusion compounds of isomeric xanthenol hosts with aniline. *CrystEngComm*, 7: 731-734.

3. Curtis, E., Nassimbeni, L.R., Su, H. & Taljaard, J.H. (2006) Xanthenol clathrate: Structure and Solid-Solid Reaction. *Crystal Growth and Design*, 6: 2716-2719.

4. Etter, M.C, Macdonald, J.C. & Bernstein, J. (1990) Graph-set analysis of hydrogen-bond patterns in organic crystals, *Acta Crystallographica*, B46: 256-262.

5. Macrae, C. F., Eddington, P. R., McCabe, P., Pidcock, E,. Shields, G. P., Taylor, R., Towler, M. & van de Streek, J (2006) Mercury: visualization and analysis of crystal structures, *Journal of Applied Crystallography*, 39: 453-457.

6. Barbour, L. J. (1999) *SECTION*- a computer program for the graphic display of cross sections through a unit cell. *Journal of Applied Crystallography*, 32: 353-354.

7. Spek, A. L. (2008) *PLATON* - A Multipurpose Crystallographic Tool. Utrecht University: Utrecht, The Netherlands.

8. Flynn, J. H. & Wall, L. A. (1966). A Quick, Direct Method for the Determination of Activation Energy from Thermogravimetric Data. *Journal of Polymer Science, Polymer Letters***,** B4(5): 323-328.

9. Ozawa, T. (1965) A New Method of Analyzing Thermo Gravimetric Data. *Bulletin of the Chemical Society of Japan*. 38(11): 1881-1886.

10. Dean, J. A. (1999) *LANGE'S HANDBOOK OF CHEMISTRY, 15th edition.* McGraw-Hill Inc.

CHAPTER 6
CONCLUSION

The inclusion ability of a series of hydroxyl hosts with a variety of guests was investigated in this study. The host 9-(4-methoxyphenyl)-9*H*-xanthen-9-ol **(A1)** forms inclusion compounds with aniline **(A1·ANI),** 3-picoline **(A1·3PIC),** morpholine **(A1·MORPH),** *N*-methylacetamide **(A1·NMA, A1·2NMA** and **2A1·2NMA)** and *N*-methylformamide (**A1·NMF·H_2O)**, their structures have been elucidated.

Non-isothermal kinetics of desolvation were performed for **A1·3PIC** and **A1·MORPH** which yielded activation energy ranges of 42-63 and 49-72 kJ/mol respectively. These results correlate to the higher onset temperature observed for **A1·MORPH** with the observation that the morpholine guests are trapped in cavities whereas the 3-picoline guests lies in channels. The packing of both these structures are characterised by (Host)-OH···N-(Guest) hydrogen bonds.

A structure of **A1·½ANI** which crystallises in $P\bar{1}$ with Z=2, has been previously reported.[1] **A1·ANI** crystallises in the monoclinic space group $P2_1/c$ with Z=4. For both structures the host atoms occupy general positions while the guest is located on a centre of inversion at Wyckoff position *a*. Both structures are stabilised by (Host)-OH···O-(Host) hydrogen bonds. For the **A1·½ANI,** two host molecules form a centrosymmetric dimer at Wyckoff position *h* as shown in Figure 6.1, whereas in **A1·ANI** the host hydrogen bonds via the hydroxyl moiety of one molecule to the methoxy oxygen of a second molecule, forming chains running in the [001] direction (Figure 6.2). For both structures the host-guest ratio is 1:½, with the aniline guest situated in cavities. The two inclusion compounds formed are polymorphs.

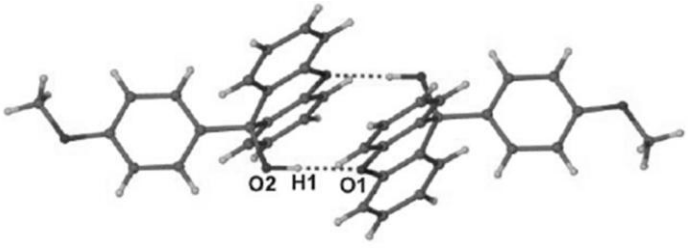

Figure 6.1: Hydrogen bonding in **A1·½ANI.**

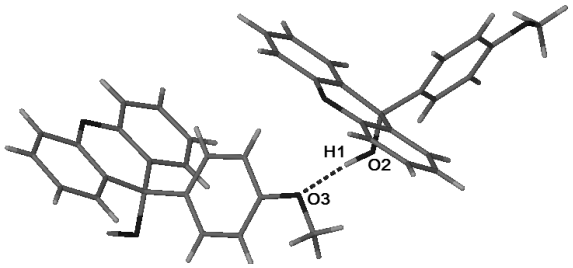

Figure 6.2: Hydrogen bonding in **A1·ANI.**

The host **A1** was dissolved in equimolar mixtures of NMA/DMA (**A1·NMA)**, NMA/DIOX (**A1·2NMA**) and NMA/ANI (**2A1·2NMA**), with host-guest ratios of 1:1, 1:2 and 2:2 respectively. The host **A1** preferentially enclathrated the guest *N*-methylacetamide (NMA) in each instance. For these structures the hosts and guests are hydrogen bonded to one another forming chains with their guests located in channels. **A1·NMA** and **2A1·2NMA** are polymorphs.

The hydrate **A1·NMF·H_2O** was successfully solved in the triclinic space group $P\bar{1}$. The **A1·NMF·H_2O** hydrogen bond pattern may be described according to Etter's notation as $R_4^2(8)$ and $R_6^6(16)$. In this structure**,** the host molecules pack to form channels along [100] in which the guests reside.

The host 9-(3-methoxyphenyl)-9*H*-xanthen-9-ol **(A2)** forms inclusion compounds with morpholine (**A2·MORPH**), *N*-methylacetamide (**A2·NMA**) and *N*-methylformamide (**A2·NMF**), with host-guest ratios 1:1. The crystal structure of the apohost crystallised in P*bca* with Z = 8. **A2·MORPH** and **A2·NMF** were solved in $P\bar{1}$, whereas **A2·NMA** solved in $P2_1/n$. The morpholine and the *N*-methylacetamide guests occupy channels, whereas the *N*-methylformamide guest is situated in cavities. The packing is stabilised by host···guest hydrogen bonds.

The host compound **A1** and **A2** differ only by the position (*para* and *meta*) of the methoxy group. When these hosts include *N*-methylacetamide the structures are stabilised by (Host)-OH···O-(Guest) and (Guest)-NH···O-(Guest) hydrogen bonds which form chains.

The host 5-(4-methoxyphenyl)-5*H*-dibenzo[a,d]cyclohepten-5-ol **(A26)** forms inclusion compounds with morpholine (**A26·MORPH**) and aniline (**A26·ANI)**. **A26·MORPH** and **A26·ANI** structures crystallise in the spacegroup *Pc* and $P\bar{1}$ respectively. The packing of these structures are characterized by (Host)-OH···O-(Host) hydrogen bonding with guest molecules situated in cavities.

The host compounds **A28** ($C_{21}H_{15}OCl$), **A31** ($C_{22}H_{15}OF_3$) and **A32** ($C_{25}H_{18}O$) form inclusion compounds with morpholine. All three structures were solved successfully in the triclinic space group $P\bar{1}$ with the host molecules hydrogen bonded to the morpholine guests.

For the **A28·MORPH** structure the guest molecules are located in intersecting channels down [100] and [010]. In **A31·MORPH** and **A32·MORPH** the guest molecules reside in cavities, therefore these structures are clathrates.

The host compounds **A26**, **A28**, **A31** and **A32** were dissolved in equimolar mixtures of pyridine/morpholine. It was observed that these host compounds preferentially enclathrated the morpholine guest in each case.

These host compounds included small organic guests which reveals the versatility of these hosts. The structures formed have Host···Host and/or Host···Guest hydrogen bonds, which is further stabilized by weak van der Waals interactions.

References

1. Jacobs, A., Nassimbeni, L. R. & Taljaard, J.H. (2006) Inclusion compounds of isomeric xanthenol hosts with aniline. *CrystEngComm*, 7: 731-734.